ELECTROOPTIC MODULATION OF INFRARED RADIATION IN PLANAR CADMIUM SULPHIDE WAVEGUIDES

A THESIS

submitted to the Faculty of Engineering

of the University of Glasgow

for the degree of

Doctor of Philosophy

by

James Alexander McMurray

September 1976.

INDEX

ABSTRACT

This thesis incorporates a study of optical waveguiding and electrooptic phase modulation in both planar and rectangular waveguides of cadmium sulphide formed by evaporation in a clean high vacuum system. Single mode propagation in multimode structures is considered throughout this investigation.

Laser radiation at 1.15 μm was guided in planar thin polycrystalline films of cadmium sulphide evaporated onto amorphous substrates. The evaporation parameters were studied in the context of minimising the optical attenuation. A minimum loss of 5 $dBcm^{-1}$ for the TE_o mode was obtained with films of apparent optimum stoichiometry and structure. Films grown epitaxially onto single crystal substrates have exhibited TE_o mode losses of 2 $dBcm^{-1}$.

The thin polycrystalline films of cadmium sulphide were successfully adapted into an Al-SiO-CdS-SiO-Al planar multilayer configuration which formed the basis of a low electrical drive power optical phase modulator. The structure was completely evaporated and unlike previous thin film modulators does not rely on the use of single crystal substrates and waveguides. The power per unit bandwidth was minimised by careful choice of buffer and guide thicknesses with particular attention made to the additional attenuation from the metal electrodes. An experimental structure with a guide thickness of 1.4 μm and buffer thicknesses of 0.45 μm required 11.5 mW/MHz^{-1} drive power for a phase change of 1 radian and a diffraction limited electrode area of 10.0x0.5 mm^2. A theoretical description of the multilayer type electrooptic phase modulator is given and shown to adequately account for the experimental results.

Tapered film coupling between 7059-glass films and cadmium sulphide optical waveguides was also demonstrated with phase modulation in the composite structure. The structure provides a low insertion loss and also facilitates coupling between optical

fibres and thin film devices which is an essential prerequisite for a fully optical communications link.

The fabrication of rectangular waveguides formed from thin polycrystalline films of cadmium sulphide by ion beam etching, selenium diffusion, chemical etching and evaporation onto preferentially etched silicon substrates is described. The most promising results have been 15 $dBcm^{-1}$ for a 20 μm x 2.0 μm cadmium sulphide guide evaporated onto a preferentially etched silicon substrate and 15-20 $dBcm^{-1}$ for a 5 μm x 4 μm guide formed by selenium diffusion into cadmium sulphide ($\Delta n = 5x10^{-3}$). In both cases the results refer to the lowest order TE mode. The results of an electrooptic phase modulator based on a 20 μm x 2 μm guide evaporated onto an etched silicon substrate are presented. For an electrode area of 5.0 x 0.02 mm^2 a drive power of 1.45 $mWMHz^{-1}$ for 1 radian phase change and a base bandwidth of 4.7 GHz into a 50Ω load are predicted.

A theoretical design study of directional couplers which exchange light through the electrooptic effect from one output port to the other is presented and proposals for a device using selenium diffused cadmium sulphide rectangular waveguides requiring 61 volts for switching are given.

ACKNOWLEDGEMENTS

I wish to express my thanks to Professor J. Lamb for the provision of the research facilities in the Department of Electronics and Electrical Engineering, and for his interest and encouragement during the course of this research.

Sincere gratitude is also due to my supervisor Dr. C.R. Stanley for helpful guidance and advice throughout this work and in the preparation of the thesis.

I should also like to thank the staff and my fellow research students for their help at various stages in this work; in particular Mr. R.H. Hutchins for his constant interest and encouragement and Dr. M. Kawabe for help with the selenium diffusion.

The technical assistance of Messers Boyle, Brownlie, Orr and Piechowiak is gratefully acknowledged and thanks is due to Miss J. Harper who typed the thesis.

This work was supported by a grant from the Science Research Council.

CHAPTER 1

INTRODUCTION

The idea of using optical frequencies as the carrier for ultra high information rates has been considered for well over twenty years but it has only been with the advent of the laser some fifteen years ago that interest in optical communications began to expand rapidly. In 1969 Miller[1] stated the difficulties of a free space optical communications link using bulk optical components and proposed a solution whereby the optical devices could be miniaturised and combined on a single substrate with interconnections by means of rectangular waveguides (transmission lines). Because of its analogy with the miniaturisation of electrical components on a single "chip" (substrate) to form an integrated circuit Miller adopted the terminology "integrated optics" to describe this field of research. The benefits of such devices are a reduction in size and weight, rigidity, ease of alignment and freedom from environmental effects such as interference.

Prior to Miller's proposals several workers had studied thick dielectric waveguides[2,3] in which the light was coupled into the structures by focussing onto a polished end of the film. Such structures were invariably multimode and it was not until Tien et al[4] developed the prism-film coupler*, which enabled efficient excitation of discrete modes in thin film waveguides, that "integrated optics" began to expand rapidly. Concurrent with this progress low loss planar waveguides were also reported[5]. Integrated optics is mainly concerned with a thin film fabrication technology which has progressed from the initial development of passive planar waveguides to active waveguides incorporating devices such as modulators and switches often with lateral confinement of the guided wave. At the commence-

* The prism-film coupler was first reported by L.V. Iogansen, Sov. Phys. Tech. Phys. 7, P295 (1962).

ment of this research a large amount of effort had been given to the theoretical and experimental studies of coupling light into dielectric waveguides[6,7,8]; investigations of active rectangular waveguides were just appearing[9] and a number of active devices had been reported[10,11].

During the course of this research the dramatic reductions in the losses of optical fibres have led to the realisation of large bandwidth experimental communication links using semiconductor laser/LED transmitters and photodiode receivers[12]. The subsequent result has been the development of planar optical waveguides in the expectation that thin film "integrated optical" circuits can provide a means of inexpensive multiplexing and demultiplexing within the transmitter and terminal stages respectively. Thin film waveguide devices have demonstrated a number of functions which have direct microwave counterparts. In addition to the many passive devices such as directional couplers[13], lenses[14] and prisms[15], laser action[16], frequency conversion[17], deflection[18], switching[19], and modulation[20] have all been reported. Electrooptic modulators employing various materials such as lithium niobate[21], gallium arsenide[22] and Cd(S,Se)[11] have all been demonstrated. The majority of interest is now concentrated on gallium arsenide in which it is envisaged that all the functions required for an integrated optical circuit can be performed[23]. In addition lithium niobate, which has very large electrooptic and acoustooptic coefficients and low waveguide attenuation[24], has enabled very low drive power devices to be fabricated. Recently investigations have begun into interactions between devices on the same substrate and into the problem of efficient coupling between low index silica fibres and devices fabricated in high index guides[25].

The main goal of integrated optics has been towards the production of a high bandwidth optical communications link. However, the techniques are also finding application in the areas of displays and interfacing electronics to optical memories where bulk optical

components are used at present, the reduction in size and weight, rigidity and ease of alignment being key advantages.

The basic requirement of any thin film device is a high quality film and in the field of integrated optics this means the fabrication of dielectric waveguides with low attenuation. The level of technology required for this is extremely complex with approximately four orders of magnitude improvement in film loss required compared to dielectric layers used in optical filters. In fibre optical technology the transmission line can be drawn from high purity bulk material and losses approaching the intrinsic scatter level can be achieved[26]. However, the planar technology required for integrated optics does not permit the use of a similar technique and the dielectric waveguides must be formed directly onto a substrate with the light confined in one dimension, a slab waveguide, (Fig. 1.1a) or in two dimensions, a rectangular waveguide, (Fig. 1.1b). Rectangular waveguides represent a greater technological challenge due to the additional scatter loss from the sides of the guide.

Initially waveguides were fabricated in passive noncrystalline materials such as glasses and organosilicons. The need for active devices quickly led to investigations of crystalline films which require a more stringent fabrication technology than do their amorphous counterparts. Most methods of thin film deposition have been used including evaporation[27], sputtering[28], proton implantation[29], diffusion[30,31] (both in and out), ion exchange[32] and chemical vapour deposition[23]. Initially the bulk of active waveguides were based on semiconductor materials such as gallium arsenide[34], zinc sulphide[4], zinc oxide[35,36] and various diffused guides formed by II-VI compound mixing[9]. However, in and out diffusion of the ferroelectrics such as lithium niobate and lithium tantalate[37] have been shown to produce waveguides with low loss. All these guides with the exception of zinc sulphide, which possessed high waveguide attenuation and very

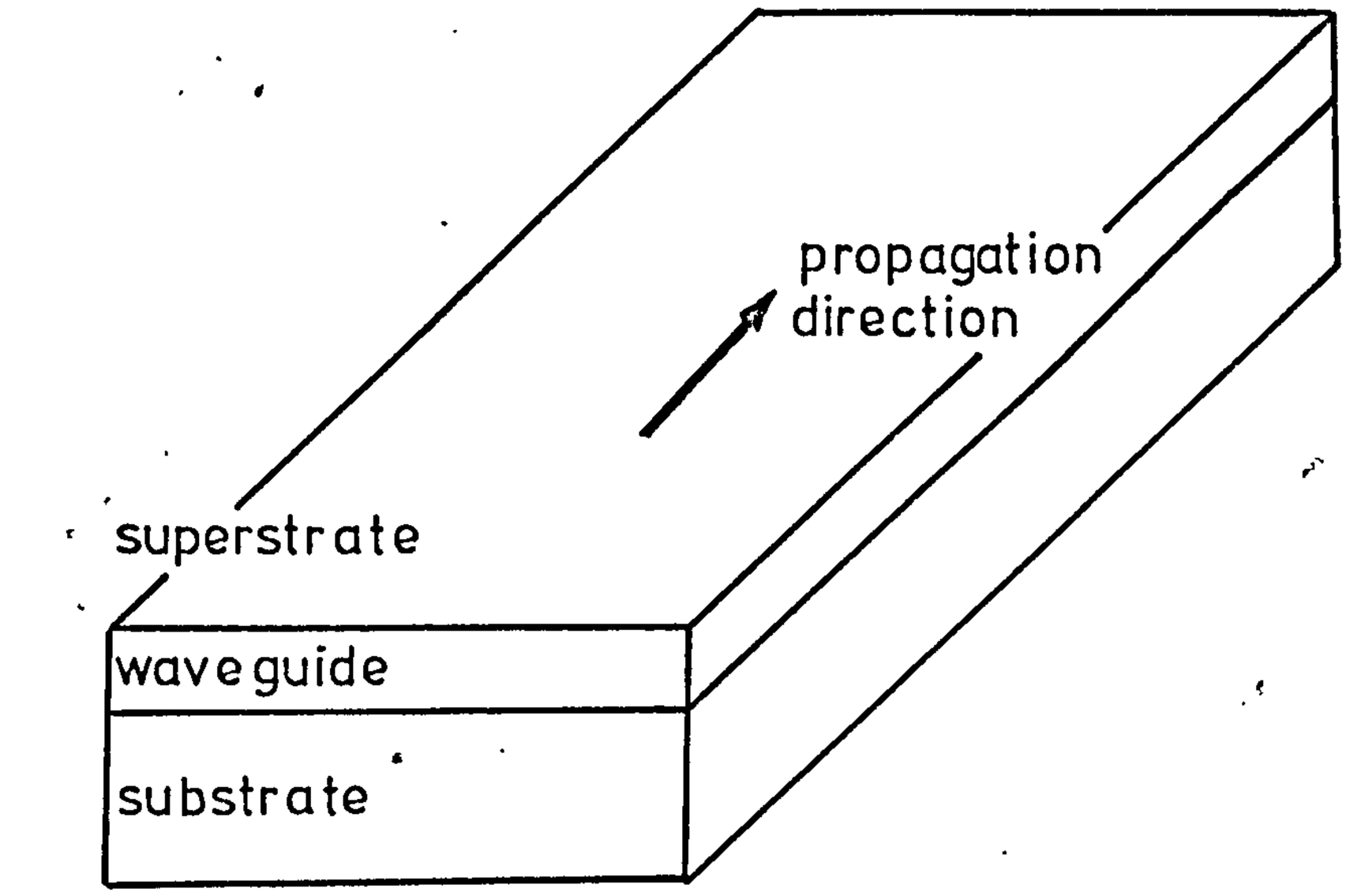

(a) Slab waveguide

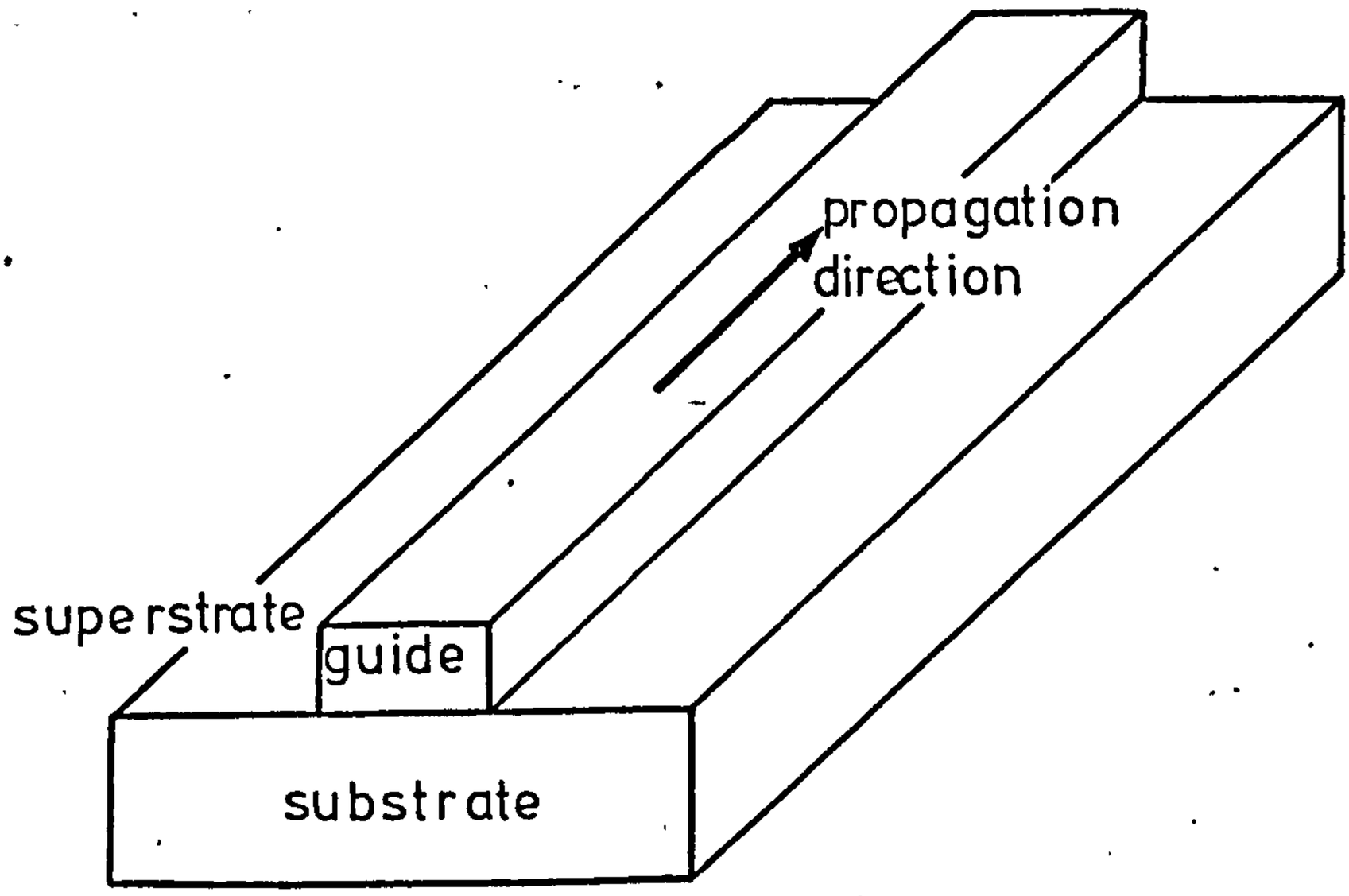

(b) Rectangular waveguide

FIGURE 1.1 Waveguide structures

little crystallographic structure, were based on single crystal substrates.

For most device applications rectangular waveguides, with their lateral confinement of the guided light, provide lower cross-talk interference and enable closer packing of devices on a substrate. They also permit a change of propagation direction and in the case of electrooptic phase modulators lead to a lower power per unit band width requirement through reduced capacitance. For these reasons most recent waveguide fabrication has been directed toward the production of low loss, active rectangular waveguides with the main emphasis on gallium arsenide and its isomorphs[38], and the ferro-electrics lithium niobate and lithium tantalate[39]. Some interest still continues in the II-VI diffused compounds[40] which were the first active rectangular waveguides to be reported[11]. In late 1974 Schmidt et al[24] demonstrated that titanium diffused into lithium niobate produced low loss rectangular waveguides and subsequently this optical waveguide fabrication technology has given way to device fabrication.

The importance of coupling optical fibres to thin film devices has now been fully appreciated and the reflection loss problems associated with butting low refractive index fibres to high index films has not yet been solved. An alternative method of coupling is to taper the waveguide to allow its propagation constant to match to a mode in the fibre. This permits almost 100% power transfer but requires that the waveguide be grown on a low index substrate. Recently some work has been reported on the sputtering of the ferro-electrics to form low loss waveguides[41] which would permit efficient fibre-film coupling.

It has been apparent since work began on integrated optics that the modulator would be an essential element of any optical communications system. A recent review article by Kaminow[20] illustrates

the large amount of research effort that has gone into the production of such devices. Many interactions have been used to modulate guided optical waves using a particular property of the waveguide or substrate. Modulation by electroabsorption effects such as injected free carrier absorption[42] or through the electrooptic[21], magnetooptic[43] and acousto-optic[44] effects have all been demonstrated. Films used for magneto-optic interactions tend to be very lossy and effects such as Faraday rotation and the Cotton-Mouton effect rely on a rapidly changing magnetic field to induce modulation; hence the bandwidth of such devices is small. In acoustooptic modulators (deflectors) diffraction of the light beam occurs by means of an r.f. generated surface acoustic wave which usually requires larger powers for unit modulation bandwidth than do electrooptic modulators. There is the problem of interaction with other devices on the same substrate. Such devices are also limited by the bandwidth of the transducer used to launch the surface acoustic wave although they do not require increased power for increased bandwidth. Thus much research effort has been concentrated on modulators using the electrooptic effect as these devices can achieve very wide bandwidths with low modulation voltages.

The electooptic effect was discovered over a century ago in 1875 by Kerr[45] when he observed refractive index changes in certain liquids, such as carbon disulphide, on the application of an electric field across the liquid. The effect he noticed was a refractive index change proportional to the square of the applied electric field and is consequently known as the quadratic or Kerr effect. Subsequently in 1906 Pockels[46] discovered the existence of an effect in crystals of quartz and tourmaline which had a linear dependence between applied electric field and induced refractive index change. This effect is now known as the Pockels or linear electrooptic effect and is the one most often used for electrooptic modulation as many crystals of high

optical quality possess large linear coefficients. Prior to the advent of guided wave optics bulk electrooptic modulators were diffraction limited in both the thickness and width directions. This resulted in large voltages being required for modulation due to the distance between the electrodes. The planar waveguide geometry permits distances of a few microns between the elcctrodes and thus large electric fields are set up for only small applied voltages. When lateral confinement of the wave occurs diffraction limiting conditions no longer apply and very low power per unit bandwidth figures result.

It is obvious that the electrooptic effect will normally result in phase modulation. For many applications amplitude modulation is more desirable and a number of systems have been proposed and demonstrated as amplitude modulators. These include grating diffraction modulators[47] in which a periodic change in refractive index, induced through the electooptic effect, gives rise to a diffracted light beam, an electrooptically controlled directional coupler[48,49] in which thc light is transferred from one guide to another, a Mach-Zenhder thin film interferometer[50] and a push-pull thin-film optical modulator based on two phase modulators in the arms of a Jamin interferometer[51]. However, much of the work has concentrated on the production of low drive power phase modulators with two electrode geometries proposed (Fig 1.2). The multilayer configuration (Fig. 1.2a) is the more efficient since most of the electric field appears across the waveguide while with the transverse electrode geometry of Fig. 1.2b the fringing fields do not induce such a large refractive index change for the same applied voltage. However to use the multilayer structure requires a highly orientated crystalline film to be grown on an amorphous substrate while single crystal substrates can be used with the transverse electrode geometry.

The majority of modulators reported to date have been based on

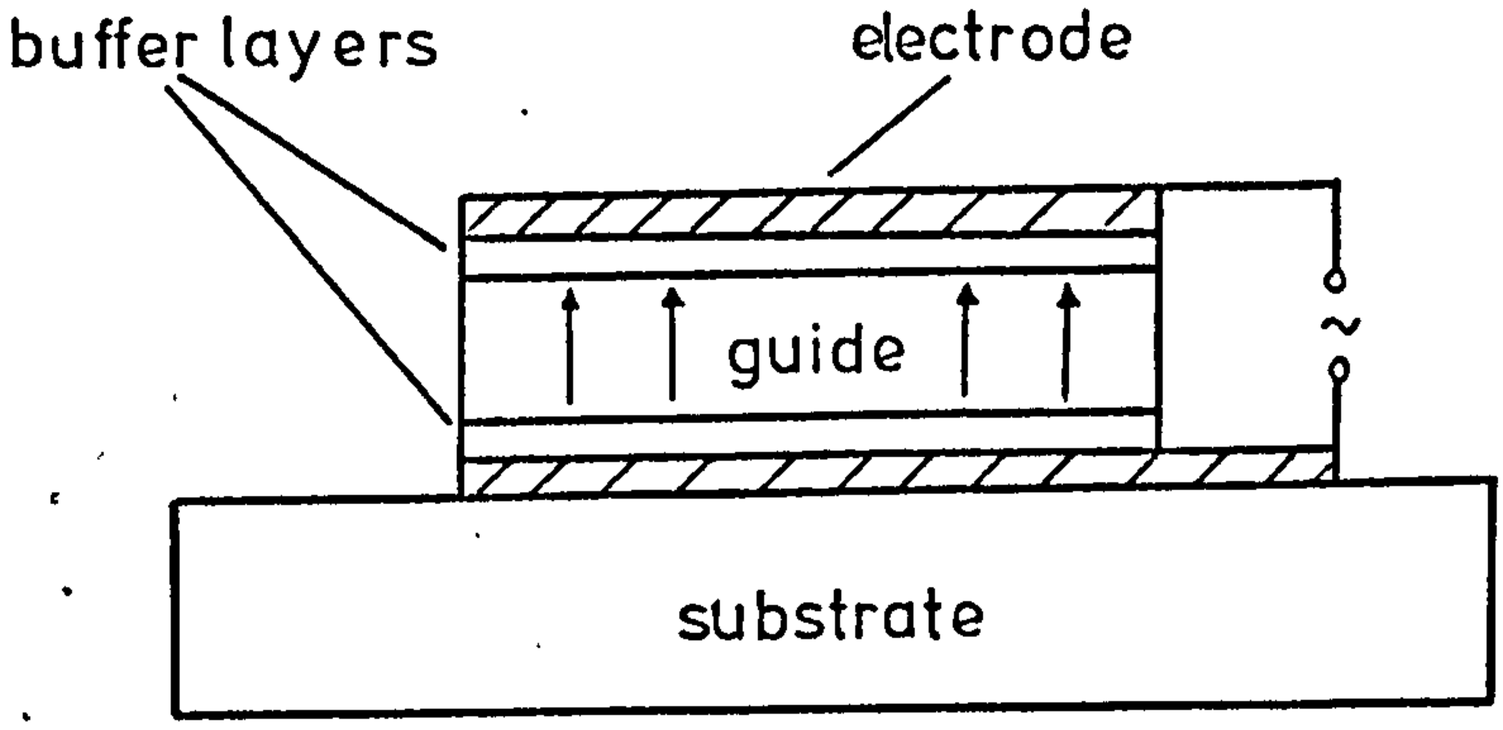

(a) Multilayer structure

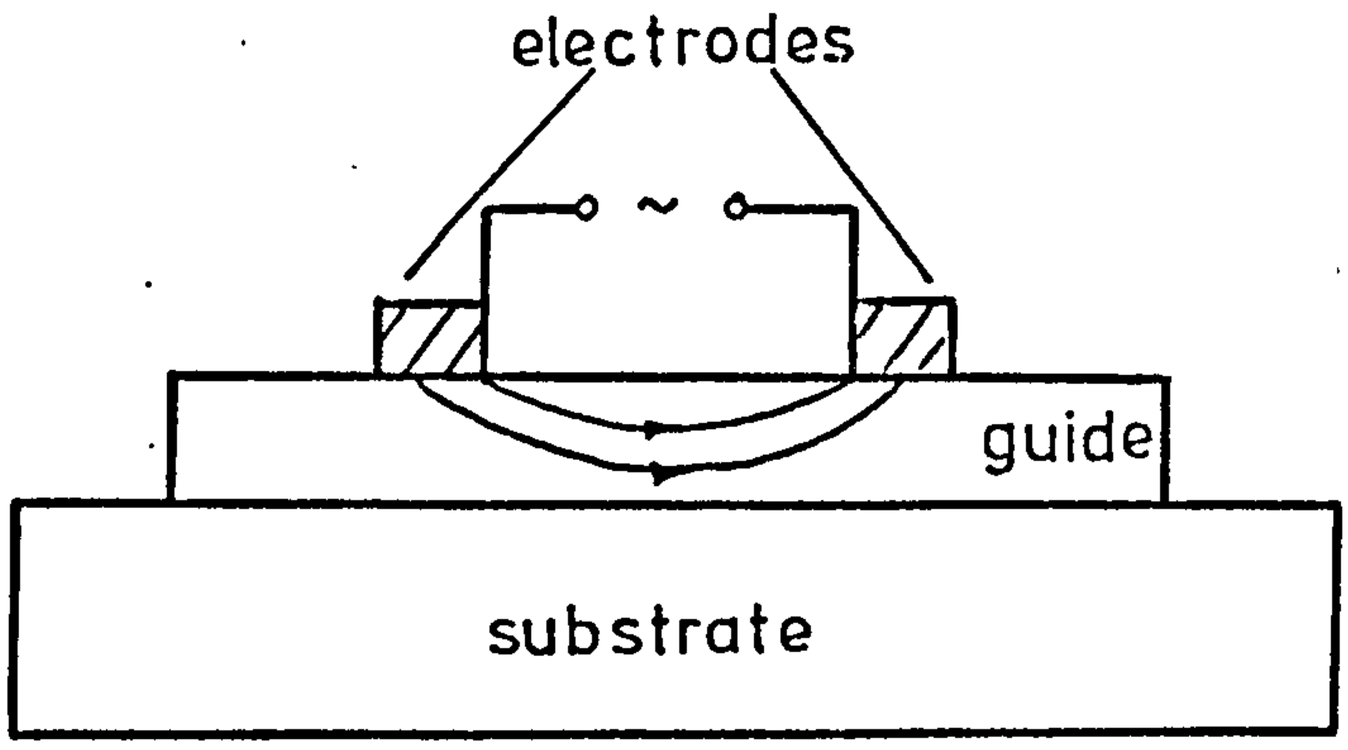

(b) Transverse electrode structure

FIGURE 1.2 Modulator geometries

single crystal substrates employing the transverse electrode scheme. The ferroelectrics lithium niobate and lithium tantalate have proved the most successful due to the low waveguide losses possible with these materials. The first waveguide phase modulator was produced in gallium arsenide[22]. In mid 1973 Kaminow et al[10] reported an electro-optic waveguide phase modulator in out-diffused lithium niobate and later that year Martin[11] reported a rectangular waveguide phase modulator based on diffusion into single crystals of II-VI semiconductor compounds. Subsequently, several modulating structures have been produced in gallium arsenide[52], lithium niobate[53] and zinc oxide[54]. The lowest power per unit bandwidth of 1.7 $\mu WMHz^{-1}$ for one radian phase change at 633 nm is attributed to Kaminow et al[55] for a titanium diffused lithium niobate rectangular waveguide modulator.

All modulators are formed from high index materials and there is a significant problem when coupling such waveguides efficiently to low refractive index silica fibres. For modulators based on lithium niobate and gallium arsenide coupling to fibres is achieved by butting the fibre to the film and problems associated with accurate alignment and reflection losses give rise to a low transfer of optical energy. Thus although the waveguide loss is low the overall fibre-fibre insertion loss may still be high. The alternative method to fibre-film coupling is to phase match the film mode to a mode in the fibre and under these circumstances close to 100% power transfer is possible. This method can, however, only be used if the substrate is of a lower refractive index than the optical fibre. When this condition applies the waveguide can be tapered to reduce its propagation constant to that of a fibre mode. To date the cadmium sulphide electrooptic phase modulator described in this thesis is the only such device amenable to the latter coupling technique.

Cadmium sulphide was selected as a material which could be vacuum evaporated with a high degree of c-axis orientation parallel to

the incident vapour stream[56]. The high degree of inherent crystallinity meant that amorphous substrates can be used and hence a modulator based on the multilayer structure (Fig. 1.2a) could be employed with a concomittant reduction in power per unit bandwidth. The structure was completely evaporated and is the only such device to have been reported. The modulator was subsequently considered as the basis of an electrooptically controlled directional coupler, proposed by Miller[1], in which the optical signal can be switched between the two output ports.

The aims of this research were essentially threefold.

(1) To develop planar waveguides of cadmium sulphide by evaporation onto amorphous substrates and to reduce the waveguide losses to a tolerable level at which meaningful experiments could be carried out.

(2) To study both theoretically and experimentally the multilayer electrooptic phase modulator using slab waveguides of cadmium sulphide and to prove its compatability with a phase matched fibre-film coupling technology.

(3) To fabricate rectangular waveguides based on the evaporated cadmium sulphide thin films and demonstrate a low power per unit bandwidth modulator based on these guides; further to study both theoretically and experimentally the possibility of producing an electrooptically switched directional coupler based on the rectangular waveguides of cadmium sulphide.

This thesis is organised into four parts.

Part 1 is concerned with the growth and optical waveguiding in cadmium sulphide thin films. In chapter 2 the basic properties of slab waveguides are summarised with particular reference to the case of cadmium sulphide. Chapter 3 outlines the growth kinetics, nucleation and preparation of cadmium sulphide thin films. The basic film properties, mode analysis and optical attenuation of the films are described in chapter 4.

Part II is devoted to a theoretical and experimental study of planar multilayer cadmium sulphide waveguide modulators. In chapter 5 a general theoretical analysis for multilayer waveguides is developed and applied to the specific case of an Al-SiO-CdS-SiO-Al modulator structure. The experimental results of the modulators are described in chapter 6 along with the results of a novel composite modulator structure.

Part III is concerned with work towards a low power per unit bandwidth electrooptic phase modulator based on rectangular cadmium sulphide waveguides and an electrooptically switched directional coupler based on selenium diffused rectangular cadmium sulphide waveguides. In chapter 7 the theory for rectangular waveguides is briefly outlined and modifications to the theory are made to account for the case of strongly asymmetric waveguides near cut-off. Experimental fabrication details for rectangular cadmium sulphide waveguides follow and the chapter is concluded with the results of a low power per unit bandwidth modulator. The theoretical design criteria for electro-optically switched directional couplers are evolved in chapter 8 and applied to the case of cadmium sulphide waveguides. A design based on selenium diffusion into polycrystalline cadmium sulphide thin films is proposed.

Part IV contains the conclusions on this study and outlines some proposals for future work.

PART I

Cadmium Sulphide Thin Film Waveguides

SYNOPSIS

A great deal of effort has gone into the evaluation of various materials which may be suitable as optical waveguides. However, little has been reported on good quality crystalline films grown on amorphous substrates. Cadmium sulphide is one of a small group of II-VI compounds that tend to grow with the c-axis preferentially orientated parallel to the incident vapour stream. This high degree of crystallinity is maintained with films grown on amorphous substrates. Other materials such as zinc sulphide and zinc oxide had been demonstrated to have large optical attentuation and cadmium sulphide was chosen for its ease of vacuum evaporation. The major problem is producing semiconductor guides of low loss and the value of 2 $dBcm^{-1}$ for planar single crystal films of cadmium sulphide (TE_o mode, $\lambda = 1.5\ \mu m$) remains one of the lowest waveguide attenuations reported.

In this part the first chapter considers the theory of planar dielectric waveguides in both isotropic and anisotropic media, in particular the specific case of cadmium sulphide. Light beam coupling to thin film waveguides is considered in chapter 2. Chapter 3 deals with a theoretical resume of the growth and nucleation of evaporated cadmium sulphide films drawn from published literature and concludes with details of the experimental apparatus and growth conditions. The final chapter discusses the characterization of the thin films through the evaluation of waveguide and other parameters. The results are fully discussed in the context of the factors governing waveguide attenuation.

CHAPTER 2: THEORY OF PLANAR OPTICAL WAVEGUIDES

The theory of propagation of light in dielectric thin films is of fundamental importance to the understanding of cadmium sulphide waveguides and associated devices considered in later chapters. There are two well established approaches to the evaluation of waveguide propagation; both have been extensively reported in the literature and will only be briefly summarized. The first is known as the "ray optics" approach[57] and the second involves a solution obtained through electromagnetic field theory[58].

It has been shown that a continuum of modes exists associated with the waveguide[59]. This can be subdivided into two broad classifications; guided modes where the fields are confined by the waveguide and radiation modes[57] where the fields are unguided. Only the former will be considered in this thesis.

In this chapter a simple three layer planar waveguide geometry will be considered as shown in Fig. 2.1. All the media will be assumed isotropic and the theory will be extended to the case of three anisotropic media. The specific case of the cadmium sulphide waveguide will then be evaluated. Beam coupling to the waveguides will also be discussed.

2.1 PROPAGATION IN ISOTROPIC MEDIA

The ray optics approach considers the light to be a series of plane waves which propagate along a zig-zag path (Fig. 2.2) with the reflections at the guide-substrate/superstrate interfaces occurring due to total internal reflection. In order to satisfy the criteria for guided modes the refractive indices must be such that $n_o < n_1 > n_2$. When the wave is totally reflected it suffers a phase change[60] which can be geometrically represented as a shift on reflection called the Goos-Haenchen shift[61] (Fig. 2.3). For propagation the waves must interfere constructively; that is for one round trip within the waveguide the total phase change should be an integral number of 2π.

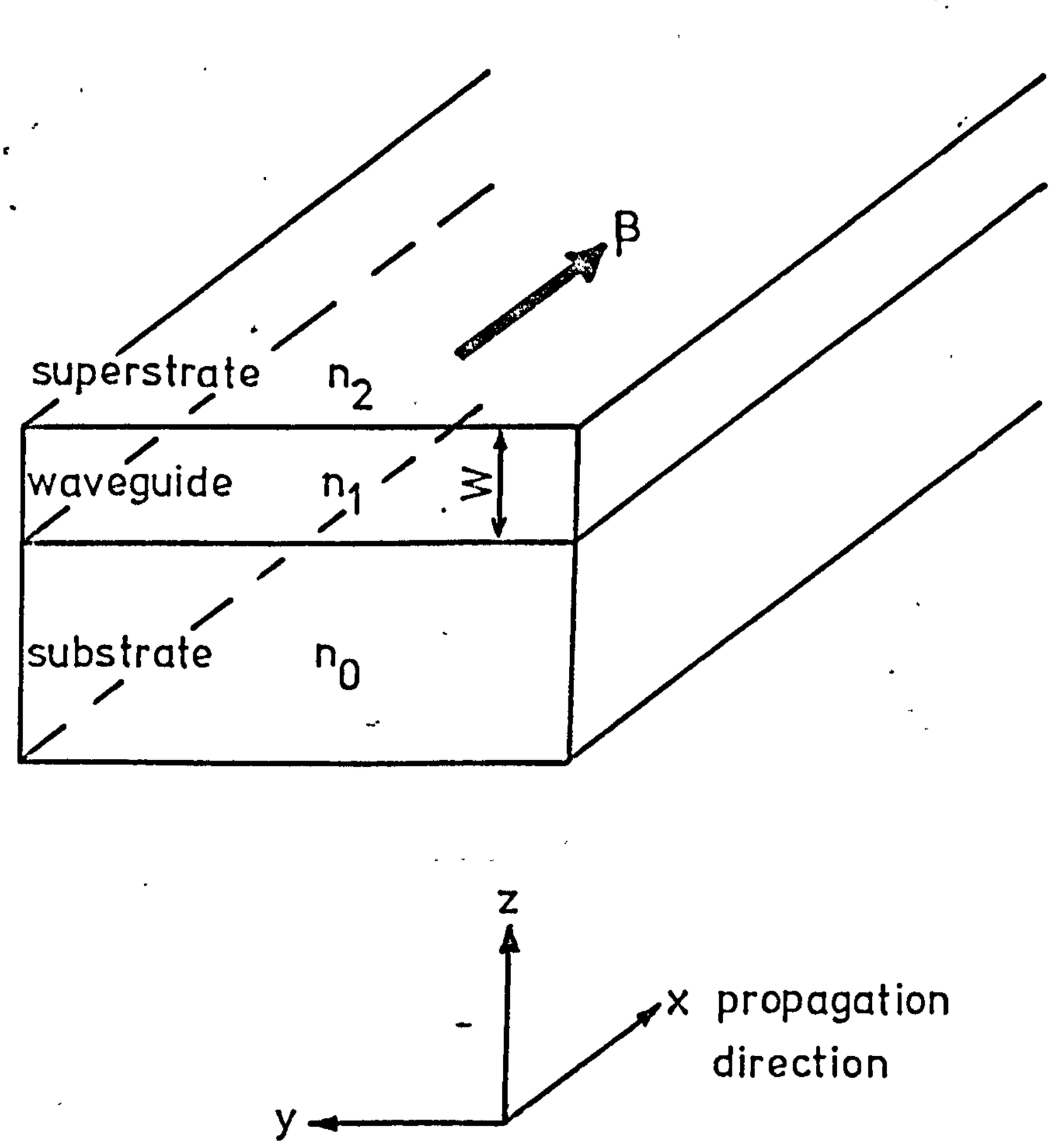

FIGURE 2.1 Planar isotropic waveguide geometry

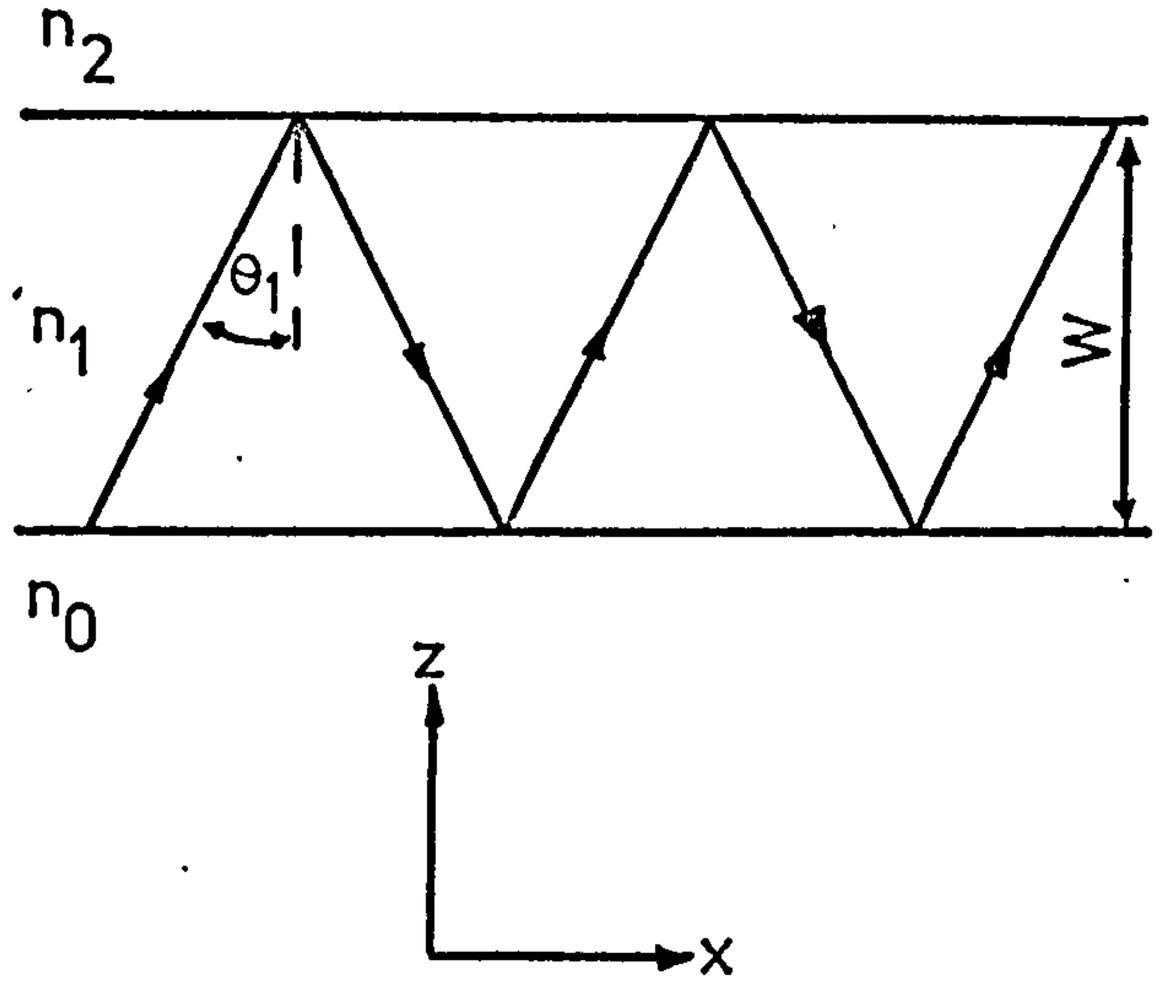

FIGURE 2.2 Ray optics representation of a guided wave

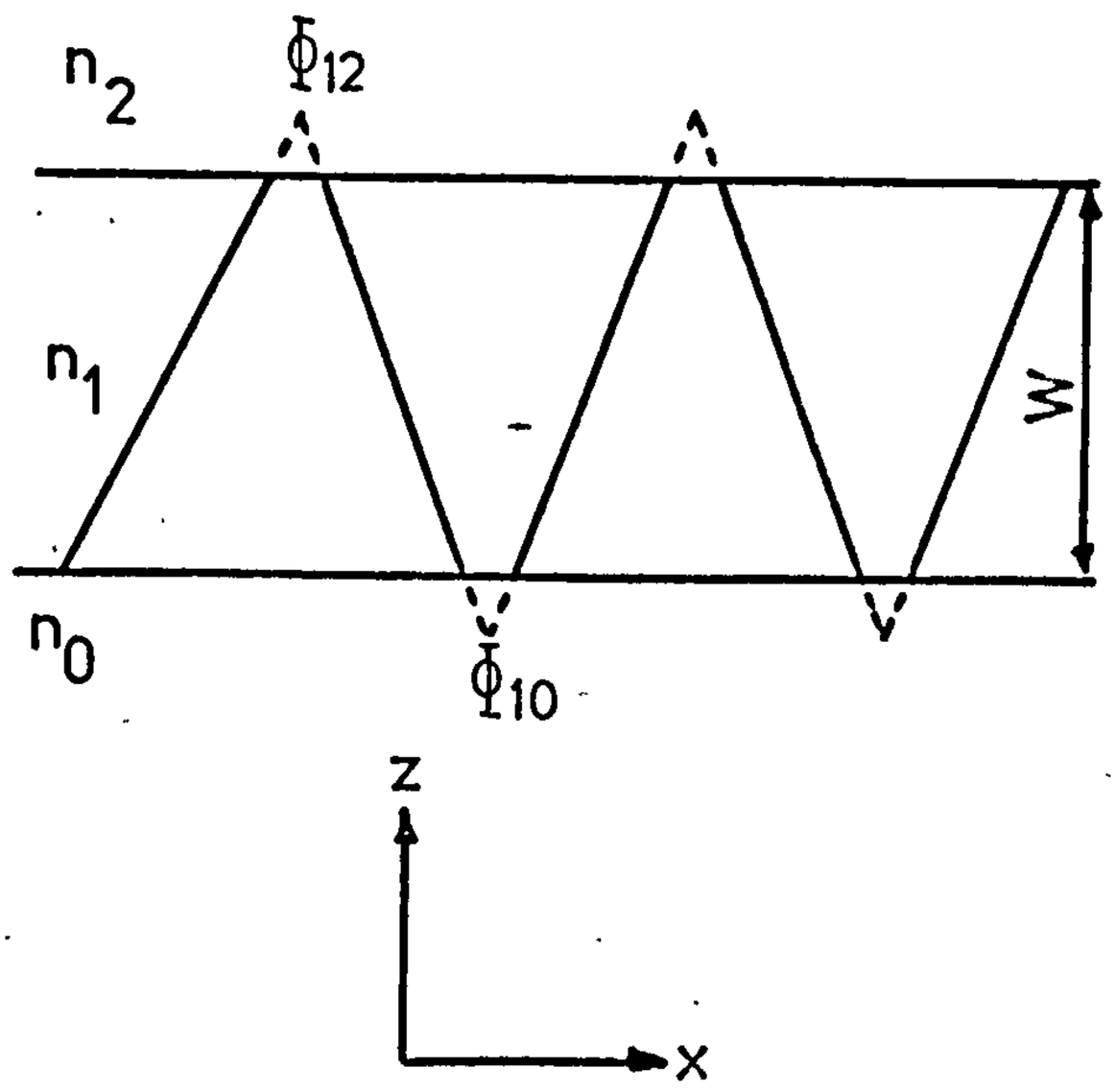

FIGURE 2.3 Phase change on reflection represented by the Goos-Haenchen shift

These above criteria yield the equation

$$2kn_1 W\cos\theta_1 - 2\phi_{10} - 2\phi_{12} = 2m\pi \qquad (2.1)$$

as the condition for guided modes. Where $k = 2\pi/\lambda$, the wave number, ϕ_{10} and ϕ_{12} are the phase changes on reflection and m is an integer = 0, 1, 2 --- , known as the mode number.

For total internal reflection[60]

$$\tan\phi_{12} = (n_1^2\sin^2\theta_1 - n_2^2)^{\frac{1}{2}} / n_1\cos\theta_1 \qquad (2.2)$$

$$\tan\phi_{10} = (n_1^2\sin^2\theta_1 - n_0^2)^{\frac{1}{2}} / n_1\cos\theta_1 \qquad (2.3)$$

for the TE waves, and

$$\tan\phi_{12} = n_1^2(n_1^2\sin^2\theta_1 - n_2^2)^{\frac{1}{2}} / n_2^2 n_1\cos\theta_1 \qquad (2.4)$$

$$\tan\phi_{10} = n_1^2(n_1^2\sin^2\theta_1 - n_0^2)^{\frac{1}{2}} / n_0^2 n_1\cos\theta_1 \qquad (2.5)$$

for the TM waves.

The phase constant β is defined as

$$\beta = kn_1\sin\theta_1 \qquad (2.6)$$

and the wave velocity v as

$$v = c\,(k/\beta) \qquad (2.7)$$

Combining the above equations yields

$$kW(n_1^2-\beta/_k^2)^{\frac{1}{2}} = m\pi + \tan^{-1}\frac{(\beta/_k^2-n_2^2)^{\frac{1}{2}}}{(n_1^2-\beta/_k^2)^{\frac{1}{2}}} + \tan^{-1}\frac{(\beta/_k^2-n_0^2)^{\frac{1}{2}}}{(n_1^2-\beta/_k^2)^{\frac{1}{2}}} \qquad (2.8)$$

for the TE waves, and

$$kW(n_1^2-\beta/_k^2)^{\frac{1}{2}} = m\pi + \tan^{-1}\frac{n_1^2(\beta/_k^2-n_2^2)^{\frac{1}{2}}}{n_2^2(n_1^2-\beta/_k^2)^{\frac{1}{2}}} + \tan^{-1}\frac{n_1^2(\beta/_k^2-n_0^2)^{\frac{1}{2}}}{n_0^2(n_1^2-\beta/_k^2)^{\frac{1}{2}}} \qquad (2.9)$$

for the TM waves.

Equations (2.8) and (2.9) are known as the transcendental equations and are used to predict waveguide propagation in any three layer isotropic, lossless slab waveguide.

Electromagnetic field theory can be used to derive equations (2.8) and (2.9). For a time harmonic field in non-magnetic, isotropic, source free media Maxwell's equations can be expressed as

$$\nabla \times \mathbf{E} = -\mu_o \dot{\mathbf{H}} \tag{2.10a}$$

$$\nabla \times \mathbf{H} = \varepsilon_o n^2 \dot{\mathbf{E}} \tag{2.10b}$$

$$\nabla \cdot \mathbf{E} = 0 \tag{2.10c}$$

$$\nabla \cdot \mathbf{H} = 0 \tag{2.10d}$$

and yield the wave equation

$$\nabla^2 \mathbf{E} = \mu_o \varepsilon_o n^2 \frac{\partial^2 \mathbf{E}}{\partial t^2} \tag{2.11}$$

Applying the appropriate boundary conditions to equation (2.11) the transcendental equations (2.8) and (2.9) can be derived. The TE waves have field components E_y, H_x and H_z and the TM waves have field components H_y, E_x and E_z. Inside the waveguide there is a sinusoidal field variation with m + 1 generally determining the number of field nodes. The field outside the waveguide decays exponentially in the z direction and is called the evanescent field. The proportion of optical power carried in these evanescent fields depends critically on the waveguide thickness and the refractive index discontinuity and is an important consideration when metal boundaries are in close proximity to the waveguide.

Both methods of solution have been outlined as each has advantages in a given situation and both will be utilised further in this thesis.

Equations (2.8) and (2.9) cannot be solved explicity for β, the phase constant, as the right hand side of the equation is a transcendental function of β. However by choosing values of phase constant the guide thickness can be calculated knowing the refractive indices, wavelength of operation and mode number. A computer program was written to plot normalised phase constant ($\beta/_k$) versus guide

thickness (W) for a number of TE and TM modes. The flow diagram is detailed in Appendix A1. Fig. 2.4 shows $\beta/_k$ versus W for an air-CdS- glass substrate system at a wavelength of 1.15 μm. It can be seen that there is a minimum thickness that will support a guided mode known as the cut-off thickness. This occurs when $\beta/_k = n$ where n is the larger surrounding refractive index.

$$W_{\text{cut-off TE}} = \left\{m\pi+\tan^{-1}\left[(n_0^2-n_2^2)^{\frac{1}{2}}/(n_1^2-n_0^2)^{\frac{1}{2}}\right]\right\} / k(n_1^2-n_0^2)^{\frac{1}{2}} \quad (2.12)$$

$$W_{\text{cut-off TM}} = \left\{m\pi+\tan^{-1}\left[n_1^2(n_0^2-n_2^2)^{\frac{1}{2}}/n_2^2(n_1^2-n_0^2)^{\frac{1}{2}}\right]\right\} / k(n_1^2-n_0^2)^{\frac{1}{2}} \quad (2.13)$$

For the air - CdS - glass system the cut-off thickness for the TE_o mode is 0.057 μm. When the surrounding indices are the same the cut-off thicknesses for the TE and TM modes are equal and for the special case of the m = 0 mode there is a guided mode for an infinitely thin film. Under such conditions the evanescent fields penetrate deeply into the surrounding media.

As the waveguide thickness increases the number of possible modes also increases and the β/k of each tends to the guide refractive index for increasing guide thickness. For very wide guides the phase constants of the modes become indistinguishable and plane waves propagate in the guide. In this situation the majority of the light energy is contained within the waveguide.

2.2 PROPAGATION IN OPTICALLY ANISOTROPIC MEDIA

Cadmium sulphide is an anisotropic material and hence the three layer structure of section 2.1 must be modified to take into account the refractive index anisotropy. Fig. 2.5 illustrates a waveguide where the three media are considered anisotropic. The refractive indices n_0, n_1 and n_2 have been replaced by the dielectric tensors $[\varepsilon_1]$, $[\varepsilon_2]$ and $[\varepsilon_3]$ respectively. The most general form of the tensor is

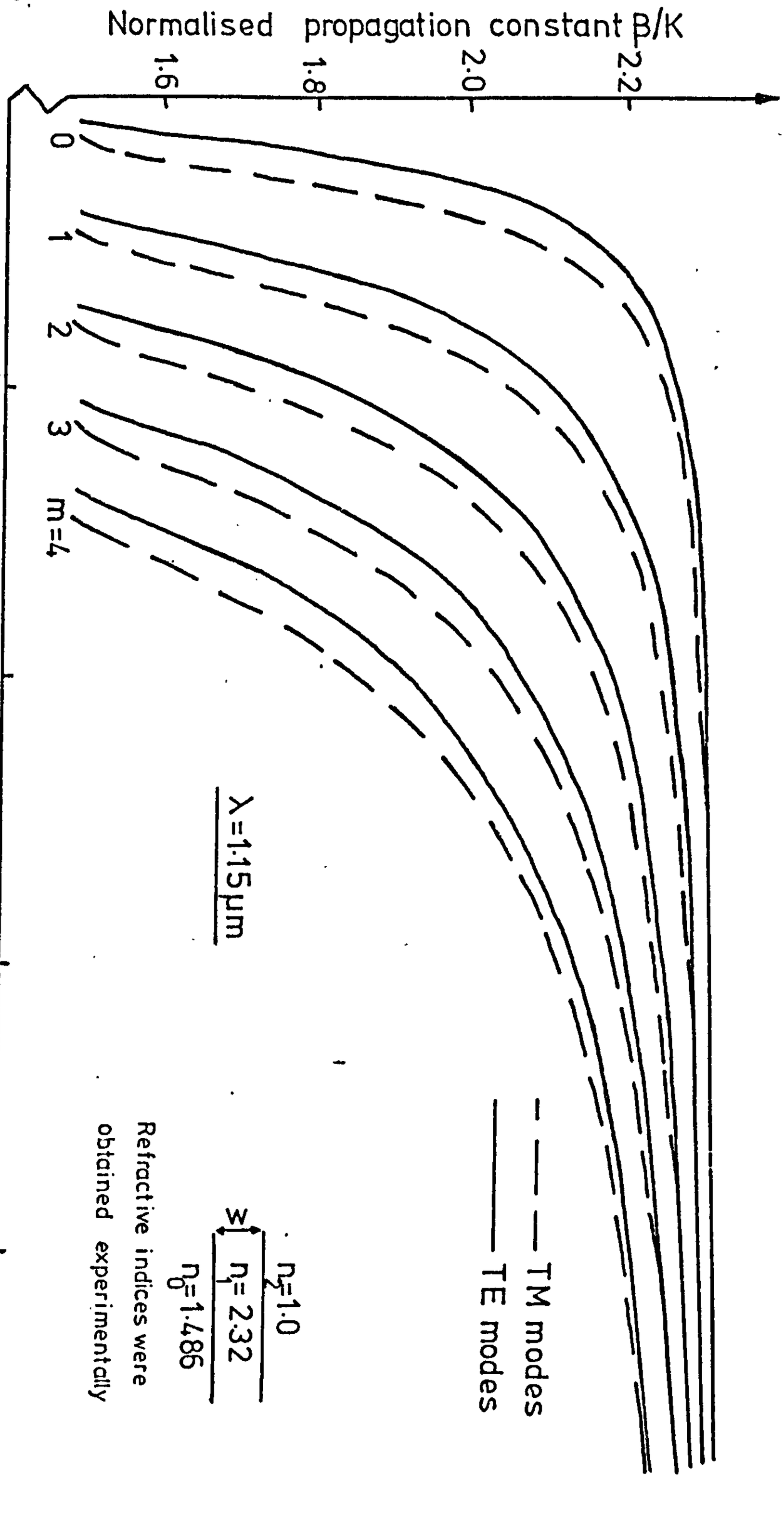

FIGURE 2.4 Normalised propagation constant versus guide thickness

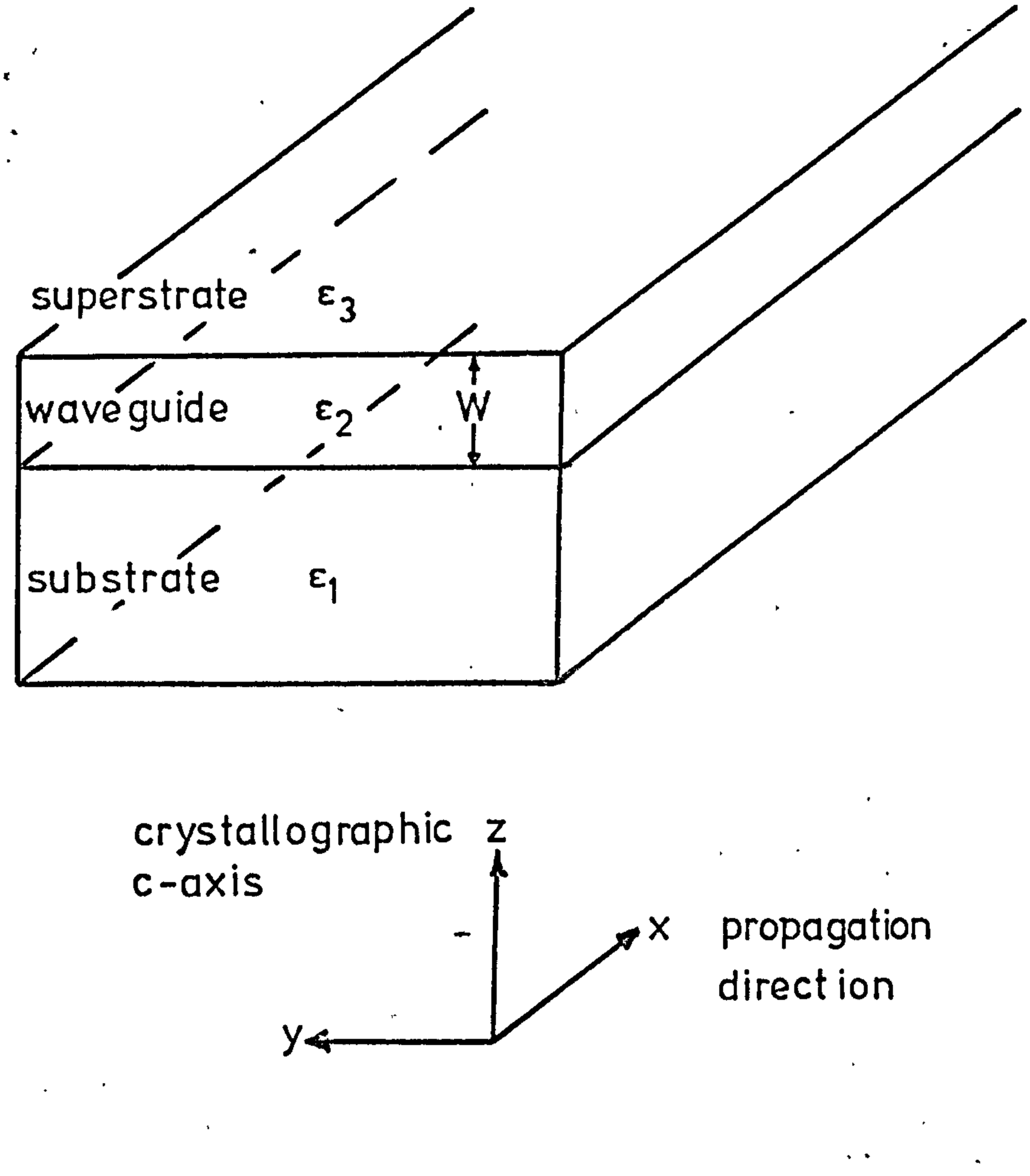

FIGURE 2.5 Planar anisotropic waveguide geometry

$$\left[\varepsilon\right] = \varepsilon_o \begin{bmatrix} k_{xx} & k_{xy} & k_{xz} \\ k_{yx} & k_{yy} & k_{yz} \\ k_{zx} & k_{zy} & k_{zz} \end{bmatrix} \tag{2.14}$$

and solutions of such waveguide systems have been published[62]. However; in order to simplify the model the geometric axes will be considered to be parallel to the crystallographic axes, reducing the off diagonal elements of the tensor to zero[63]. Thus the dielectric tensors $\left[\varepsilon_1\right]$, $\left[\varepsilon_2\right]$ and $\left[\varepsilon_3\right]$ are of the form

$$\left[\varepsilon\right] = \varepsilon_o \begin{bmatrix} k_{xx,} & 0 & 0 \\ 0 & k_{yy} & 0 \\ 0 & 0 & k_{zz} \end{bmatrix} \tag{2.15}$$

The three layer system can be solved readily following an analysis of Yamamoto et al[64] since there is no interaction among independent modes.

Maxwell's equations for a time harmonic field in non-magnetic, source free media

$$\nabla \times \mathbf{E} = -\mu_o \dot{\mathbf{H}} \tag{2.16a}$$

$$\nabla \cdot \mathbf{E} = 0 \tag{2.16b}$$

$$\nabla \times \mathbf{H} = \varepsilon_o \left[k\right] \dot{\mathbf{E}} \tag{2.17a}$$

$$\nabla \cdot \mathbf{H} = 0 \tag{2.17b}$$

yield the wave equation

$$\nabla^2 \mathbf{E} = \mu_o \varepsilon_o \left[k\right] \frac{\partial^2 \mathbf{E}}{\partial t^2} \tag{2.18}$$

Noting that there is no variation along the y coordinate and applying the boundary conditions to equation (2.18) the mode equations for TE and TM modes are derived.

$$kW(k_{2yy}-\beta/_k{}^2)^{\frac{1}{2}} = m\pi + \tan^{-1}\frac{(\beta/_k{}^2-k_{1yy})^{\frac{1}{2}}}{(k_{2yy}-\beta/_k{}^2)^{\frac{1}{2}}} + \tan^{-1}\frac{(\beta/_k{}^2-k_{3yy})^{\frac{1}{2}}}{(k_{2yy}-\beta/_k{}^2)^{\frac{1}{2}}} \qquad (2.19)$$

for TE waves, and

$$kW\left(\frac{k_{2zz}}{k_{2xx}}\right)^{\frac{1}{2}}(k_{2xx}-\beta/_k{}^2)^{\frac{1}{2}} = m\pi + \tan^{-1}\frac{k_{2zz}{}^{\frac{1}{2}}k_{2xx}{}^{\frac{1}{2}}(\beta/_k{}^2-k_{1xx})^{\frac{1}{2}}}{k_{1zz}{}^{\frac{1}{2}}k_{1xx}{}^{\frac{1}{2}}(k_{2xx}-\beta/_k{}^2)^{\frac{1}{2}}}$$

$$+ \tan^{-1}\frac{k_{2zz}{}^{\frac{1}{2}}k_{2xx}{}^{\frac{1}{2}}(\beta/_k{}^2-k_{3xx})^{\frac{1}{2}}}{k_{3zz}{}^{\frac{1}{2}}k_{3xx}{}^{\frac{1}{2}}(k_{2xx}-\beta/_k{}^2)^{\frac{1}{2}}} \qquad (2.20)$$

for TM waves.

2.3 WAVEGUIDE PROPAGATION IN THE CASE OF CADMIUM SULPHIDE

Cadmium sulphide is a positive uniaxial material; with $k_{xx} = k_{yy} = n_o^2$ and $k_{zz} = n_e^2$ where n_o and n_e are the ordinary and extra-ordinary refractive indices respectively. The superstrate and substrate are taken to be isotropic and when these conditions are substituted into equations (2.19) and (2.20) the following equations result;

$$kW(n_{1o}^2-\beta/_k{}^2)^{\frac{1}{2}} = m\pi + \tan^{-1}\frac{(\beta/_k{}^2-n_2^2)^{\frac{1}{2}}}{(n_{1o}^2-\beta/_k{}^2)^{\frac{1}{2}}} + \tan^{-1}\frac{(\beta/_k{}^2-n_0^2)^{\frac{1}{2}}}{(n_{1o}^2-\beta/_k{}^2)^{\frac{1}{2}}} \qquad (2.21)$$

for TE waves, and

$$kW\left(\frac{n_{1e}}{n_{1o}}\right)(n_{1o}^2-\beta/_k{}^2)^{\frac{1}{2}} = m\pi + \tan^{-1}\frac{n_{1o}n_{1e}}{n_2^2}\frac{(\beta/_k{}^2-n_2^2)^{\frac{1}{2}}}{(n_{1o}^2-\beta/_k{}^2)^{\frac{1}{2}}}$$

$$+ \tan^{-1}\frac{n_{1o}n_{1e}}{n_0^2}\frac{(\beta/_k{}^2-n_0^2)^{\frac{1}{2}}}{(n_{1o}^2-\beta/_k{}^2)^{\frac{1}{2}}} \qquad (2.22)$$

for TM waves, where n_{1o} and n_{1e} are the waveguide ordinary and extra-ordinary refractive indices respectively.

Equation (2.21) is identical to the mode equation (2.8) derived for isotropic media and verifies that a TE mode will always be formed by an ordinary ray whatever the value of β for the chosen

geometry of Fig. 2.5.

Let the birefringence of a crystal B be defined as

$$B = n_e - n_o \tag{2.23}$$

Substituting (2.23) in (2.22) for n_{1e} yields

$$kW\left(1+\frac{B}{n_{1o}}\right)\left(n_{1o}^2-\beta/_k{}^2\right) = m\pi + \tan^{-1}\frac{n_{1o}^2}{n_2^2}\left(1+\frac{B}{n_{1o}}\right)\frac{\left(\beta/_k{}^2-n_2^2\right)^{\frac{1}{2}}}{\left(n_{1o}^2-\beta/_k{}^2\right)^{\frac{1}{2}}} \tag{2.24}$$

$$+ \tan^{-1}\frac{n_{1o}^2}{n_0^2}\left(1+\frac{B}{n_{1o}}\right)\frac{\left(\beta/_k{}^2-n_0^2\right)^{\frac{1}{2}}}{\left(n_{1o}^2-\beta/_k{}^2\right)^{\frac{1}{2}}}$$

The similarity between equation (2.24) and the mode equation (2.9) is marked. The only difference between the isotropic and anisotropic cases is a factor $\left(1 + \frac{B}{n_{1o}}\right)$ in every term of the TM mode equation for an anisotropic film of cadmium sulphide.

The birefringence of cadmium sulphide is small (B = 0.01) and since n_o is equal to 2.32 the percentage change in each term of equation (2.24) is 0.43%. Fig. 2.6 shows a plot of $\Delta\beta/_k$ versus the birefringence B for an air - CdS - glass system for the TM_o mode of a 1 μm thick cadmium sulphide waveguide which calculated the change in normalised propagation constant from the isotropic value for varying amounts of birefringence. The difference in $\beta/_k$ can be seen to be extremely small and for all further waveguide analyses, cadmium sulphide will be considered to be isotropic.

2.4 BEAM COUPLING TO THIN FIIM WAVEGUIDES

There are many methods of efficiently coupling free space propagating light into a mode of a thin film waveguide. These include edge focussing,[66] tapered film coupling,[67] holographic coupling,[68] grating coupling[69] and prism coupling[4]. All have been the subject of extensive theoretical and experimental studies and only a brief description of the latter two will be given since they form an integral

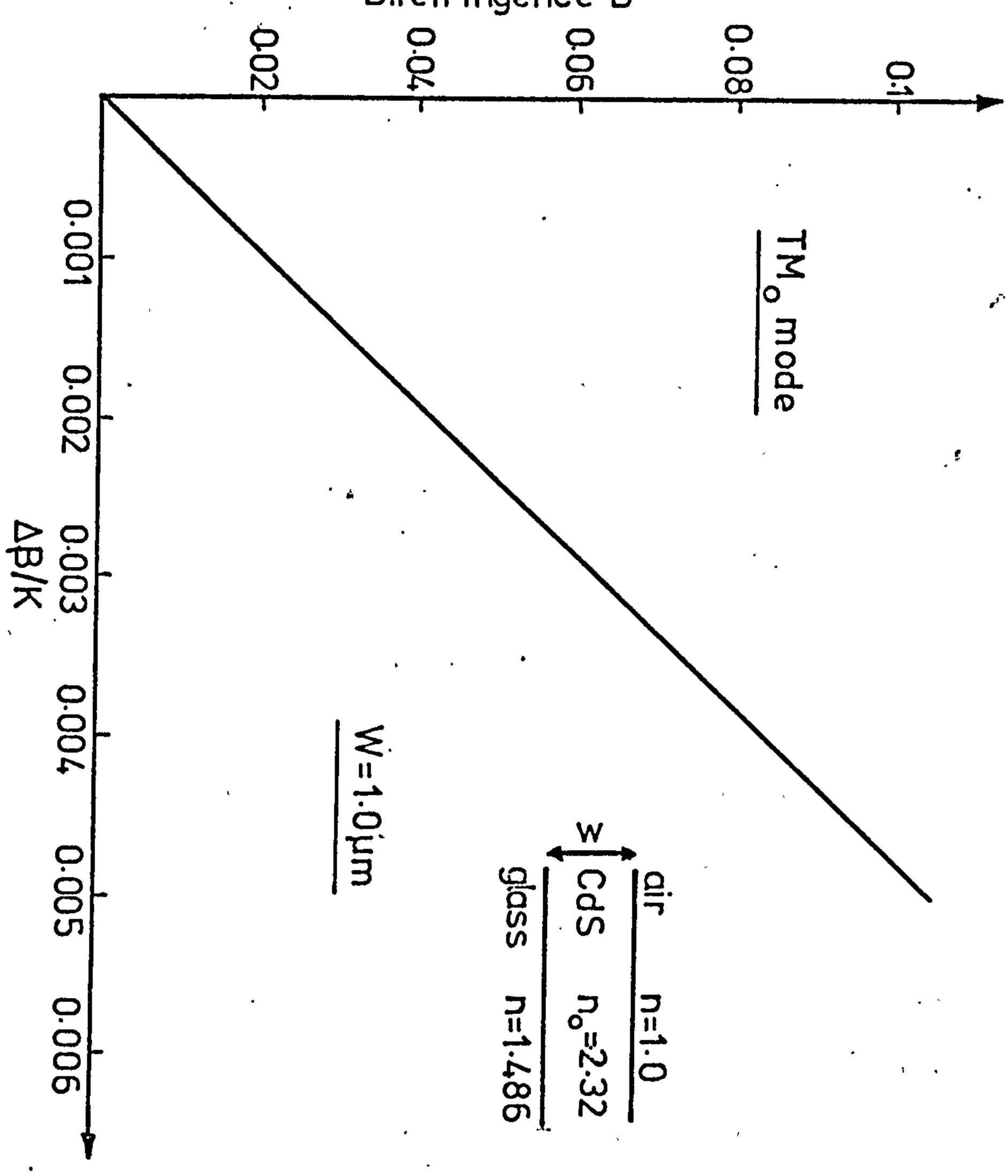

FIGURE 2·6 Graph illustrating effect of birefringence on the propagation constant of the TM_o mode

part of the experiments described in later chapters. Both methods allow the efficient excitation of discrete modes in a multimode waveguide.

2.4.1 THE GRATING COUPLER

This type of coupler is produced by forming a thin phase grating (usually in photoresist) on top of the waveguide (Fig. 2.7a) or by etching a pattern directly into the waveguide or substrate (Fig. 2.7b). One of the diffraction orders of the grating is used to couple light into the waveguide mode by adjusting the angle of the incoming beam such that the diffracted beam has the same phase velocity along the film direction as the guided mode. Such couplers have typical input efficiencies of $\sim 40\%$ [69] although an efficiency of 70% has been reported.[70]

Grating couplers have the advantage of compactness, rigidity and compatability with a planar thin film technology. Photoresist gratings are inefficient on cadmium sulphide due to the large refractive index difference between the two materials resulting in a small perturbation. The gratings were consequently ion etched into the substrate to improve the coupling efficiency. However, because of the processing involved in preparing the gratings, prism couplers were used extensively in most experiments.

2.4.2 THE PRISM COUPLER

Prism couplers enable accurate calculation of mode propagation constants, the launching of light at any chosen point on the film and have a theoretical maximum input efficiency of 81% [7].

In this type of coupler, coupling takes place through the surface of the film. The evanescent field associated with the total internal reflection of light at the boundary between the prism base and the air gap allows the light to "tunnel" into the waveguide

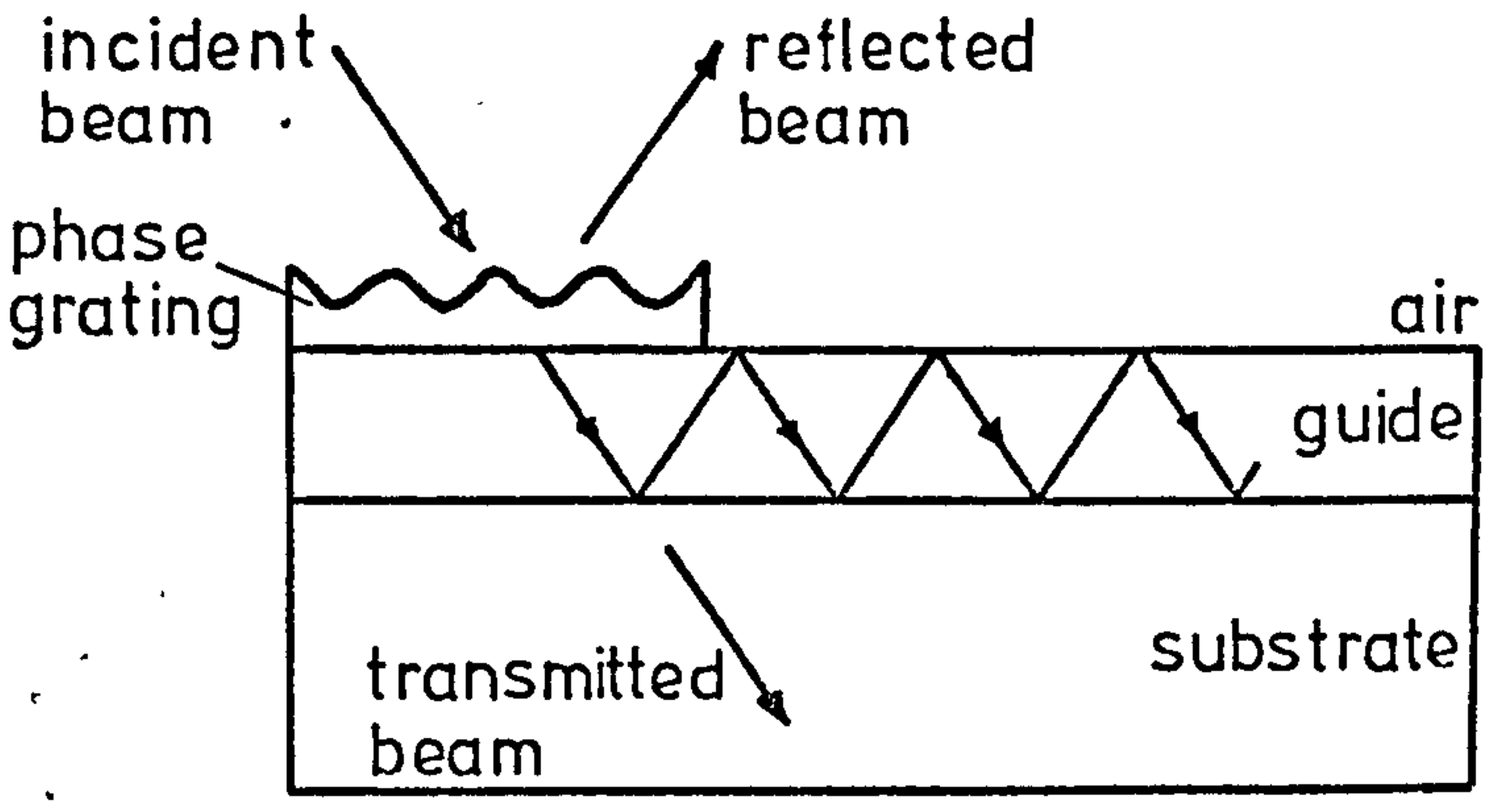

(a) Thin film grating coupler

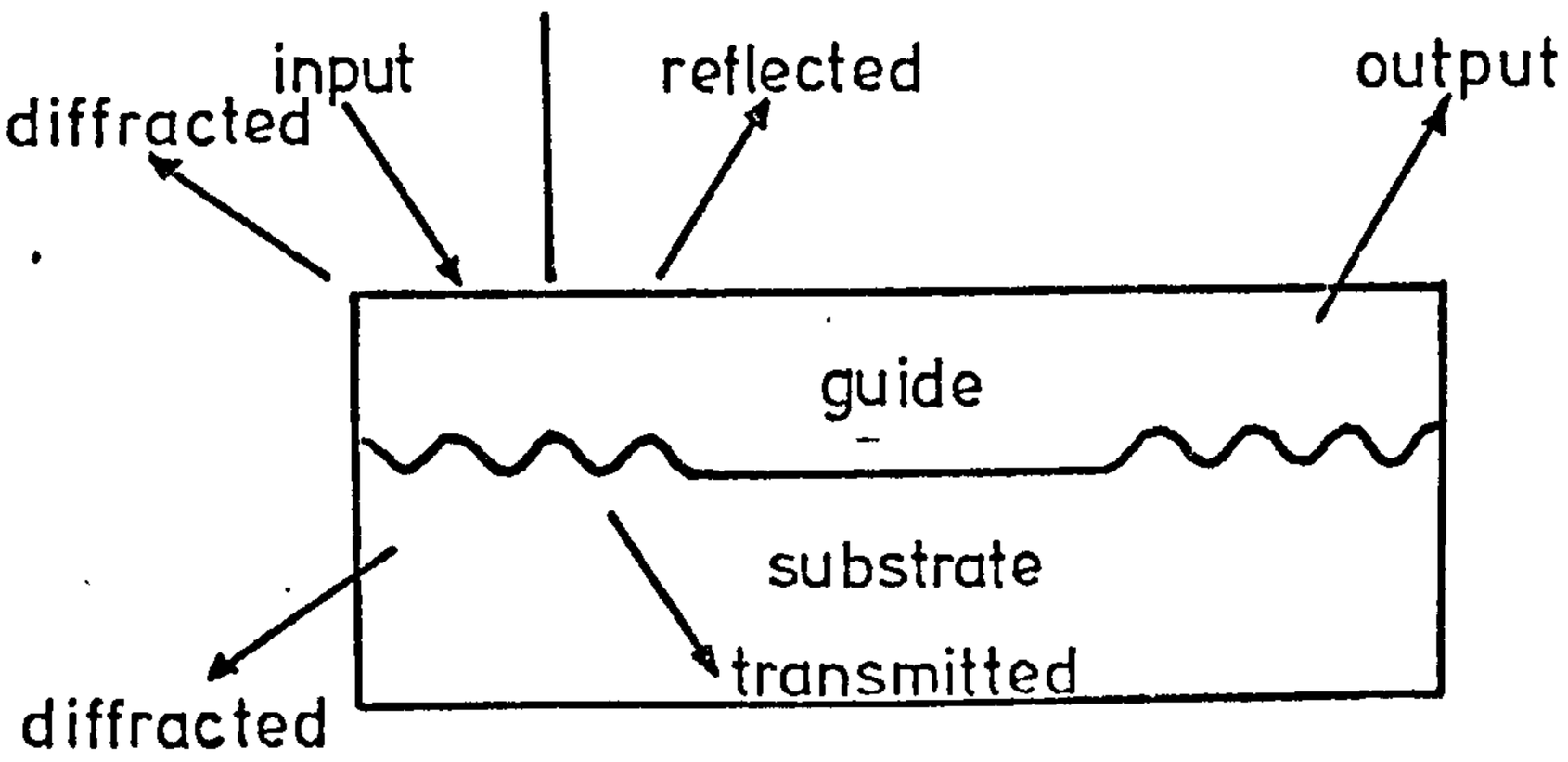

(b) Etched grating coupler

FIGURE 2·7 Phase grating couplers

(Fig. 2.8). Coupling proceeds to a guided mode when the angle of incidence on the lower prism face is such that the evanescent field in the gap region travels with the same phase velocity along the film direction as the guided mode. As the coupler is reciprocal to prevent the light leaking back out of the waveguide the prism is truncated after the maximum light energy has been transferred to the film.

The propagation constants of the modes can be obtained by measuring the synchronous coupling angles for the modes. The measurement of two or more mode angles permits the film refractive index and thickness to be calculated from the mode equation provided the surrounding indices and wavelength of operation are known. A numerical method is used to solve the equations and the flow diagram for the computer program is given in Appendix A2. This method was used to evaluate most of the films grown.

The prism coupler used for launching light into the cadmium sulphide thin films was made from rutile. This is a highly birefringent material[71] and was cut with the crystal axes as shown in Fig. 2.8 to allow a constant prism refractive index for both TE and TM modes. The TE mode has its E-field parallel to the c-axis and is hence subject to extraordinary refractive index while the TM mode E-field vectors rotate through the ordinary refractive index plane.

The large birefringence of rutile enables the design of a coupler which will launch equal powers in both a TE and a TM mode by using the birefringence to compensate for $\beta_{TE} > \beta_{TM}$ in a given waveguide structure. Such a prism could be useful, for instance, to excite TE and TM modes in an amplitude modulating structure. The design of the prism is described in detail in Appendix B.

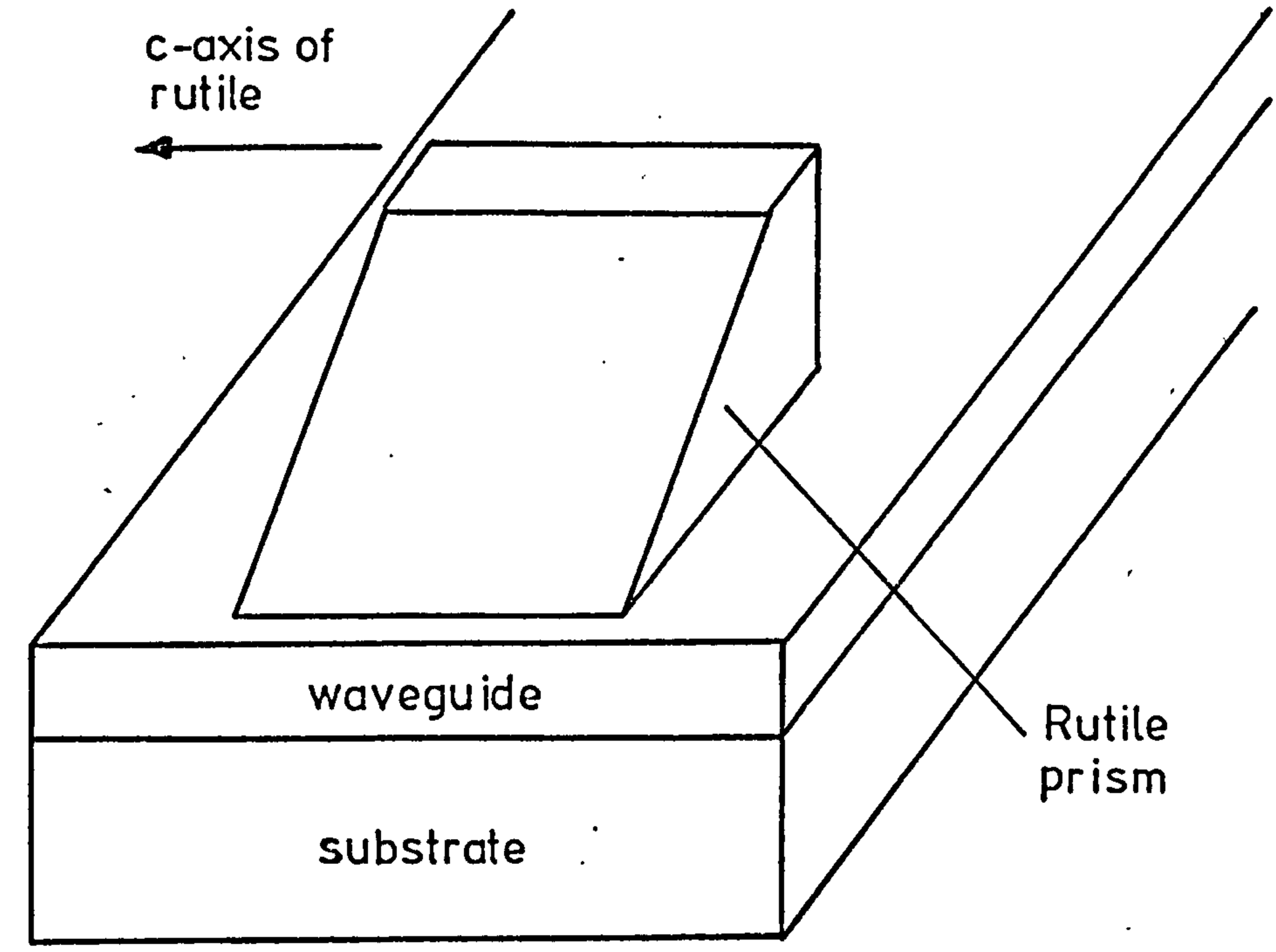

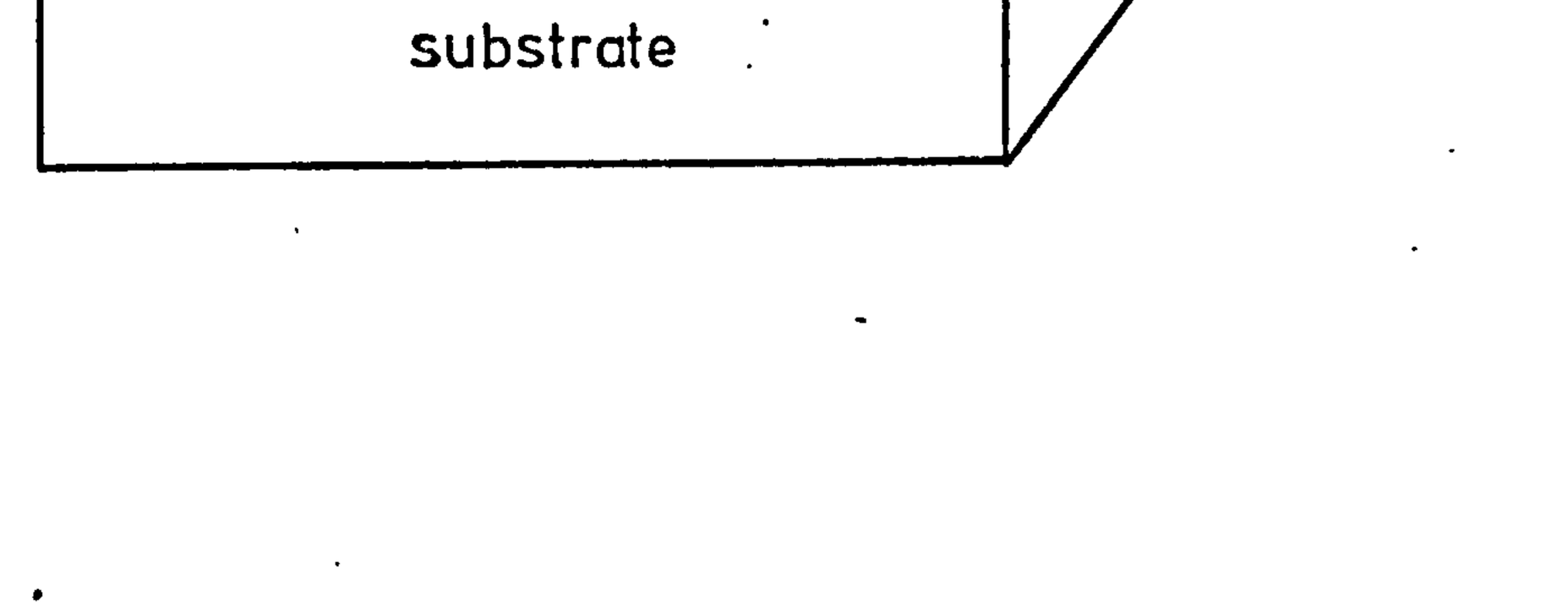

FIGURE 2·8 Prism-film coupler

CHAPTER 3: GROWTH OF EVAPORATED CADMIUM SULPHIDE THIN FILMS

Cadmium sulphide thin films have been the subject of a great deal of research over many years. Apart from sputtering of the compound cadmium sulphide[72], evaporation of either the elements cadmium and sulphur, compound cadmium sulphide or a combination of both have been amongst the most frequently used deposition techniques. However, deposition procedures have varied considerably causing wide fluctuations in the reported properties of the thin films. This tends to indicate that the physical properties of cadmium sulphide thin films are very dependent on their method of preparation and post evaporation treatments. The film quality depends not only on the vapour pressures, substrate temperature and impurity concentration of the charge but also on the evaporation rates, vapour composition, source temperature and nature of the substrate and surface morphology.

Previous work has always involved optimising the evaporation conditions to produce the best electrical, optical or structural property of the cadmium sulphide thin film[73]. This research differs in that the optical property (the waveguide loss) which is being optimised has not previously been considered. However, this parameter was related to optimizing some of the more common thin film parameters namely the structure and stoichiometry. The films were mainly grown on amorphous, inert (no chemical reactivity with the incident vapour) substrates as these were to form the basis of subsequent devices. The film were thus polycrystalline although some films of cadmium sulphide were deposited on single crystal substrates.

A theoretical and experimental study of source temperature, impinging vapour rates, composition of vapours, reaction processes and nucleation was not considered to be within the scope of this research. The underlying principles involved are however of paramount importance in obtaining an understanding of how the properties of thin films respond to changes in their structure and composition

as well as being essential to the control of their characteristics. Consequently, the first part of this chapter deals broadly with the principles involved in cadmium sulphide evaporation kinetics, nucleation and film growth and is drawn extensively from published work. The deposition equipment is then outlined and finally the deposition procedure and conditions are described.

3.1 MODEL OF CADMIUM SULPHIDE EVAPORATION

3.1.1 KINETICS OF CADMIUM SULPHIDE EVAPORATION

Thermal evaporation of compound cadmium sulphide in vacuum is a common technique used to deposit cadmium sulphide thin films and can be performed where there is either an equilibrium between the vapour and solid or where there is a non equilibrium. The latter condition is the one that normally prevails during vacuum evaporation.

Cadmium sulphide is known to dissociate upon evaporation into a vapour composed predominantly of cadmium atoms and sulphur (S_2) molecules together with smaller amounts of the heavier species of sulphur[74]. In general this vaporization will occur through a series of reaction steps one of which will be the rate determing step depending on the condition of the reaction. There have been many studies to determine the reaction steps[75] and the rate determining step[76] and many different processes have been discovered. To obtain the same evaporation rate it is thus essential to have the same processes occurring in each evaporation. Not only should the inputs to the evaporator be kept constant to maintain a constant source temperature but also the composition of the charge must be identical to maintain the same reaction steps.

The condensation of a single component or elemental vapour onto a solid surface is a function of complex adsorption, surface diffusion and nucleation phenomena[77]. When the vapour consists of two components the interaction between the two components as well as

their condensation and reevaporation must be taken into consideration. No comprehensive description of the mechanism of cadmium sulphide condensation has been published although a few experimental studies have been concerned with the kinetics of condensation[77]. During condensation the following events are considered to occur. The impinging atom or molecule is attracted to the surface of the substrate by some force (eg Van der Waals forces) and as a result loses its velocity component normal to the surface provided the kinetic energy is not too large. The vapour atom is then physically adsorbed and will move across the surface until it either interacts with other adsorbed atoms to form a stable nucleus (chemically absorbed) or it reevaporates or desorbs into the vapour phase. Condensation is thus an equilibrium between adsorption and desorption processes.

The two coefficients normally used to describe the properties of impinging atoms are the accommodation and sticking coefficients. The sticking or condensation coefficient is defined as the probability of an impinging particle being adsorbed, thermally equilibrated and incorporated into the surface. The accommodation coefficient is used to describe the degree of thermal equilibrium of the substrate surface particles incident onto and subsequently ejected from it (it is an indication of the amount of energy interchange between the substrate). These coefficients are controlled by the type of substrate employed, substrate temperature and the impinging rate and composition of the vapour. The latter condition is set by the source (evaporator) conditions and thus the substrate temperature becomes the single most important parameter governing the thin film stoichiometry. A theoretical and experimental analysis of binary vapours reported by Gunther[78] is based on an extension of the well established theory for a single component vapour. He demonstrates that for compounds with

a lower vapour pressure than either of the single components (as is the case with cadmium sulphide) accurate control of the substrate temperature is the single most important criterion for depositing exactly stoichiometric layers of the compound. Provided the incident vapour rates are sufficiently large then for a substrate temperature at which the sticking coefficients of the single components are zero stoichiometry is possible.

The vapour-substrate-nuclei reaction at the substrate surface is illustrated in Fig. 3.1. The components of the vapour are considered to be absorbed onto the surface and to undergo an equilibrium reaction between formation of compound cadmium sulphide, complexes of cadmium and sulphur, and free cadmium and sulphur which can be desorbed. Adjustment of the vapour rates and composition and the substrate temperature shift the equilibrium position of this reaction and can lead to the deposition of stoichiometric films of cadmium sulphide.

3.1.2 GROWTH AND CRYSTALLINITY OF CADMIUM SULPHIDE FILMS

Many of the important physical properties of cadmium sulphide films are sensitive to the method of deposition and the processing techniques. The microstructure including crystallographic phases, crystallite size and orientation, and surface features such as roughness and uniformity depend on factors including substrate temperature, deposition rate and angle, and ambient pressure. These variations influence the electrical and optical properties and cause non-bulk behaviour.

The absorbed atoms react with each other to form nuclei and this is known as the nucleation stage in film growth. The nuclei will grow or decay until a certain critical size is reached beyond which they will no longer decay.[79] The growth stage then occurs when the nuclei agglomerate into small islands which eventually join up to form a continuous deposit and finally a complete film. As

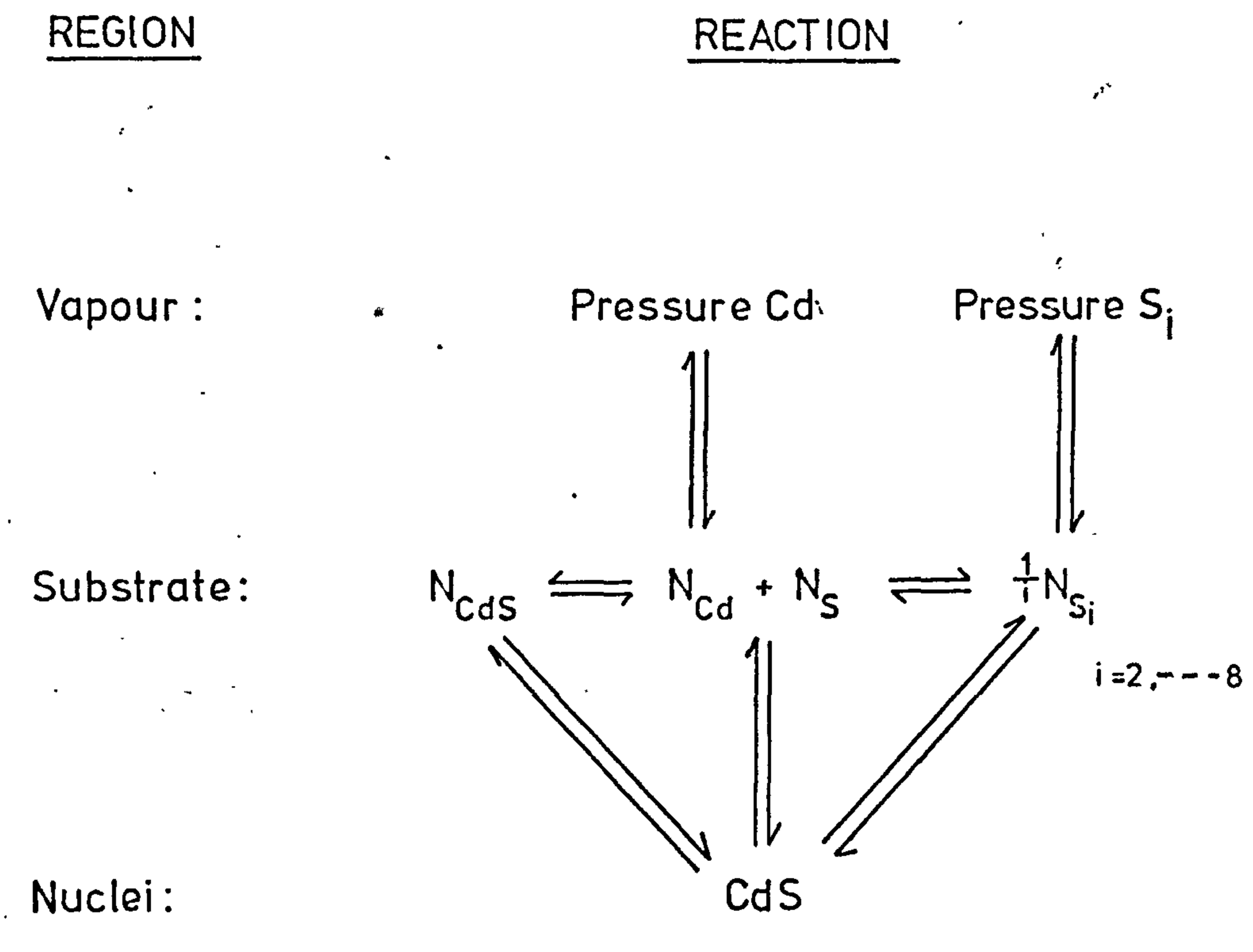

FIGURE 3.1 Schematic representation of the condensation process for CdS films

the islands grow in size they orientate themselves to achieve an equilibrium shape but once large islands form they cannot change shape rapidly enough before further growth occurs and thus necks are produced between the islands[80]. Grain boundaries occur in the necks of differently oriented crystallites and the size of the islands at this critical stage in the growth governs the grain size. The larger the grain size the better will be the thin film structure and the lower the optical scatter loss. Thus it is important to achieve growth conditions which will produce large grains. The deposition parameters affect the agglomeration rate through the sticking coefficients and absorbed particle mobility; thus a larger grain size will be obtained if the growth rate is slow[81].

For films evaporated onto inert amorphous substrates the important crystallographic considerations are the grain or crystallite size and the orientation of the film. The grain size is affected by the growth rate, substrate temperature, vapour velocity parallel to the surface, inertness and smoothness of the surface and finally deposition angle. For large grain size, therefore, a high substrate temperature appears desirable. However high substrate temperatures tend to inhibit growth as do absorbed impurities and residual gases owing to the reduction in sticking coefficient and the low rate of surface diffusion. There should thus exist an optimum substrate temperature for the best film structure.

Polycrystalline films of cadmium sulphide have crystallographic order in the c-axis direction; this is known as fibre axis texture or preferred orientation. Fibre texture may develop at any stage of the deposition and is strongly dependent on deposition parameters[56]; substrate temperature, deposition rate and angle, type and surface structure of substrate, although the latter may not influence the final stages of growth. Fibre texture arises because

of the differing growth rates of the various crystallite orientations at a given time[82]. Since initial crystallites usually have an equilibrium form, preferred orientation is possible on amorphous surfaces. When preferred orientation occurs the texture axis is commonly inclined towards the direction of incidence of the vapour stream[56]. Most common crystal defects can occur in cadmium sulphide thin films either by an extension of substrate imperfections into the crystal structure or when the islands are coalescing during the nucleation-growth phase.

Cadmium sulphide films predominantly have a wurtzite structure but the zinc blend structure has also been detected[83,84]. Films deposited on amorphous substrates usually exhibit a degree of preferred orientation with the c-axes of the crystallites normal to the substrate surface in the initial layers arising from the nucleation conditions. As the film thickness increases the growth conditions determine the preferred orientation and the c-axes tend to align themselves in the direction of the incident vapour stream.

3.2 DEPOSITION EQUIPMENT

3.2.1 VACUUM SYSTEM

A schematic diagram of the vacuum system assembled for the evaporation of cadmium sulphide is shown in Fig. 3.2. It maintained a working vacuum between 5×10^{-8} and 10^{-7} Torr during cadmium sulphide deposition and had an ultimate vacuum pressure of 10^{-9} Torr, produced by a combination of ion and titanium sublimation pumping. The rotary pump was connected through a molecular sieve trap to prevent oil migration from the pump contaminating the vacuum chamber. The whole system was baked to $100^{o}C$ before each evacuation of the chamber to remove the water vapour and achieve the ultimate vacuum of 10^{-9} Torr

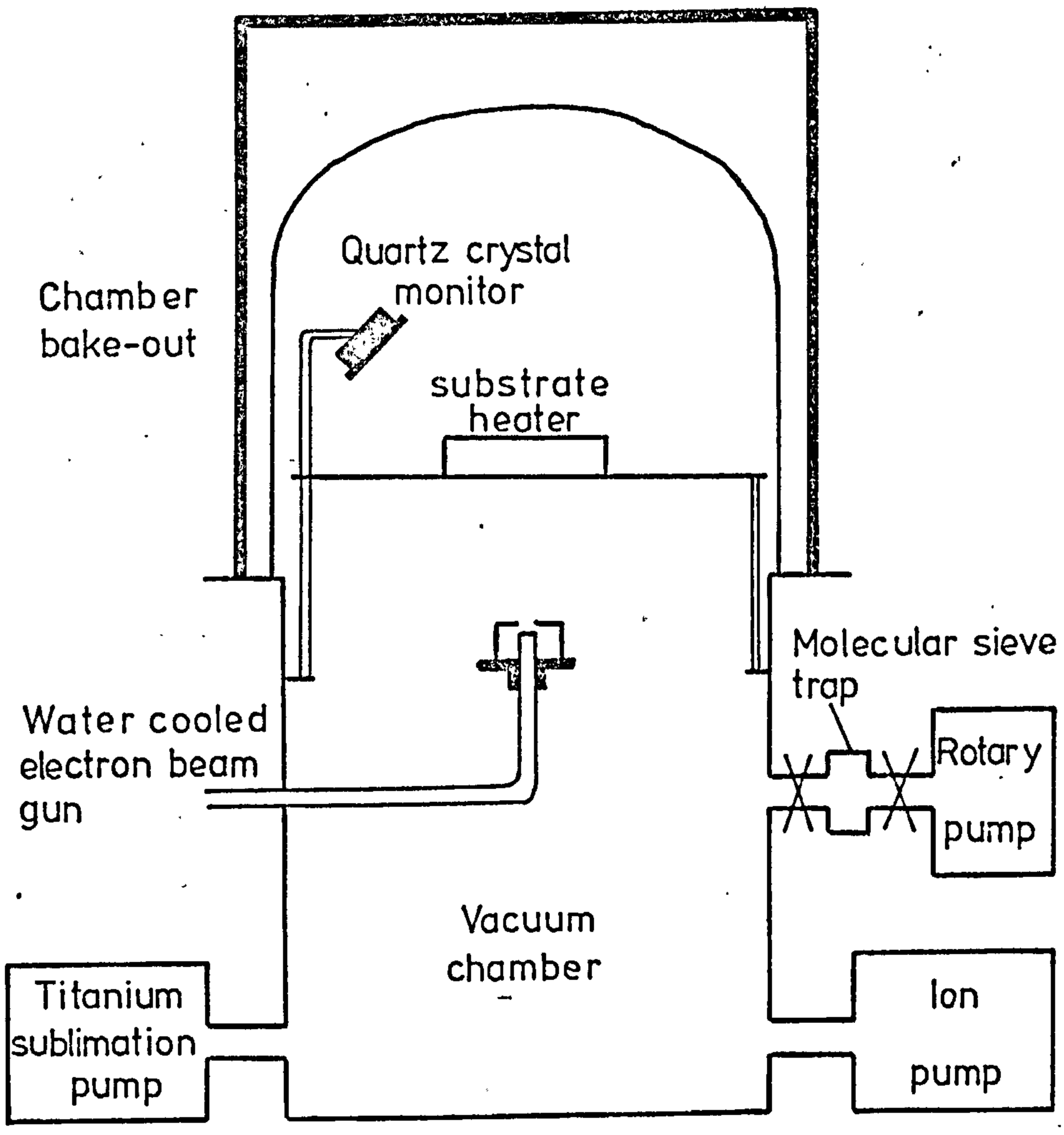

FIGURE 3.2 Schematic diagram of CdS evaporation apparatus

The electrical pumping system is inherently much slower than a conventional diffusicn pumped vacuum system but the reduced level of hydrocarbon contamination and the lower background level of other residual gases outweighed this disadvantage. This level of cleanliness was considered essential to producing consistent results.

3.2.2 EVAPORATION CHAMBER

A schematic diagram of the evaporation chamber is shown in Fig. 3.2. The evaporation of compound cadmium sulphide was carried out using an electron gun evaporator, type EG2 (Vacuum Generators), with a maximum rating of 2kW. The beam was electrostatically focussed onto the source to give a beam diameter of approximately 1mm. The cadmium sulphide charge was contained in a water cooled copper hearth. Electron beam evaporation was chosen as a convenient means of depositing cadmium sulphide with out risk of contamination from the evaporator.

The substrate heater, a stainless steel block with radiant heaters, was placed in a direct line of sight to the source and normal to the impinging vapour stream in order to induce c-axis growth of the crystallites normal to the plane of the substrate. The temperature was controlled to $\pm$ 1^{o}C by means of a proportional controller with a temperature gradient along a three inch glass substrate of less than 1^{o}C. The substrate temperature was monitored by a platinum resistance thermometer located in the stainless steel block in order that temperature measurements were always made from the same position. This temperature, which will be called the substrate temperature, was between 0^{o} and 30^{o}C higher than the front face of the substrate.

The growth rate was estimated using a quartz crystal thickness monitor (Edwards Speedivac Model 1) which was also used to calculate the film thickness.

All the evaporation chamber fittings were cleaned regularly to prevent excessive outgasing from previous cadmium sulphide deposits.

3.3 DEPOSITION PROCEDURE AND CONDITIONS

The properties of an evaporated cadmium sulphide film depend critically on the deposition procedure and conditions. It is thus important to outline how the various parameters were controlled during an evaporation such that reliable and reproducible films could be fabricated. The various parameters that could be controlled were substrate temperature, source-substrate distance, rate of evaporation, source material, substrate material, ultimate pressure and ambient pressure during evaporation. The latter two were dealt with in section 3.2 amd the rest will be considered below.

The parameters were controlled by setting the evaporator variables and finally the substrate conditions since there is an interrelation of parameters when a cadmium sulphide film is grown from the compound. Two different cadmium sulphide starting materials were used and required quite different growth conditions (see chapter 4). The material was, however, always used in a fine powder form and packed into the hearth in the same manner (for the same input conditions to the electron beam gun a lower growth rate was observed for crystalline lumps). The minimum power attainable from the electron beam power supply was 8 watts and during evaporations it was always maintained at that level to produce the slowest evaporation rate. The source-substrate distance was set to a height of 2" which permitted a reasonable film uniformity over a 1.5" diameter region of the substrate. With the above variables held constant the substrate temperature was used to adjust the condensation and reevaporation rates of the vapour components to produce the optimum film structure.

To produce a thin film suitable for experimental investigations considerable care had tc be exercised in the predeposition treatment of the substratcs. The cleanliness of the substrate surface was of paramount importance because of the marked influence it had on the final physical and adhesive properties of the deposited films. It

was necessary to outgas the substrate and the substrate heater at 100°C during the bake-out stage in order that the ultimate vacuum may still be attained when the substrate is at a temperature of greater than 200°C. In the interests of film adhesion it was found advisable to allow the substrate to cool to below 60°C before removing it from the vacuum chamber.

CHAPTER 4: CADMIUM SULPHIDE THIN FILM CHARACTERIZATION

Cadmium sulphide had not previously nor has subsequently been used by other research workers as a material for thin film dielectric waveguides. The rationale for this work is the ease with which cadmium sulphide can be vacuum evaporated and the preferential c-axis orientation of the films when grown onto most substrates be they amorphous, polycrystalline or single crystal. These properties are of fundamental importance when the device structures discussed in chapters 6, 7 and 8 are considered.

Cadmium sulphide is a group II-VI semiconductor compound and some of its basic properties are listed in Table 4.1. It has a band gap of 2.42eV, exhibits a small birefringence of 0.01 and possesses the hexagonal wurtzite structure with the c-axis orientated perpendicular to the plane of the film. It shows good transmission properties in the range 1-14 microns[85] and hence is most useful as an infrared material.

The films of cadmium sulphide were evaporated from two different starting materials (high purity single crystal cadmium sulphide grown by Eagle Picher and "Optran Grade" polycrystalline lump produced by B.D.H.) using the apparatus described in chapter 3. Substrates of different materials were used and a variety of evaporation conditions employed.

The results of analytical techniques other than waveguide analysis are described in section 4.1 for amorphous substrates of glass and fused silica. Section 4.2 describes the waveguide evaluation while films grown on single crystal substrates of spinel are considered in section 4.3. Subsequent modifications to the growth conditions are described in section 4.4 and section 4.5 concludes with a discussion of the factors which contribute to waveguide loss.

Molecular weight		144.48
Refractive index -	ordinary	2.32 (λ=1.15 μm)
	extraordinary	2.336
Transmission limits -	long wavelength	16 μm
	short wavelength	0.52 μm
Thermal conductivity		3.8×10^{-2} cal.cm^{-1}sec^{-1}°C^{-1}
Thermal expansion		4.2×10^{-6} °C^{-1}
Band gap		2.42 eV
Lattice spacing		4.137Å
Hall mobility -	electrons	300 cm^{2}v^{-1}sec^{-1}
	holes	50 cm^{2}v^{-1}sec^{-1}
Effective mass ratio -	electrons	0.17
	holes	0.6

TABLE 4.1 Some basic properties of CdS

4.1 ANALYTICAL TECHNIQUES

The aim of the subsequent analyses was to provide information which would enable thin films of cadmium sulphide with the lowest possible propagation loss to be produced and to understand the reasons for any remaining attenuation. Film appearance is the first obvious indication of film quality and Fig. 4.1 shows the dramatic change in film stoichiometry caused by varying the substrate temperature. The dark brown films indicate an excess of cadmium and as the substrate temperature is increased a 1:1 cadmium: sulphur ratio is established. Raising the substrate temperature still further leads to sulphur rich films which are characterized by the cloudy appearance.

A number of other basic thin film properties were measured and are discussed in the following subsections.

4.1.1 BAND EDGE

Band edge measurements were carried out to gain an understanding of the transmission properties of the thin films in the wavelength region to be considered for optical waveguiding. Two conventional spectrometers were used to cover the wavelength range from 0.35 microns to 2.5 microns. Films were grown for a range of substrate temperatures, (20^{o}-300^{o}C) and growth rates (1000-3000 $\text{Å}\,\text{min}^{-1}$). Both the single crystal and polycrystalline starting materials were used. The amorphous glass substrates used throughout this analysis transmitted into the near ultra-violet and therefore did not interfere with the band edge measurements. The film thicknesses varied for each evaporation, although similar input conditions to the electron beam gun were used, due to the variation in substrate temperature. This thickness variation was taken into consideration when comparing the results.

Fig. 4.2 illustrates plots of band edge versus substrate temperature for different growth rates and both starting materials.

Substrate temperature (°C)
23
94
136
147
160
173
193
258

FIGURE 4.1 Cadmium sulphide thin films grown from Eagle Picher material

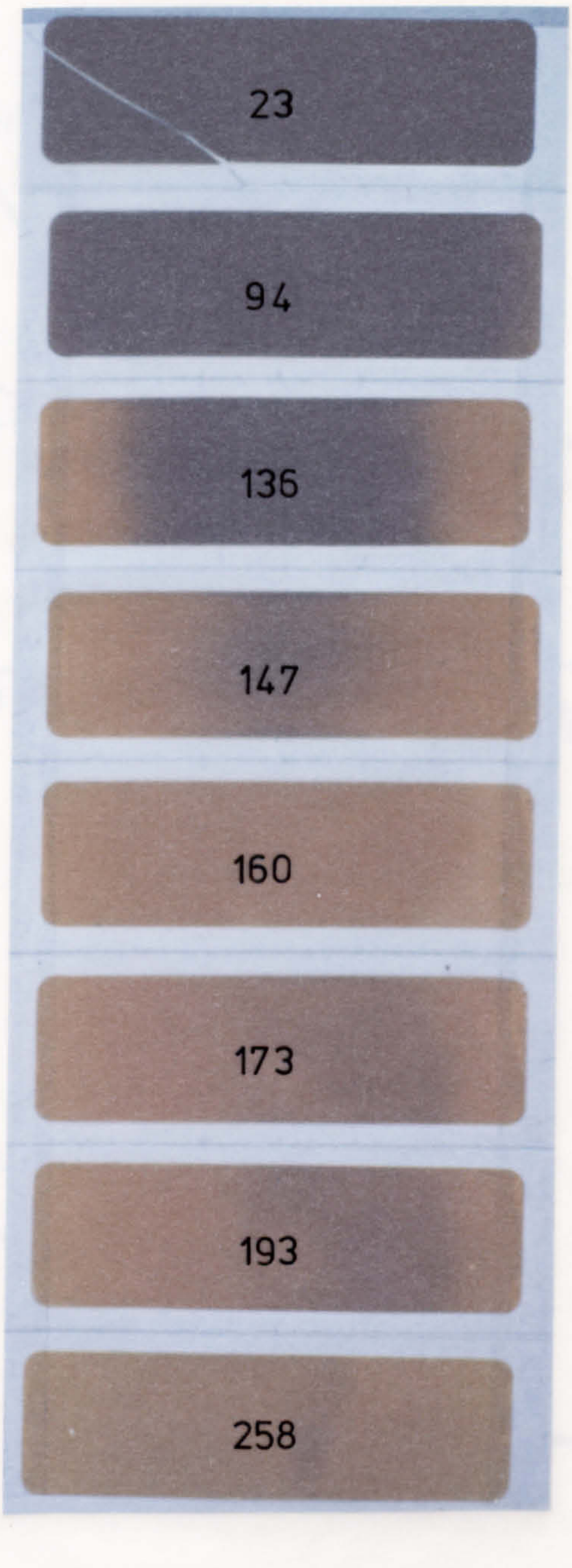

FIGURE 4.1 Cadmium sulphide thin films grown from Eagle Picher material

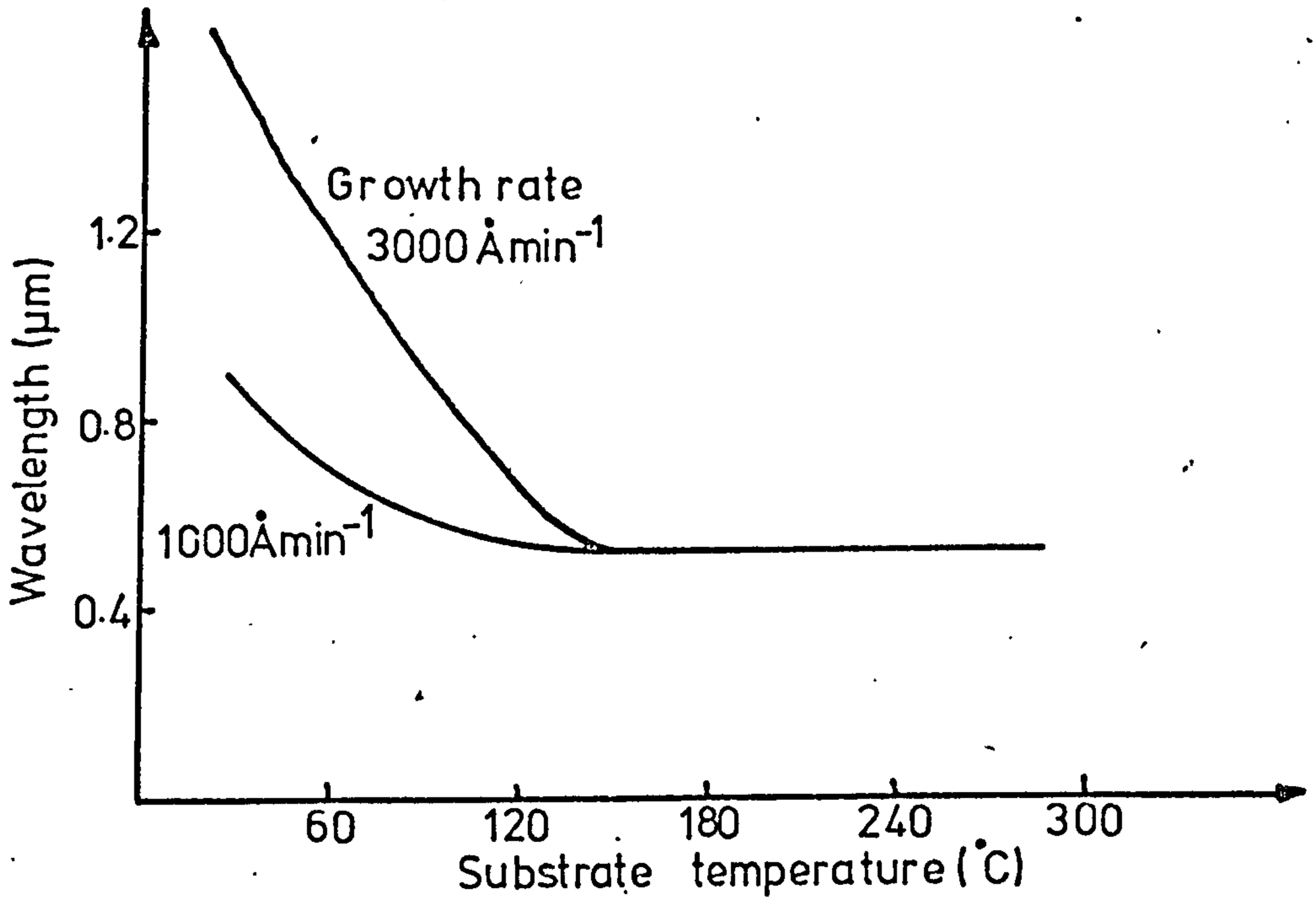

(a) Eagle Picher material

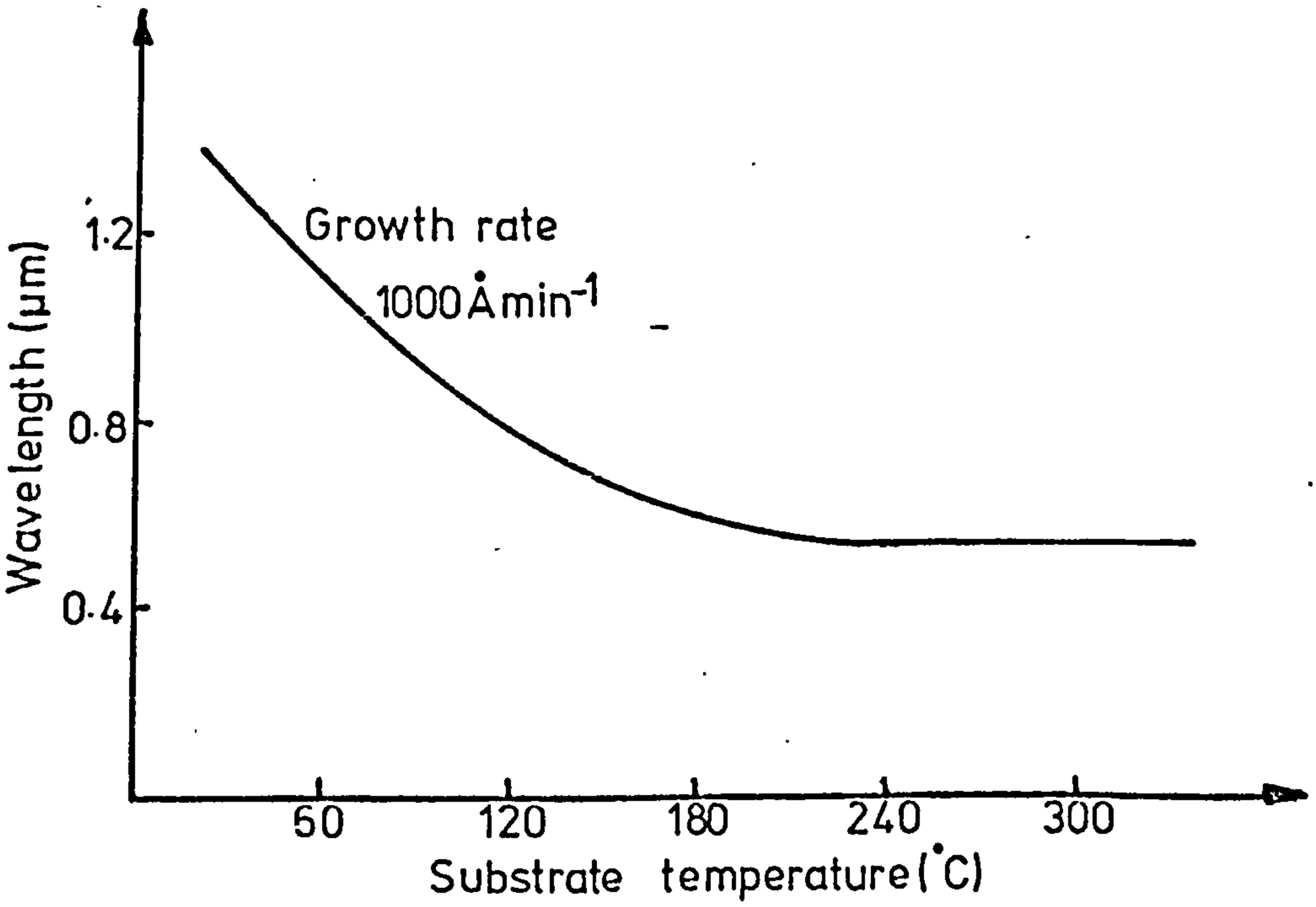

(b) Optran Grade material

FIGURE 4.2 Band edge versus substrate temperature

The band edge is less abrupt in low temperature cadmium rich films and extends towards 1 μm. As the cadmium: sulphur ratio approaches 1:1 the band edge becomes much sharper and tends to the bulk single crystal value of 520 nm. The band edge remains at 520 nm for high temperature films. The lower growth rate films (1000 Å min^{-1}) have a band edge nearer the bulk value of 520 nm for the same substrate temperature.

The band edge measurements suggest that in films which are deficient in sulphur the structure disorder gives rise to a large number of trapping levels in the band gap which serve to reduce its effective width. For films whose band edge is greater than 600 nm the absorption at 1.15 μm becomes significant and these films have a large optical waveguide attenuation at this wavelength.

4.1.2 RESISTIVITY

Resistivity is a property of a cadmium sulphide film that has frequently been used by a large number of workers as a figure of merit when gauging film quality[73]. Resistivity is affected by the free carrier concentration level and the electron mobility. The latter factor is a strong function of the film structure while the free carrier concentration should indicate the level of free carrier absorption loss. The resistivity measurements were carried out using a four-point probe method described by Valdes[86]. The input resistance of the meters available meant that resistivities of greater than $10^4 \Omega cm$ could not be measured; for cadmium sulphide films of this resistivity free carrier absorption should be negligible. Film resistivity was calculated as the average value of a series of measurements made over a central region of the film.

The cadmium sulphide films were grown on amorphous glass substrates (non-conducting) over a range of substrate temperatures, growth rates and source materials. The thickness variations of the

films were taken into account in the calculation of resistivity.

Fig. 4.3 shows graphs of resistivity versus substrate temperature for different growth rates and both starting materials. With the single crystal starting material the resistivity rises with increasing substrate temperature. The polycrystalline material on the other hand passes through a maximum resistivity value. The resistivity was greater for the slower growth rate.

In the films grown from the single crystal material the resistivity appears dominated by the free carrier level which arises because of the high sulphur concentration in this material. However, with the films grown from the polycrystalline material the structural order dictates the concentration of free carriers with the maximum in resistivity occurring at the optimum film structure. For all films the mobility varied by less than one order of magnitude and hence had a less significant effect on the resistivity changes. The different compositions of the two source materials also account for the lower substrate temperatures of the single crystal material for the same resistivity.

4.1.3 PHOTOCONDUCTIVITY

Photoconductivity measurements were made on the cadmium sulphide thin films to provide a more accurate indication of the regions of the spectrum in which strong absorption was likely to occur and hence those wavelengths to be avoided when waveguide evaluation was attempted. There is obvious photoconductivity at wavelengths near the band edge but the main concern was the presence of trapping levels causing a photoconductive signal in the 0.6-1.15 micron region.

Aluminium electrodes were evaporated directly through a metal foil mask and contacts were made by attaching gold wires to the

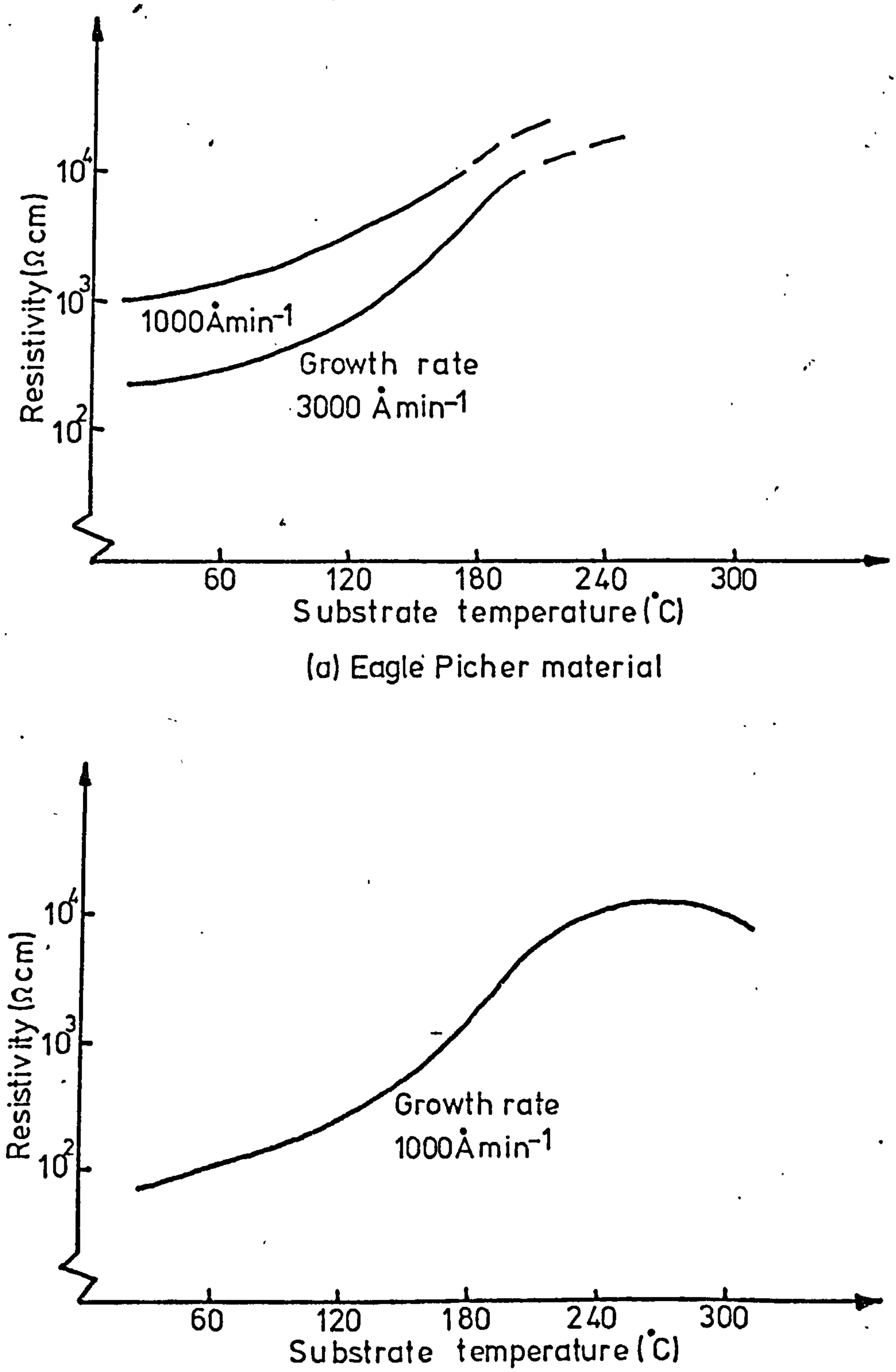

FIGURE 4.3 Resistivity versus substrate temperature

electrodes using a silver suspension. Three discrete laser wavelengths (0.633 μm, 0.9 μm and 1.15 μm) were used in the investigation to provide high intensity probes. The light was directed normally through the film between the electrodes and the photoconductivity measured under a.c. conditions for increased sensitivity.

A strong photoconductive signal at 633 nm was exhibited by all the films. This is in keeping with the strong fluorescence observed at 610 nm in the films. The measurements at 0.9 μm and 1.15 μm showed a slight photoconductive signal for the low substrate temperature films. Although no photoconductivity was detected with normally indicent light for films grown above 100°C, a small signal was measured in these films by guiding the light between the electrodes. The optimum substrate temperatures were 160°C for the single crystal starting material and 260°C for the polycrystalline lump and yielded films with a trap density responsible for absorption at 1.15 μm of less than 10^{15} cm^3.

The measurements confirmed that either 0.9 μm or 1.15 μm are suitable wavelengths for propagation in cadmium sulphide waveguides. The results show no evidence of a sulphur trapping level at about leV[87] which would affect waveguide loss at 1.15 μm.

4.1.4 MICROSCOPIC FIIM ANALYSIS

Microscopic analysis is one of the most important techniques available for gauging the film quality and hence the optical waveguide loss. The films were examined using a scanning electron microscope at University College London, X-ray analysis was carried out by Standard Telecommunication Laboratories, Harlow and transmission electron microscope studies made by the Chemistry Department, Glasgow University. The SEM and X-ray work was carried out on films grown on glass substrates while the TEM analysis was for a film grown on sodium chloride.

The SEM study was carried out by cleaving the glass substrate

and examining the surface and the cleaved edge of the film. The results have subsequently been repeated in the department and Fig. 4.4 shows micrographs of two films grown at different substrate temperatures. The much larger grain size of the higher temperature material is apparent and is significant from optical loss considerations. In both films the fibre texture is apparent, the larger the grain size the lower the waveguide loss. The initial film layers have no discernible crystal structure (amorphous region) and this causes some additional waveguide loss particularly in thinner films (< 1μm).

The X-ray analysis was carried out to gain a quantitative idea as to the preferred orientation of the c-axes. The results show that on amorphous glass substrates the c-axes are within $\pm$ 20° of the normal to the plane of the film.

With transmission electron microscopy the first few hundred angstroms of film growth can be examined in detail. However, ionic substrates were used to facilitate separation of the film from the substrate. Cadmium sulphide on sodium chloride was found to grow epitaxially which is in agreement with other published results[88] but gives no insight into the initial growth layers on amorphous glass substrates.

4.2 WAVEGUIDE EVALUATION

Waveguiding was attempted with visible radiation of 0.633 μm but due to trapping levels within the band gap no guiding was observed in any film produced. The next helium-neon transition at 1.15 μm was thus used in the majority of waveguide analyses. Most thin film information was routinely obtained by the optical methods described below.

4.2.1 MODE CONSTANT MEASUREMENTS

Two types of coupler were used for launching the 1.15 μm radiation into the cadmium sulphide thin films. The first method

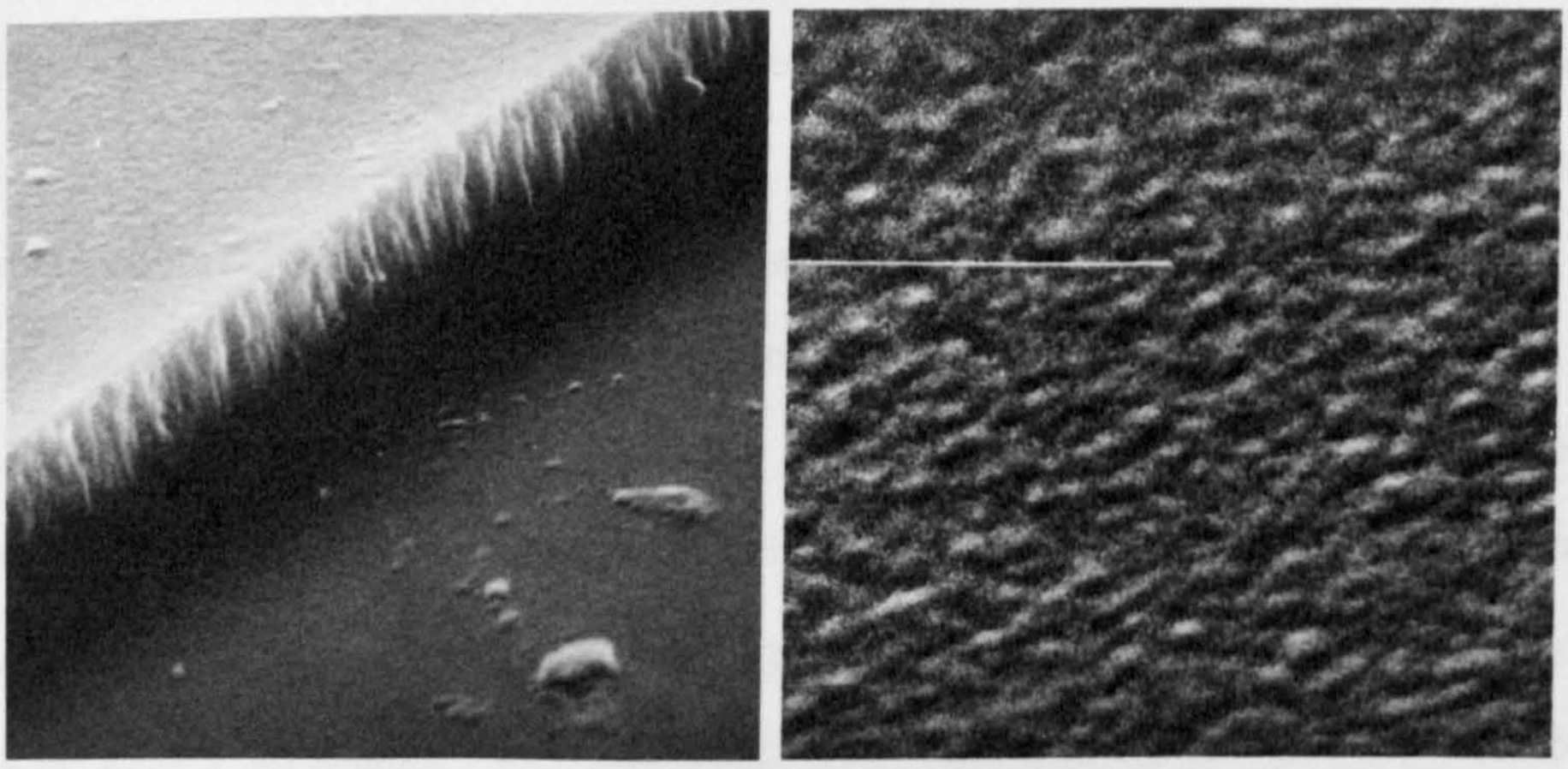

Cleaved edge magnification 10K Surface magnification 40K

(a) Substrate temperature 23°C

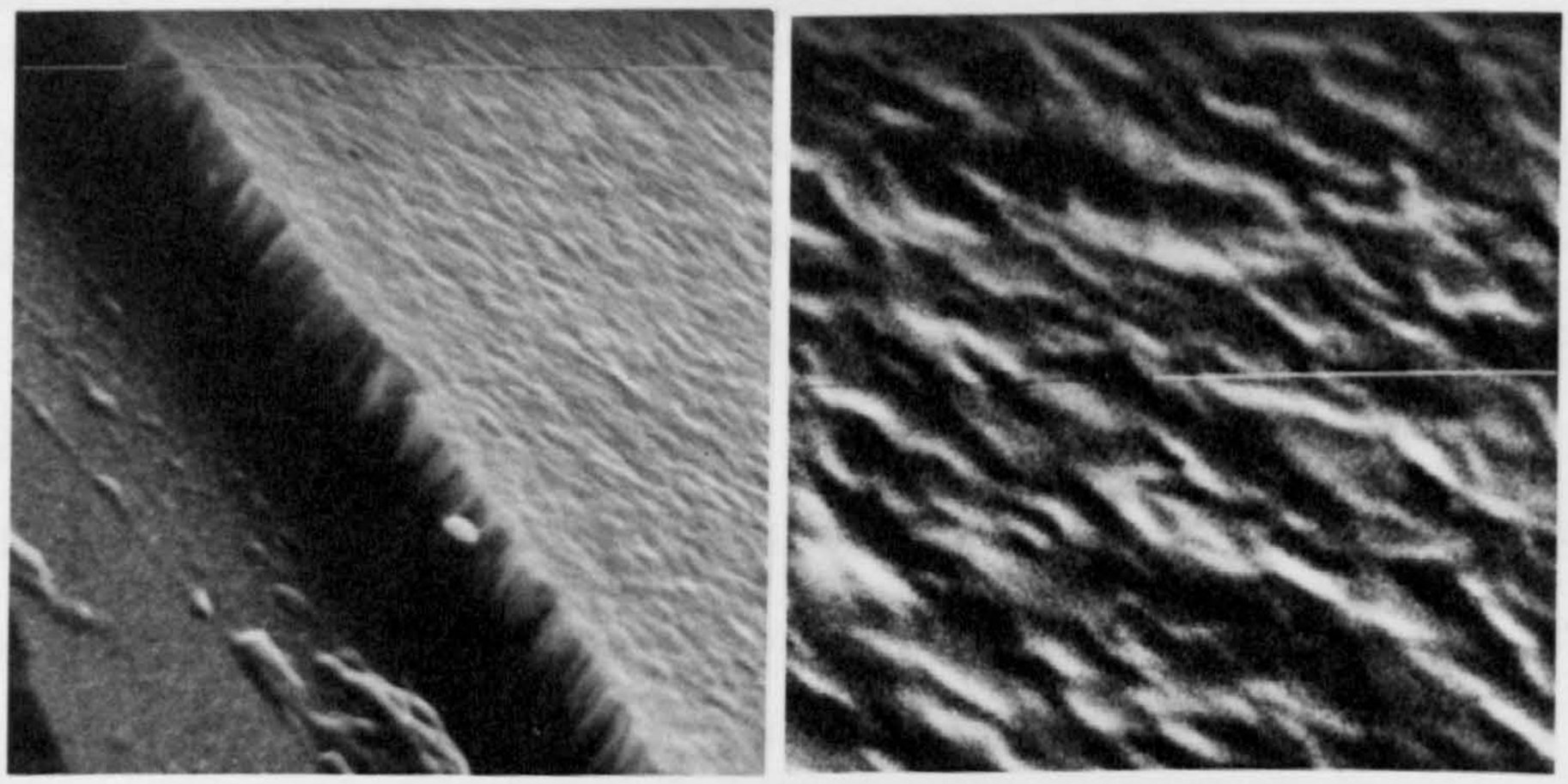

Cleaved edge magnification 10K Surface magnification 40K

(b) Substrate temperature 260°C

FIGURE 4.4 Scanning electron micrographs of cadmium sulphide

employed a grating which had been formed by etching a phase pattern in the substrate (Fig. 5.4a) and the second used a rutile prism coupler (Fig. 4.5b). A photo resist grating deposited directly onto the cadmium sulphide film did not induce a sufficient phase perturbation, due to the large refractive index difference between the cadmium sulphide and photoresist films, to allow efficient coupling. A glass or fused silica substrate covered with a film of Shipley AZ1350 photoresist was exposed to a 476.5 nm argon ion interferometer[89] and the required grating periodicity of Λ = 0.76 μm produced. The edges of the phase gratings were produced by contact printing using a white light source. The gratings were then ion beam etched for 30 minutes to define the phase pattern in the substrate. The combination of a vacuum evaporated cadmium sulphide film and the etched grating produced a coupler with a compact planar structure and a coupling efficiency of 35% for 1.15 μm radiation in the TE_o film mode. Rutile prisms provided a much simpler means of characterizing the cadmium sulphide waveguides but repeated application of the prism did cause surface damage to the film. These couplers had launching efficiencies of 65% for 1.15 μm radiation coupled to the TE_o mode. The refractive indices of the prism were measured experimentally at 1.15 μm to be n_o = 2.472 and n_e = 2.732 which confirm the values calculated from the dispersion relations given by de Vore[71] for rutile.

The combination of a quarter-wave plate and a Glan-laser calcite polariser was used to select either the TE or TM polarisation without significant lateral displacement of the 1.15 μm input beam. The position of the infrared beam on the input coupler was located by means of a 0.633 μm laser beam collinearly aligned with the infrared beam to within 0.5 milliradians. The infrared radiation was monitored by either a Kodak phosphor card or a vacuum image converter tube both of which gave visual displays of the 1.15 μm light directly incident

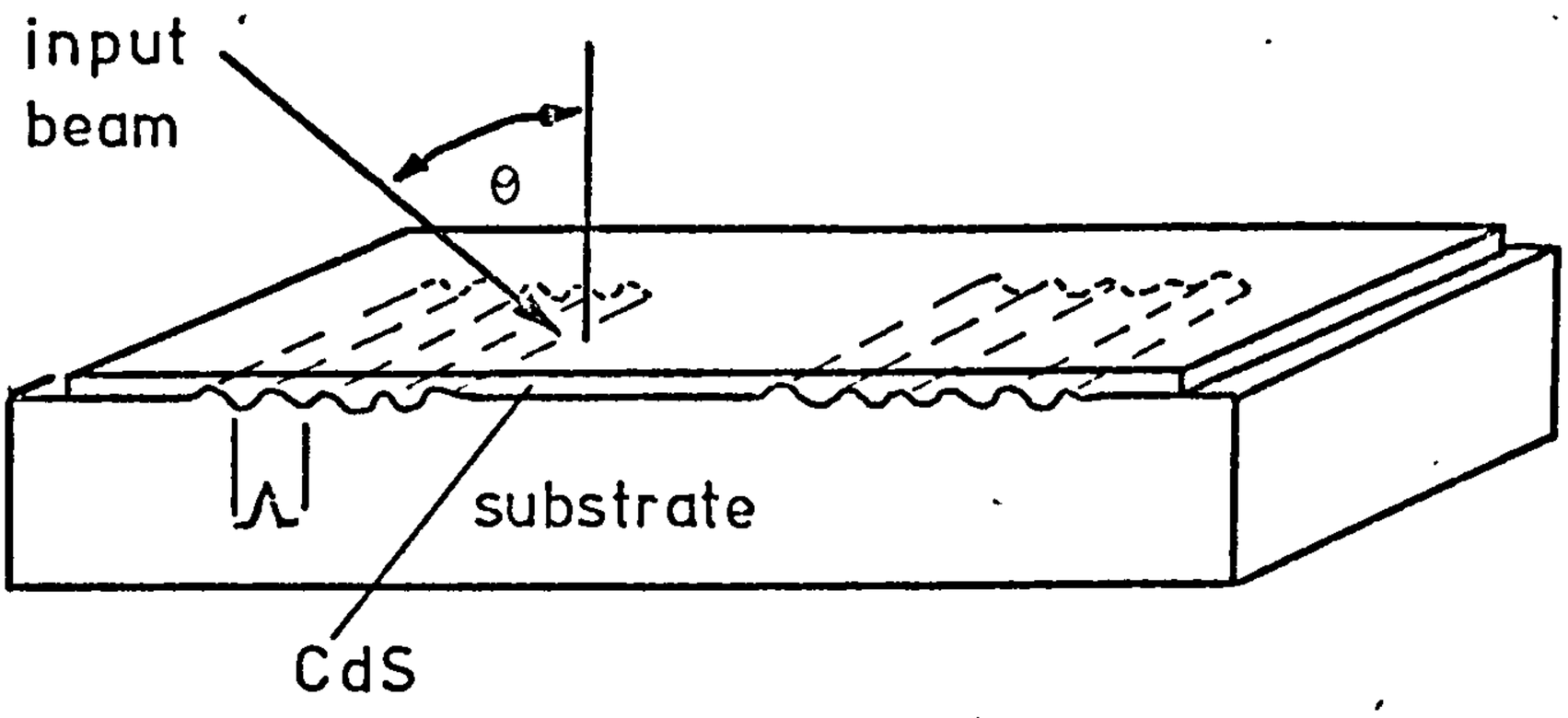

(a) Ion-etched grating couplers

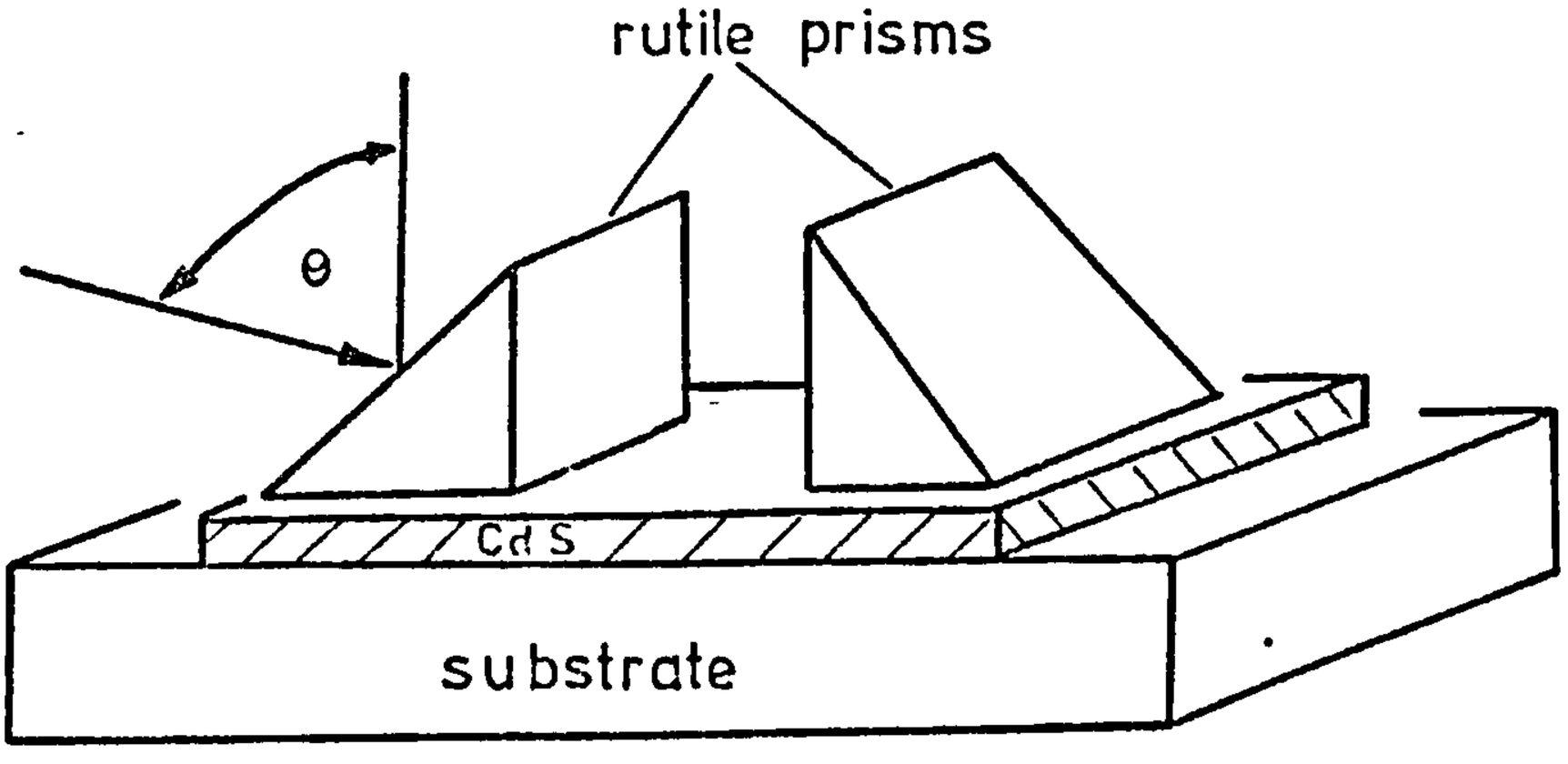

(b) Rutile prism couplers

FIGURE 4.5 CdS coupler schemes

on them. In later experiments an image converter (Electrophysics model IRV 7100) was available which allowed direct observation of the infrared beam in the cadmium sulphide thin film. Coupling to the waveguides was achieved by observation of the input beam after reflection from the base of the prism or the phase grating. A black line was observed through the up-converted beam when power was coupled into the waveguide. At the output coupler a bright spot corresponding to the mode launched in the guide was seen along with the "m-lines"[57] associated with energy coupled into other waveguide modes through scattering. The existence of a waveguide mode was further confirmed by scratching the cadmium sulphide film (once all the measurements had been made) at which radiation from the output coupler ceased.

The most accurate estimates of film refractive index and thickness were determined by computer calculations (Appendix A2) using the known refractive indices of the prism and substrate, and the angles measured between the incident laser beam direction and the plane of the film for which synchronous coupling into the TE or TM waveguide modes occurred. The effective indices ($\beta/_k$) for the modes were derived from these angles and a knowledge of either the rutile prism geometry or the phase grating period. Subsequently, the film thickness for each value of $\beta/_k$ from a set of modes was calculated using the appropriate characteristic equation for the mode and a selected value of guide refractive index. The refractive index was then varied until the values of film thickness were the same for each mode. For the prism coupler film thicknesses could be calculated to $\pm$ 1% and refractive indices to better than $\pm$ 0.1%. The refractive indices and thicknesses of a number of cadmium sulphide films are listed in Table 4.2 along with other data relating to the films. Every film analysed exhibited a small birefringence with $\Delta n = n_{TM} - n_{TE} = 0.01$. The values of n_{TM} and n_{TE} are comparable with the bulk indices of single

Film No.	Polarization	Caculated Refractive Index	Calculated Thickness μm	Measured Thickness μm	Resistivity Ω.cm	TE_o Propagation loss, $dBcm^{-1}$
1	TE	2.330	1.498	1.21	$\sim 10^3$	15
2	TE TM	2.330 2.339	1.278 1.280	1.21	$> 10^4$	< 5
3	TE TM	2,312 2.323	0.858 0.853	0.79	$5x10^3$	11
4	TE TM	2.322 2.335	1.313 1.315	1.33	$\sim 10^3$	16
5	TE TM	2.323 2.343	2.091 2.090	2.05	$3x10^3$	8
6	TE TM	2.328 2.344	1.295 1.273	1.275	$\sim 10^3$	16

TABLE 4.2 Summary of the main characteristics of a number of CdS films.

crystal cadmium sulphide given by n_o=2.32 and n_e=2.336 at 1.15 μm[65].

The small birefringence found in cadmium sulphide thin films can be neglected when considering waveguide analysis and thus Abeles method[90] was used to check the refractive index. Good correlation was obtained with the refractive indices calculated from the mode angles even though the absolute error was ± 0.5% due to the gradient of the tangent function. Only films grown around the optimum substrate temperature could be analysed by the mode angle method. In every case the refractive index was within ± 0.6% of the bulk single crystal value of 2.32 at 1.15 μm.

Two further techniques were used to check the film thickness; firstly, deposition monitoring and secondly by a mechanical technique. The film deposition was recorded using a quartz crystal thickness monitor and this could be calibrated to give film thicknesses to within ± 5% if repeated runs under identical condition were used. However, since the quartz crystal was kept at a fixed temperature it was not accurate to more than ± 10% when deposition conditions were changed. Measurement of the film thickness was also obtained using a sliding stylus instrument (G.V. Planar surfometer type SF100). This instrument is capable of measuring steps in films (ie film thickness at edge of film) to an accuracy of ± 0.05 μm up to a film thickness of 1.5 μm and ± 2% thicker films. This method gave good agreement with the values calculated from TE and TM mode angles as seen from the results in Table 4.2

4.2.2 LOSS MEASUREMENTS

Attenuation measurements provide the most important quantitative information about the cadmium sulphide thin films used as waveguides. The propagation losses of the 1.15 μm guided modes were determined by a number of techniques. The first method involved the extrapolation of loss from a relative power measurement on all

the accountable beams directed at and eminating from the input and output couplers both on and slightly away from the synchronous coupling angles. This method will also give a relative measure of the launching efficiency of the particular coupler. Alternatively, by treating the rutile output coupling prism as 100% efficient[7] the loss could be calculated by recording the relative output powers as the spacing between the undisturbed input coupler and the output coupling prism was varied. Repeated application of a prism can cause increased attenuation due to damage of the surface. Consequently, the first measurement was made at the extremity of the light beam in the film and then as successive measurements were made the prism was moved progressively towards the input coupler. These two methods are potentially the most accurate as the actual power of the guided mode was measured.

The final method involved scanning the cadmium sulphide film with a small area germanium photodiode and recording the power scattered out of the film as a function of position along the film. This method measures all the light being guided in the film including that which has been scattered to the other waveguide modes. Such light has however been lost from the launched mode and should be considered in attenuation measurements. Fig. 4.6 illustrates a plot of scattered light intensity versus distance for a cadmium sulphide waveguide along with typical curves for 1.15 μm and 0.633 μm propagation in an r.f. sputtered 7059 glass* film. It is concluded from these curves that large scattering centres, easily identifiable in the 7059 glass films, are absent from the cadmium sulphide films.

Measurements by all three methods gave virtually identical results due to the fact that there was very little scatter between the modes. A plot of waveguide loss for the TE_o mode versus substrate temperature for varying growth rates is shown in Fig. 4.7 for both

* Corning Glass Co. U.S.A.

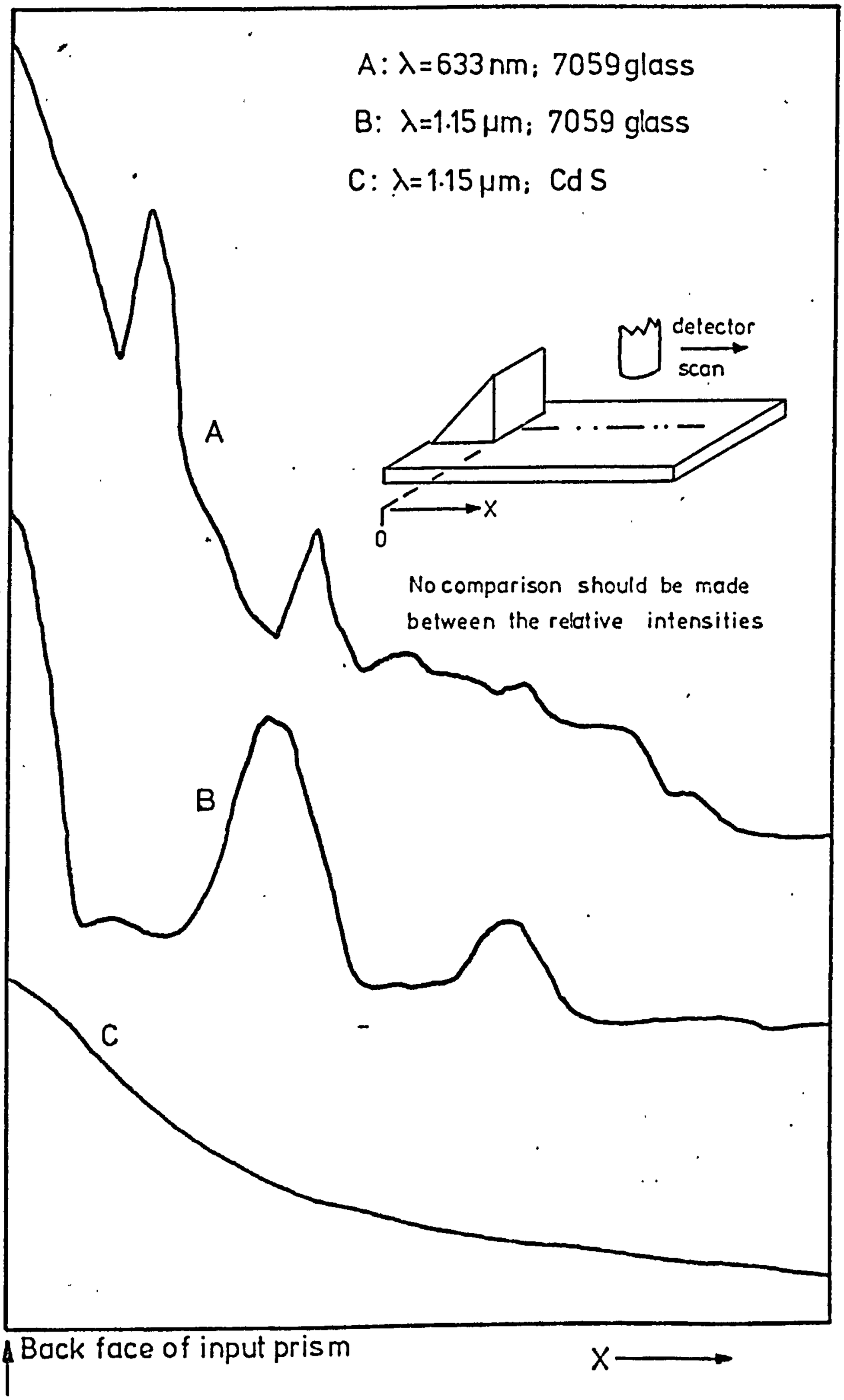

FIGURE 4.6 Scattered light intensity as a function of distance

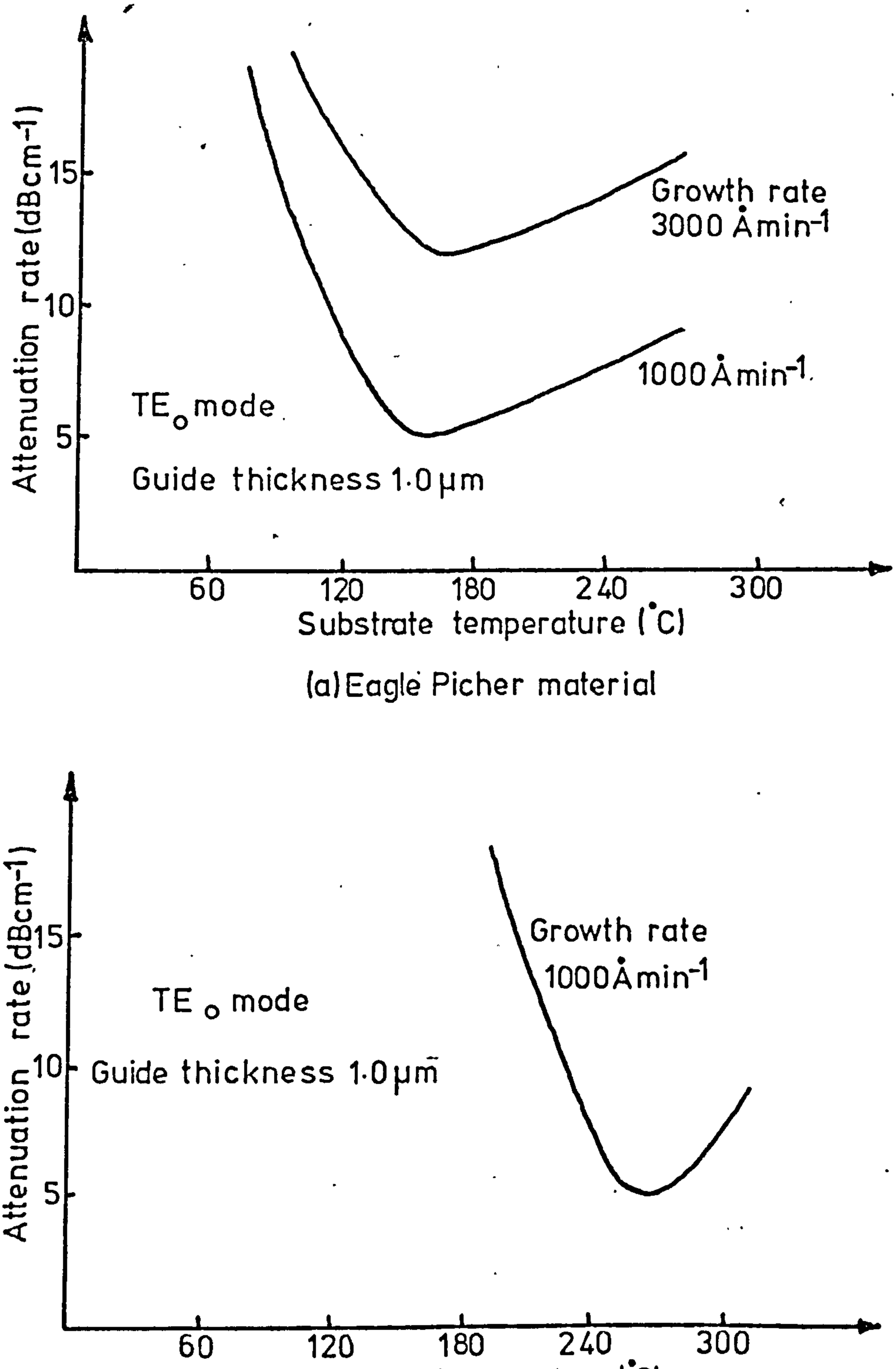

FIGURE 4.7 TE_o mode attenuation versus substrate temperature

cadmium sulphide starting materials. The curves illustrate that there is an optimum range of substrate temperatures over which the lowest loss waveguides can be formed corresponding to the best film structure and stoichiometry. Table 4.3 shows the losses for the TE_o, TE_1 and TE_2 modes in the waveguide exhibiting the lowest TE_0 mode loss. For amorphous glass films it is possible to estimate the level of bulk absorption[57]. However since cadmium sulphide guides possess several sources of loss, including free carrier absorption, and scattering from the initial amorphous region, grain boundaries and the surface, it is not possible to make such an estimate.

The TM mode losses in all these films were too large to be measured and hence only TE modes were considered. The lowest loss for a TE_o mode in a polycrystalline cadmium sulphide film grown on an amorphous substrate was found to be 5 $dBcm^{-1}$ for films of thickness greater than 1.2 μm. For thinner cadmium sulphide films the loss increased dramatically and this will be considered in more detail in section 4.4.

Photoconductive signals were observed from the cadmium sulphide guides when planar aluminium electrodes were placed parallel to and on either side of the propagation path. Monitoring of the signals produced by the 1.15 μm radiation proved to be an extremely effective method of tuning onto the synchronous coupling angles for the TE and TM modes, particularly when film propagation loss precluded the observation of an output beam.

4.3 SINGLE CRYSTAL SUBSTRATE ANALYSIS

Device fabrication requires that amorphous substrates be used for the cadmium sulphide film growth. However, it is valuable to consider cadmium sulphide thin films grown onto single crystal substrates of < 111 > spinel, where the films should be epitaxial, to investigate further the causes of waveguide loss. "Optran grade"

TABLE 4.3 Total propagation losses measured in film 2

Mode	β/K	Total propagation attenuation ($dBcm^{-1}$)
TE_0	2·296	5·0
TE_1	2·195	6·3
TE_2	2·017	8·7

polycrystalline material was used in this analysis since the more expensive single crystal material had no benefit in terms of waveguide loss. The cadmium sulphide was evaporated at a rate of 1000Åmin^{-1} onto the single crystal spinel substrates for a range of substrate temperatures around the temperature for minimum optical loss waveguides on amorphous substrates. Similar experimental procedures to these already detailed in sections 4.1 and 4.2 were followed.

The resistivity of the films measured was greater than 10^4Ωcm. Scanning electron micrographs and X-ray analyses showed the films to be of better crystalline quality with a c-axis spread of less than $\pm 5^o$ about the normal to the plane of the film. The refractive indices were measured to be within $\pm$ 0.5% of the bulk single crystal value. Optical loss, however, showed a very marked improvement (Fig. 4.8) with a minimum loss of 2 $dBcm^{-1}$ being recorded for a film deposited at 258°C. With these films the substrate temperature was much more critical and control to $\pm 1^oC$ was important.

The single crystal substrate films are largely free of grain boundaries and the initial amorphous regions. For amorphous substrates the loss can thus be improved by increasing the grain size and reducing the thickness of the amorphous region.

4.4 SUBSEQUENT IMPROVEMENTS TO THIN FILMS

For the cadmium sulphide waveguides the sources of loss are free carrier absorption, and scattering from the initial amorphous region, grain boundaries and the surface. Calculations have shown free carrier absorption to be negligible and the loss scans of Fig. 4.6 indicate that surface scatter is also insignificant. The main causes of waveguide attenuation for films grown on amorphous substrates are the initial disordered structure and scattering from the grain boundaries. Increased grain size and reduced thickness of the initial amorphous region should lead to lower cadmium sulphide thin film losses.

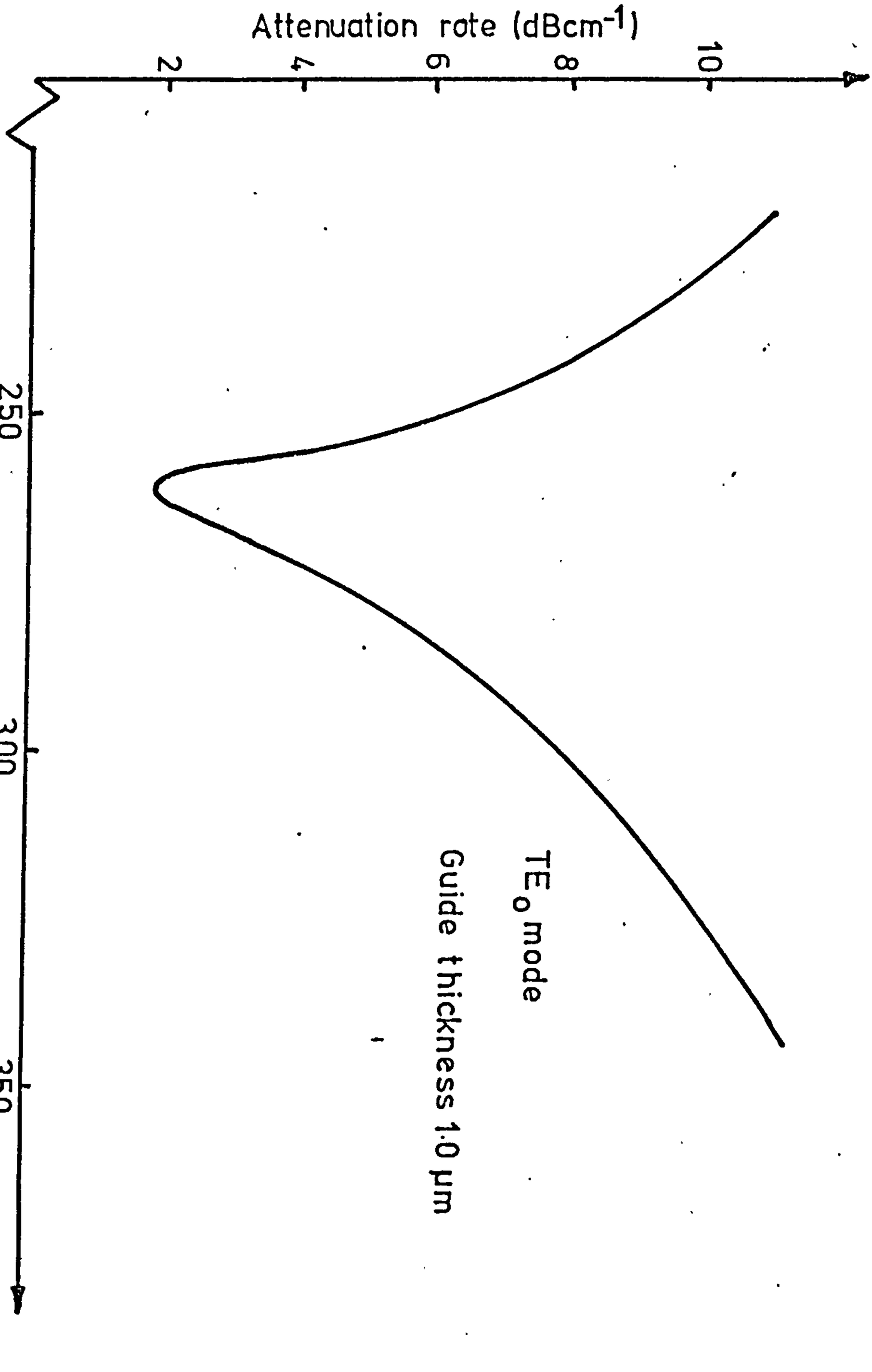

FIGURE 4.8 TE_o mode attenuation versus substrate temperature for CdS grown on ⟨111⟩ spinel

Modifications were made to the electron beam power supply such that the minimum growth rate could be reduced from 1000 to 100 $Åmin^{-1}$. The optical loss was measured for a range of film thicknesses grown onto amorphous substrates at the optimum temperature of 260°C. Both a fast growth rate of $3000A^{o}min^{-1}$ and a slow growth rate of $200A^{o}min^{-1}$ were used, the resultant waveguide attenuation versus film thickness for the TE_o mode being plotted in Fig. 4.9. It was found that for very thin films the losses were much less for the slower growth rate but for films of greater than 1 μm thickness the TE_o mode loss tended to the same limiting value of 5 $dBcm^{-1}$. The initial disordered regions of the cadmium sulphide thin film have therefore been greatly improved by allowing the initial structure more time to become ordered with the slower growth rate. However, once the film is established the growth rate is not critical and the ultimate grain size does not appear to be affected by the rate. Thin films carry more of the optical power in the disordered amorphous region and thus there is a dramatic improvement in the loss of these films. With thicker films a lesser amount of power is carried in that region and changes in the loss are not found.

Post-deposition annealing in a nitrogen atmosphere for 2 hr. at a temperature of 350°C was carried out. The films possessed a sharper band edge borne out by the accompaning colour change and also reduced photoconductivity of 0.633 μm. The resistivity also increased from $8x10^{3}$Ωcm to greater then 10^{4}Ωcm. Scanning electron micrographs showed that the grain size and amorphous region had not altered indicating that no recrystallisation had occurred. The resistivity increase must therefore be largely attributed to a reduction in the free carrier concentration level. Optical guiding at 1.15 μm showed no change from the preannealed value and illustrated further the small contribution to loss from free carrier absorption. The results indicate that the trapping levels within the band gap caused by the

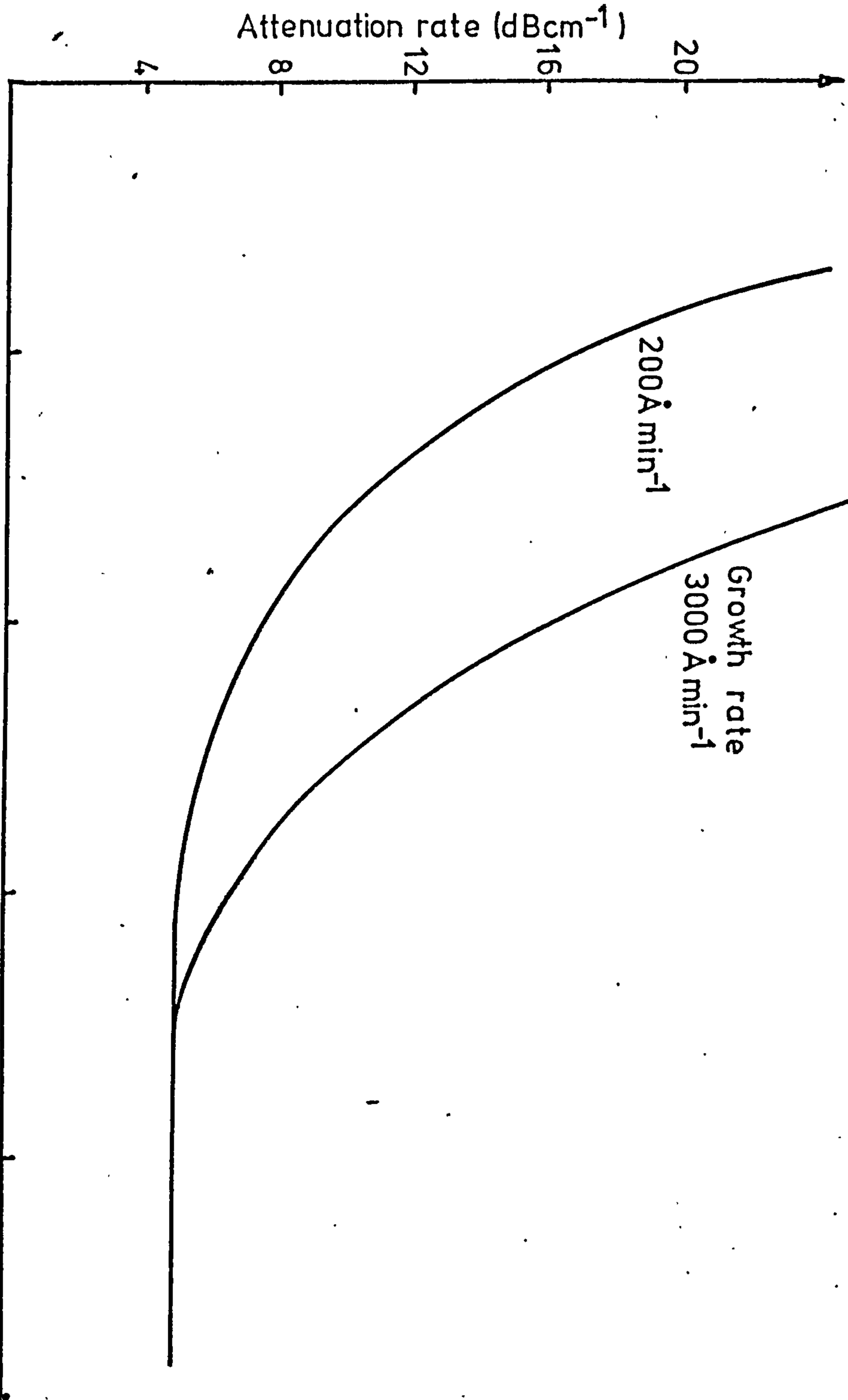

FIGURE 4.9 TE_o mode attenuation versus guide thickness for CdS grown on glass substrates

lattice defects in the cadmium sulphide are being filled by nitrogen atoms. However, none of these trapping levels makes a significant contribution to the waveguide attenuation at 1.15 μm. The photoconductive response at 0.633 μm was reduced. Coupling of that laser wavelength was possible but the waveguide losses were greater than 40 $dBcm^{-1}$.

4.5 DISCUSSION OF RESULTS

The results of sections 4.2 and 4.4 have shown that it is difficult to improve the propagation loss below 5 $dBcm^{-1}$ for cadmium sulphide films grcater than 1.2 μm thick grown on amorphous substrates. The films are of apparent optimum stoichiometry and structure with the substrate temperature maintained at $260^{o} \pm 10^{o}C$ for the polycrystalline starting material. The improved loss of 2 $dBcm^{-1}$ for the TE_{o} mode in cadmium sulphide films grown on < 111 > spinel single crystal substrates was incidental to the main objectives since devices were to be fabricated on amorphous substrates. However, the results did indicate that the main source of waveguide attenuation in the films grown on amorphous substrates was the structural quality of the films. The fabrication of low loss waveguides has proved a difficult problem but the figure of 2 $dBcm^{-1}$ for cadmium sulphide on spinel still remains one of the best results for a semiconductor.

The final film loss has proved to be independent of starting material although the substrate temperature required for minimum waveguide attenuation was $160^{o}C$ in the case of the single crystal material and $260^{o}C$ for the polycrystalline evaporant. In both cases a slow growth rate reduced the loss in films less than 1 μm thick. The different substrate temperatures were due to the varying compositions of the two starting materials. The greater sulphur content of the single crystal material was confirmed by mass spectra recorded during film deposition (see Fig. 4.10). The polycrystalline material was

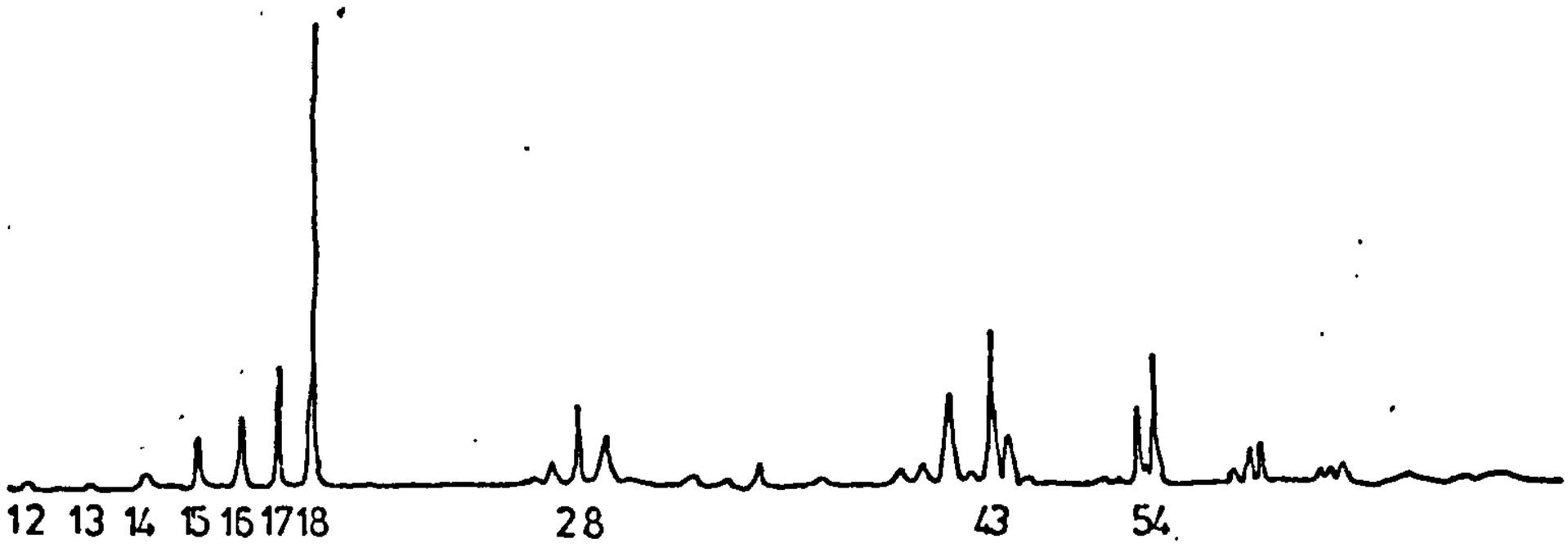

(a) Chamber background

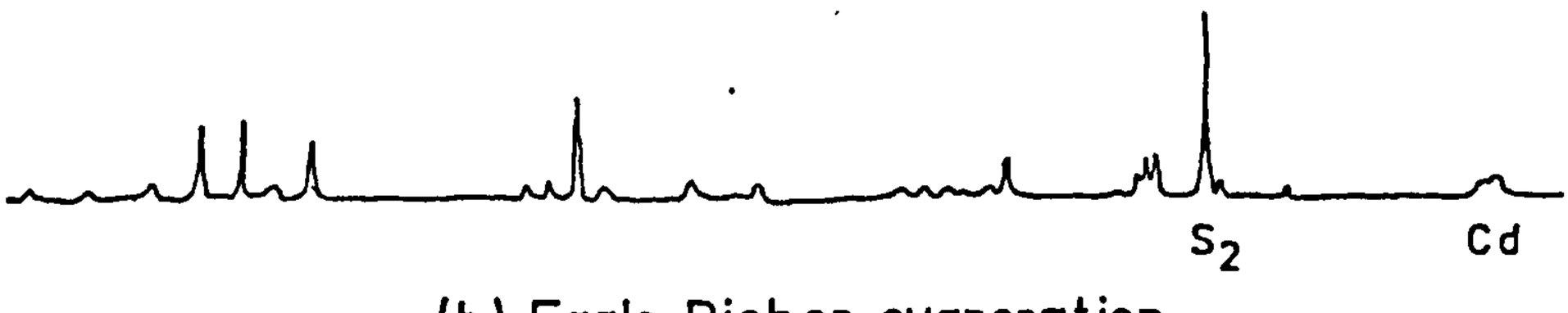

(b) Eagle Picher evaporation

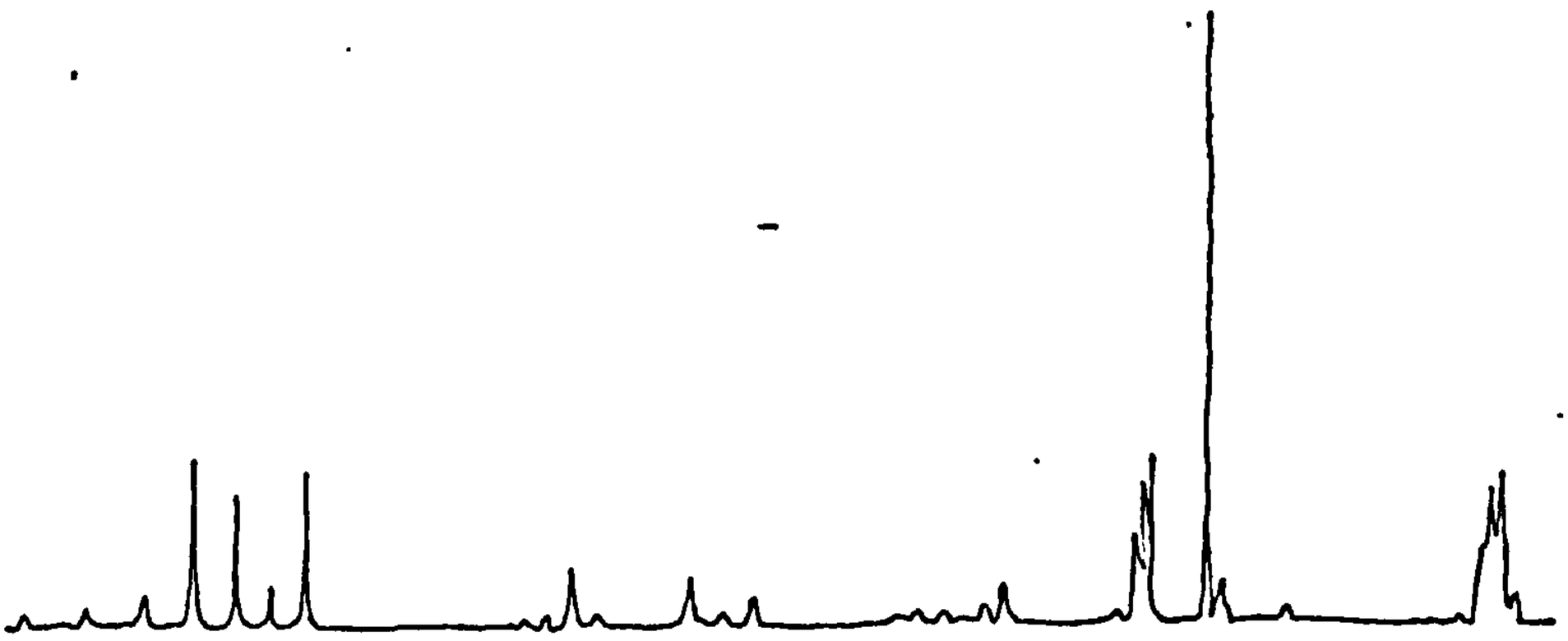

(c) Optran Grade evaporation

FIGURE 4.10 Mass spectral data from CdS evaporations

therefore chosen for all subsequent experiments on the basis of its considerably lower cost and availability.

Calculations have shown free carrier absorption to have a negligible contribution to waveguide attenuation and this has been borne out in the resistivity measurements on the basic films as well as in the resistivities measured in samples before and after annealing. Losses of 5 $dBcm^{-1}$ for the TE_o mode were measured in films at a wavelength of 0.904 μm and further indicate that the sulphur deficiency trapping level at about leV is not contributing to the loss at 1.15 μm. The cadmium sulphide films appear to be dominated by scattering at the grain boundaries and in the amorphous region which forms during the initial 100-200$\mathring{A}$ of film growth.

The single crystal films grown on the < 111 > spinel substrates are free from grain boundaries and do not possess an initial amorphous growth region. Greater than 50% of the loss in the cadmium sulphide films grown on amorphous substrates can therefore be attributed to scattering from the grain boundaries and the disordered amorphous region. Surface scatter is negligible and gross defects are absent as the loss scan of Fig. 4.6 shows no large peaks as is the case with r.f. sputtered glass films.

Although there is no preferred orientation within the plane of the cadmium sulphide film grown on amorphous substrates, the c-axes grow within $\pm$ 20° to the normal of the plane of the film and this property can be used in the design of the electrooptic phase modulator.

PART II

ELECTROOPTIC MODULATION IN SLAB WAVEGUIDES

SYNOPSIS

The full bandwidth available to optical communication links requires the utilisation of optical signal processing. As part of such a system the modulator will play an important role. The main advantage that a thin film device has over its bulk counterpart is that confinement of the optical beam below the diffraction limit leads to a device requiring a very low drive power. Electrooptic modulators not only require less drive power than do acoustooptic and magnetooptic modulators but also have a potentially much greater bandwidth.

The electrooptic effect in the partially orientated cadmium sulphide waveguides described in part 1 has been used to produce a phase modulator. The device described here has the advantage that it is a completely evaporated structure and unlike all other such previously reported modulators does not depend on epitaxial growth onto a single crystal substrate. A multilayer configuration (Fig. 5.1a) can therefore be employed in preference to a transverse electrode configuration (Fig. 5.1b) as in the former case the phase change is greater for a given applied voltage[54]. The device exploits the fact that the cadmium sulphide films grow with a high degree of c-axis orientation perpendicular to the plane of the film and for TE mode propagation use can be made of the r_{13} electrooptic coefficient. Buffer layers are essential for the elimination of additional propagation loss by isolating the waveguide from the metal electrodes.

Part II of this thesis is divided into two chapters, the first deals with a general theoretical analysis of the multilayer electro-optic thin film modulator and a theoretical optimisation for the specific case of the Al-SiO-CdS-SiO-Al stacked structure (Fig. 5.1a). The second chapter is concerned with the device fabrication, the experimental techniques for measuring electrooptically induced phase

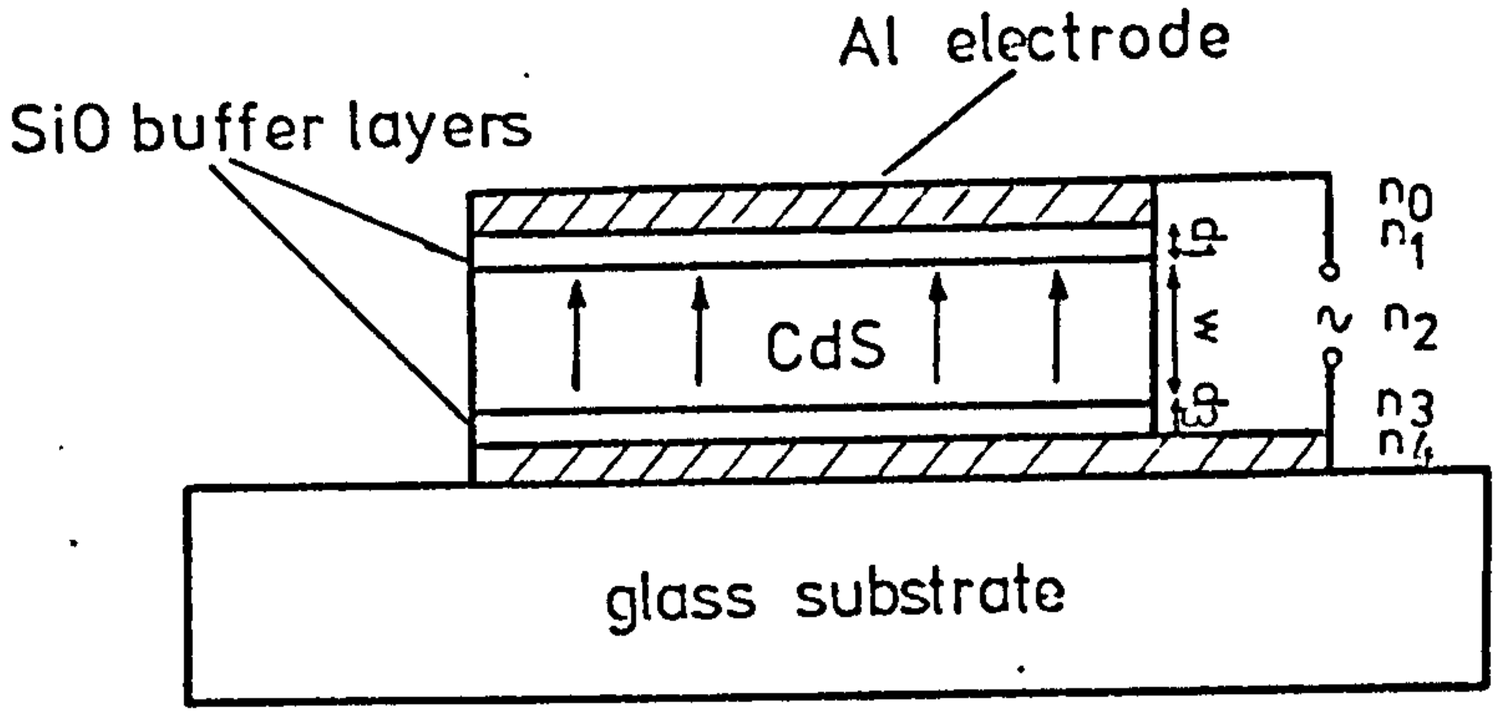

(a) Multilayer structure

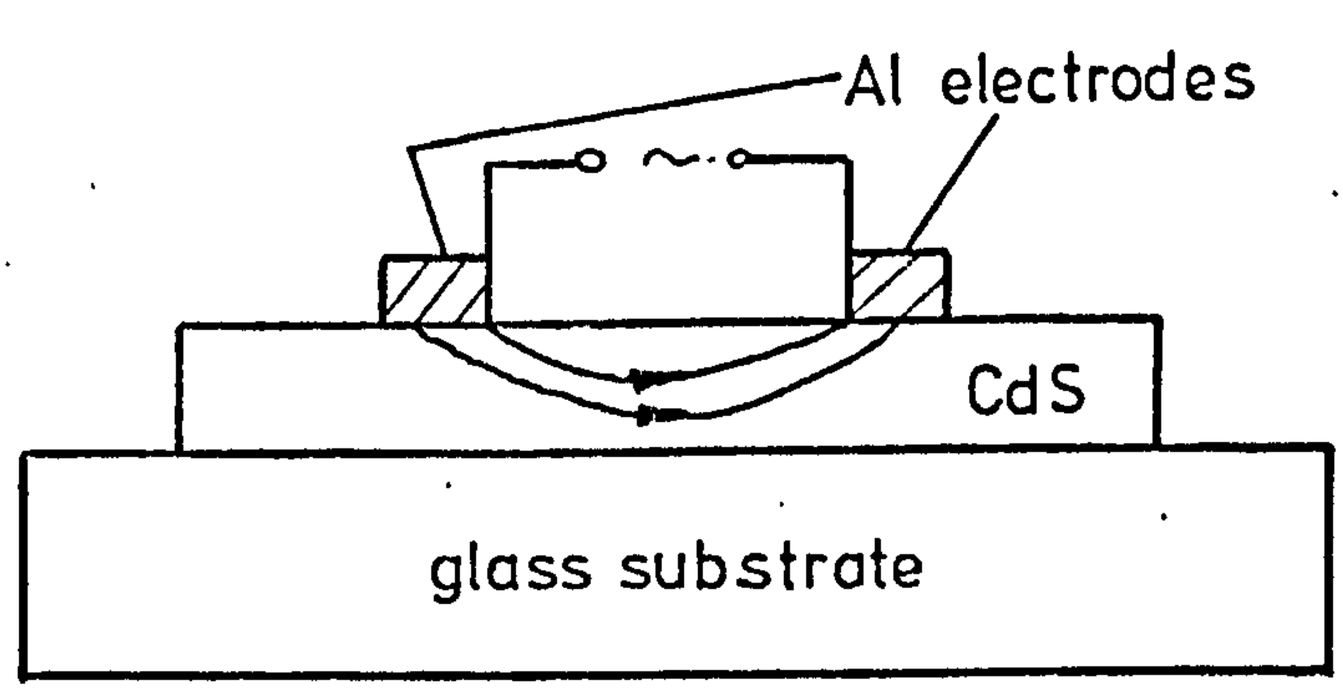

(b) Transverse electrode structure

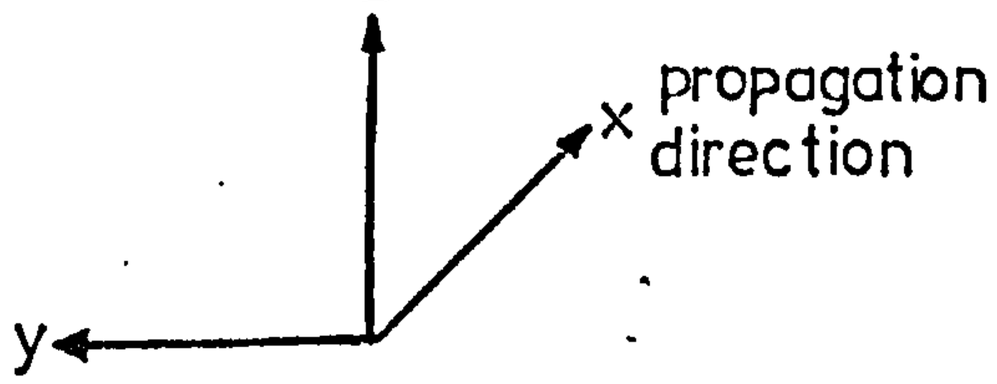

FIGURE 5.1 CdS electrooptic modulator geometries

changes and the results from several modulators. A novel composite modulator structure is also described along with concluding discussion on the slab waveguide phase modulators.

CHAPTER 5: MODULATOR DESIGN CONSIDERATIONS

The modulator described in this chapter induces a phase change through the electrooptic effect although in many cases amplitude modulation is preferable as the demodulation process is simpler. Discrete single mode operation is assumed throughout the analysis. In section 5.1 the electrooptic effect with particular reference to cadmium sulphide is characterised to relate the relevant refractive index changes to the applied electric field. The equations describing TE and TM mode propagation in lossy waveguides are given in section 5.2 and from these an expression relating phase change to refractive index change is derived for TE modes in section 5.3. The specific case of TE mode propagation in an Al-SiO-CdS-SiO-Al stacked structure is then considered and the various layer thicknesses optimised for a minimum in the power required for unit modulation bandwidth for one radian phase change.

5.1 THE ELECTROOPTIC EFFECT

The theory of the electrooptic effect has been detailed in many books[63,91] and only the salient features of the effect will be outlined.

An electrooptic material is one whose dielectric properties change under the application of an electric field in the manner described by equation (5.1);

$$N = n_o + aE + bE^2 + \ldots\ldots \qquad (5.1)$$

where N is the refractive index, n_o is the unperturbed refractive index and a and b are constants. Non-zero b represents the quadratic (or Kerr) effect while a non-zero a represents the linear (or Pockels) effect. It is this latter effect which dominates in the case of cadmium sulphide.

Single crystal cadmium sulphide is a hexagonal material with

6mm symmetry[92]. The electrooptic matrix is therefore given by[93]

$$r_{ij} = \begin{vmatrix} 0 & 0 & r_{13} \\ 0 & 0 & r_{23} \\ 0 & 0 & r_{33} \\ 0 & r_{42} & 0 \\ 0 & 0 & r_{51} \\ 0 & 0 & 0 \end{vmatrix}$$

where the subscripts 1, 2, 3 relate to the orthogonal x, y, z axes of Fig. 5.1a respectively with z parallel to the crystallographic c-axis. The refractive index changes of immediate interest are those which result from the application of an electric field parallel to the z-direction;

$$\Delta n_1 = -\tfrac{1}{2} r_{13} n_1^3 E_3 \qquad (5.2a)$$

$$\Delta n_2 = -\tfrac{1}{2} r_{13} n_2^3 E_3 \qquad (5.2.b)$$

$$\Delta n_3 = -\tfrac{1}{2} r_{33} n_3^2 E_3 \qquad (5.2.c)$$

Since cadmium sulphide is a positive uniaxial material, $n_1 = n_2 = n_o$ and $n_3 = n_e$, where n_o and n_e are the ordinary and extraordinary refractive indices respectively. Equations (5.2) can thus be rewritten as

$$\Delta n_{1,2} = \Delta n_o = -\tfrac{1}{2} r_{13} n_o^3 E_3 \qquad (5.3a)$$

$$\Delta n_3 = \Delta n_e = -\tfrac{1}{2} r_{33} n_e^3 E_3 \qquad (5.3.b)$$

At 1.15 μm the appropriate data for cadmium sulphide is as follows,

$$n_o = 2.32, \quad n_e = 2.336^{65}$$

$$r_{13} = 1.1\text{x}10^{-12}\ \text{m.V}^{-1}, \quad r_{33} = 2.4\text{x}10^{-12}\ \text{m.V}^{-1}\ ^{92}$$

For the structure geometry of Fig. 5.1a, TE modes travel in the x-direction with their E-field polarized in the y-direction, similarly TM modes propagate in the x-direction with the H-field polarized in the y-direction. The TE modes will therefore experience the smaller refractive index change associated with r_{13}. It is important to note that since the refractive index changes in the x and y directions are the same, the crystallographic orientation in the x-y plane is of no consequence for an useful electrooptic effect. This point is particularly relevant in view of the polycrystalline nature of the cadmium sulphide films grown on amorphous substrates. The case of the TM mode is more complex due to the E-field vector being the resultant of the E-fields in the x and z directions which depend on the propagation constant ($\beta/_k$) of the mode. TM modes are considered for completeness in Appendix C although they are of no practical use in the case of cadmium sulphide due to their high optical losses.

With bulk modulators the light is unconfined both laterally and in the thickness dimension and therefore it is the diffraction of the beam which eventually limits the aperture of the structure[92]. Equation (5.4) gives the design criterion for a diffraction limited modulator;

$$d^2/_L = S^2 4\lambda/n\pi \qquad (5.4)$$

where d is the width, L the length, n the refractive index, λ the wavelength and S a safety factor made equal to six for ease of alignment. Planar optical waveguides benefit from the one dimensional confinement in the thickness direction enabling the electrodes to be brought closer together. The final width, however, still depends on the diffraction limit in the lateral dimension. This is overcome by using rectangular waveguides where no diffraction effects occur, but as will be discussed in part III these structures are very much more difficult to fabricate.

5.2 THE BASIC WAVEGUIDE EQUATIONS

The effect of refractive index anisotropy for the case of cadmium sulphide was considered in section 2.3 and found to be insignificant. Cadmium sulphide waveguides are therefore treated as isotropic in the following analysis.

The structure of Fig. 5.1a can be considered on the basis of a solution of 5 or 7 layers depending on whether the thicknesses of the metal electrodes are important. Calculations have shown metal thicknesses to be unimportant for electrodes of acceptable resistivity and thus only a five-layer lossy waveguide structure will be considered. The term lossy refers to the fact that each layer will be considered to have a complex dielectric constant (the real part relating to refractive index and the imaginary part relating to loss).

For time harmonic fields in linear isotropic, non-magnetic, source free media Maxwell's equations can be expressed as

$$\nabla x E = - \mu_o \dot{H} \tag{5.5}$$

$$\nabla x H = \varepsilon_o \underset{\sim}{n}^2 \dot{E} \tag{5.6}$$

$$\nabla \cdot E = 0 \tag{5.7}$$

$$\nabla \cdot H = 0 \tag{5.8}$$

Applying the appropriate vector identity yields from equations (5.5) - (5.8) the wave equation

$$\nabla^2 E = \mu_o \varepsilon_o \underset{\sim}{n}^2 \frac{\partial^2 E}{\partial t^2} \tag{5.9}$$

where $\underset{\sim}{n}$ is complex and equivalent to n - jk.

Applying the boundary conditions at each interface, equation (5.9) can be solved using the usual determinant relation[58] and the following transcendental (mode) equations derived after some algebraic manipulation;

$$\underset{\sim}{\gamma}_2 W = m\pi + \tan^{-1}\left(\frac{\underset{\sim}{P}}{\underset{\sim}{\gamma}_2}\right) + \tan^{-1}\left(\frac{\underset{\sim}{Q}}{\underset{\sim}{\gamma}_2}\right) \tag{5.10}$$

for TE waves, and

$$\underset{\sim}{\gamma}_2 W = m\pi + \tan^{-1}\left(\frac{\underset{\sim}{n}_2^2}{\underset{\sim}{n}_o^2}\frac{\underset{\sim}{P}'}{\underset{\sim}{\gamma}_2}\right) + \tan^{-1}\left(\frac{\underset{\sim}{n}_2^2}{\underset{\sim}{n}_4^2}\frac{\underset{\sim}{Q}'}{\underset{\sim}{\gamma}_2}\right) \tag{5.11}$$

for TM waves, where

$$\underset{\sim}{P} = j\underset{\sim}{\gamma}_1 \frac{\frac{\underset{\sim}{\gamma}_o}{j\underset{\sim}{\gamma}_1} + \tanh j\underset{\sim}{\gamma}_1 d_1}{1 + \frac{\underset{\sim}{\gamma}_o}{j\underset{\sim}{\gamma}_1}\tanh j\underset{\sim}{\gamma}_1 d_1} \tag{5.12}$$

$$\underset{\sim}{Q} = j\underset{\sim}{\gamma}_3 \frac{\frac{\underset{\sim}{\gamma}_4}{j\underset{\sim}{\gamma}_3} + \tanh j\underset{\sim}{\gamma}_3 d_3}{1 + \frac{\underset{\sim}{\gamma}_4}{j\underset{\sim}{\gamma}_3}\tanh j\underset{\sim}{\gamma}_3 d_3} \tag{5.13}$$

$$\underset{\sim}{P}' = j\underset{\sim}{\gamma}_1 \frac{\frac{\underset{\sim}{n}_1^2}{\underset{\sim}{n}_o^2}\left(\frac{\underset{\sim}{\gamma}_o}{j\underset{\sim}{\gamma}_1}\right) + \tanh j\underset{\sim}{\gamma}_1 d_1}{1 + \frac{\underset{\sim}{n}_1^2}{\underset{\sim}{n}_o^2}\left(\frac{\underset{\sim}{\gamma}_o}{j\underset{\sim}{\gamma}_1}\right)\tanh j\underset{\sim}{\gamma}_1 d_1} \tag{5.14}$$

$$\underset{\sim}{Q}' = j\underset{\sim}{\gamma}_3 \frac{\frac{\underset{\sim}{n}_3^2}{\underset{\sim}{n}_4^2}\left(\frac{\underset{\sim}{\gamma}_4}{j\underset{\sim}{\gamma}_3}\right) + \tanh j\underset{\sim}{\gamma}_3 d_3}{1 + \frac{\underset{\sim}{n}_3^2}{\underset{\sim}{n}_4^2}\left(\frac{\underset{\sim}{\gamma}_4}{j\underset{\sim}{\gamma}_3}\right)\tanh j\underset{\sim}{\gamma}_3 d_3} \tag{5.15}$$

$$\underset{\sim}{\gamma}_o = \left(\underset{\sim}{\beta}^2 - k_o^2 \underset{\sim}{n}_o^2\right)^{\frac{1}{2}} \tag{5.16}$$

$$\underset{\sim}{\gamma}_1 = \left(\underset{\sim}{\beta}^2 - k_o^2 \underset{\sim}{n}_1^2\right)^{\frac{1}{2}} \tag{5.17}$$

$$\underset{\sim}{\gamma}_2 = \left(k_o^2 \underset{\sim}{n}_2^2 - \underset{\sim}{\beta}^2\right)^{\frac{1}{2}} \tag{5.18}$$

$$\underset{\sim}{\gamma}_3 = \left(\underset{\sim}{\beta}^2 - k_o^2 \underset{\sim}{n}_3^2\right)^{\frac{1}{2}} \tag{5.19}$$

$$\underset{\sim}{\gamma}_4 = \left(\underset{\sim}{\beta}^2 - k_o^2 \underset{\sim}{n}_4^2\right)^{\frac{1}{2}} \tag{5.20}$$

$\underset{\sim}{\beta}$ is the complex phase constant $\underset{\sim}{\beta} = \beta' + j\beta''$ and k_o is the wave number. From equations (5.10) and (5.11) it is possible to plot the normalised phase constant(β'/k_o) and the attenuation (β'') versus guide thickness

for varying buffer thicknesses. A computer program was developed for this purpose and the flow diagram is contained in Appendix A3.

The mode equations reduce to those for a five-layer, lossless, isotropic structure when the imaginary component of the refractive index $\underset{\sim}{n}$ is set to zero. By setting $d_1 = d_3 = 0$ equations (5.10) and (5.11) reduce to the three layer isotropic situation described by equations (2.8) and (2.9) respectively thus confirming the validity of the above expressions.

5.3 PHASE CHANGE AND MODULATOR CALCULATIONS

5.3.1 PHASE CHANGE

The relation between phase change and applied voltage is obtained by differentiating the characteristic equations (5.10) and (5.11) with respect to the guide refractive index. It is not necessary at this stage to keep the generalised five-layer solutions. To simplify calculations a symmetrical structure will therefore be considered, ie $\underset{\sim}{n}_0 = \underset{\sim}{n}_4$, $\underset{\sim}{n}_1 = \underset{\sim}{n}_3$ and $d_1 = d_3 = d$. Thus equations (5.10) and (5.11) reduce to

$$W(k_{o\sim 2}^2 n_2^2 - \underset{\sim}{\beta}^2)^{\frac{1}{2}} = m\pi + 2\tan^{-1}\frac{(\underset{\sim}{\beta}^2 - k_{o\sim 1}^2 n_1^2)^{\frac{1}{2}}\left[\dfrac{(\underset{\sim}{\beta} - k_{o\sim o}^2 n_o^2)^{\frac{1}{2}}}{(\underset{\sim}{\beta}^2 - k_{o\sim 1}^2 n_1^2)^{\frac{1}{2}}} + \tanh(\underset{\sim}{\beta}^2 - k_{o\sim 1}^2 n_1^2)^{\frac{1}{2}} d\right]}{(k_{o\sim 2}^2 n_2^2 - \underset{\sim}{\beta}^2)^{\frac{1}{2}}\left[1 + \dfrac{(\underset{\sim}{\beta}^2 - k_{o\sim o}^2 n_o^2)^{\frac{1}{2}}}{(\underset{\sim}{\beta}^2 - k_{o\sim o}^2 n_o^2)^{\frac{1}{2}}} \tanh(\underset{\sim}{\beta}^2 - k_{o\sim 1}^2 n_1^2)^{\frac{1}{2}} d\right]} \quad (5.21)$$

for TE waves, and

$$W(k_{o\sim 2}^2 n_2^2 - \underset{\sim}{\beta}^2)^{\frac{1}{2}} = m\pi + 2\tan^{-1}\frac{\underset{\sim 2}{n^2}(\underset{\sim}{\beta}^2 - k_{o\sim 1}^2 n_1^2)^{\frac{1}{2}}\left[\dfrac{\underset{\sim 1}{n^2}(\underset{\sim}{\beta}^2 - k_{o\sim o}^2 n_o^2)^{\frac{1}{2}}}{\underset{\sim o}{n^2}(\underset{\sim}{\beta}^2 - k_{o\sim 1}^2 n_1^2)^{\frac{1}{2}}} + \tanh(\underset{\sim}{\beta}^2 - k_{o\sim 1}^2 n_1^2)^{\frac{1}{2}} d\right]}{\underset{\sim o}{n^2}(k_{o\sim 2}^2 n_2^2 - \underset{\sim}{\beta}^2)^{\frac{1}{2}}\left[1 + \dfrac{\underset{\sim 1}{n^2}(\underset{\sim}{\beta}^2 - k_{o\sim o}^2 n_o^2)^{\frac{1}{2}}}{\underset{\sim o}{n^2}(\underset{\sim}{\beta}^2 - k_{o\sim 1}^2 n_1^2)^{\frac{1}{2}}} \tan(\underset{\sim}{\beta}^2 - k_{o\sim 1}^2 n_1^2)^{\frac{1}{2}} d\right]} \quad (5.22)$$

for TM waves.

Equations (5.21) and (5.22) can then be differentiated with respect to $\underset{\sim}{n}_2$ to yield expressions for $d\underset{\sim}{\beta}$ in terms of $d\underset{\sim}{n}_2$. For TE guided modes the expression is;

$$d\underset{\sim}{\beta} = \frac{k_o^2 n_2^2 \frac{W}{\gamma_2} + 2\cos^2\phi k_o^2 n_2 Y}{2\cos^2\phi \underset{\sim}{\beta}(X+Y+\frac{Z}{\underset{\sim}{\gamma}_1})\frac{\beta W}{\underset{\sim}{\gamma}_2}} d\underset{\sim}{n}_2 \qquad (5.23)$$

where

$$X = \underset{\sim}{\gamma}_1 \frac{\left[\underset{\sim}{\gamma}_2(\underset{\sim}{\gamma}_1 + \underset{\sim}{\gamma}_o \tanh \underset{\sim}{\gamma}_1 d)\right] - \underset{\sim}{\gamma}_1\underset{\sim}{\gamma}_2(\underset{\sim}{\gamma}_o + \underset{\sim}{\gamma}_1 \tanh \underset{\sim}{\gamma}_1 d)\tanh \underset{\sim}{\gamma}_1 d}{\underset{\sim}{\gamma}_o\left[\underset{\sim}{\gamma}_2(\underset{\sim}{\gamma}_1+\underset{\sim}{\gamma}_o \tanh \underset{\sim}{\gamma}_1 d)\right]^2} \qquad (5.24)$$

$$Y = \frac{\underset{\sim}{\gamma}_1 (\underset{\sim}{\gamma}_o+\underset{\sim}{\gamma}_1 \tanh \underset{\sim}{\gamma}_1 d)(\underset{\sim}{\gamma}_1+\underset{\sim}{\gamma}_o \tanh \underset{\sim}{\gamma}_1 d)}{\underset{\sim}{\gamma}_2\left[\underset{\sim}{\gamma}_2(\underset{\sim}{\gamma}_1+\underset{\sim}{\gamma}_o \tanh \underset{\sim}{\gamma}_1 d)\right]^2} \qquad (5.25)$$

$$Z = \frac{(\underset{\sim}{\gamma}_o+2\underset{\sim}{\gamma}_1 \tanh \underset{\sim}{\gamma}_1 d)}{\underset{\sim}{\gamma}_2(\underset{\sim}{\gamma}_1+\underset{\sim}{\gamma}_o \tanh \underset{\sim}{\gamma}_1 d)} + \frac{\underset{\sim}{\gamma}_1^2 d\,\mathrm{sech}^2 \underset{\sim}{\gamma}_1 d}{\underset{\sim}{\gamma}_2(\underset{\sim}{\gamma}_1+\underset{\sim}{\gamma}_o \tanh \underset{\sim}{\gamma}_1 d)}$$

$$- \frac{\underset{\sim}{\gamma}_2\underset{\sim}{\gamma}_1(\underset{\sim}{\gamma}_o+\underset{\sim}{\gamma}_1 \tanh \underset{\sim}{\gamma}_1 d)\ (1+\underset{\sim}{\gamma}_o d\,\mathrm{sech}^2 \underset{\sim}{\gamma}_1 d)}{\left[\underset{\sim}{\gamma}_2(\underset{\sim}{\gamma}_1+\underset{\sim}{\gamma}_o \tanh \underset{\sim}{\gamma}_1 d)\right]^2} \qquad (5.26)$$

$$\phi = \tan^{-1} \frac{\underset{\sim}{\gamma}_1(\underset{\sim}{\gamma}_o+\underset{\sim}{\gamma}_1 \tanh \underset{\sim}{\gamma}_1 d)}{\underset{\sim}{\gamma}_2(\underset{\sim}{\gamma}_1+\underset{\sim}{\gamma}_o \tanh \underset{\sim}{\gamma}_1 d)} \qquad (5.27)$$

Using equations (5.3) and (5.23) the general expression for phase change in terms of electric field across the guide can be derived.

$$d\beta' = \mathrm{Re}\left[F(W,d,\underset{\sim}{\beta})\right] \cdot d\underset{\sim}{n}$$

$$\approx -\tfrac{1}{2} rn^3 E \cdot \mathrm{Re}\left[F(W,d,\underset{\sim}{\beta})\right] \qquad (5.28)$$

where $F(W,d,\underset{\sim}{\beta})$ is a function of guide thickness, buffer thickness and phase constant defined by equation (5.23).

To complete the understanding of the device, the electric field of equation (5.28) must be correlated with the voltage applied between the metal electrodes, V_{TOT}. The various layers can be thought of as individual capacitors, all connected in series. The phase change $\Delta\phi$ in terms of the voltage driving the modulator is then given by

$$\Delta\phi = - \frac{\frac{1}{2}rn^3 \mathrm{Re}\left[F(W,d,\underset{\sim}{\beta}) \right] V_{TOT} \varepsilon_1'^2}{(2d\varepsilon_1'\varepsilon_2' + W\varepsilon_1'^2)} \qquad (5.29)$$

where ε_1' and ε_2' are the real parts of the complex dielectric constants of the buffer and guiding films respectively.

The theoretical performance of a multilayer electrooptic phase modulator is fully described by equations (5.10), (5.11), (5.23) and (5.29).

5.3.2 MODULATION ENHANCEMENT

In bulk electrooptic modulators the normalised phase change that occurs is equal to the refractive index change induced and thus always has a modulation sensitivity equal to unity. Fig. 5.2 illustrates an interesting phenomenon which occurs with the Al-SiO-CdS-SiO-Al waveguide modulator and similar structures[94]. For high order modes in this well confined structure a modulation sensitivity of greater than unity is realised for propagation constants slightly away from cut-off; that is, the phase change occurring for a given refractive index change (or applied voltage) can be greater for a waveguide modulator with low refractive index buffer layers than for a similar bulk modulator. Indeed the larger the refractive index difference between the guide and buffer films (tighter mode confinement) the greater the enhancement that occurs. It is possible to have an enhancement three times that of the bulk modulator counterpart[94].

The physical significance of the effect can be explained by considering the ray optics analogy for light propagating in a thin

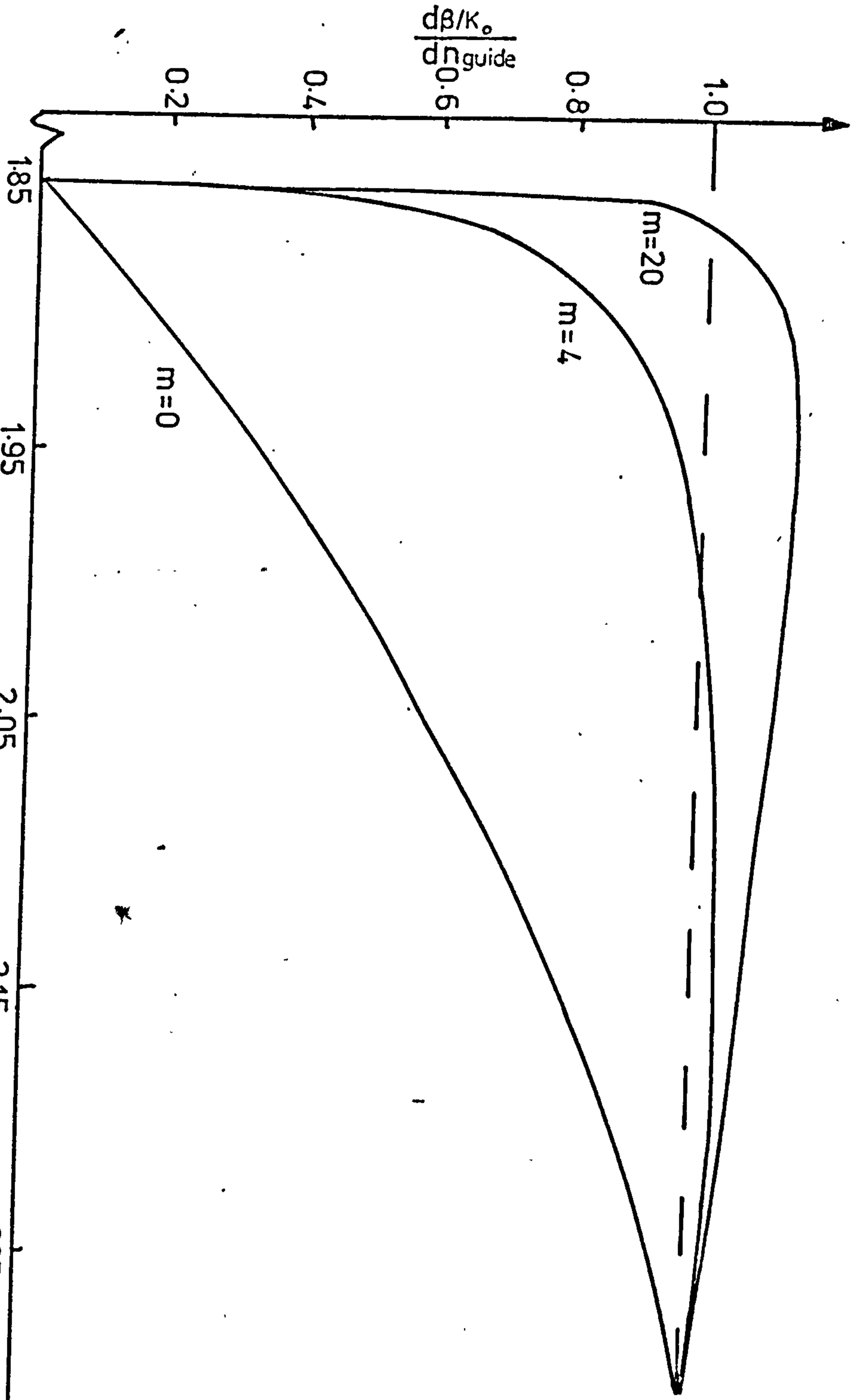

FIGURE 5.2 Modulation sensitivity enhancement

film. Normally the amount of optical power travelling in the guide is low for higher order modes due to the large evanescent fields penetrating into the buffer layers. However, with a large refractive index difference between the guide and buffer layers the wave is more tightly confined within the guide and more optical power is carried in that region. The external electric field applied across the electrooptic guide thus has a greater effect on the optical wave. The zig-zag path of the wave through the guide is much greater in length for the higher order modes and the result is a modulation sensitivity of greater than unity. This effect has not been seriously considered in the case of cadmium sulphide as the attenuation of the higher order modes was too severe.

5.4 OPTIMISATION OF THE Al-SiO-CdS-SiO-Al MODULATOR STRUCTURE

The Al-SiO-CdS-SiO-Al multilayer (Fig. 5.1a) was used for the modulation experiments of chapter 6 and in the following sub-sections calculations for this specific device are presented.

5.4.1 PARAMETERS GOVERNING MODE PROPAGATION

The normalised waveguide propagation constant for TE (m = 0, 1, 2 and 3) modes as a function of guide thickness is shown in Fig. 5.3 for fixed buffer layer thicknesses of 0.1 μm and 0.5 μm. The form of the curve is similar to that of a conventionally bounded guide without the presence of metal electrodes but deviations occur near cut-off as the buffer thickness decreases. In this situation the evanescent fields will penetrate through the buffer layers and be influenced by the metal electrodes. The increasing attenuation rate for higher mode numbers for a fixed buffer layer thickness of 0.5 μm is illustrated in Fig. 5.4 while Fig. 5.5 depicts the manner in which additional TE_o mode attenuation decreases with increasing buffer thickness. Both curves agree with physical representation of the

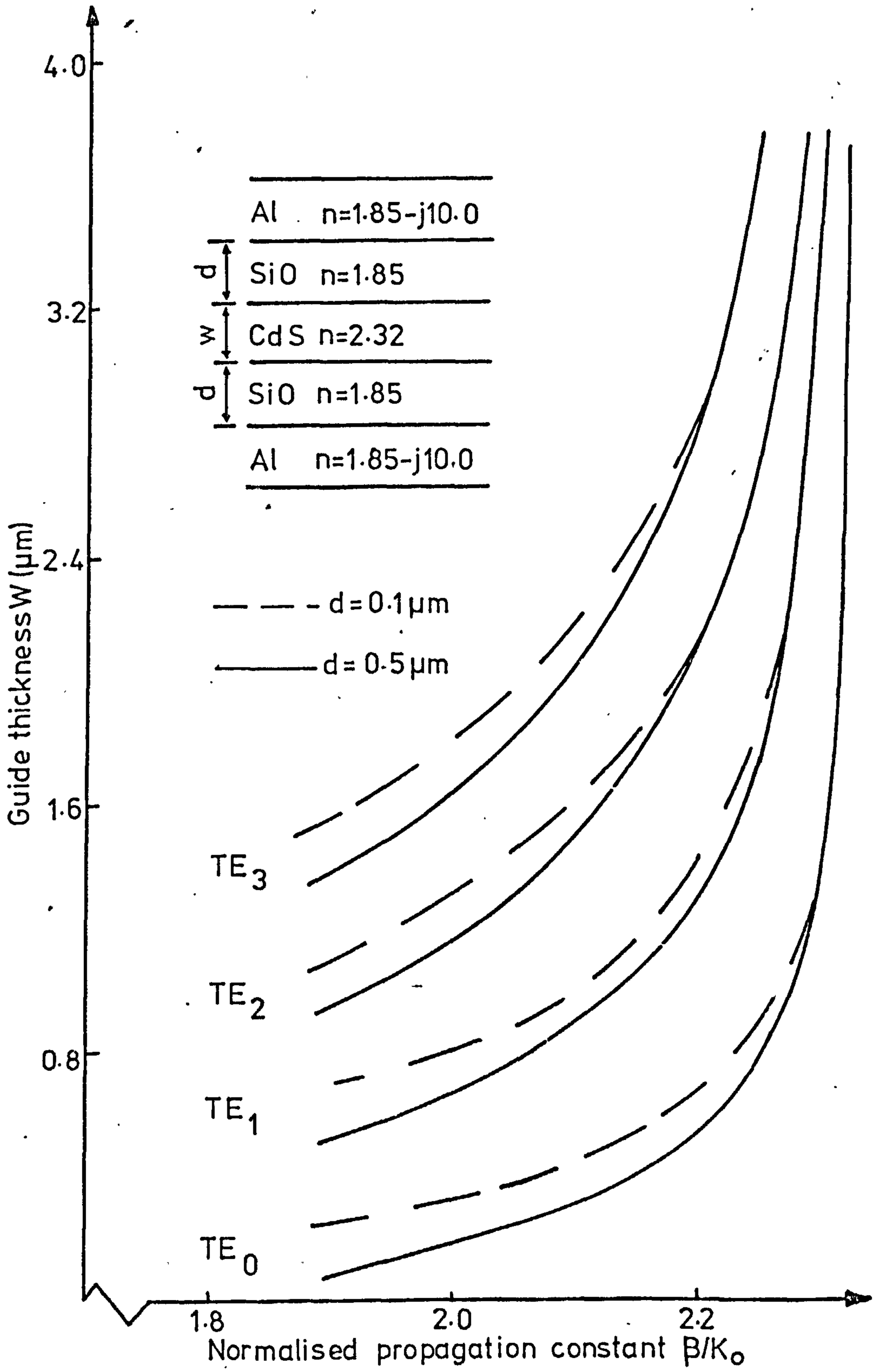

FIGURE 5.3 Guide thickness versus normalised propagation constant

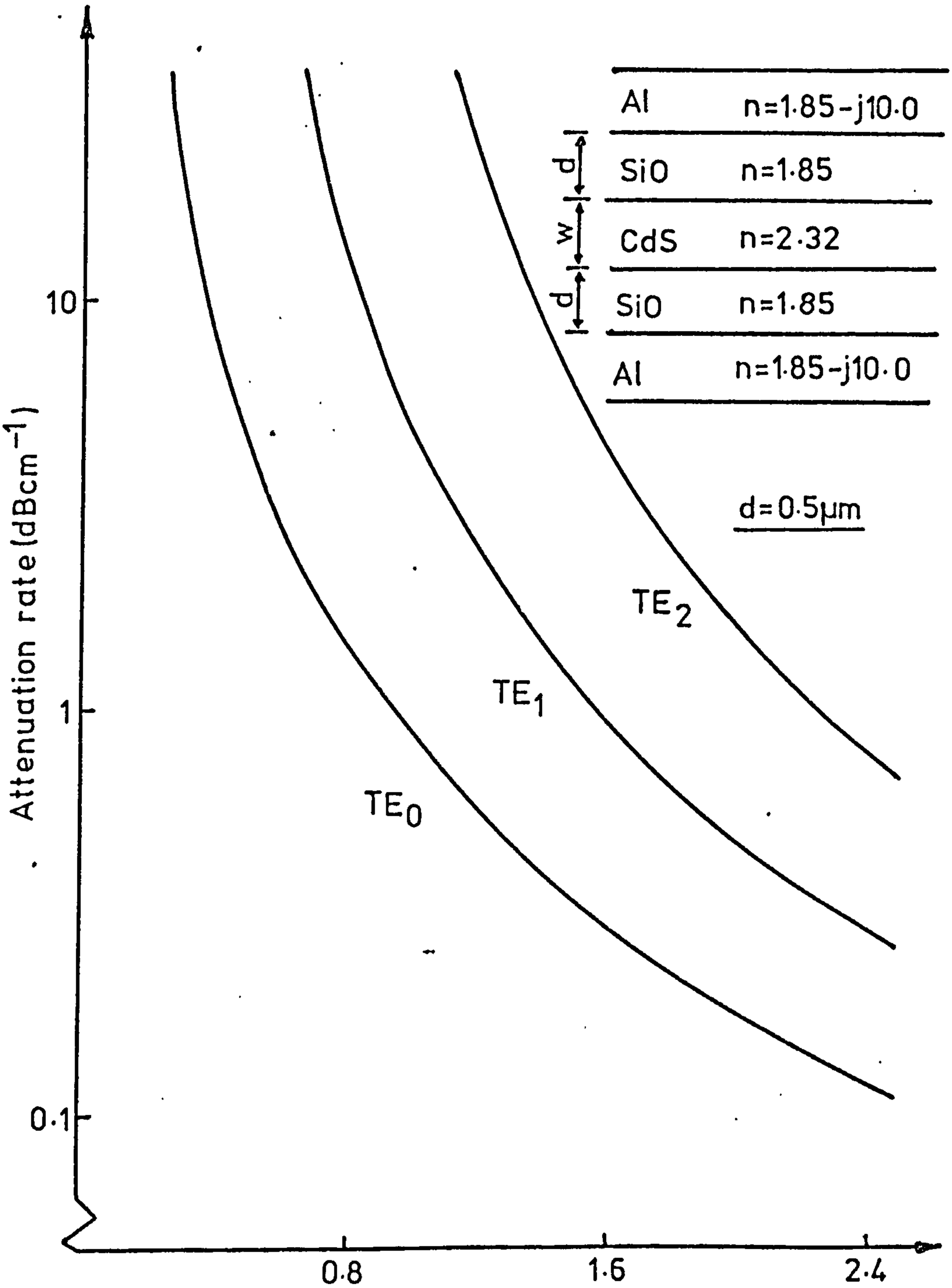

FIGURE 5.4 Attenuation rate versus guide thickness

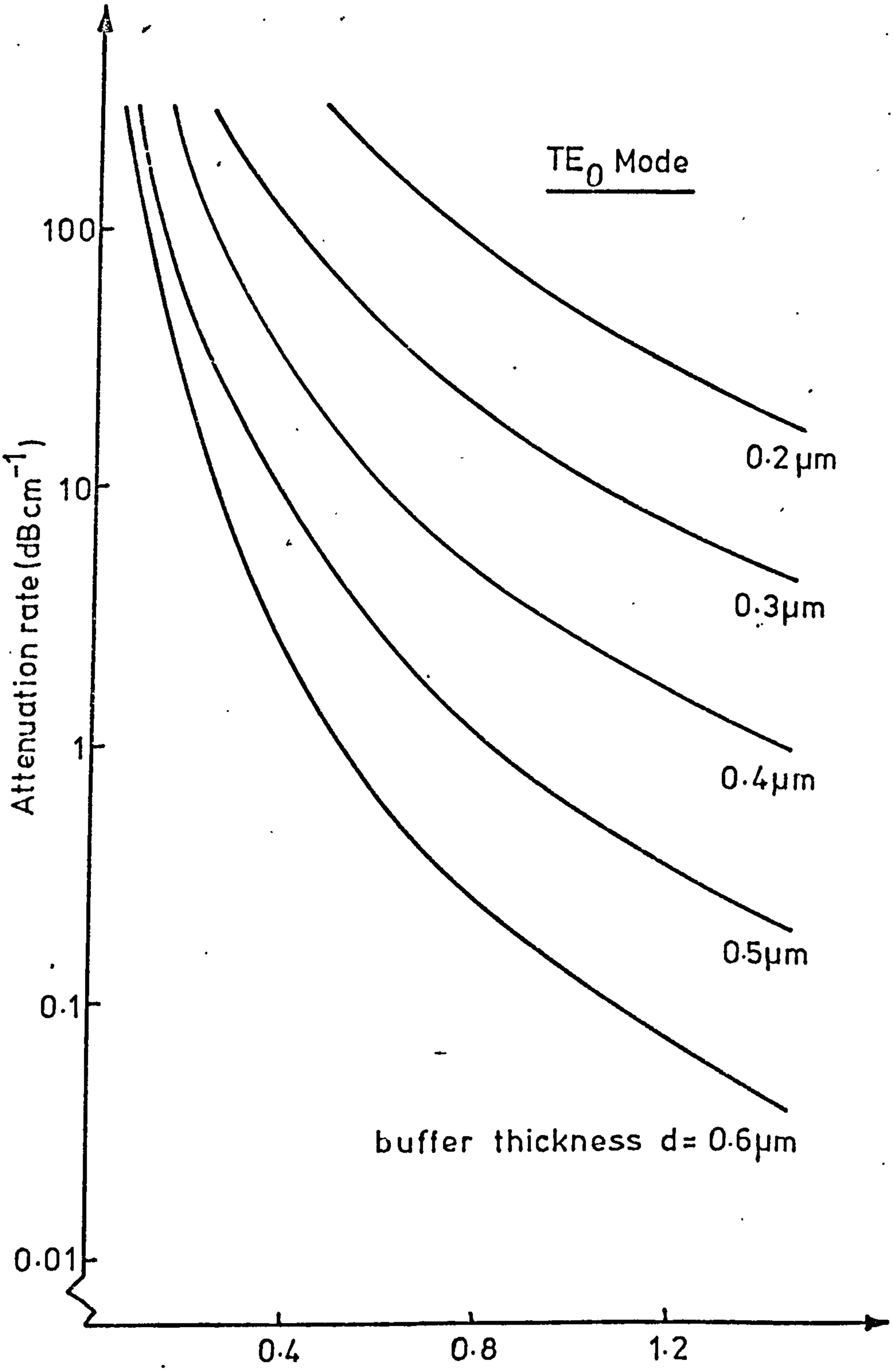

FIGURE 5.5 Attenuation rate versus guide thickness

evanescent field penetrating through the buffer layers to the metal electrodes. The variation of $\Delta\phi$ with guide thickness for the TE (m = 0, 1 and 2) modes is shown in Fig.5.6 (constant buffer layer thickness) while decreasing buffer thickness causes an increase in $\Delta\phi$ for all values of guide thickness (Fig. 5.7). Both Figs. 5.6 and 5.7 illustrate that $\Delta\phi$ passes through a maximum value which depends on the order of the propagating mode, the guide thickness and the buffer layer thickness. Fig. 5.8 further emphasises the very sharp peak for optimum guide and buffer thicknesses by illustrating an isometric plot of phase change for the TE_o mode. The physical explanation of the maximum in $\Delta\phi$ is as follows; for large guide thicknesses $\Delta\phi$ is small since the electric field strength responsible for the refractive index changes will be small for a given voltage applied to the complete structure. As the guide thickness is reduced so the electric field strength across the guide increases resulting in an increase in $\Delta\phi$. However, as the guide thickness approaches the cut-off value so $\Delta\phi$ will again decrease due to a smaller proportion of the total power of the guided mode being carried within the electrooptic waveguide.

In a practical modulator structure, buffer layer thicknesses cannot be reduced indefinitely to take advantage of the concomitant increase in $\Delta\phi$. The effects of increasing attenuation rate must also be considered. A compromise must therefore be reached between an useful value of $\Delta\phi$ and an acceptable additional attenuation resulting from the presence of the metal electrodes. A series of constant attenuation rate and phase change contours were therefore drawn on the axes of buffer layer thickness versus guide thickness to assist with the modulator design. The contours for the Al-SiO-CdS-SiO-Al structure are shown in Fig. 5.9 are are similar to those presented by Chang and Loh[95] for two 10.6 μm modulator structures based on single crystal gallium arsenide films. It is important to emphasise

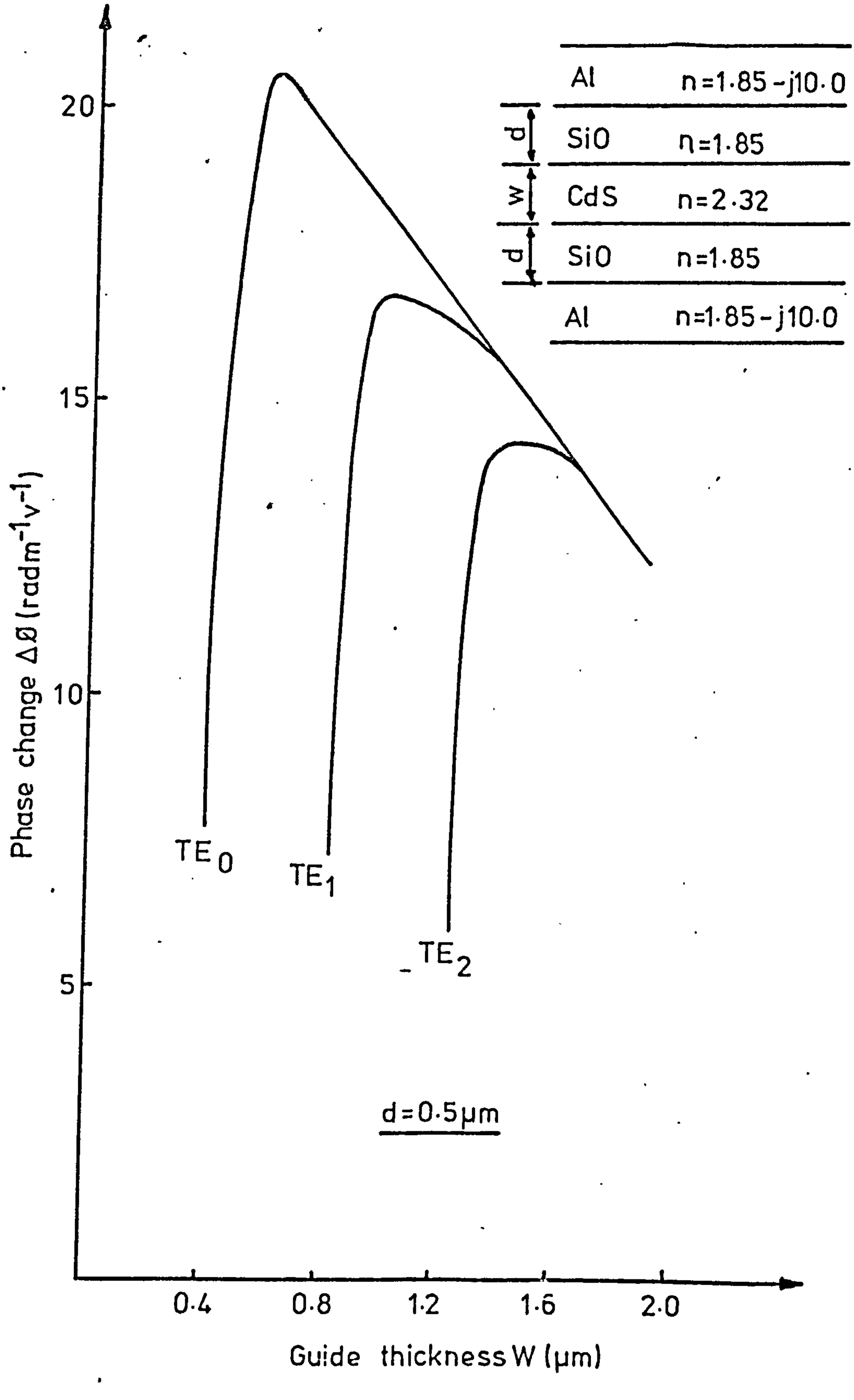

FIGURE 5.6 Phase change versus guide thickness

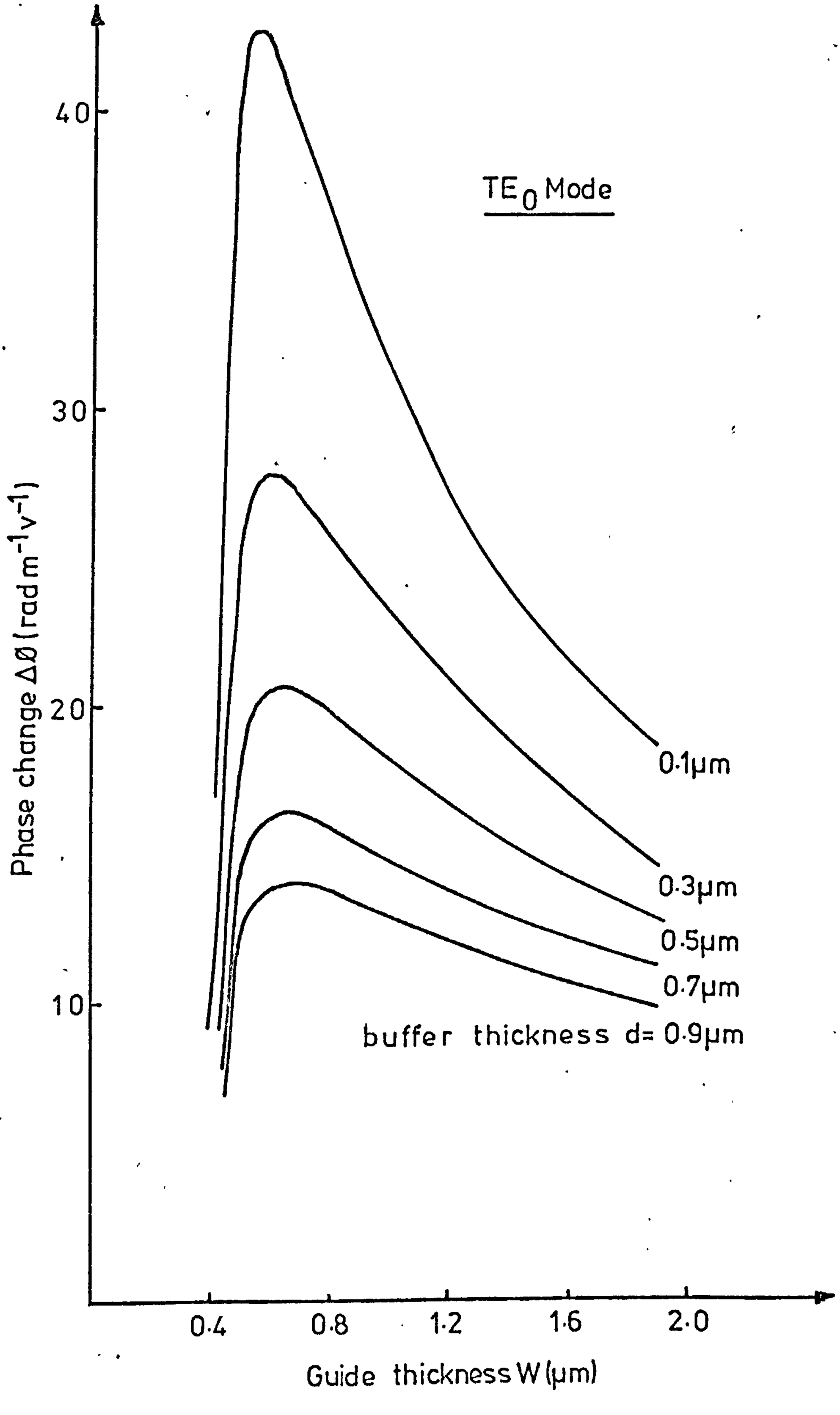

FIGURE 5.7 Phase change versus guide thickness

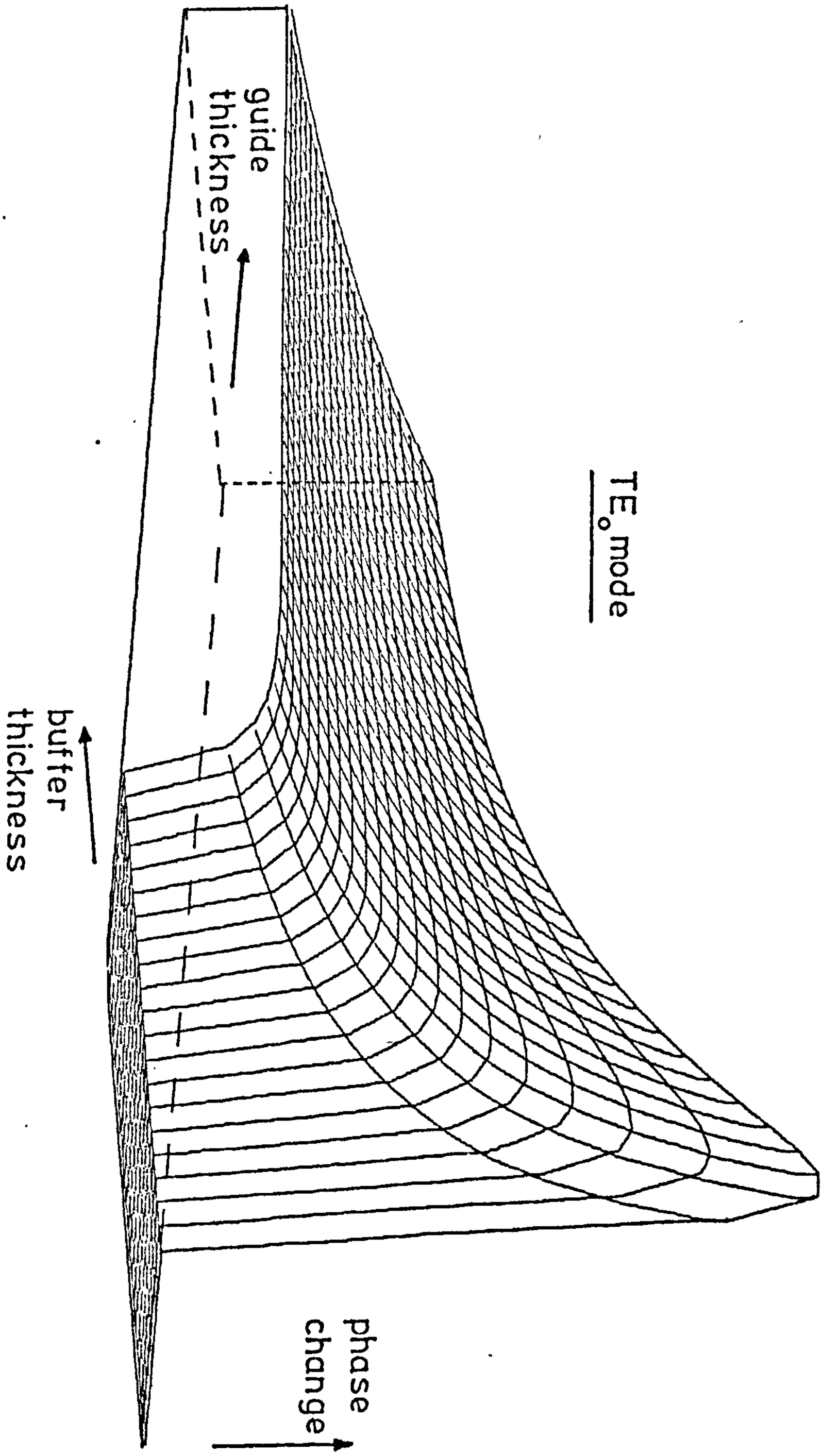

FIGURE 5.8 Isometric plot of phase change

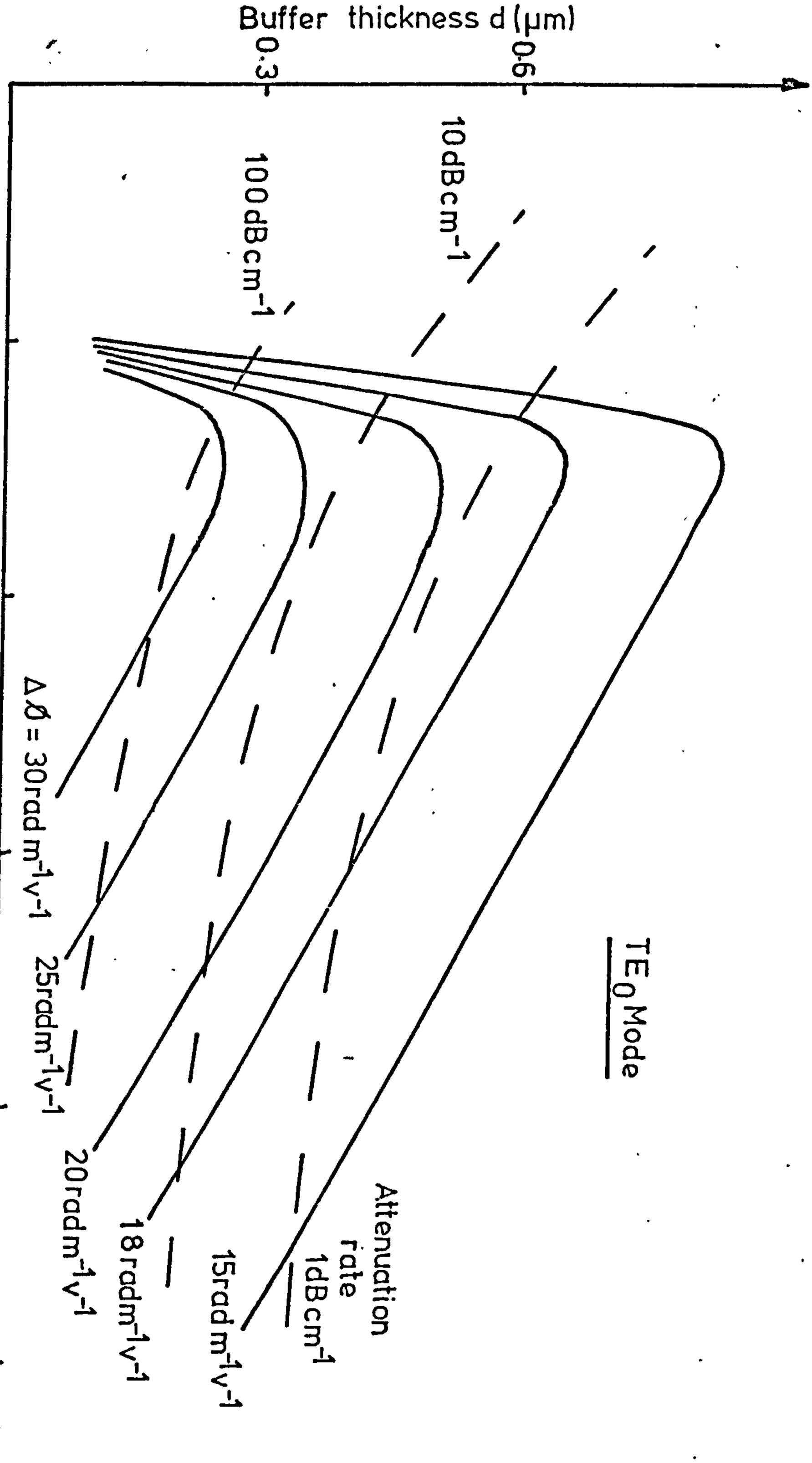

FIGURE 5.9 Constant phase change and attenuation rate contours

that the attenuation rate contours represent the additional attenuation introduced by the aluminium metal electrodes and do not include the inherent losses of the waveguide, ie scatter and absorption losses.

5.4.2 MINIMISATION OF DRIVE POWER

The modulator design is optimised on the basis of minimising a figure of merit, the power per unit bandwidth expressed as $mWMHz^{-1}$. Power per unit bandwidth P is given by

$$P = \pi C_m V_{TOT}^2 \qquad (5.30)$$

where C_m is the modulator capacitance. It is evident that a reduction in voltage is more effective in minimising P than a reduction in capacitance. This is equivalent to maximising the phase change $\Delta\phi$ of Fig. 5.9. An acceptable additional loss figure of 1 $dBcm^{-1}$ was chosen and the loss contour traced until $\Delta\phi$ is a maximum. The corresponding guide and buffer layer thicknesses were noted. At an attenuation rate of 1 $dBcm^{-1}$ the maximum phase change for the Al-SiO-CdS-SiO-Al structure is 19.5 $radm^{-1}V^{-1}$ for a guide thickness of 0.65 μm and buffer thicknesses of 0.55 μm. In a planar guide the mode is unbounded in the lateral direction and the minimum electrode width calculated from equation (5.4) was 500 μm including a safety factor of S = 6. For an electrode length of 10 mm, the total capacitance of the modulator would be 122 pF and the maximum base bandwidth with a 50Ω load would be 50 MHz. The theoretical power per unit bandwidth figure for a 1.15 μm TE_o guided mode and one radian phase change would be 10.0 $mWMHz^{-1}$.

5.4.3 MINIMISATION OF DRIVE POWER CONSIDERING CADMIUM SULPHIDE WAVEGUIDE LOSS

The loss contours of Fig. 5.9 illustrated the additional loss occurring in the structure due to the presence of metal elec-

trodes and optimisation along these curves is only possible if losses from other sources (eg waveguide) are less prevalent. As predicted from the loss measurements on basic cadmium sulphide waveguides (Fig. 4.9) modulators with guide thicknesses of less than 1 μm will possess large waveguide attenuation. A new optimum modulator design must therefore be sought in which the scatter and absorption losses of the cadmium sulphide are taken into account. This is achieved by following the 0.5 $dBcm^{-1}$ additional loss contour of Fig. 5.9 until an acceptable guide thickness is reached for which the contribution to loss from the amorphous region of the cadmium sulphide film is not dominant. The corresponding value of $\Delta\phi$ represents the maximum attainable phase change in a realistic modulator, ie a modulator in which the total losses, including waveguide and electrode attenuation, are acceptable. A guide thickness of 1.4 μm and buffer layer thicknesses of 0.45 μm give a phase change of 0.16 $radV^{-1}$ for an electrode length of 10 mm. The associated modulator capacitance and power per unit bandwidth are 94 pF and 11.2 $mWMHz^{-1}$ for $\Delta\phi$ = 1 radian respectively. The maximum base bandwidth into a 50Ω load is 68 MHz.

It should be pointed out that although silicon monoxide was chosen as the buffer layer improved modulator performance should theoretically be possible if a material with a lower refractive index and higher dielectric constant, such as magnesium fluoride, could be used. The low refractive index would lead to tighter confinement of the mode and hence thinner buffer layers could be deposited for a similar additional electrode attenuation. Higher buffer layer capacitance and consequently a smaller voltage drop across the buffer layers would then be possible through the reduced thickness and higher dielectric constant.

The possibility of using a low loss waveguide with cadmium sulphide electrooptic buffer layers was considered as a way of overcoming the high attenuation losses of the cadmium sulphide. However, for low drive power modulation most of the optical power must propagate in the electrooptic regions. The lowest drive power will result when the waveguide thickness becomes zero thus reverting to the situation already considered. For the lowest drive power modulation in a particular waveguide situation the electrooptic material should be made the waveguide.

CHAPTER 6: ELECTROOPTIC PHASE MODULATION IN CADMIUM SULPHIDE

At the start of this research only a few electrooptic modulator structures had been demonstrated[10,11] with power per unit bandwidths similar to those predicted in chapter 5 for the cadmium sulphide modulator. Recently, however, several modulators based on titanium diffused lithium niobate waveguides have shown exceptionally low power per unit bandwidth figures[55] (1.7 $\mu W\ MHz^{-1}$ for 1 radian phase change at 0.633 μm). With the exception of a zinc oxide structure[54] all reported modulators rely on the electrooptic effect in a waveguiding film supported on a single crystal substrate.

Although the modulators described in this chapter do not compare with recent devices in terms of their power per unit bandwidth figures they are important because of their method of fabrication. The structure is completely evaporated and uses well oriented polycrystalline films of cadmium sulphide grown on amorphous, low refractive index substrates. This not only enables a multilayer stacked structure to be employed but allows highly efficient phase matched coupling of the high refractive index waveguide to a low refractive index silica fibre, a problem that has not been satifactorily solved for any other modulator. If the waveguide losses for cadmium sulphide could be made comparable to titanium diffused lithium niobate waveguides then very low modulator drive powers will be possible.

The waveguides used in the following phase modulation experiments were all multimode but efficient excitation of a single discrete mode was possible. Since the scattering between the modes was small the propagating power was retained by the launched mode. Although TM modes were subject to the larger r_{33} electrooptic coefficient only the TE_o mode was considered because of the high waveguide losses of the other modes.

The structure fabrication is discussed in section 6.1 and the

experimental apparatus used for the analysis of the modulator performances described in section 6.2. The results of these analyses are presented in section 6.3 and discussed in section 6.4. In section 6.5 a composite modulator structure which should permit highly efficient fibre-film coupling is discussed and the results presented. Concluding remarks on the electrooptic slab waveguide modulator are given in section 6.6.

6.1 STRUCTURE FABRICATION

Although all the theoretical and empirical knowledge was available to fabricate the phase modulator there were several experimental difficulties to overcome before the device could finally be produced. These were entirely associated with the differential expansion between the various layers which made up the multilayer dielectric stack. Problems occurred with the adhesion of the top buffer layer to the evaporated cadmium sulphide waveguide which manifested itself as either crazing of the buffer layer or both the cadmium sulphide film and the buffer layer. The sputtering of insulators such as 7059 glass and silicon dioxide proved unsuitable owing to surface damage of the cadmium sulphide from back sputtering. Evaporated glass and silicon dioxide films crazed on exposure to the atmosphere. Silicon monoxide was selected because of its thermal compatability with cadmium sulphide even though its high refractive index of 1.85 at 1.15 μm meant that slightly thicker buffer layers were required. Its dielectric constant of 4.72, however, partly compensated for the thicker buffer layers by increasing the capacitance of the buffer layers and so reducing the voltage dropped across them.

The aluminium electrodes and silicon monoxide buffer layers were evaporated in a conventional diffusion pumped coating unit (Edwards High Vacuum 12E) while the cadmium sulphide layers were grown

by the method described in chapter 3. The successive layers were deposited through straight-edge masks. The top electrode pattern with electrodes of 0.5 x 5mm^2 to 5 x 5 mm^2 area was defined in photo-resist and the aluminium electrodes formed using the "lift-off" technique. Thermal expansion problems during the deposition of the silicon monoxide meant that it had to be evaporated for 30 second periods with 10 minutes between the evaporations to prevent the substrate temperature rising more than 3^{o}C. Alternatively, radiation shields could have been employed to prevent the substrate temperature rising. For good adhesion of silicon monoxide to cadmium sulphide the silicon monoxide must be evaporated onto a cold substrate. A check on the refractive index of the silicon monoxide using Abeles method[90] confirmed that the material, with a refractive index of 1.85 at a wavelength of 1.15 μm, was consistently near the monoxide rather than the dioxide of silicon.

Several structures were fabricated with varying guide and buffer layer thicknesses to verify the theory of chapter 5. A scanning electron micrograph of one such structure is shown in Fig. 6.1.

6.2 PHASE CHANGE MEASUREMENT TECHNIQUES

Coupling of the 1.15 μm radiation into and out of the cadmium sulphide modulator structure was achieved by means of rutile prism couplers. The phase measurements were made in the interferometers illustrated in Fig. 6.2. Both homodyne and heterodyne detection were employed as ways of determining the electrooptically induced phase changes. The Bragg cell, used for producing a frequency shifted reference signal for heterodyne detection, was removed from the apparatus during the homodyne measurements. A photodetector with the necessary sensitivity and response was also an important consideration.

6.2.1 DETECTOR CONSIDERATIONS

1.15 μm lies in a region of the spectrum where there is a

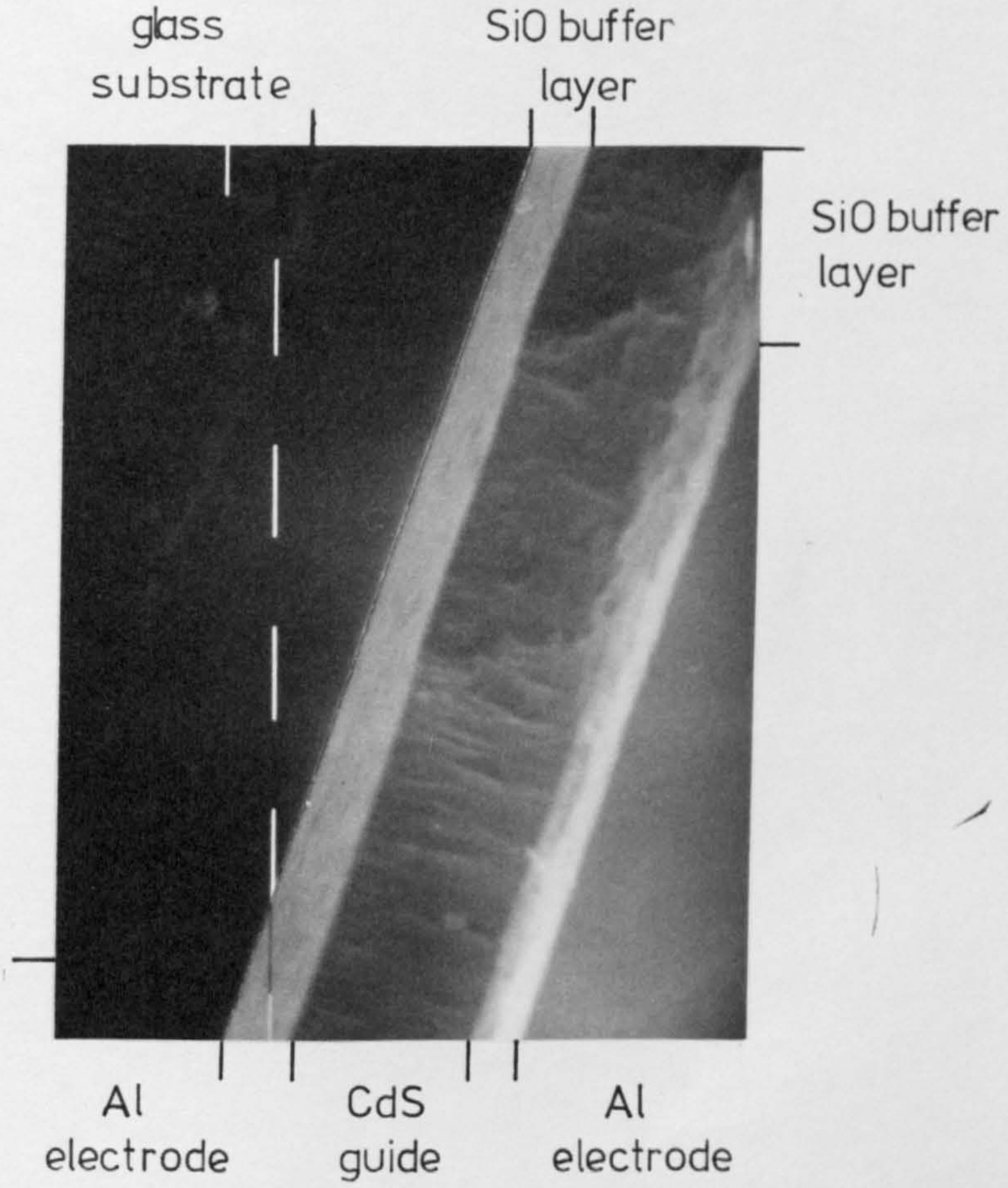

FIGURE 6.1 Scanning electron micrograph of cleaved edge of a multilayer Al-SiO-CdS-SiO-Al modulator (magnification 10K)

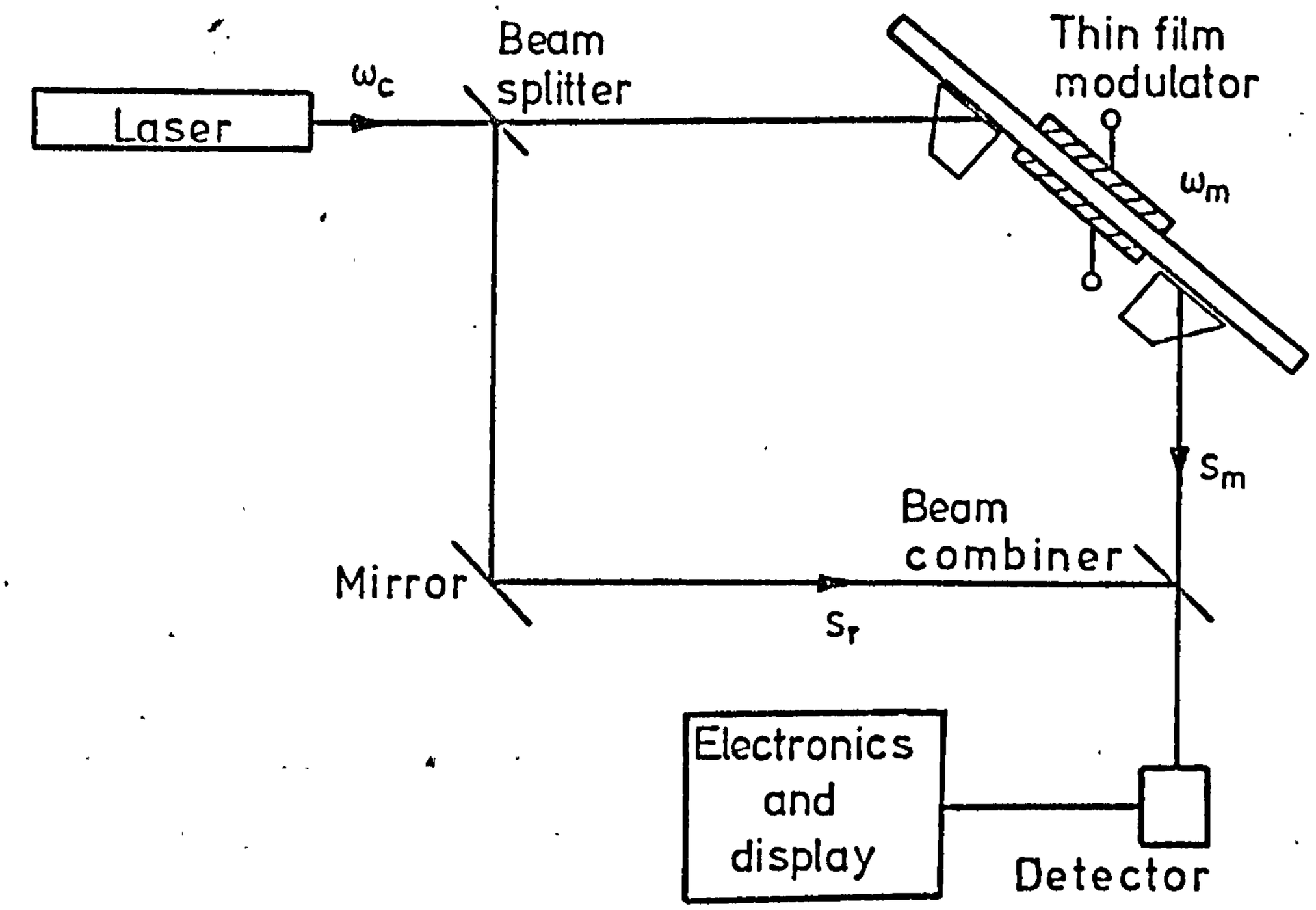

(a) Homodyne detection

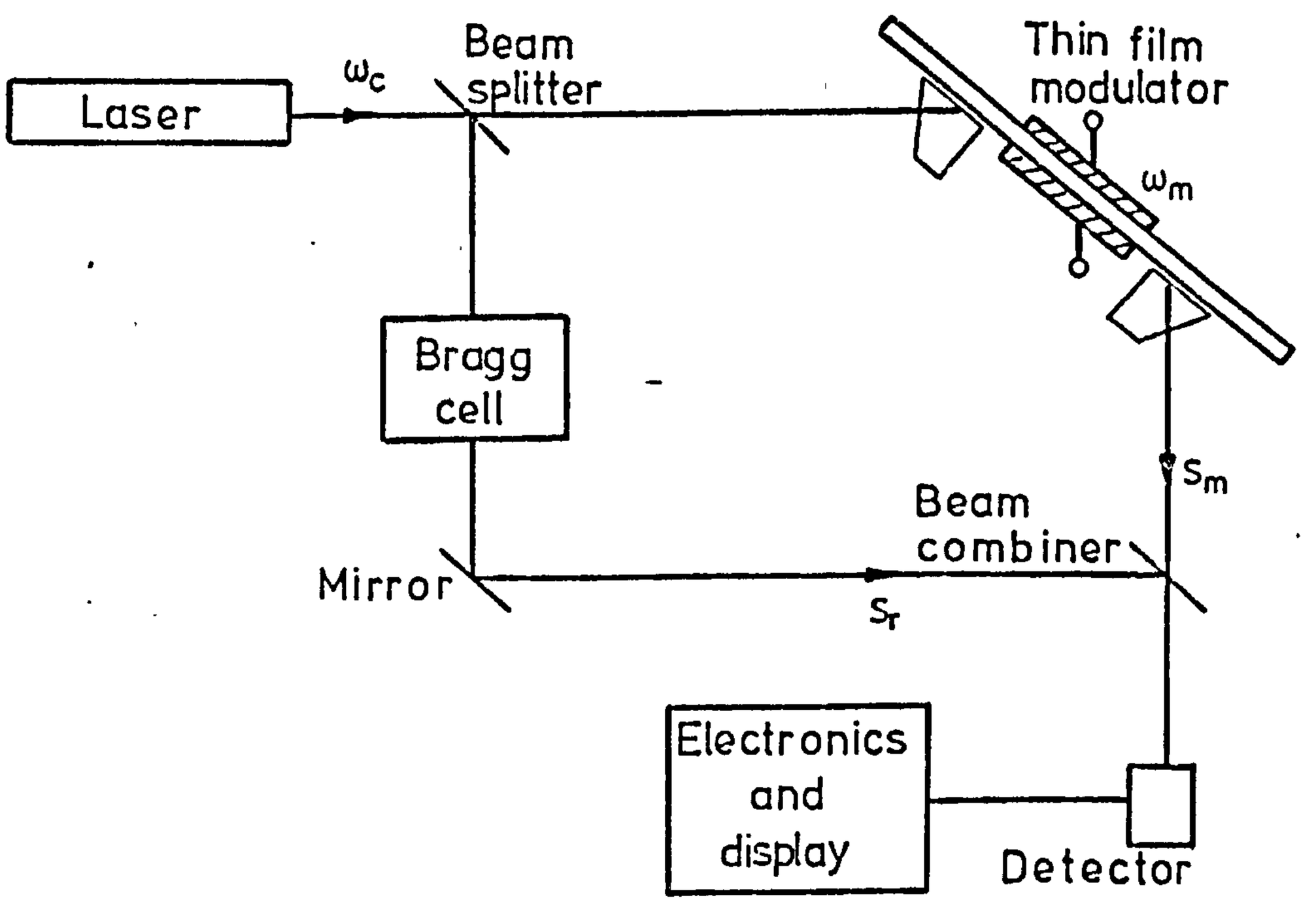

(b) Heterodyne detection

FIGURE 6.2 Interferometer detection systems

dearth of detectors with both a high sensitivity and a fast response. For high sensitivity a germanium detector is ideal but in its normal mode of operation is very slow (typically 50 kHz). Silicon detectors, which have a fast response time, have low sensitivity at 1.15μm and even those enhanced for 1.06 μm operation have a small gain-bandwidth product at 1.15μm. The near infrared detectors, such as indium antimonide and indium arsenide, although possessing good response times have very little sensitivity at 1.15 μm. The germanium avalanche photodetector is the only device with both the required sensitivity and response time to suit the modulator experiments. Due to their low production yield such devices are not manufactured commercially; however, one was obtained from the United States Air Force and without it the results of section 6.3 could not have been obtained. The device was a TIXL 57 germanium avalanche photodetector with a TIXL151 trans-impedance amplifier. The detector circuit is shown in Fig. 6.3.

6.2.2 HOMODYNE DETECTION

In theory homodyne detection optical signals is a simpler technique than heterodyne detection but in practice demands better mechanical stability of the optical equipment. Homodyne detection essentially involves the mixing of a signal and reference beam on the surface of a square-law response photodetector. The local oscillator (reference beam) is set to the same frequency as the carrier and the beams must be collinearly incident on the detector surface to prevent phase cancellation[96,97]. When the reference beam is a proportion of light split from the main beam (Fig. 6.2a) it is more difficult to lock the phases of the two beams.

The signal from the reference arm is given by;

$$S_r = E_r \cos(\omega_c t + \phi_r) \qquad (6.1)$$

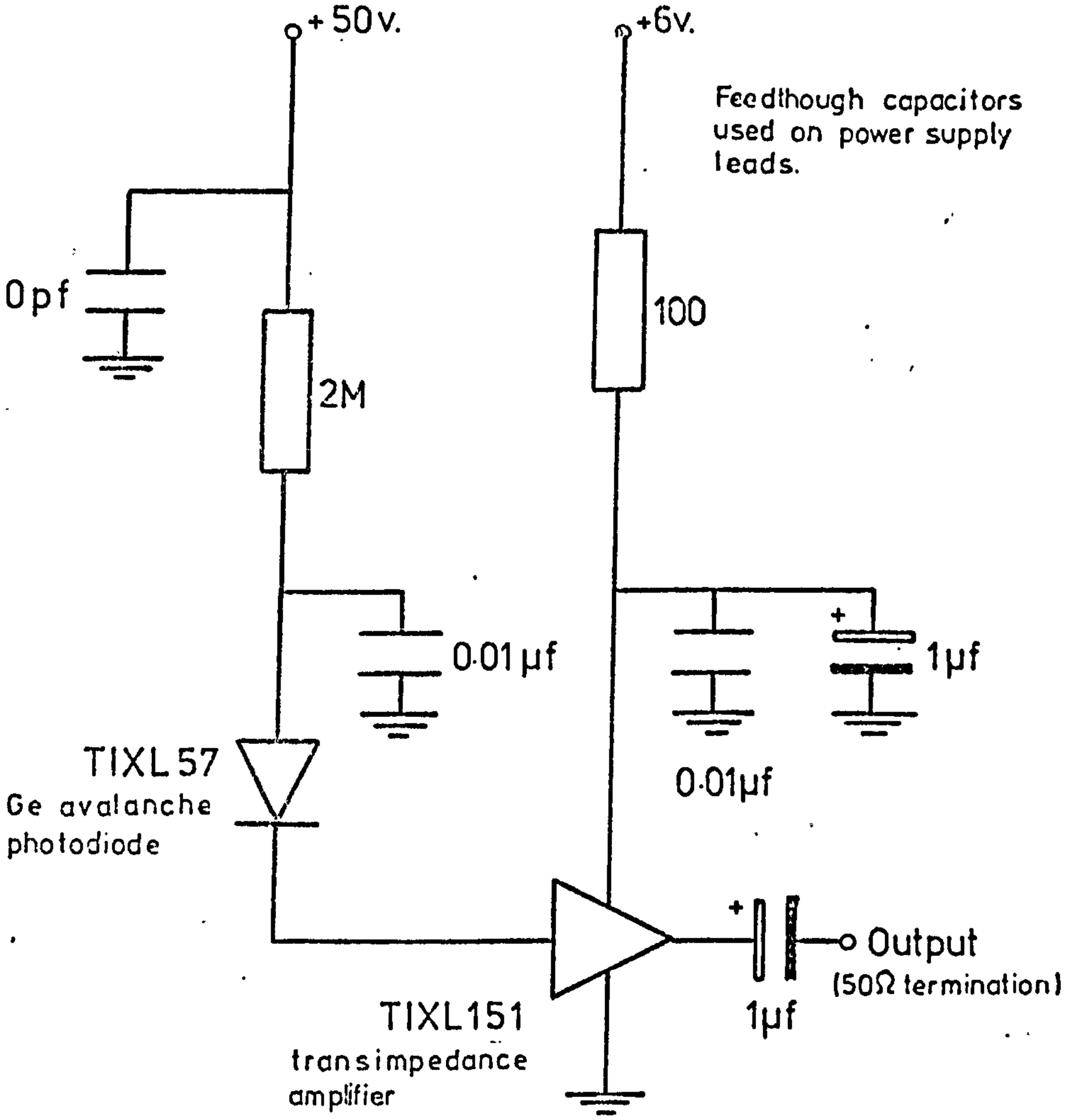

FIGURE 6.3 Germanium avalanche detector electronics

where E_r is the optical field amplitude, ω_c is the carrier frequency and ϕ_r is the static phase shift in the reference arm. The signal from the modulator is;

$$S_m = E_m \cos (\omega_c t + \alpha \sin \omega_m t + \phi_m) \qquad (6.2)$$

where E_m is the optical field amplitude, ω_m the modulating frequency, ϕ_m the static phase shift in the signal path and α is the maximum phase change in the modulator. It is important to appreciate that α is directly proportional to the voltage applied across the modulator. The instantaneous photodetector current, I_D, is thus proportional to

$$\left[E_r \cos (\omega_c t + \phi_r) + E_m \cos (\omega_c t + \alpha \sin \omega_m t + \phi_m)\right]^2 \qquad (6.3)$$

If the d.c. and optical frequency components are neglected the signal current at the modulation frequency is

$$i_{\omega_m} = G (I_r I_m)^{\frac{1}{2}} \cos (\alpha \sin \omega_m t + \phi) \qquad (6.4)$$

where ϕ is a static phase difference given by $(\phi_m - \phi_r)$ and G is the detector conversion factor. I_r and I_m are proportional to the intensities of the reference and signal beams respectively. The output from the photodetector is thus a cosine function of an a.c. modulating signal with amplitude α, plus a static phase component proportional to the optical path difference between the reference and signal beams.

The theoretical variation of i_{ω_m} versus $\omega_m t$ for three values of ϕ is illustrated in Fig. 6.4. ϕ in addition to its dependence on the optical path length difference can be more simply varied by the application of a d.c. voltage to the modulator in series with the a.c. modulating signal. This will impose a fixed phase change via the electrooptic effect and hence enable the path difference between the reference and signal beams to be either cancelled or enhanced depending

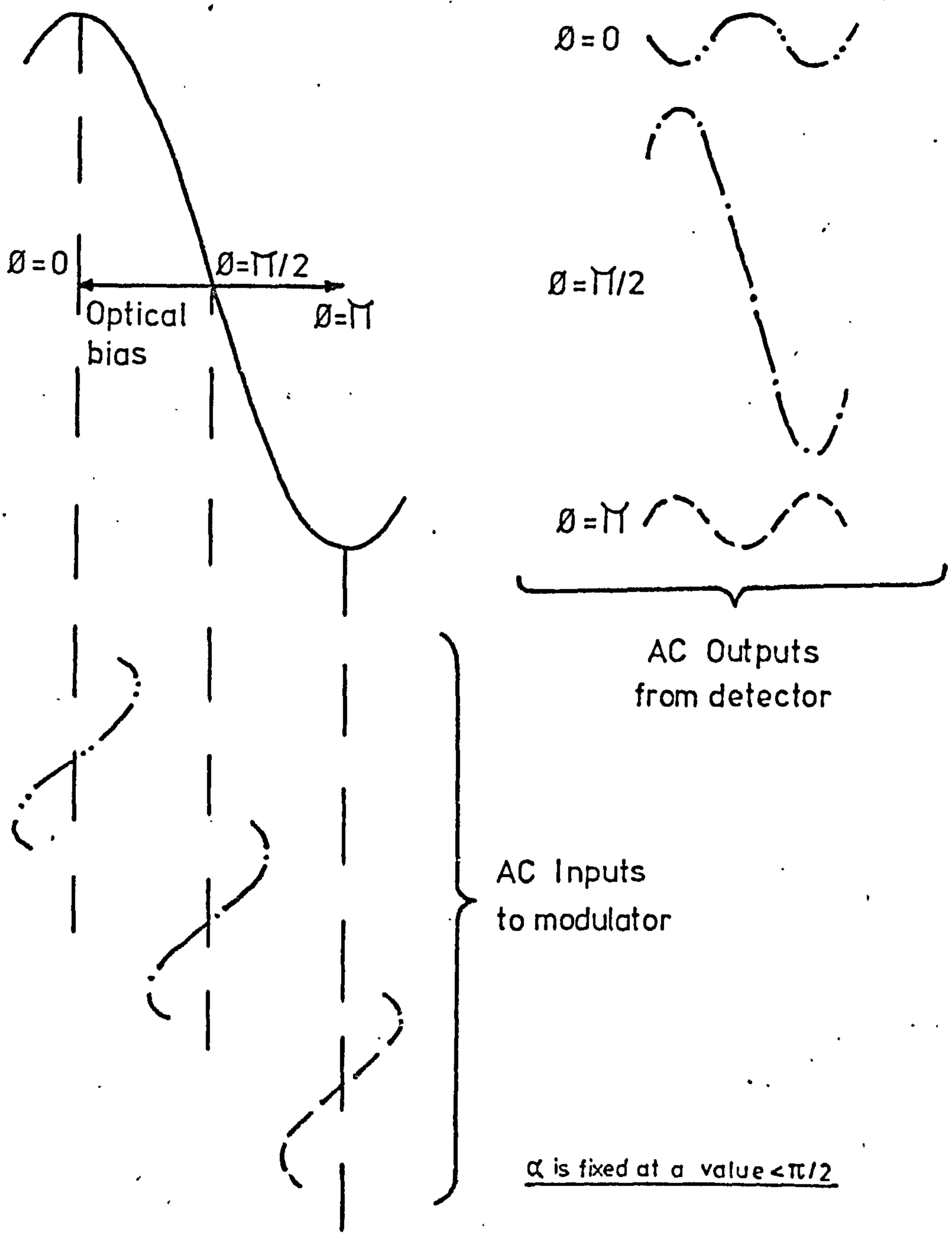

FIGURE 6.4 Theoretical variation of i_{ω_m} versus $\omega_m t$

on the polarity of the voltage. Referring to Fig. 6.4, it can be seen that a fixed phase bias can be applied anywhere between $n\pi$ and $(n + 1)\pi$ ($n = 0, \pm 1, \pm 2$ ---) by using a combination of the inherent phase difference and the d.c. electrooptic phase change.

Fig. 6.5 shows that the output signal from the photodetector will be severely distorted when the phase term ($\alpha \sin \omega_m t + \phi$) exceeds the limits bounded by $n\pi$ and $(n + 1)\pi$. It is the onset of symmetrical distortions, ie the simultaneous distortion of the maxima and minima which signifies the detection of an additional π change of phase produced by the modulating signal on the electrooptic structure.

The bias point at which maximum undistorted a.c. signal is obtained is given by $\phi = (2n + 1)\pi/2$. At this point on the cosine curve the signal can swing between $(2n + 1)\pi/2$ and $n\pi$ on the negative half cycle and between $(2n + 1)\pi/2$ and $(n + 1)\pi$ on the positive half cycle without suffering severe distortion. Under these conditions the peak to peak a.c. modulating voltage represents the number of volts required for a π phase change in the modulator, the $\lambda/2$ voltage.

The linearity of phase change with applied voltage is also important. A check on this parameter can be made by initially applying a small a.c. signal about the $(2n + 1)\pi/2$ bias point and subsequently increasing the d.c. bias until one set of peaks is on the point of severe distortion. The a.c. voltage and the concomitant change in the d.c. voltage are recorded. If linearity exists then

$$2\Delta V_{dc} + V_{ac} = V_{ac} \text{ (for } \pi \text{ phase change)} = V_{\lambda/2} \qquad (6.5)$$

Equation (6.5) can be rewritten as

$$\text{phase change} = \pi \left[1 - \frac{2\Delta V_{dc}}{V_{\lambda/2}} \right] \qquad (6.6)$$

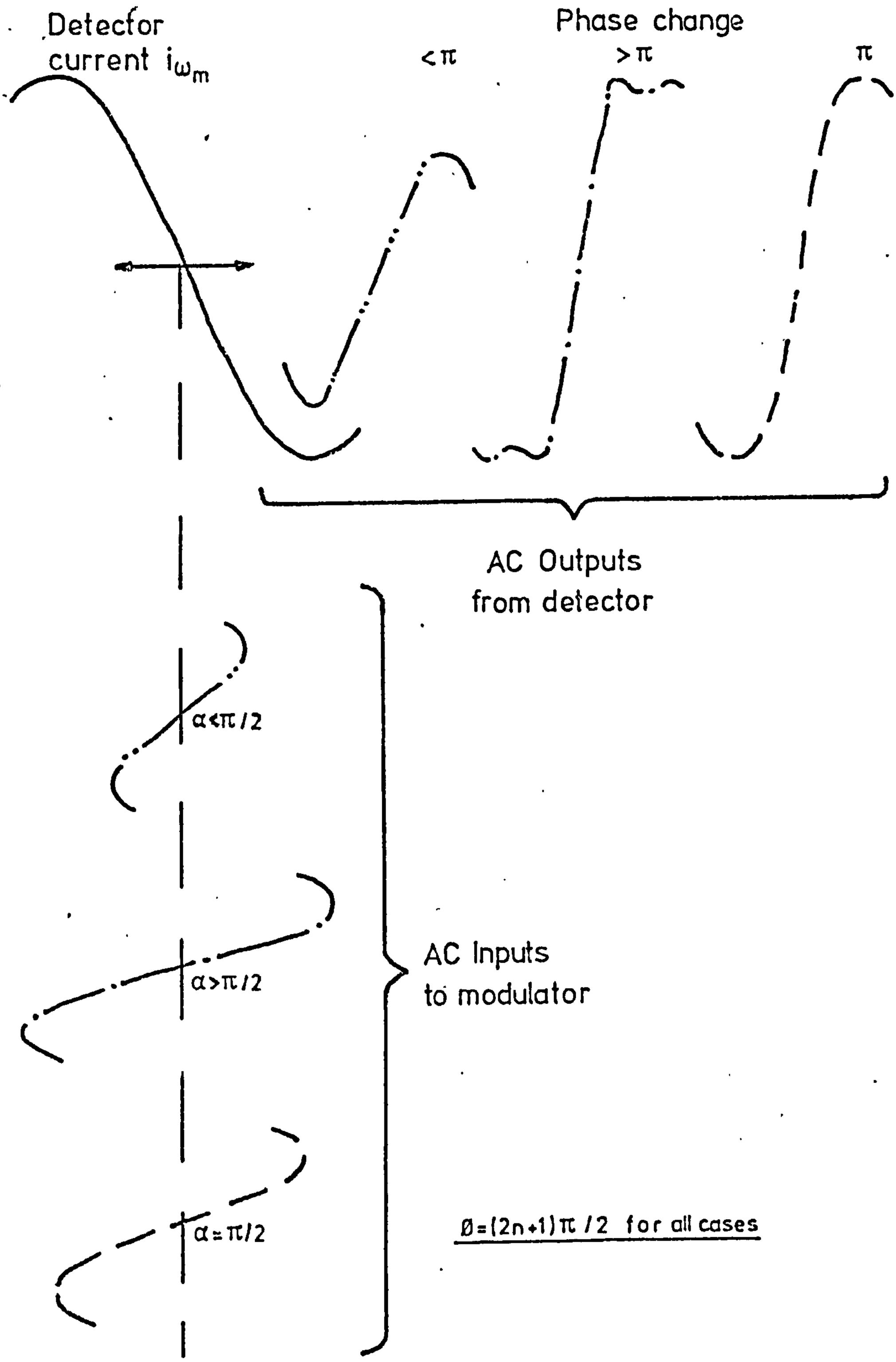

FIGURE 6.5 Detection of a π phase change - i_{ω_m} versus $\omega_m t$

Hence the phase change deduced from equation (6.6) should be linearly proportional to the a.c. voltage applied across the modulator, V_{ac}.

The experimental evidence confirming the above analysis was obtained using the system shown in Fig. 6.2a. The signal from the detector was displayed on an oscilloscope after amplification in a wideband amplifier. A narrow-band tuned amplifier is inappropriate for these measurements as even the most severely distorted waveform is modified to a sine wave. The location of the $(2n + 1)\pi/2$ bias point was achieved by applying an a.c. modulating signal which is sufficiently large to produce distortion at both the maxima and minima of the photodetector output. The d.c. bias is then altered until the trace is symmetrical with equal amounts of distortion at the positive and negative peaks; this corresponds to the required bias point. With the bias set at the $(2n + 1)\pi/2$ point the a.c. modulating signal is reduced until severe distortion is just eliminated. V_{ac} now equals $V_{\lambda/2}$. The peaks of the cosine output become slightly flattened prior to the onset of severe distortions.

Some experimental traces are illustrated in Fig. 6.6. Fig. 6.6a shows symmetrical distortions representing bias about $\phi = (2n + 1)\pi/2$ but with an a.c. signal corresponding to α greater than $\pi/2$. Bias at $\phi = (2n + 1)\pi/2$ and an a.c. signal with $\alpha = \frac{\pi}{2}$ is illustrated in Fig. 6.6b with the peak to peak value of this a.c. signal representing the voltage required for a π phase change. Fig. 6.6c illustrates an optical bias with ϕ less than $(2n + 1)\pi/2$ and Fig. 6.6d an optical bias of ϕ greater than $(2n + 1)\pi/2$ in both cases α is approximately $\pi/2$. The accuracy with which the voltage for a π phase change could be measured was $\pm$ 2%.

The phase change in the modulators can thus be simply and readily measured by means of this homodyne detection and display arrangement. This method is ideally suited to thin film modulators where the small voltages required can be derived from a simple signal

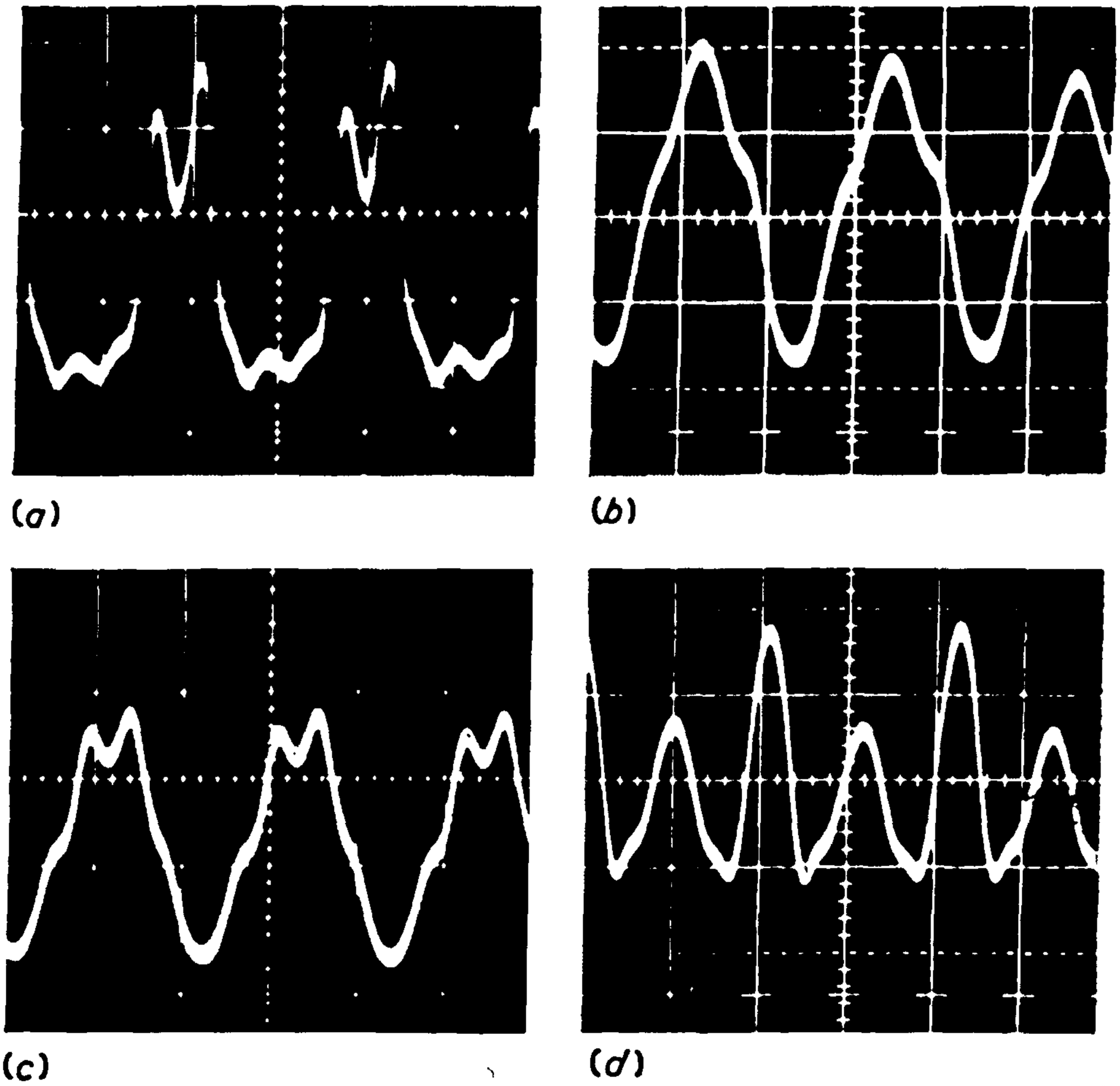

Figure 6·6 Experimental oscilloscope traces – time base 1 ms cm^{-1}. (*a*) DC optical bias near $(2n+1)\pi/2$ point but AC signal too large ($\alpha > \pi/2$); (*b*) correct optical bias and signal just small enough to prevent distortion; peak-to-peak voltage represents voltage for π phase change; (*c*) optical bias less than $(2n+1)\pi/2$ with $\alpha \approx \pi/2$; (*d*) optical bias greater than $(2n+1)\pi/2$ with $\alpha \approx \pi/2$

generator.

6.2.3 HETERODYNE DETECTION

Heterodyne detection has the advantage that random phase fluctuations not associated with the modulating signal are elminated by electronic processing. In this case the local oscillator is set to a frequency slightly different from the carrier frequency and this is most readily achieved using a liquid filled Bragg cell. Such a device was constructed following the design of DeLaRue[98] and operated with a 20 MHz quartz crystal transducer. Heavy water (D_2O) was used as the diffracting medium as deionised water is unsuitable at 1.15 μm due to the severe optical attenuation at this wavelength. The signal from the photodetector then contains the modulation as a phase modulation on an I.F. Bragg frequency and can thus be detected by discriminator electronics or displayed directly on a spectrum analyser. Interpretation of the results recorded on a spectrum analyser requires the use of Bessel functions to extract the relevant phase data[96]. Discrete phase changes can be deduced from the more obvious behaviour of the carrier and sidebands such as where $J_o = J_1$ of $J_o = 0$ (ie when the amplitude of the carrier and first sidebands are equal or when the carrier amplitude is equal to zero). For a continuous plot of phase change versus voltage applied to the modulator the amplitude of J_o alone could be followed.

In both detection methods the beams were focussed onto the photodetector surface with a 0.33 m focal length lens to reduce the required alignment criterion from better than 0.5 milliradians to approximately 3 milliradians. The beam splitter used was a piece of Schott BaSF52 glass 10 mm thick so that the reflections from the two surfaces could be separated by a pin-hole. The detection system performance would have been enhanced had a polarising beam splitter

been available since the use of a $\lambda/2$ plate would have permitted compensation of the insertion loss of the modulator. Maximum detection sensitivity is obtained when the two beams have approximately equal power densities[97].

Frequency response measurements can be obtained using either homodyne or heterodyne detection by noting the voltage required for a specific fixed phase change over the operating frequency range. This information along with the capacitance and impedance data allows the theoretical and experimental bandwidths to be computed and compared. Both homodyne and heterodyne detection were used for all measurements with similar results.

6.3 SUMMARY OF RESULTS

Several modulators were constructed with different guide and buffer thicknesses in order to verify experimentally the predictions of the curves in Fig. 5.9. Table 6.1 lists the results obtained from six modulators and includes for comparison their theoretically calculated performances. Sample curves of frequency versus applied voltage for 1 radian phase change are shown in Fig. 6.7 for modulator C and Fig. 6.8 illustrates the phase change versus applied voltage for the same modulator. The results obtained from a modulator made to the theoretical design of section 5.4.3 are given in Table 6.2. In all cases there is a good agreement between the theoretical predictions and the experimental results. The structures have tolerated 150 volts without breakdown.

The unanticipated roll-off occurring in the frequency response curve (Fig.6.7) for frequencies less than 1 MHz is considered in the following section.

6.3.1 DIELECTRIC PERMITTIVITY MEASUREMENTS

Erroneous results with capacitors formed by sandwiching cadmium

Modulator	Guide Thickness (μm)	Buffer Thickness (μm)	Electrode Area (mm^2)	Theoretical Power per Unit Bandwidth ($mW\ MHz^{-1}$)	Experimental Power per Unit Bandwidth ($mW\ MHz^{-1}$)	Theoretical Cut-Off Frequency with 600Ω Load (MHz)	Experimental Cut-Off Frequency with 600Ω Load (MHz)
A	1.45	0.4	5.0 x 5.0	226.5	230.0	1.1	1.4
			5.0 x 2.0	90.6	90.0	2.2	2.1
			5.0 x 1.0	45.3	45.7	5.5	5.2
B	1.0	0.6	5.0 x 5.0	227.5	225.0	1.09	1.2
			5.0 x 1.0	45.5	46.0	5.45	5.3
C	1.5	0.5	5.0 x 5.0	276.0	270.0	1.2	1.6
			5.0 x 2.0	110.4	105.0	3.0	4.0
			5.0 x 1.0	55.2	55.0	6.0	6.5
			5.0 x 0.5	27.6	27.0	12.0	13.0
D	1.1	0.4	5.0 x 5.0	194.0	205.0	0.94	1.2
			5.0 x 2.0	77.6	85.0	2.35	2.4
			5.0 x 1.0	38.8	39.5	4.7	5.0
E	1.05	0.5	5. 0 x 5.0	200.0	215.0	1.01	0.95
			5.0 x 2.0	80.0	81.0	2.02	2.2
			5.0 x 1.0	40.0	45.0	5.05	5.4
F	1.5	0.95	5.0 x 5.0	339.0	340.0	1.7	2.0
			5.0 x 2.0	135.6	125.0	4.2	4.0
			5.0 x 1.0	67.8	70.0	8.4	8.5
			5.0 x 0.5	33.9	34.0	16.8	17.0

TABLE 6.1 Comparison between theoretical calculations & experimental results for a number of modulators.

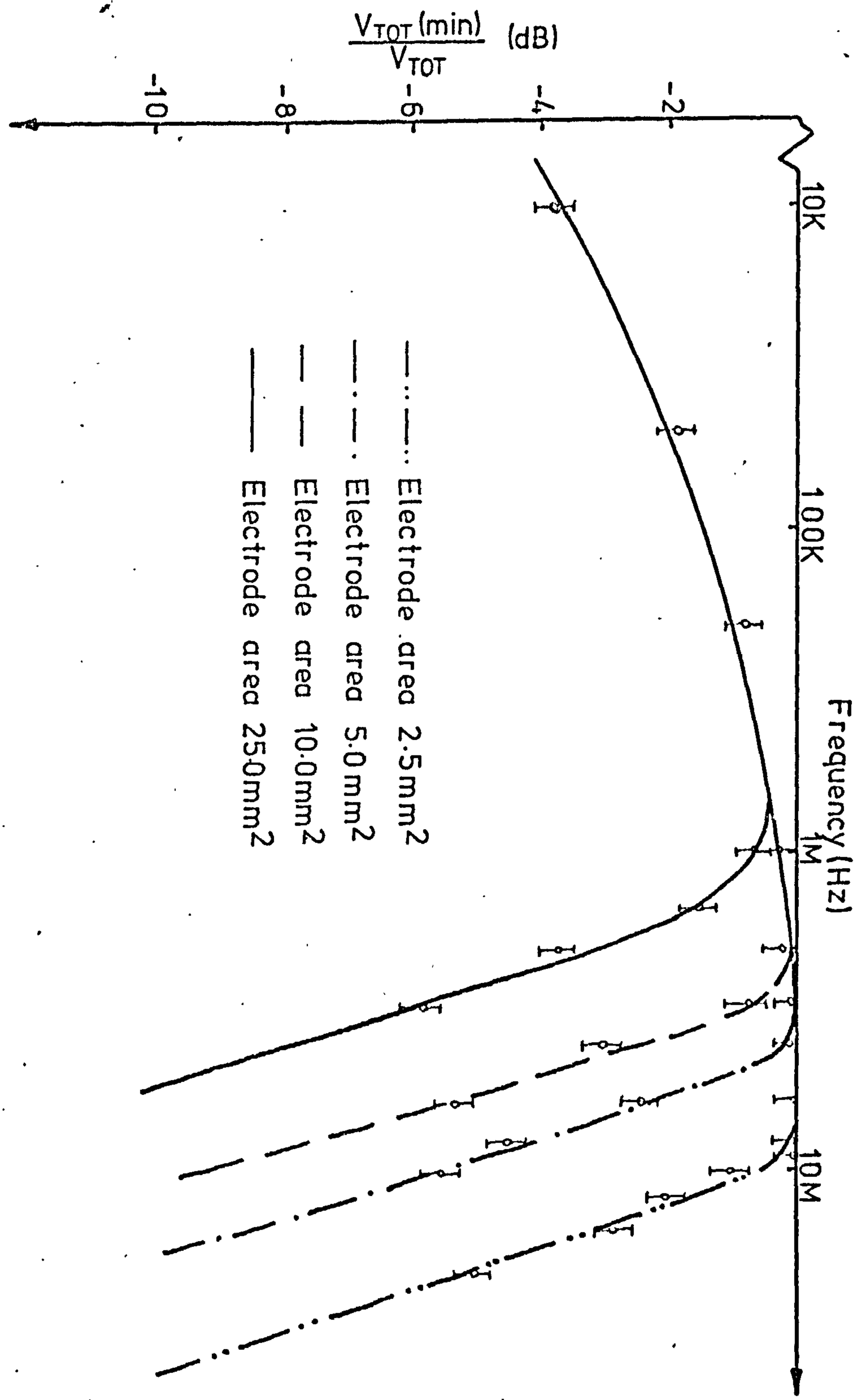

FIGURE 6.7 Frequency response plot for modulator C

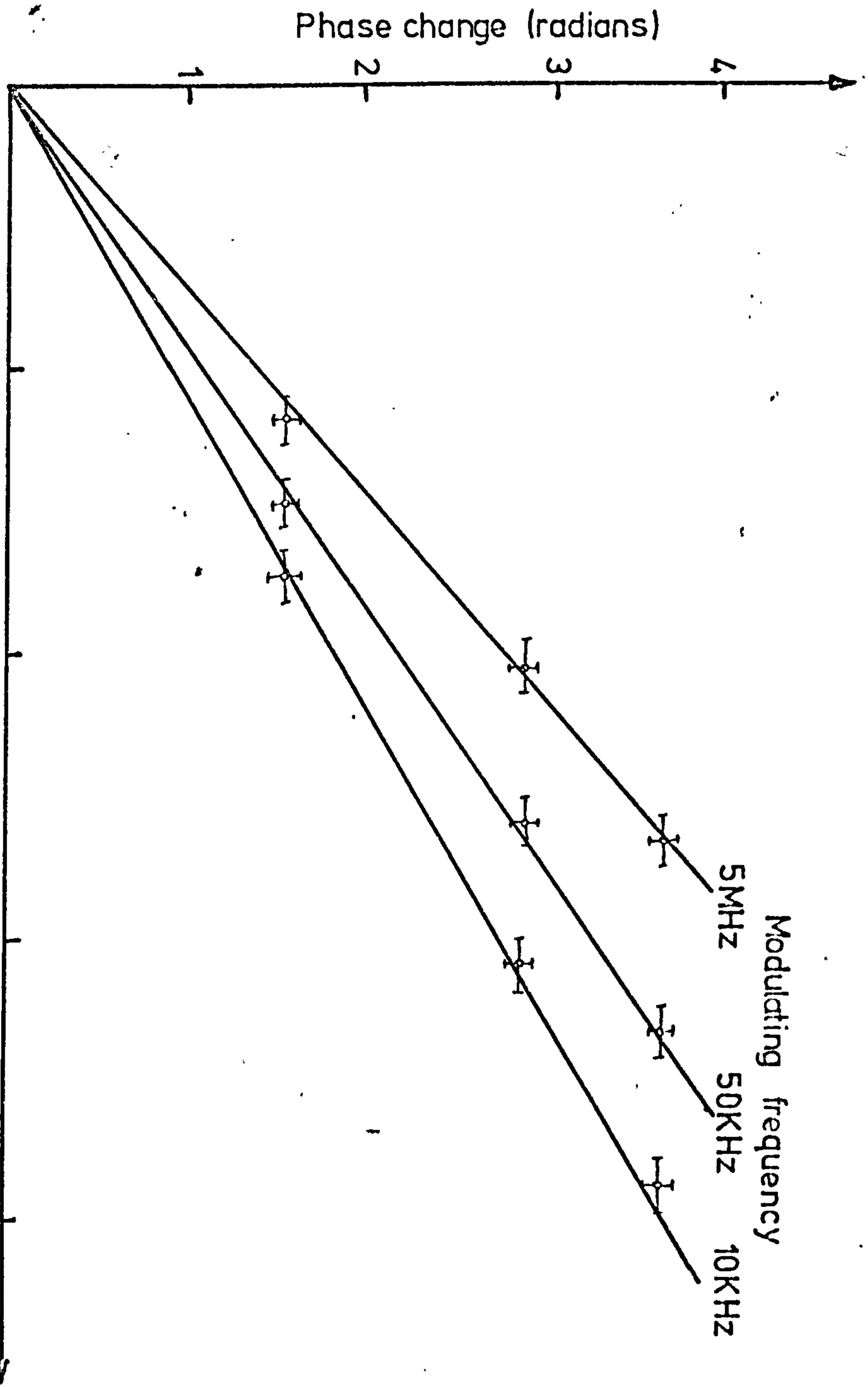

FIGURE 6.8 Phase change versus applied voltage for modulator C

Guide Thickness (μm)	Buffer Thickness (μm)	Electrode Area (mm^2)	Theoretical Power per Unit Band-width ($mW\ MHz^{-1}$)	Experimental Power per Unit Band width ($mW\ MHz^{-1}$)	Theoretical Cut-Off Frequency with 600Ω Load (MHz)	Experimental Cut-Off Frequency with 600Ω Load (MHz)
1.4	0.45	10.0 x 5.0	112.0	115.0	0.56	0.6
		10.0 x 2.0	44.8	45.0	1.41	1.6
		10.0 x 1.0	22.4	22.5	2.83	3.0
		10.0 x 0.5	11.2	11.5	5.65	6.0

TABLE 6.2 Comparison between Theoretical and Experimental figures for an optimized Al-SiO-CdS-SiO-Al Structure.

sulphide between metal electrodes occurred due to a semiconductor-metal junction capacitance effect. The dielectric relaxation was therefore measured experimentally by forming several parallel plate capacitors with individual films of silicon monoxide and an SiO-CdS-SiO stack sandwiched between metal electrodes. The thin film dielectric constantswere deduced by extrapolation from the capacitance measurements. Fig. 6.9 shows the dielectric constants of silicon monoxide and cadmium sulphide versus frequency in the range 1 KHz to 10 MHz. It is evident that at low frequencies (less than 1 MHz) the roll-off of the phase modulators is largely due to the increasing dielectric constant of the cadmium sulphide guide although the silicon monoxide does make a small contribution. The loss associated with dielectric relaxation, tan δ, did not appear to be significant.

6.4 DISCUSSION OF RESULTS

The results of section 6.3 show excellent agreement with the theoretically predicted modulator performances of section 5.4. The frequency response characteristics of the Al-SiO-CdS-SiO-Al phase modulators are adequately explained when the behaviour of the thin film dielectric constants and RC time constant effects are taken into consideration. As predicted from the basic cadmium sulphide waveguide losses modulators with guide thicknesses of less than 1 μm have losses which precluded testing of these structures. In general insertion loss levels of less than 10 dB for the modulators were required to permit the alignment of the detection equipment. The major limiting factor on modulator performance apart from the waveguide loss, was the diffraction limited width of the top electrode.

All measurements in this chapter have been made on modulators in which there has been no confinement of the guided wave in the lateral direction. It is of interest to calculate the performance

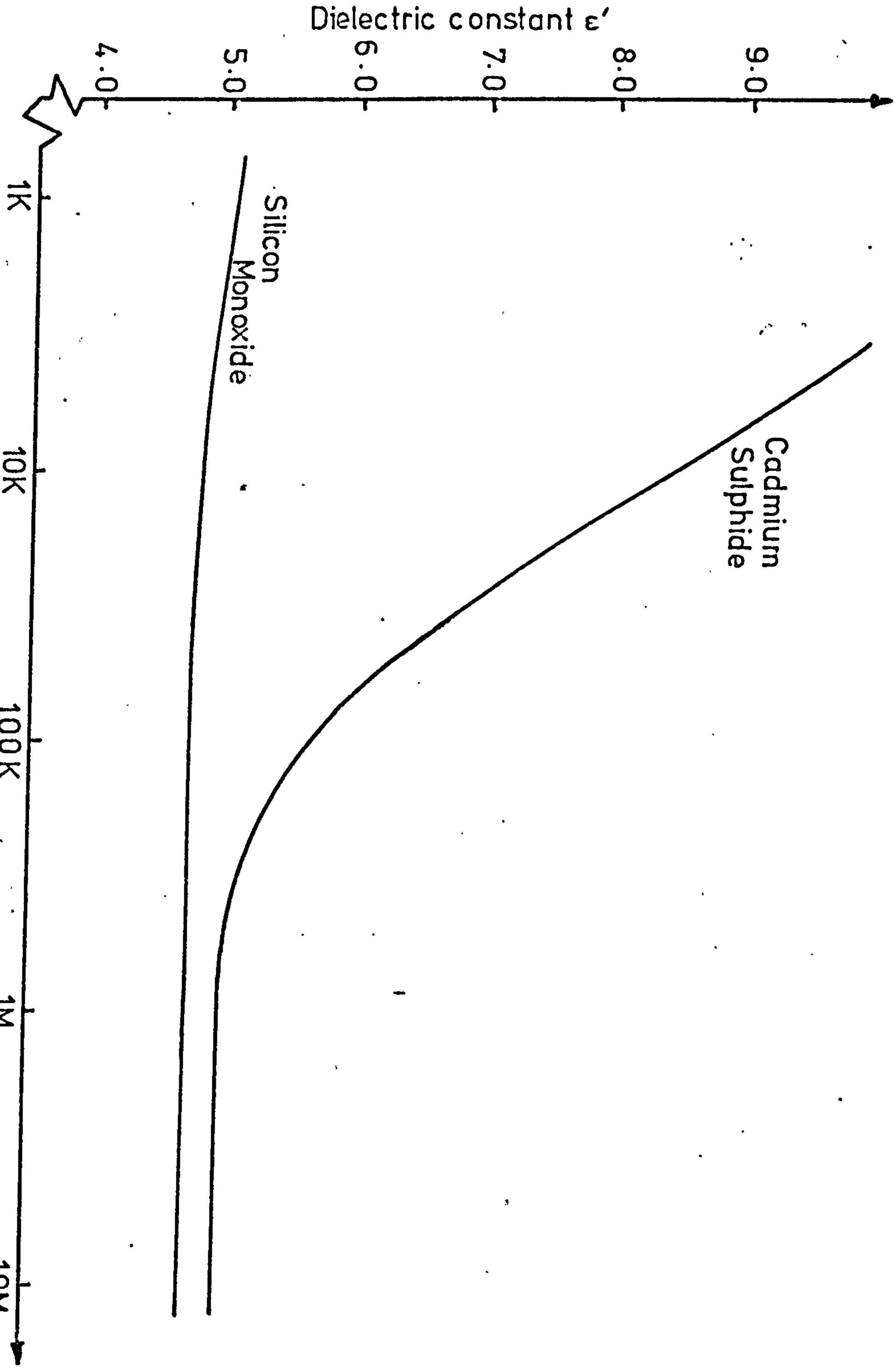

FIGURE 6.9 Dielectric constant versus frequency for thin films of CdS and SiO

figures for a modulator based on a rectangular optical waveguide of cadmium sulphide. Two dimensional confinement would allow a reduction in the electrode width by a factor of 25 times below that permitted in the diffraction limited case, ie a decrease from 500 μm to 20 μm. The power per unit bandwidth figure for the realistic modulator structure considered in section 5.4.3 would become 450 $\mu W \cdot MHz^{-1}$ with a maximum base bandwidth into a 50Ω load of 1.7 GHz. Since the wavelength of operation is 1.15 μm the performance figures would approach those modulators[55] currently showing the most promise. The above figure is, however, based on the assumption that the planar cadmium sulphide waveguide loss of 5 $dBcm^{-1}$ can be maintained in rectangular waveguides (this is a severe problem as will be seen in chapter 7).

6.5 THE COMPOSITE MODULATOR STRUCTURE

Tien et al[15] proposed and demonstrated a hybrid circuit technology whereby individual passive devices such as lenses, prisms and reflectors in zinc sulphide are linked by means of a low refractive index organosilicon waveguide. The coupling to and from high index zinc sulphide was achieved by tapering the edges of the zinc sulphide. Providing the taper was sufficiently gradual then a mode in the low index guide would couple to the lowest order mode in the high index film and vice-versa at the output taper. The theory of this tapered coupling is detailed by Tien et al[99] and is based on the tapered films providing regions of guide with slowly changing effective index $(\beta/_k)$. The production of tapers in vacuum evaporated polycrystalline films of cadmium sulphide is easily achieved and thus the cadmium sulphide stacked modulator structure lends itself to this type of coupling transition. Phase matched coupling between low index waveguides and optical fibres has shown almost 100% efficiency[100] and therefore a fibre-cadmium sulphide modulator-fibre device is possible.

6.5.1 DEVICE PREPARATION

The waveguide and modulator structure Al-7059 glass-CdS-SiO-Al, is illustrated schematically in Fig. 6.10. The 7059 glass films were deposited by r.f. sputtering onto glass substrates to give a refractive index of 1.54 and a waveguide propagation loss of less than 1 $dBcm^{-1}$ at 1.15 μm. The tapers controlling the coupling between the cadmium sulphide modulator waveguide and the 7059 glass were produced by masking the substrate, during the cadmium sulphide deposition, with two 2mm thick brass plates into which a 1 mm step had been recessed by 2 mm in the base. For the evaporator geometry employed the masks gave taper lengths of approximately 50 μm for a cadmium sulphide film 1.5 μm thick. The taper induces a gradual increase in phase constant enabling a TE_o mode in the 7059 glass guide to continue to propagate as a TE_o mode in the cadmium sulphide layer and vice versa. However, some power was scattered in the tapers due to the high losses associated with the structure of very thin films of cadmium sulphide. Tapers approximately 5 μm long did not give satisfactory coupling as the $\beta/_k$ change was too abrupt, causing the power to radiate from the guide.

The 7059 glass ceased to be a waveguide between the aluminium electrodes and fulfilled the role of a buffer layer between the new waveguide, the cadmium sulphide film, and the lower metal electrode. Silicon monoxide was chosen for the upper buffer layer since it was again thermally compatible with the existing layers. The top aluminium film consisted of four electrodes of identical length but with differing widths so that capacitance effects on modulator performance could be observed. The pattern was produced by photo-lithography using the "lift-off" technique.

The phase change experienced by a TE mode as a result of a small change in the guide refractive index, Δn_o, is given by equation

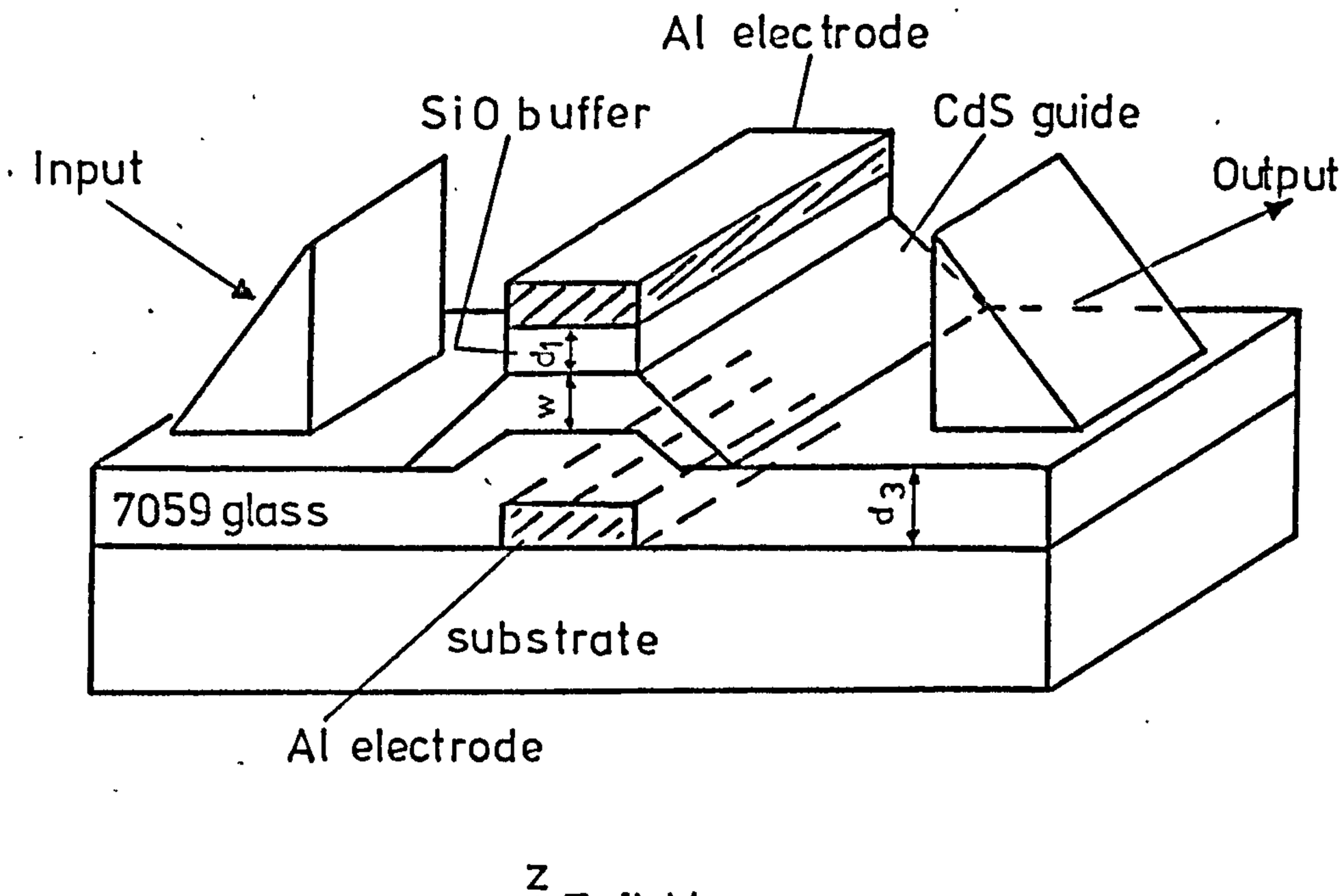

FIGURE 6.10 Schematic diagram of composite modulator structure

(6.7) which is a modified form of equation (5.28).

$$\Delta\beta' = \mathrm{Re}\left[F\left(W, d_1, d_3, \underset{\sim}{\beta}\right) \right] \Delta n_o \qquad (6.7)$$

where the function F is obtained as for the symmetrical structure of section 5.3 and depends on the waveguide thickness W, buffer layer thicknesses d_1 and d_3 and on the complex propagation constant $\underset{\sim}{\beta} = \beta' + j\beta''$. Expressing the phase change $\Delta\phi$ in terms of the total voltage applied across the modulator structure the more useful expression (equation (6.8)) is obtained.

$$\Delta\phi = \frac{-\frac{1}{2}n_o^3 r_{13} \mathrm{Re}\left[F(W, d_1, d_3, \underset{\sim}{\beta}) \right] V_{TOT}\, \varepsilon_1' \varepsilon_3'}{(d_1\varepsilon_3'\varepsilon_2' + d_3\varepsilon_1'\varepsilon_2' + W\varepsilon_1'\varepsilon_3')} \qquad (6.8)$$

ε' is the real part of the complex dielectric constant $\underset{\sim}{\varepsilon}$ and the subscripts 1, 2, 3 refer to the silicon monoxide, cadmium sulphide and 7059 glass films respectively.

Phase change measurements and frequency response data were obtained using the detection techniques described in section 6.2.

6.5.2 SUMMARY OF RESULTS

The loss characteristics of the composite waveguiding structure are illustrated by the loss scan of Fig. 6.11 which shows clearly the differing attenuation rates of the 7059 glass and cadmium sulphide films. The large area of the photodiode (cf the taper length) meant that the scattering at the taper was integrated over a larger area. However, the infrared radiation made visible with an image converter showed scattering centres at the two tapers.

The performance figures for the TE_o mode propagation through 3 modulat- structures are given in Table 6.3 along with the theoretical values calculated using equations (6.7) and (6.8). The agreement between the theoretical and measured performances is again good indicating that the effective electrooptic coefficient of the polycrystalline cadmium

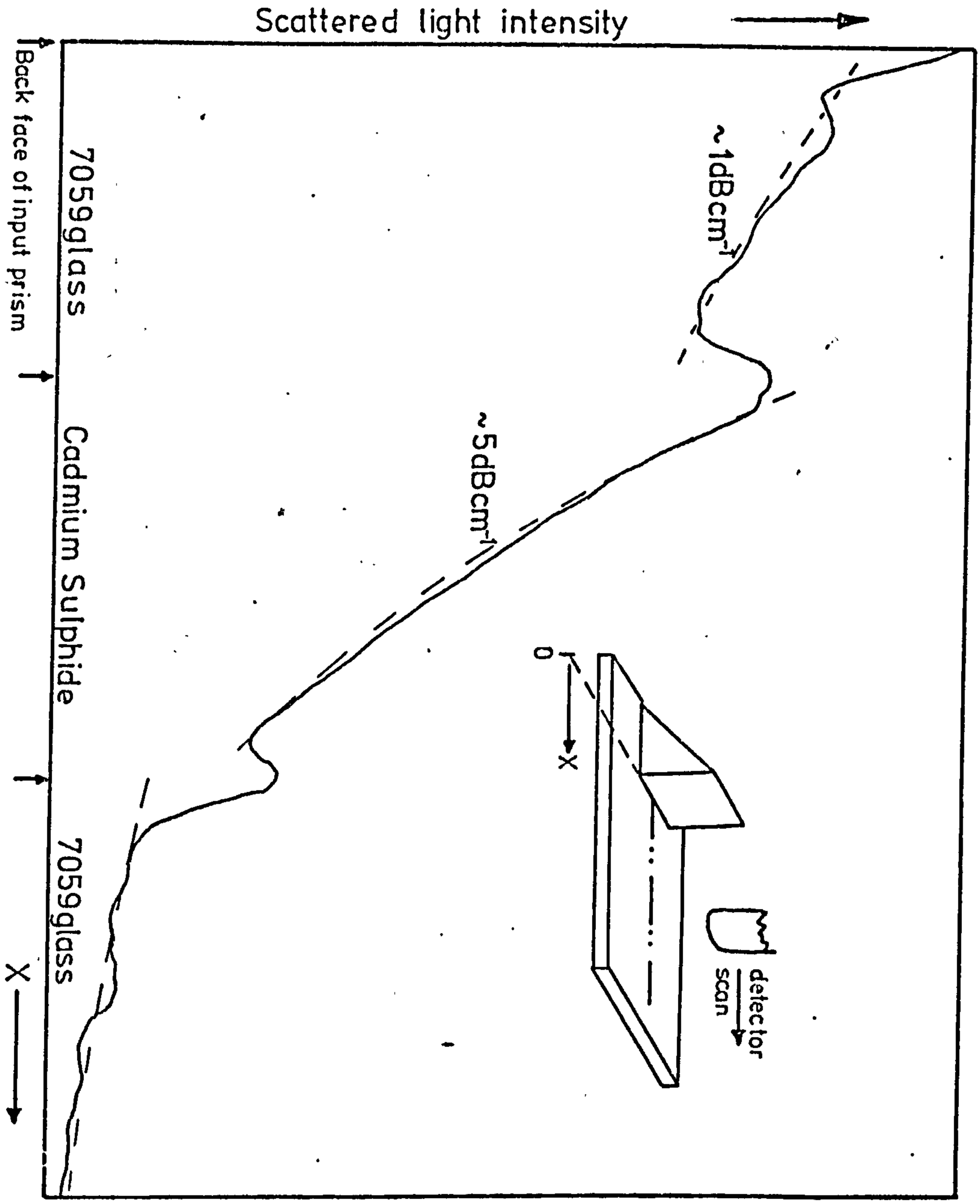

FIGURE 6·11 Scattered light intensity as a function of distance for the composite structure

Modulator	CdS Guide Thickness (μm)	7059 Glass Thickness (μm)	SiO Buffer Thickness (μm)	Electrode Area (mm^2)	Theoretical Power per Unit Bandwith. ($mW.MHz^{-1}$)	Experimental Power per Unit Bandwith. ($mW.MHz^{-1}$)	Theoretical Cut-Off Frequency (MHz)	Experimental Cut-Off Frequency (MHz)
A	1.8	1.5	0.4	5.0 x 5.0 5.0 x 2.0 5.0 x 1.0 5.0 x 0.5	204.8 152.4 76.2 38.1	310.0 150.0 80.0 33.5	1.52 3.8 7.6 15.2	1.5 3.4 7.2 16.0
B	1.4	1.5	0.4	5.0 x 5.0 5.0 x 2.0 5.0 x 1.0 5.0 x 0.5	261.2 130.6 65.3 32.7	250.0 142.5 74.5 35.0	1.36 3.4 6.8 13.6	1.0 4.0 6.0 13.0
C	1.0	1.5	0.4	5.0 x 5.0 5.0 x 2.0 5.0 x 1.0 5.0 x 0.5	244.8 122.4 61.2 30.6	240.0 103.0 64.5 31.5	1.12 2.8 5.6 11.2	1.3 2.0 6.0 11.0

TABLE 6.3 Summary of Main Characteristics of Three Modulators Comparing Theoretical and Experimental Figures

sulphide thin films is very close to the bulk single crystal value of 1.1×10^{-12} m.V^{-1}. Fig. 6.12 illustrates the frequency response of modulator A. As with the simpler modulator structure of section 6.3. the increasing value of V_{TOT} required to produce a one radian phase change is accounted for by RC effects at high frequencies and by dielectric relaxation, particularly in the cadmium sulphide, at frequencies less than 1 MHz.

6.5.3 DISCUSSION OF RESULTS

The power per unit bandwidth figures of Table 6.3 would at first sight appear large in comparison with those quoted for the symmetrical modulator (Table 6.2) and require further comment. The buffer layer thicknesses were not optimised for the modulators described nor were the electrodes as long (5mm cf. 10mm for symmetric case). These refinements were not considered necessary as it was the device feasibility which was being analysed rather than the modulator performance. To optimise the buffer layer thickness the 7059 glass film would need to be tapered over the aluminium electrode during the r.f. sputter deposition. The optical insertion loss of these devices was between 5 and 7 dB, the contribution to the overall loss from the tapers being approximately 1dB. The demonstration of phase-matched coupling between fibres and 7059 glass films[100] suggests that input and output coupling can be efficiently achieved to the Al-7059-glass-CdS-SiO-Al modulator structure by means of optical fibres.

6.6 CONCLUDING REMARKS

The phase modulation properties of the Al-SiO-CdS-SiO-Al waveguiding structure have been fully analysed both theoretically and experimentally. All the experimental observations have been adequately accounted for by the theory implying that the r_{13} electrooptic coefficient for thin polycrystalline films of cadmium sulphide is close

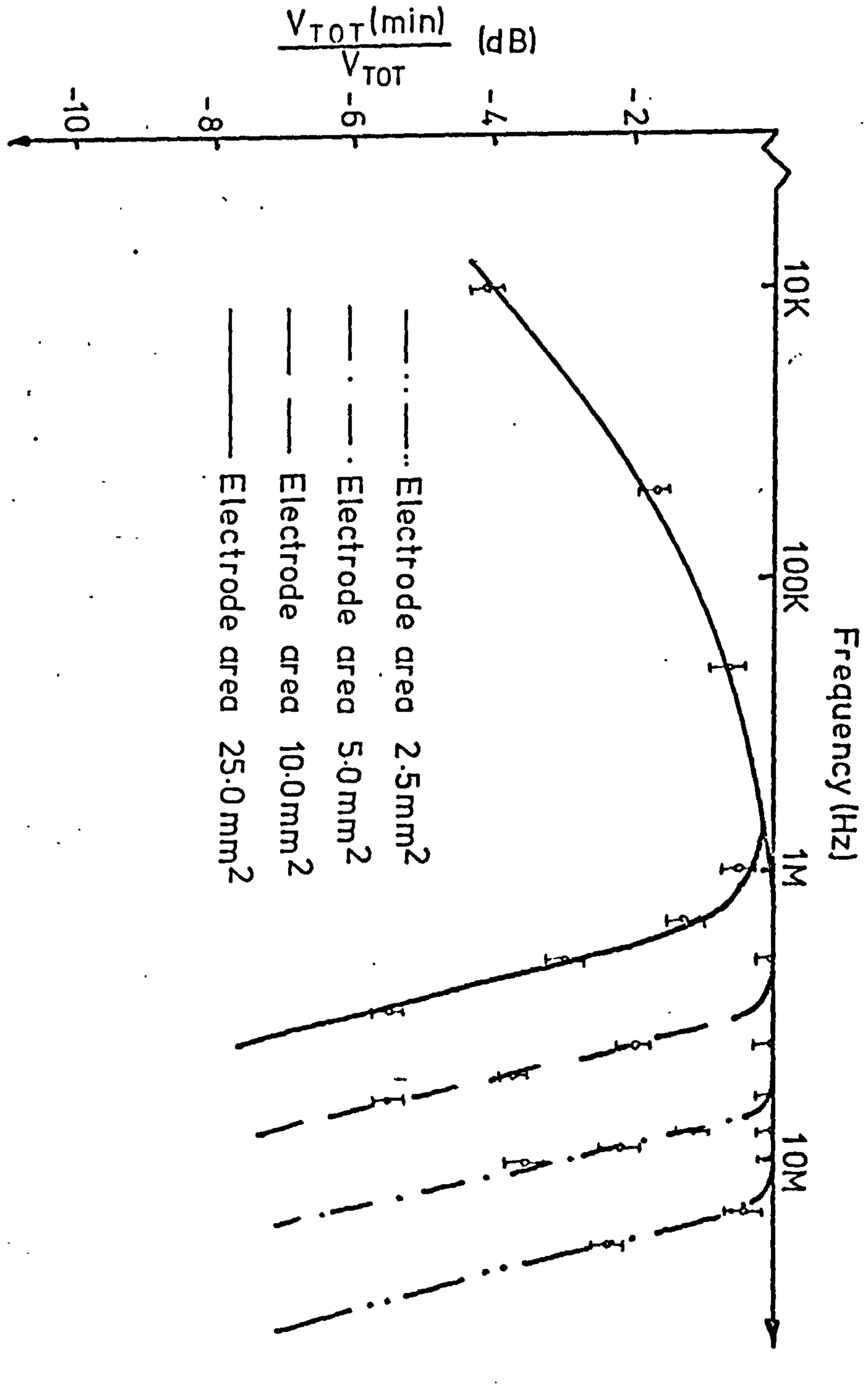

FIGURE 6.12 Frequency response plot for modulator A

to the bulk single crystal value of 1.1×10^{-12} m.V^{-1}. While the best power per unit bandwidth figure of 11.5 mW MHz^{-1} for 1 radian phase change, with a guide thickness of 1.4 μm, buffer thicknesses of 0.45 μm and an electrode area of 10x0.5 mm^2, does not compare with the lithium niobate modulators[55] the fabrication technologies are important. All the films have been vacuum evaporated and the desired electrooptic effect does not depend on epitaxial growth or single crystal substrates unlike most other modulators. The device had an insertion loss of 12 dB which, apart from the diffraction limited electrode width, is the main reason why lower power per unit bandwidths were not attained.

A method for simply and readily measuring the phase change in an electrooptic modulator by homodyne detection was devised. The static optical bias inherent in the interferometer could be varied by applying a d.c. voltage across an electrooptic structure.

The composite modulator demonstrated that the cadmium sulphide waveguide is compatible with a hybrid circuit technology which should facilitate highly efficient phase-matched coupling to and from low refractive index silica fibres.

The calculations for a rectangular waveguide modulator assembly indicated a theoretical performance comparable to the lithium niobate systems but as will be seen in chapter 7 the high waveguide losses of rectangular cadmium sulphide waveguides precludes the realisation of the lowest drive powers predicted.

PART III

RECTANGULAR WAVEGUIDES FORMED FROM CADMIUM SULPHIDE THIN FILMS, AND ASSOCIATED DEVICES

SYNOPSIS

A planar slab waveguide provides no lateral confinement of the guided light. For some devices this confinement is not necessary and in others it is not even desirable[21]. However, with the requirement of a high packing density of components on the same substrate crosstalk isolation demands the use of rectangular waveguides. In active devices such as lasers and modulators the additional confinement will lead to a reduction in electrical power requirements. The electro-optic phase modulator drive power will however be limited by the waveguide losses and the optical power densities sustainable by the guides. Directional couplers can be fabricated both in planar stacked waveguides and in rectangular waveguides placed parallel to each other in a coplanar configuration. The latter system has marked benefits in that independent voltage control can be exercised over the two guides leading to reduced switching voltages for an electrooptically controlled directional coupler, as will be seen in chapter 8.

With two further waveguide boundaries in rectangular guides the major difficulty is fabricating a device with an acceptable loss. To overcome this problem rectangular waveguides are often defined by diffusion, eg. titanium into lithium niobate. However, in these guides only a small refractive index difference can be induced between the guide and the surrounding medium. Diffusion also invariably requires the use of high refractive index single crystal substrates with the associated problems of fibre-film coupling already mentioned in part II.

The benefits of the cadmium sulphide technology described in Parts I and II have been discussed but to fully exploit these techniques they must be applicable to situations where lateral confinement of the guided wave can be induced. This part of the thesis is divided into two chapters; the first outlines rectangular waveguide theory, fabrication methods and the evolution of an electro-

optic phase modulator with lateral confinement. The second chapter presents a theoretical analysis of directional couplers and their application to optical switching in some possible cadmium sulphide waveguide structures. The approach adopted to reduce dimensional tolerances and voltage requirements is outlined.

CHAPTER 7: RECTANGULAR DIELECTRIC WAVEGUIDES

The production of an electrooptic phase modulator relies heavily on the ability to fabricate rectangular (2-d) waveguides with a low propagation loss. Once these waveguides can be satisfactorily produced then an improvement on the stacked cadmium sulphide waveguide modulator performance (drive power) outlined in chapter 6 will be possible. Low loss rectangular waveguides will also form the first step in the fabrication of an electrooptically switched directional coupler which will be discussed in chapter 8.

In section 7.1 a brief outline of the theory of rectangular waveguides is presented as a basis for the interpretation of the experiments described in section 7.2 and the analysis of the results of section 7.3. Experiments and results from a 20 μm wide electro-optic phase modulator are described in section 7.4 and concluding remarks on rectangular waveguide fabrication from an experimental standpoint are presented in section 7.5

7.1 THEORETICAL RECTANGULAR WAVEGUIDE ANALYSIS

The analysis of a rectangular dielectric waveguide is very much more complex than that of the planar waveguide described in chapter 2. Unlike the latter case or that of hollow rectangular metal waveguides the electric and magnetic fields of the rectangular dielectric waveguide cannot be expressed as simple functions exhibiting sinusoidal transverse variation in the core. The solutions can only be found exactly through detailed numerical methods. Many workers have exerted considerable effort to finding means by which the properties of the modes of a rectangular waveguide can be characterised[101]. Such studies were considered to be beyond the scope of this thesis and the rectangular waveguide theory used was based on an approximate solution derived by Marcatili[102]. The theory is briefly summarised and its limitation for modes near cut-off outlined. In most of the

rectangular waveguides described in section 7.2 the modes are well confined and the approximate theory adequately predicts mode propagation. However, for selenium diffused cadmium sulphide waveguides the modes are near cut-off and a modification is necessary to the theory to predict their behaviour.

7.1.1 SUMMARY OF PUBLISHED ANALYSES

Marcatili[102] has detailed an approximate analytical solution in closed form using simple sinusoidal and exponential functions. The waveguide geometry used is illustrated in Fig. 7.1. In his analysis the fields in the shaded regions are neglected, accounting for both the simplicity and limitations of the approach.

The analysis assumes that for well guided modes the field decays exponentially in regions 2, 3, 4 and 5; therefore most of the power travels in region 1, a small part in regions 2, 3, 4 and 5 and even less in the four shaded regions. Consequently, only a small error should be introduced if the fields are not matched along the edges of the shaded areas. The matching along the four sides of region 1 can be achieved assuming simple field distributions. The largestfield components are found to be perpendicular to the axis of propagation with the modes essentially of the TEM kind and are grouped into two families E^x_{pq} and E^y_{pq} plus a continuum of unguided modes. The main field components of the members of the first family are E_x and H_y, while those of the second are E_y and H_x. The subindices p and q represent the number of nodes of the electric or magnetic fields in the x and y directions respectively. Marcatili shows that the longitudinal propagation constant can be written as

$$\beta = (k_1^2 - k_x^2 - k_y^2)^{\frac{1}{2}} \qquad (7.1)$$

where k_x and k_y are the x and y direction propagation constants in the core and are given by

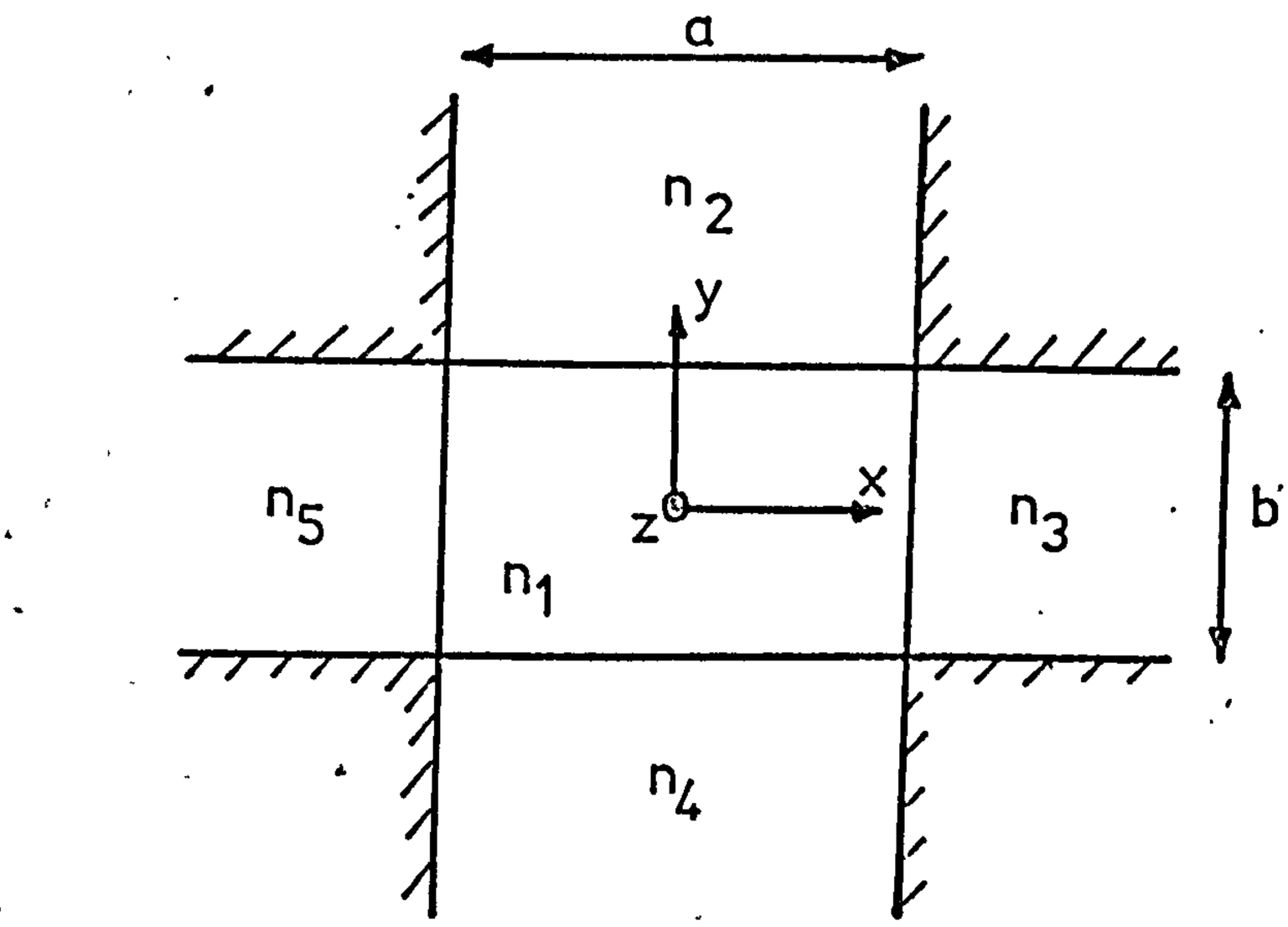

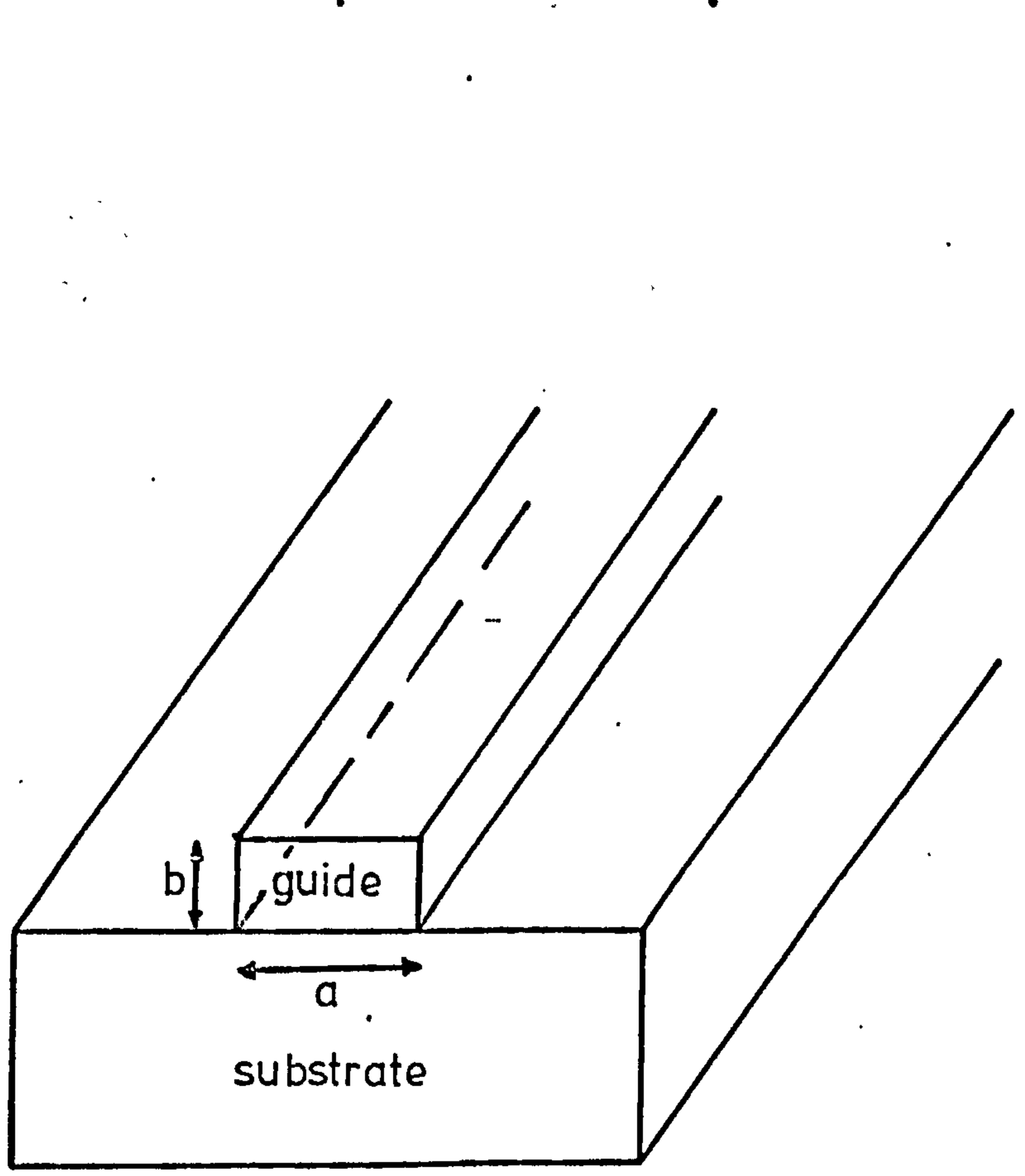

FIGURE 7.1 Rectangular waveguide geometry

$$k_x a = p\pi - \tan^{-1} k_x \xi_3 - \tan^{-1} k_x \xi_5 \qquad (7.2)$$

$$k_y b = q\pi - \tan^{-1} \frac{n_2^2}{n_1^2} k_y \eta_2 - \tan^{-1} \frac{n_4^2}{n_1^2} k_y \eta_4 \qquad (7.3)$$

for E^y_{pq} modes, and

$$k_x a = p\pi - \tan^{-1} \frac{n_3^2}{n_2^2} k_x \xi_3 - \tan^{-1} \frac{n_5^2}{n_2^2} k_x \xi_5 \qquad (7.4)$$

$$k_y b = q\pi - \tan^{-1} k_y \eta_2 - \tan^{-1} k_y \eta_4 \qquad (7.5)$$

for E^x_{pq} modes, where

$$\xi_i = \frac{1}{|k_{xi}|} = \frac{1}{\left[\left(\frac{\pi}{A_i}\right)^2 - k_x^2\right]^{\frac{1}{2}}} \quad i = 3,5 \qquad (7.6)$$

$$\eta_i = \frac{1}{|k_{yi}|} = \frac{1}{\left[\left(\frac{\pi}{A_i}\right)^2 - k_y^2\right]^{\frac{1}{2}}} \quad i = 2,4 \qquad (7.7)$$

$$A_i = \frac{\lambda}{2(n_1^2 - n_i^2)^{\frac{1}{2}}} \qquad i = 2,3,4,5 \qquad (7.8)$$

$$k_i = \frac{2\pi}{\lambda_i} = \omega\sqrt{\bar{\mu}_o \varepsilon_i} \qquad i = 1,2,3,4,5 \qquad (7.9)$$

The amplitudes of the field components in media 2,3,4 and 5 decay exponentially; therefore ξ_i and η_i are a measure of the distance the evanescent field penetrates into each of the media. If the modes tend towards cut-off the fields in the shaded region are significant and the approximate theory becomes invalid. The above equations thus apply only to the case of well guided modes away from cut-off.

In the situation where the refractive index difference between the guide and the surrounding media is large and the waveguide has a large aspect ratio the E^x_{pq} and E^y_{pq} modes can be represented as

the TE_m and the TM_m ($m = q-1$) modes of a planar waveguide. An example is illustrated for a cadmium sulphide rectangular waveguide in Fig. 7.2. For a waveguide 1.5 μm thick with air as the medium in regions 3 and 5 the phase constant of the waveguide mode is the same as that for the planar waveguide for guide widths of greater than 10 μm. This will be the case for all the rectangular waveguides described in section 7.2 with the exception of the selenium diffused cadmium sulphide waveguide (considered in section 7.1.2). For a 20 μm wide rectangular waveguide electrooptic phase modulator the expression for $d\beta$ calculated in chapter 5 can be used as the change in using the differentiated form of equation (7.1) is found to be insignificant.

7.1.2 MODIFICATION FOR GUIDES NEAR CUT-OFF

Waveguides formed by selenium diffusion into crystals of cadmium sulphide are considered to have a refractive index gradient throughout the waveguide[30]. However, for diffusion into a thin film of cadmium sulphide a stepped index profile was considered since the diffusion time would produce an even concentration of selenium throughout the waveguide channel. The small refractive index difference of 5×10^{-3} between the cadmium sulphide and the CdS_xSe_{1-x} means that the modes are near cut-off for the guides considered and the approximate theory of Marcatili does not hold. A ray optics analogy to waveguide propagation in the rectangular waveguides is considered and a modification made to the theory to more accurately describe the case of the selenium diffused waveguides.

For a CdS_xSe_{1-x} rectangular waveguide there is a large refractive index difference between region 2,4 and 1 while only a very small difference exists between regions 3, 5 and 1. Therefore a mode in the y-direction will still be well guided when a mode in the x direction is near cut-off. The situation can be described

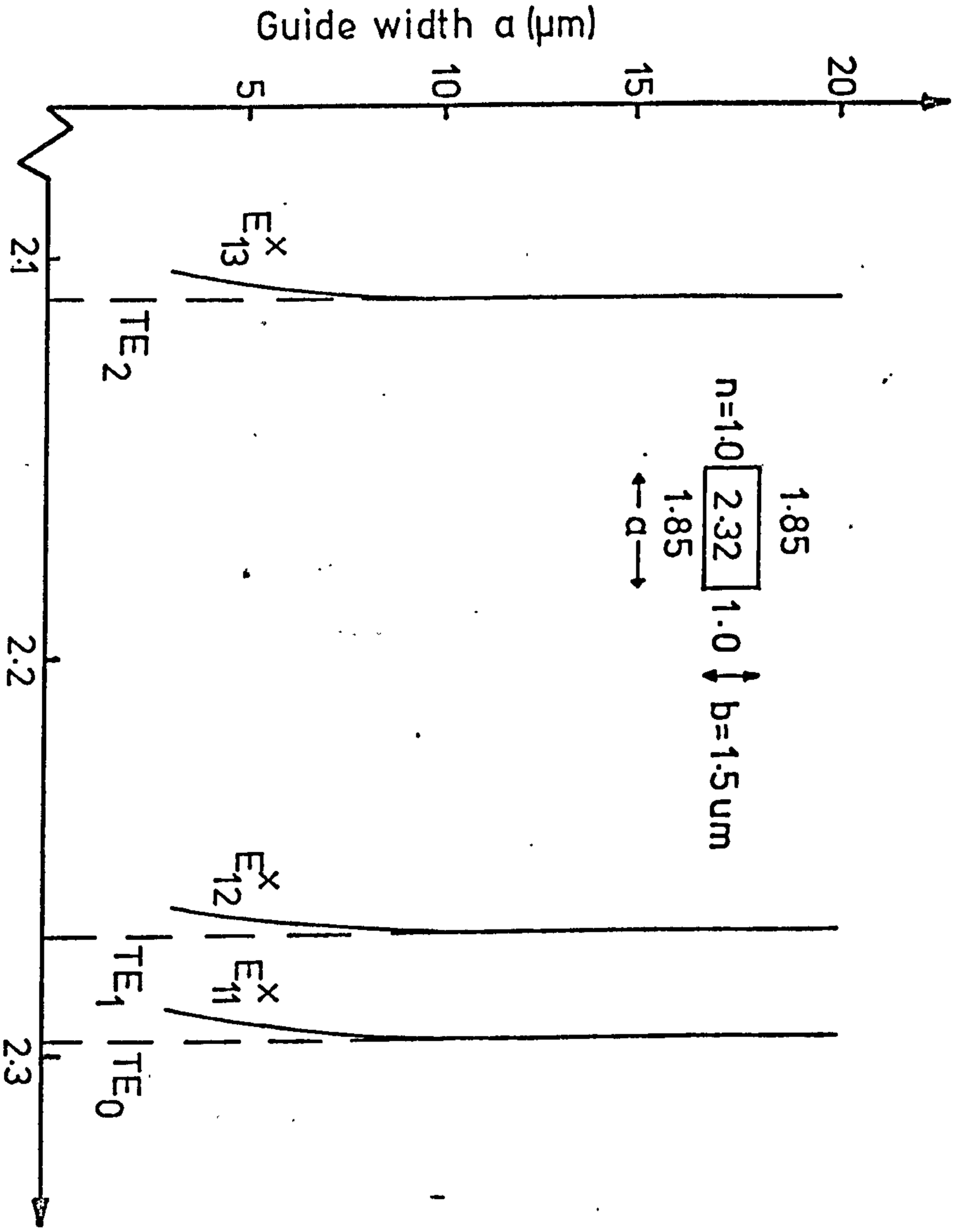

FIGURE 7.2 Normalised propagation constant versus guide width

alternatively by the large aspect ratio guide illustrated in Fig. 7.3; where the mode is near cut-off in the lateral dimension while still being well guided in the thickness direction. A ray path through such a waveguide is illustrated along with the projections of the ray on the x-z and y-z planes. The dots represent the points at which reflections from the guide-surrounding medium occur. It can be seen that, as with Marcatili's theory, the mode propagation in the rectangular guide can be represented by two slab waveguide modes. However, the reflections from the other faces slightly alter the profiles of these projected slab guides and although in the y-z plane the reflections are not significant those in the x-z plane are (Fig. 7.3). A new effective guide index is derived for the wave propagating in the x-z plane. The reflections at the x-z plane give the ray projected in that plane an effective path directly in the x-z plane. The refractive index "seen" by the wave in that plane is therefore more accurately represented by the vector k'_1 rather than the vector k_1 as defined in Fig. 7.4 and the following equations result;

$$k_1'^2 = k_x^2 + k_z^2 \tag{7.10}$$

$$k_1^2 = k_x^2 + k_y^2 + k_z^2 \tag{7.11}$$

therefore

$$k_1'^2 = k_1^2 - k_y^2 \tag{7.12}$$

Substituting k'_1 for k_1 in Marcatili's formulae will modify the expression for ξ_i giving

$$\xi_i = \frac{1}{|k_{xi}|} = \frac{1}{(\beta^2 - k_i^2)^{\frac{1}{2}}} \tag{7.13}$$

Equation (7.13) can be used to define the evanescent fields in region 3 and 5 of the CdS_xSe_{1-x} waveguide. For unity aspect ratio guides

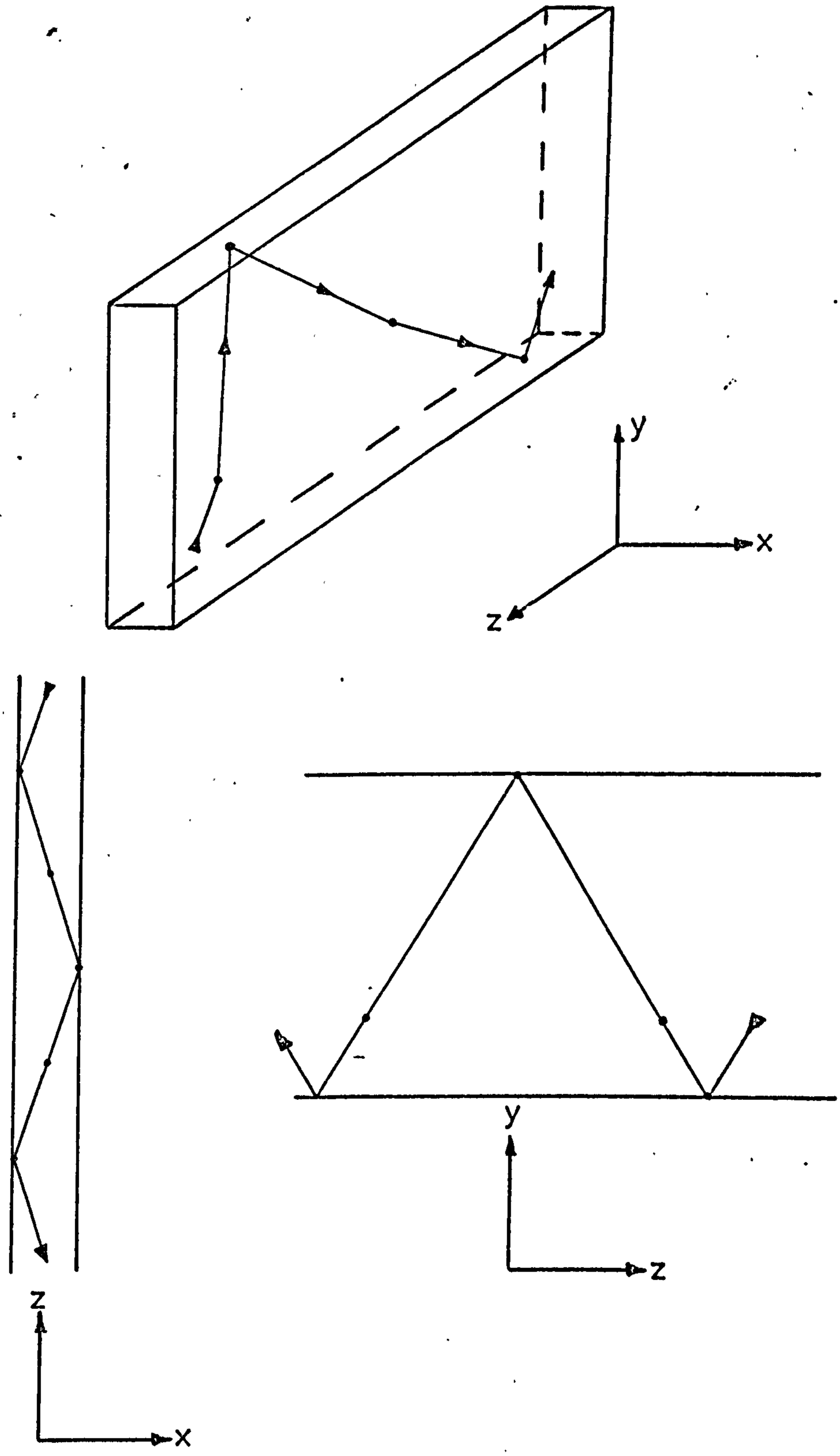

FIGURE 7.3 Ray representation of propagation in a rectangular waveguide

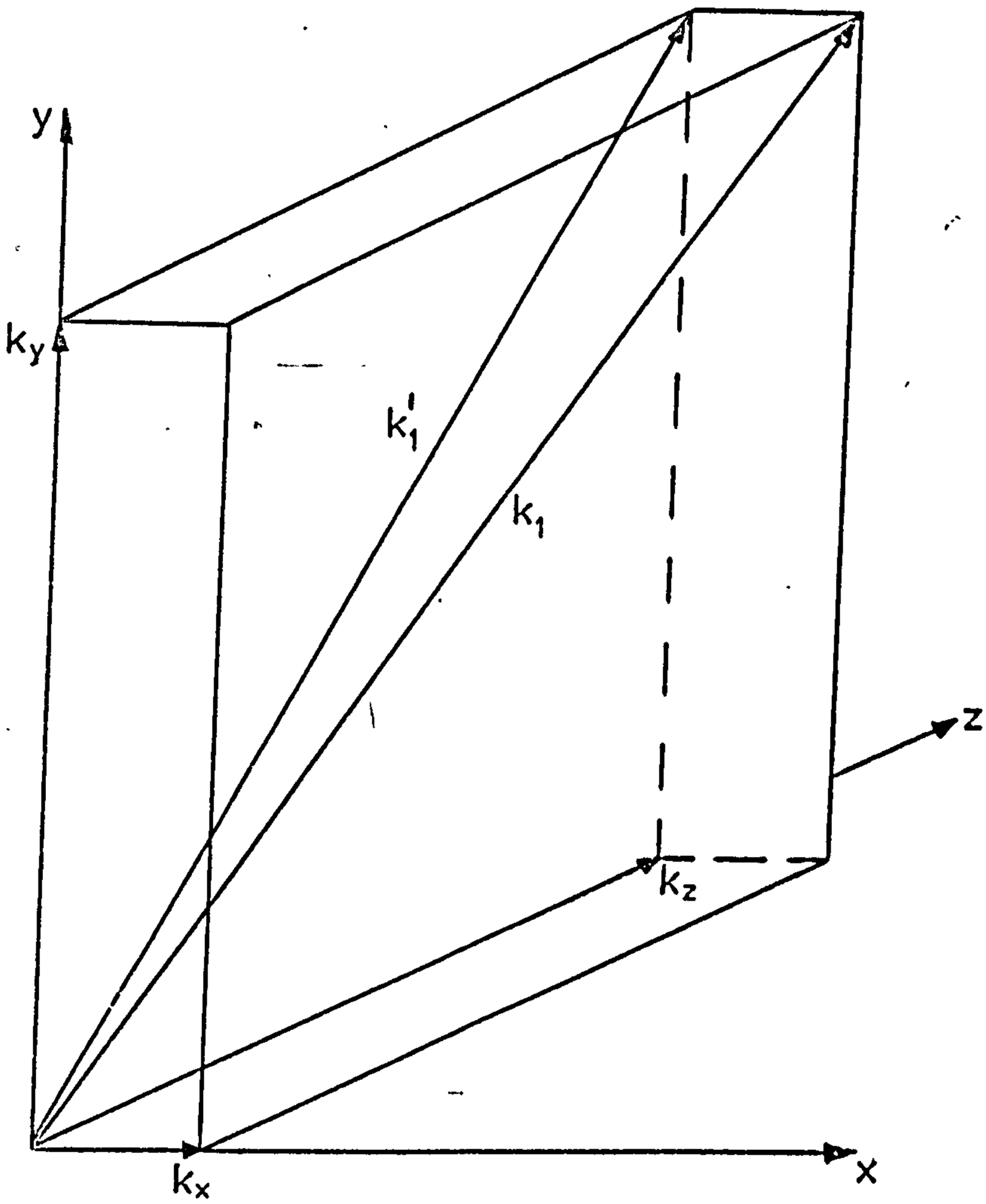

FIGURE 7.4 Vector diagram defining k_1'

the theory will breakdown as the wave is tending to cut-off in both dimensions.

The validity of the above analysis was checked by comparing the results with those of Goell's circular harmonic analysis[101] and although the aspect ratio is only 2:1 there is reasonable agreement as can be seen from Fig. 7.5. The approximation improves with larger aspect ratio guides and as the aspect ratio tends to infinity the mode equation (7.1) reduces to the form for planar waveguide propagation (equation (2.8)). The concept of a large aspect ratio guide is entirely analogous to the CdS_xSe_{1-x} waveguide (x large) in a cadmium sulphide film. A $\beta/_k$ versus guide thickness plot, illustrated in Fig. 7.6, compares the results of this analysis to those calculated directly from Marcatili's formulae.

The above analyses only provide an adequate insight into mode propagation in the rectangular dielectric waveguides described in the remainder of this thesis and should not be considered as a comprehensive theoretical analysis of 2-d waveguides.

7.2 FABRICATION OF CADMIUM SULPHIDE RECTANGULAR WAVEGUIDES

The objective was to produce rectangular dielectric waveguides based on thin, vacuum evaporated films of cadmium sulphide. The optical attenuation was to approach that of the planar waveguides described in chapter 4 so that a low drive power modulator and an optical switch could be fabricated. This, however, represented a considerable technological challenge and two main fabrication approaches were tried; firstly a modification of the cadmium sulphide film once it had been evaporated onto a substrate and secondly alterations to the substrate prior to the cadmium sulphide evaporation. Both techniques relied primarily on the formation of the waveguide pattern in photoresist and the consistency with which the pattern could be replicated into the final waveguide.

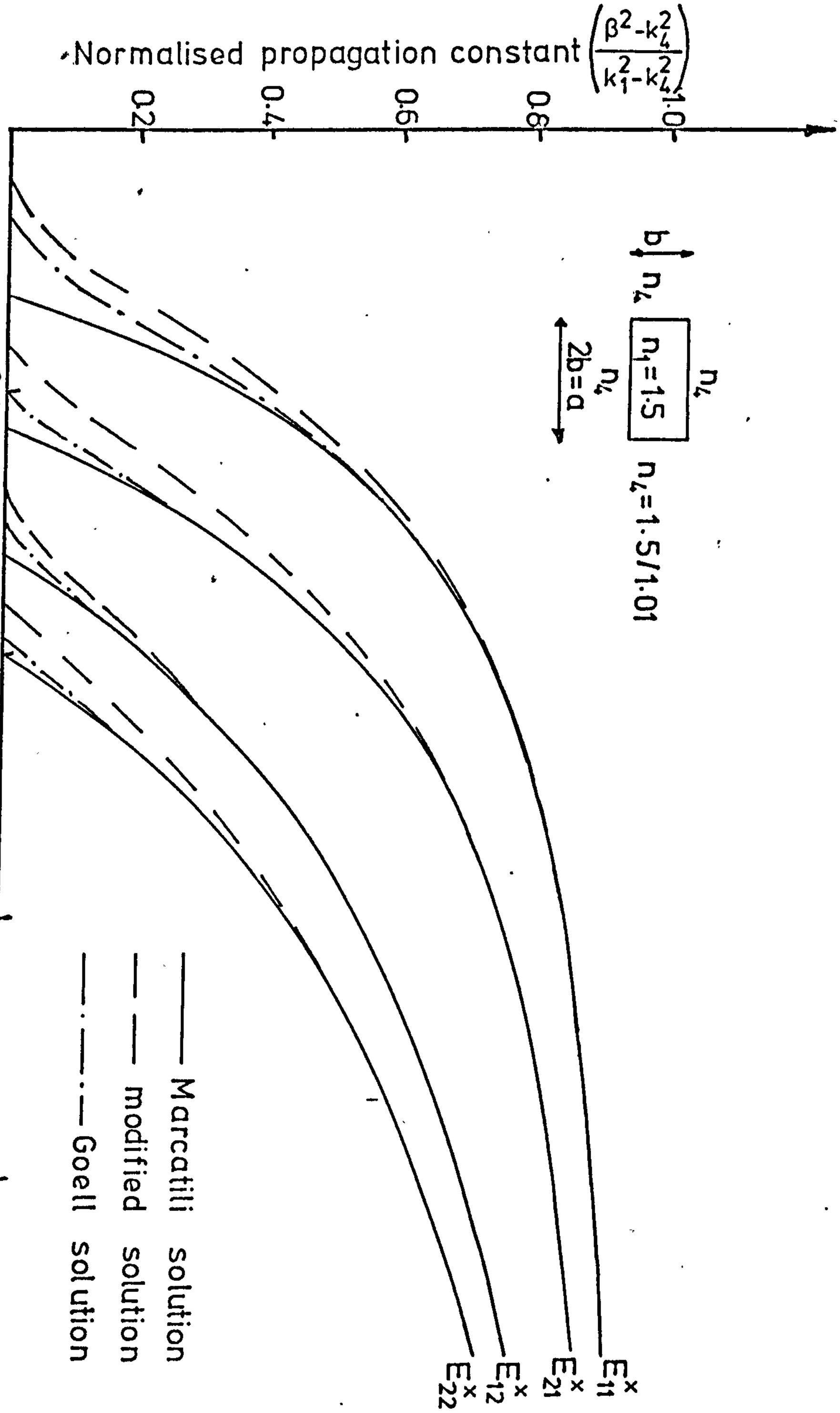

FIGURE 7.5 Normalised propagation constant versus normalised thickness comparing Goell's solutions to the modified theory

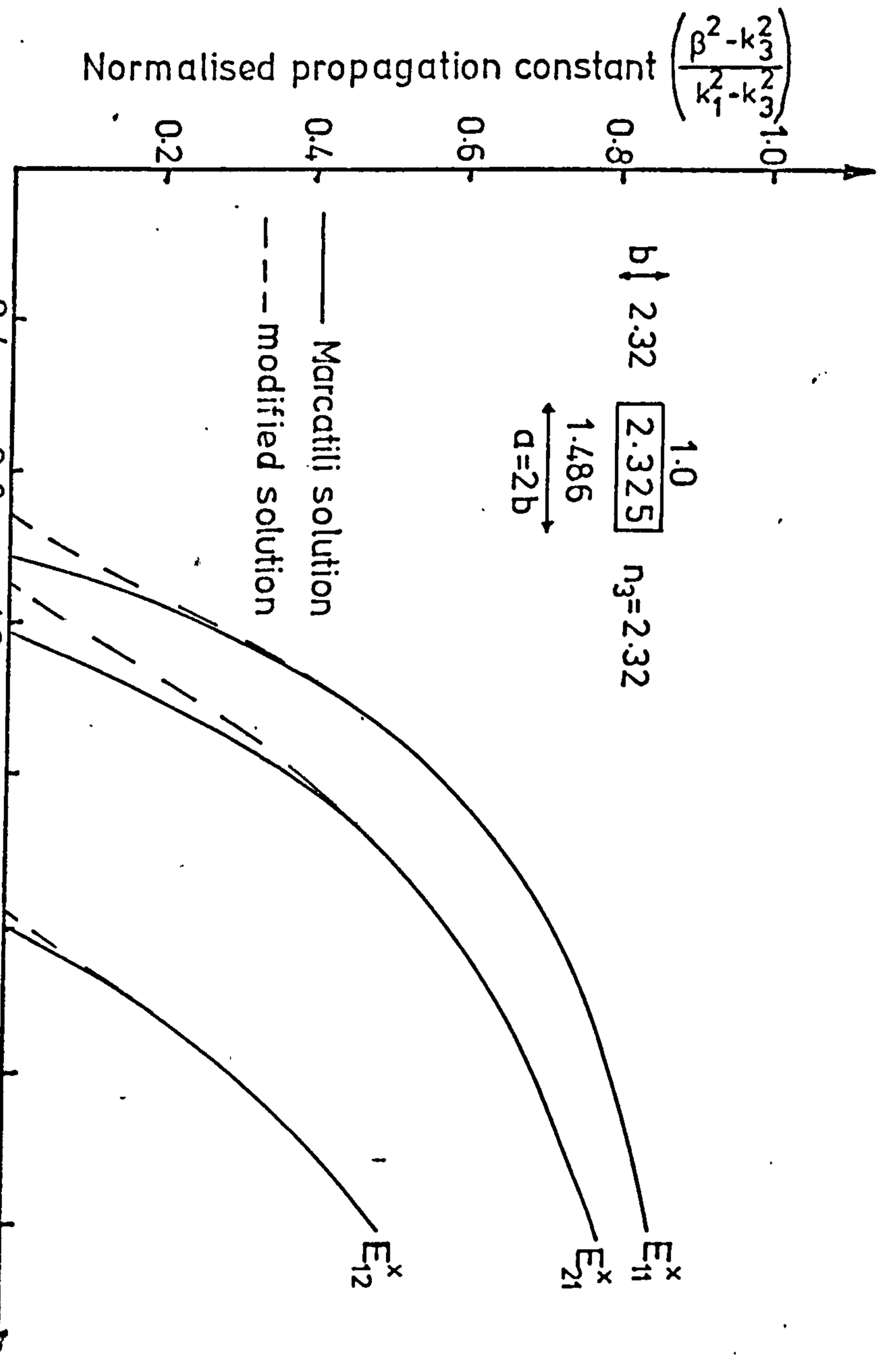

FIGURE 7.6 Normalised propagation constant versus normalised thickness for a selenium diffused rectangular CdS waveguide

Positive Shipley AZ1350J photoresist was used throughout the study because of its ability to withstand chemical and ion beam etching while at the same time producing good edge definition. When photolithography was carried out directly on the surface of a cadmium sulphide film the edges of the film had to be protected with unexposed photoresist during processing to prevent the film from detaching itself from the substrate. The waveguide dimensions were all within the capabilities of replication by conventional photolithography and exposure was carried out using contact printing through conformable masks.

7.2.1 CHEMICAL ETCHING

A waveguide pattern was defined in photoresist on the surface of a cadmium sulphide thin film. Various chemical etches for cadmium sulphide, listed in Table 7.1 along with their relative etch rates, were used to remove the unwanted cadmium sulphide leaving a rectangular waveguide pattern replicated in the remaining cadmium sulphide. It was found that both the methanol-bromine and chromic acid attacked photoresist very much more rapidly than they etched cadmium sulphide and were therefore discarded. The presence of hydrofluoric acid in the white etch tended to attack the glass substrate and cause removal of the cadmium sulphide film. Neither nitric or hydrochloric acid affected the photoresist masking but their etch rates to cadmium sulphide were much too vigorous to be controllable. A series of dilutions of the hydrochloric acid with water was tried and a 1:1 mix of $HCl:H_2O$ was found to produce a reasonably controllable etch rate. This etchant was therefore used to produce chemically etched rectangular waveguides of cadmium sulphide on glass substrates.

The waveguides produced were typically 1.5 μm thick and ranged in width from 50 μm to 20 μm in 10 μm steps. In all cases the side wall roughness was very poor with up to 3 μm variation in width

Etchant	Relative etch rate to cadmium sulphide
Nitric acid	etches vigorously
Hydrochloric acid	etches moderately fast
White etch ($1HF:4HNO_3$)	etches moderately
Methanol bromine (5% Br)	etches slowly
Chromic acid	etches slowly

TABLE 7.1 Chemical etches and their effect on cadmium sulphide

occurring. It was found impossible to improve on this edge quality which was considered to be caused mainly by the preferential etching of the cadmium sulphide crystallites. In all cases the surface finish of the cadmium sulphide was unaffected by the processing. Waveguide losses of greater than 30 $dBcm^{-1}$ were measured in the 50 μm wide guides with the losses in the narrower guides significantly larger.

7.2.2 ION BEAM ETCHING

Ion beam etching or machining is a well established technique for replicating patterns in a substrate by removal of the mask and substrate materials by sputtering and has been described in a number of review articles[103]. It has been used in many applications over the past years (eg for the production of microelectronic circuit patterns) and has now evolved as a useful technique for integrated optics applications. The high resolution capability means that it will faithfully reproduce any pattern.

The ion beam etching of cadmium sulphide, however, has some difficulties which do not arise with the etching of other materials. These are mainly due to the need to remove the remaining protective mask without damaging the cadmium sulphide film underneath. The high chemical reactivity of cadmium sulphide precludes the use of most common ion masks and indeed polymer films such as photoresist are the only materials that can be satisfactorily removed from cadmium sulphide. To enable the photoresist to withstand the ion plasma it must be baked to a temperature of 150°C for one hour prior to etching. Baking, however, seriously alters the profile of the resist as can be seen from the scanning electron micrographs (Figs. 7.7a and 7.7b) of a rectangular resist pattern on cadmium sulphide before and after baking. Baking first causes the resist to flow across the surface of the cadmium sulphide and to take up a

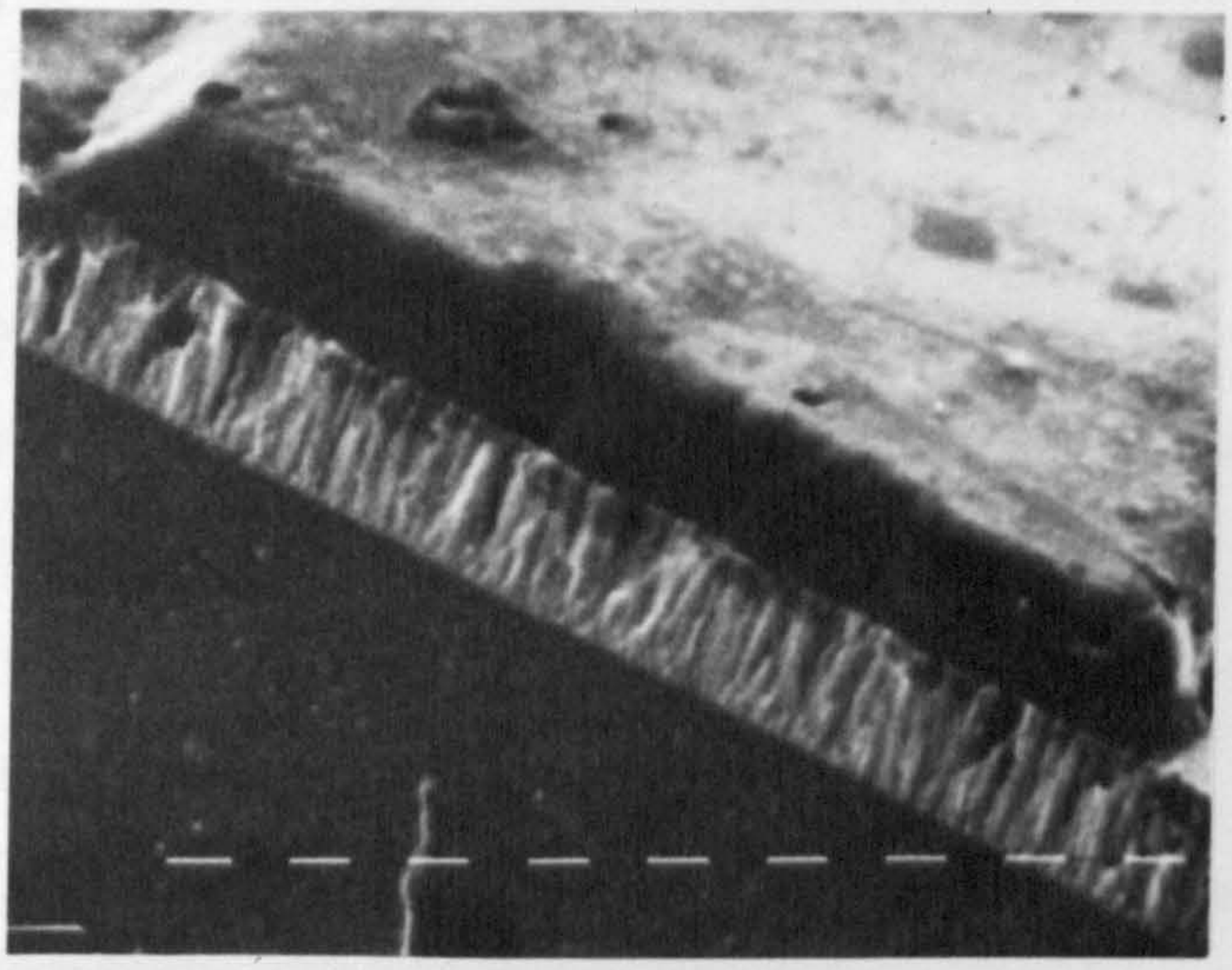

(a) Unbaked photoresist

magnification 5K

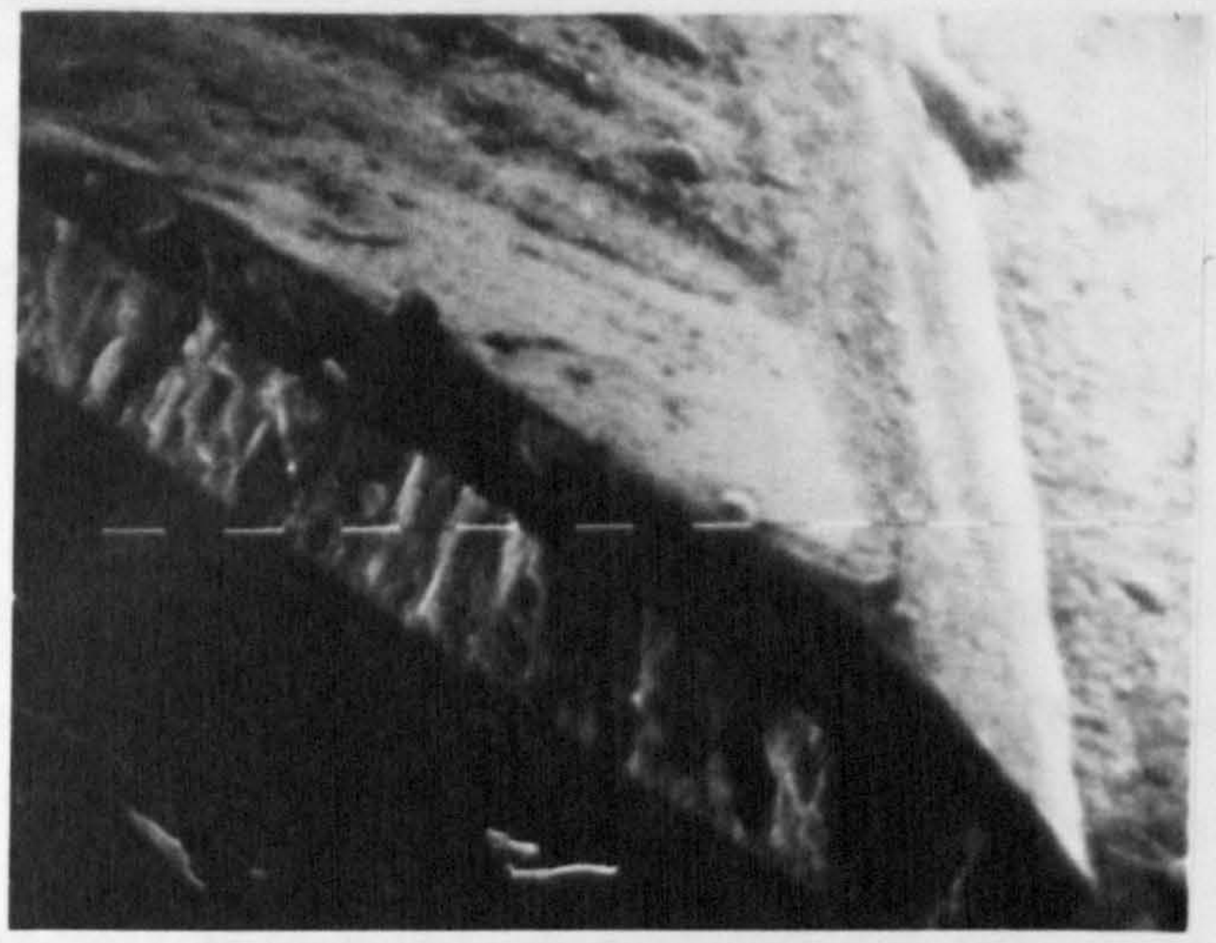

(b) Photoresist after baking for 1hr at 150°C

magnification 5K

FIGURE 7.7 Scanning electron micrographs of a 20μm photoresist ridge on a cadmium sulphide film

meniscus shape. The volatile constituents of the resist are then driven off by evaporation and the meniscus contracts still retaining the same general shape. The photoresist in this form is able to withstand the ion beam. However, as can be seen in Fig. 7.7b, the mask is no longer rectangular and when etching takes place sloping rather vertical sides in the cadmium sulphide rectangular waveguide result. Sputtering rate is a non-monotonic function of the angle of incidence of the ions and Fig. 7.8 shows schematically how this also produces sloping edges in the substrate. A combination of both the above mentioned effects gives a trapezoidal rather than a rectangular waveguide profile.

The trapezoidal shape has the disadvantage that the sloping edges are rough and lead to a large waveguide attenuation due to scattering. The roughness arises from the differential etch rates of the waveguide and mask materials. When a film is etched it is not attacked smoothly but developes a surface roughness caused by the impinging ions. When this material is completely removed the roughness will reproduce itself in the waveguide material particularly when the waveguide material etches at a faster rate than the mask material. Once the etching has been completed the remaining resist was removed by oxidation in an r.f. plasma.

The ion beam etching was carried out in an Edwards diffusion pumped coating unit with a G.V. Planar ion gun assembly. The substrates were mounted on a rotating table to provide an even etch rate and the etching was carried out in an argon atmosphere at a pressure of 4-5 microns with the ion gun set to 5 kV and 30 mA. The etch rate of cadmium sulphide was measured to be 400Å min^{-1} with the AZ1350J photoresist being etched at approximately one quarter of this rate. This differential between the etch rates meant that if rectangular masks could be formed then good edges should be possible in the cadmium sulphide rectangular waveguides.

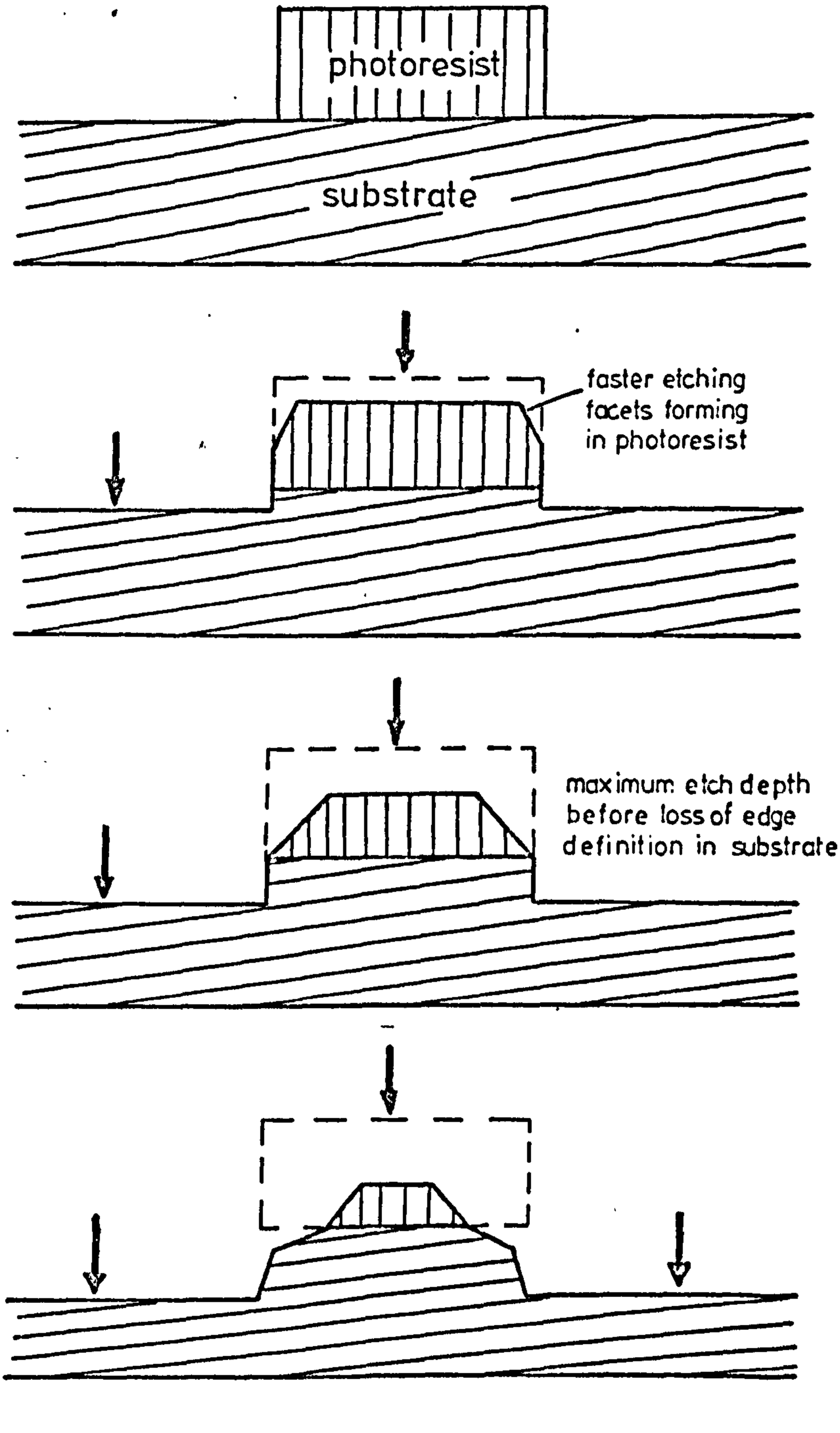

FIGURE 7.8 Schematic diagram of the stages of ion beam etching

The resist thickness, baking time and baking temperature were carefully studied with a view to producing a mask of near rectangular shape but it was found in all cases that the general shape of Fig. 7.7b resulted once all the volatile components of the resist had been driven off. The optimum thickness of photoresist film was found to be between 1 and 2 μm. The best guides achievable thus had sloping side boundaries which contributed to a higher waveguide attenuation than had been expected. Any preferential etching of crystal facets of the cadmium sulphide was masked by the sloping edge roughness. Fig. 7.9 shows that there is no obvious difference between a polycrystalline film grown on a glass substrate and a single crystal film grown on < 111 > spinel. The major contribution to waveguide loss was therefore due to the rough sloping edges caused by the poor shape of the photoresist mask. Care had to be exercised when oxidising the remaining resist as a very intense plasma could damage the surface of the cadmium sulphide.

The waveguides produced were typically 1.5 μm thick and had optical losses of 20-25 $dBcm^{-1}$ in 50 μm wide guides and greater than 30 $dBcm^{-1}$ in 20 μm wide guides.

7.2.3 SELENIUM DIFFUSION INTO CADMIUM SULPHIDE

Diffusion of selenium into single crystals of cadmium sulphide to produce a CdS_xSe_{1-x} ($x = 1 \rightarrow 0$) structure has been studied in the past[30]. It is well known that CdS_xSe_{1-x} has a higher refractive index than cadmium sulphide and the diffusion technique has thus found application in integrated optics. It has been used to form low loss rectangular waveguides in single crystal substrates of cadmium sulphide[9] because the diffuse waveguide profile meant that edge roughness from the side walls was ameliorated and hence scatter loss reduced. The refractive index profiles of these waveguides are graded rather than stepped and considerable theoretical effort has

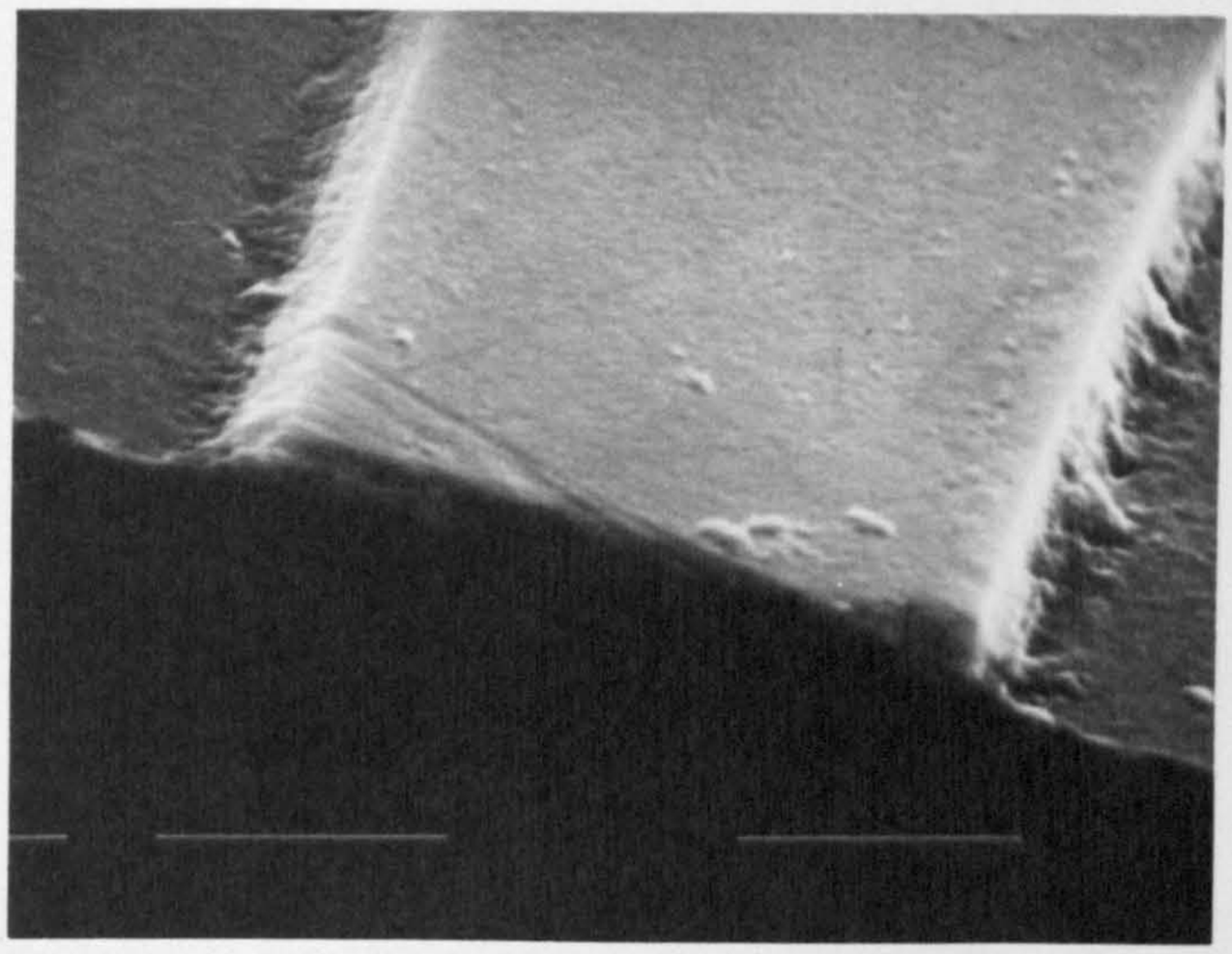

(a) Cadmium sulphide on a glass substrate

magnification 2·5K

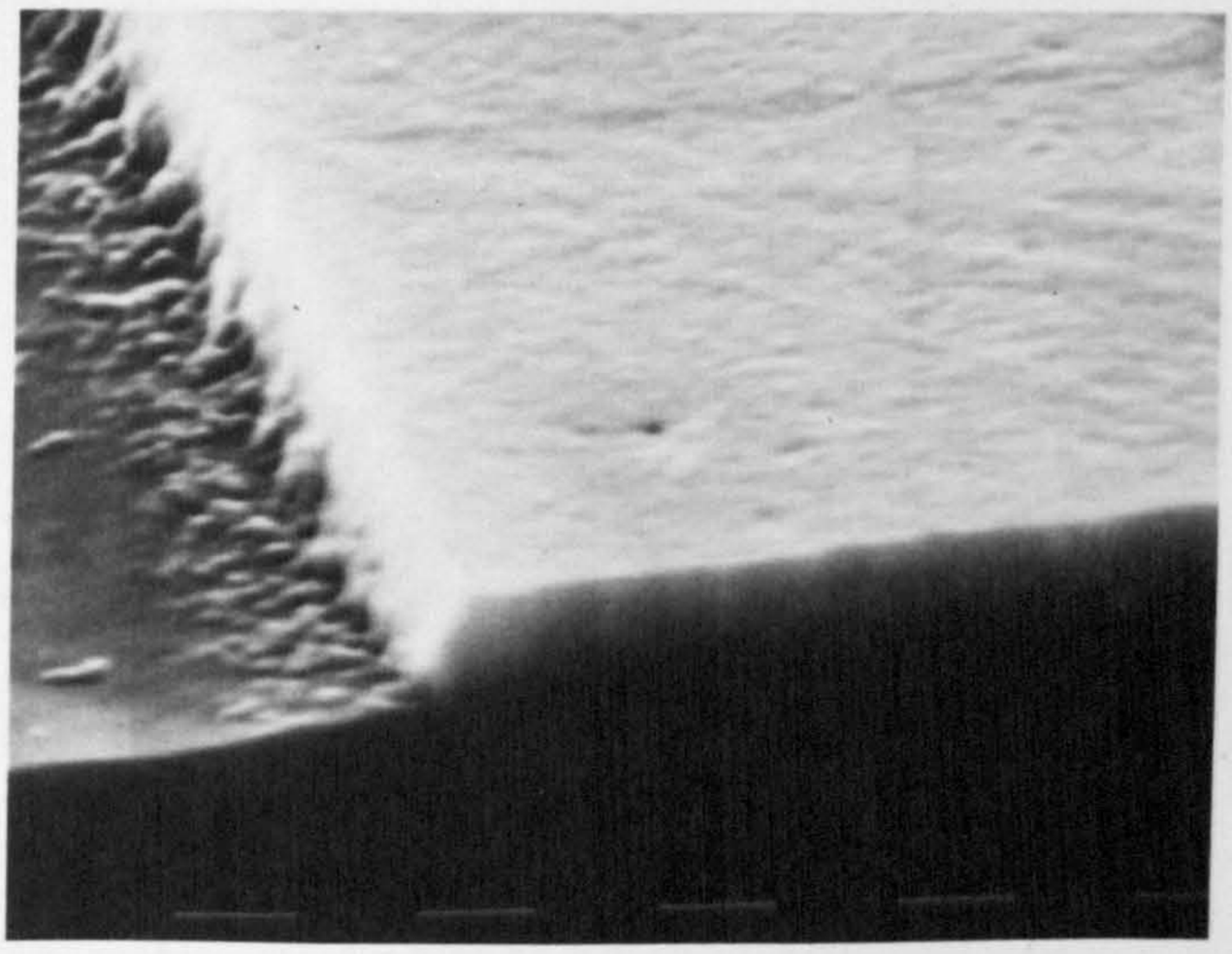

(b) Cadmium sulphide on a spinel substrate

magnification 10K

FIGURE 7·9 Scanning electron micrographs of ion beam etched cadmium sulphide waveguides

been devoted to a study of mode propagation in these structures[104]. However, a stepped index profile was assumed in the analysis of section 7.1.2 since the selenium diffusion was into thin polycrystalline films of cadmium sulphide rather than bulk single crystals.

In the first experiments the cadmium sulphide films were evaporated onto fused silica substrates and a diffusion carried out following the procedure of Taylor et al[9]. The thin film was sealed into a quartz ampoule evacuated to 10^{-6} torr along with sulphur, selenium and cadmium sulphide powder in specified molar proportions. The mass per unit volume ratios of the sulphur and selenium were 1.1 $mgcm^{-3}$ and 3.7 $mgcm^{-3}$ respectively. The ampoules were then placed in a resistance furnace and heated to 600°C. The temperature gradient over the length of the ampoule was less than 2°C and fluctuations in the mean temperature were of the order of $\pm$ 1°C. The processed ampoule was allowed to cool down to room temperature over a period of 12 hours. The resultant films all had bad surface damage with fine cracks and pit marks in which globules of recondensed selenium lay. When diffusion was carried out on films grown on spinel only the pit marks were observed indicating that the cracks were due to a difference in thermal expansion between the fused silica and the cadmium sulphide. None of the films was suitable for light guiding and the results were independent of diffusion time. It was only once the selenium concentration had been reduced to a level of 1 μgcm^{-3} that CdS_xSe_{1-x} films of an acceptable optical quality were produced. The diffusion temperature was reduced to 350°C to permit the use of glass substrates and the ampoules were sealed at half an atmosphere of nitrogen to reduce the level of sulphur diffusion out of the cadmium sulphide. The diffusions were carried out for 3 hours and the concentration of selenium in the cadmium sulphide was controlled by altering the mass per unit volume present. The diffusion coefficient

of the selenium was such that in a 3 hour diffusion the selenium will have penetrated completely through the cadmium sulphide film thus substantiating the assumption of a stepped refractive index profile.

Optical measurements on planar CdS_xSe_{1-x} waveguides confirmed losses of 7 $dBcm^{-1}$ for a refractive index increase of $5x10^{-3}$ and 12 $dBcm^{-1}$ for a refractive index change of 10^{-2}. Attempts to introduce still higher concentrations of selenium resulted in extremely large waveguide losses.

Rectangular waveguides were fabricated by masking the cadmium sulphide with a thin film of silicon monoxide in which a waveguide pattern had been replicated using the lift-off technique. The diffusion was carried out in the manner described above. Waveguiding was demonstrated in a 4 μm thick film with waveguide widths from 50 μm to 5 μm and a refractive index difference of $5x10^{-3}$. The losses measured increased from 8 $dBcm^{-1}$ for the 50 μm guide to around 15 $dBcm^{-1}$ for the 5 μm wide guide. These low waveguide losses can be attributed to the small refractive index difference causing only very slight confinement of the guided wave.

7.2.4 SUBSTRATE ETCHING

All the methods described in the previous sections have involved a modification to the cadmium sulphide film once it has been deposited. In this section two methods of modifying the substrate prior to the deposition of cadmium sulphide are discussed. The underlying principle was to form deep grooves in the substrate such that when the cadmium sulphide evaporation took place the film will not grow continuously but will break at the edges of the channels and result in the formation of rectangular waveguides either on the ridges or in the channels (see Fig. 7.10). The side walls of the cadmium sulphide rectangular guides would then be formed during the

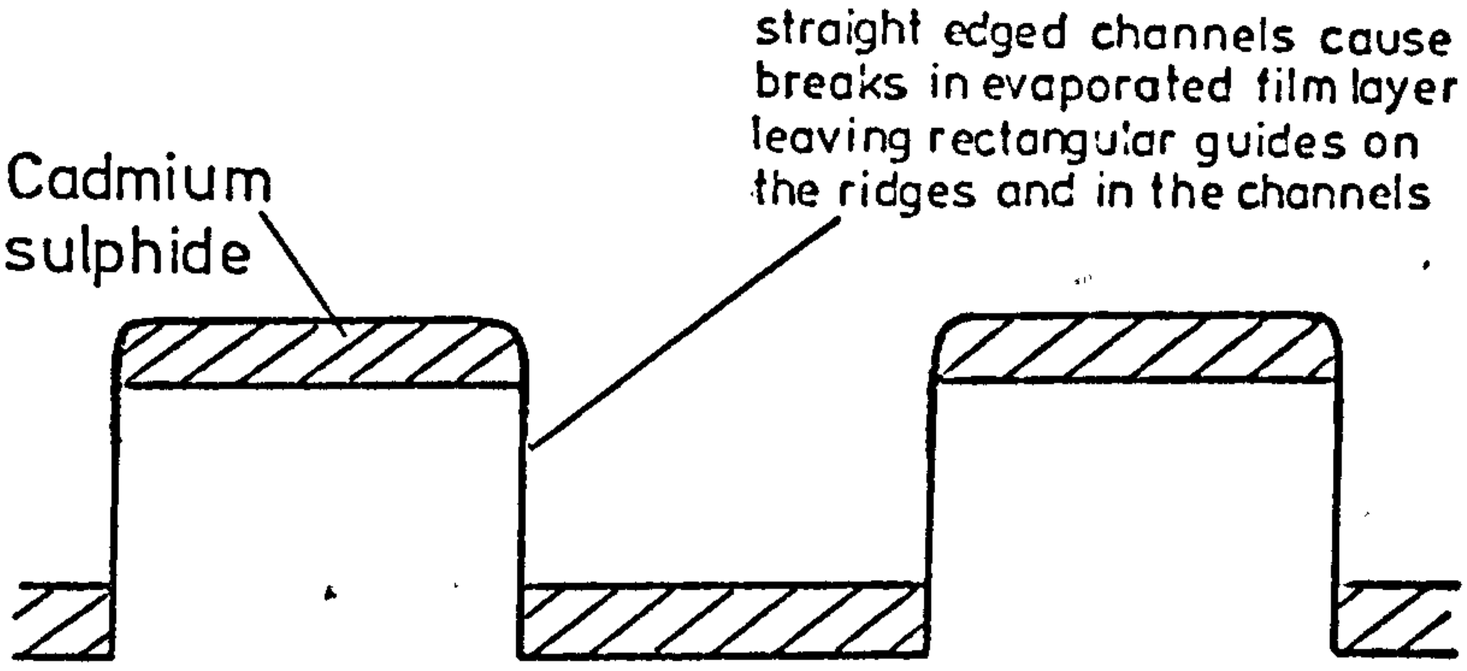

FIGURE 7·10 Schematic diagram of a cadmium sulphide thin film deposited on an etched substrate

evaporation process and the resulting scatter should be greatly reduced. The first technique involved the ion beam etching of a glass substrate and the second involved selectively etching a single crystal substrate of silicon. The slow etch rate of glass (85Å min^{-1}) meant that the channels were only ~ 1 μm deep and had sloping edges. The desired film break did not occur when the evaporation was carried out and thus the majority of effort was concentrated on the latter method.

Etches which preferentially attack the planes of silicon have been used in a variety of applications[105] and the fabrication of waveguides formed by filling etched silicon channels with PMMA has recently been reported[106]. In the department apparatus existed for the preferential etching of silicon for use in transmission electron microscopy studies and the etching of silicon waveguide channels was carried out using that apparatus. The etchant was a ternary mixture of water, amine and complexing agent which is fully described, along with the refluxing apparatus, in a paper by Finne et al[105]. The etch rates for the < 111 >, < 110 > and < 100 > planes of silicon were approximately 3:30:50 μm/hr respectively. A straight waveguide with the sides orientated parallel to the (100) direction would produce of waveguide groove with the side walls formed by perfectly smooth < 111 > planes of silicon as illustrated schematically in Fig. 7.11.

< 100 > silicon wafers (n-type, 3-4 Ωcm) polished on one side were thermally oxidised to produce a layer of silicon dioxide between 0.3 μm and 0.5 μm thick. Photolithography was carried out with the appropriate care being taken to align the waveguide edges along the (110) crystallographic directions. Buffered hydrofluoric acid was used to remove the silicon dioxide and the waveguide ridges were defined by the remaining silicon dioxide after the photoresist had been removed. The etchant then exposed the < 111 > planes of the

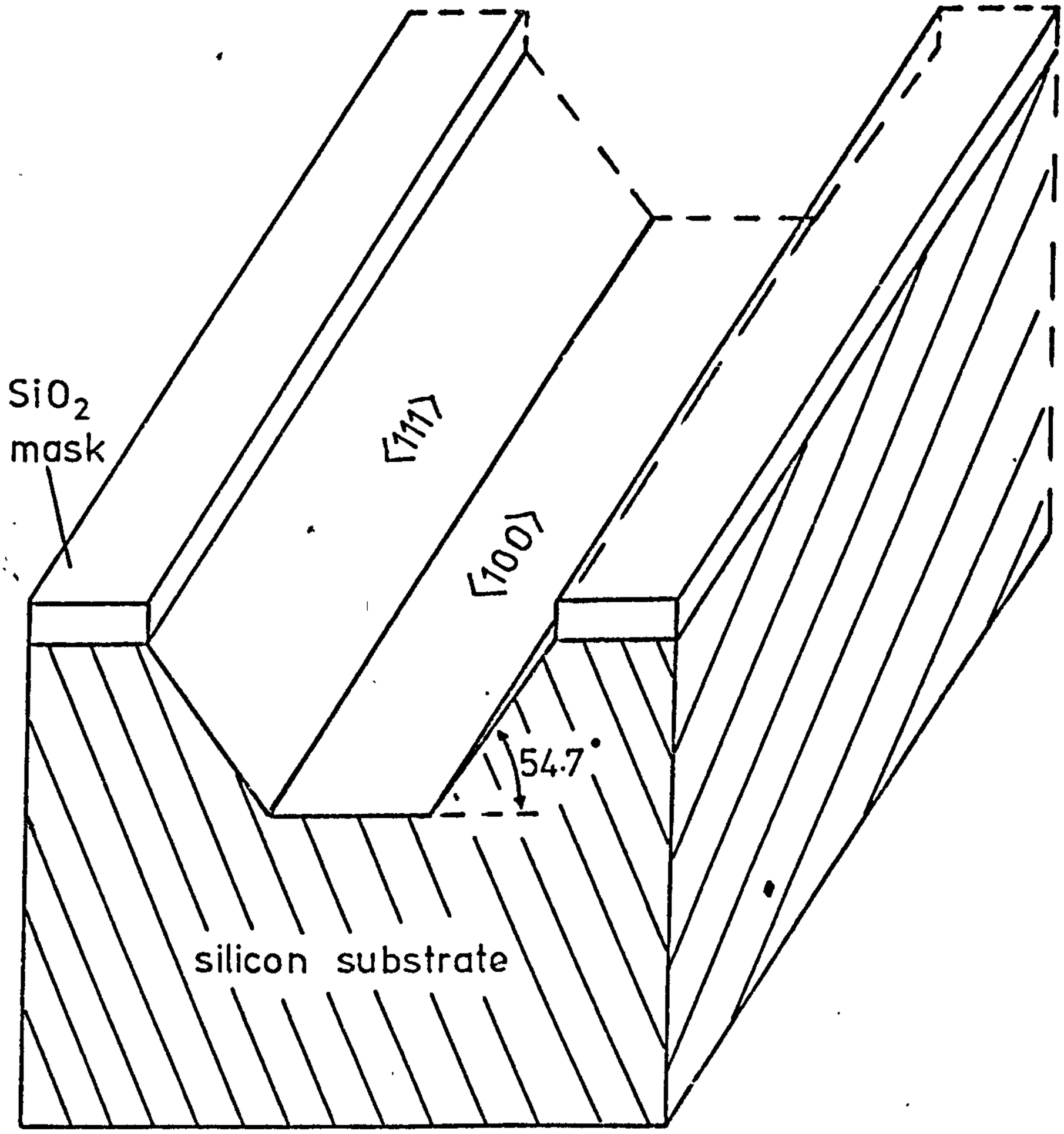

FIGURE 7·11 Schematic diagram showing the waveguide groove formed by the preferentially etched ⟨111⟩ planes of silicon

silicon due to the preferential etch rates while the silicon dioxide performed the role of the mask since it is only attached very slowly by the etchant. The etched silicon channels contained pit marks caused by crystal defects in the silicon and thus the ridges, which had remained protected by the silicon dioxide, were used as the "substrates" for the rectangular waveguides. After the etching process the remaining oxide was removed and a thick oxide buffer layer grown to eliminate waveguide attenuation from the silicon. A cadmium sulphide film was then evaporated over the substrate and rectangular waveguides were formed on the top of the etched silicon ridges which were approximately 20 μm high. Fig. 7.12 illustrates a scanning electron micrograph of the rectangular guides on the silicon ridges. The edges are very straight and do not have the roughness associated with the ion beam etched guides of Fig. 7.9.

The waveguides were typically 2.0 μm thick and had widths ranging from 50 μm to 20 μm in steps of 10 μm. The corresponding waveguide losses increased from 8dBcm^{-1} to 15 dBcm^{-1}.

7.3 SUMMARY OF RESULTS

A critical review of the loss figures obtained for the various fabrication techniques shows that the waveguide attenuation is dominated by scatter from the side walls (excluding the diffused waveguides). Table 7.2 summarises the minimum waveguide attenuation possible using the current technologies. It was estimated that waveguide losses of less than 15 dBcm^{-1} were required to perform experiments on an electrooptic modulator with lateral confinement and since the chemically etched and ion beam etched waveguides had losses of at least 30 dBcm^{-1} they were excluded from further consideration. However, both the guides formed using selectively etched silicon substrates and those formed by selenium diffusion represent possible bases for device fabrication. Waveguides evaporated onto etched silicon have

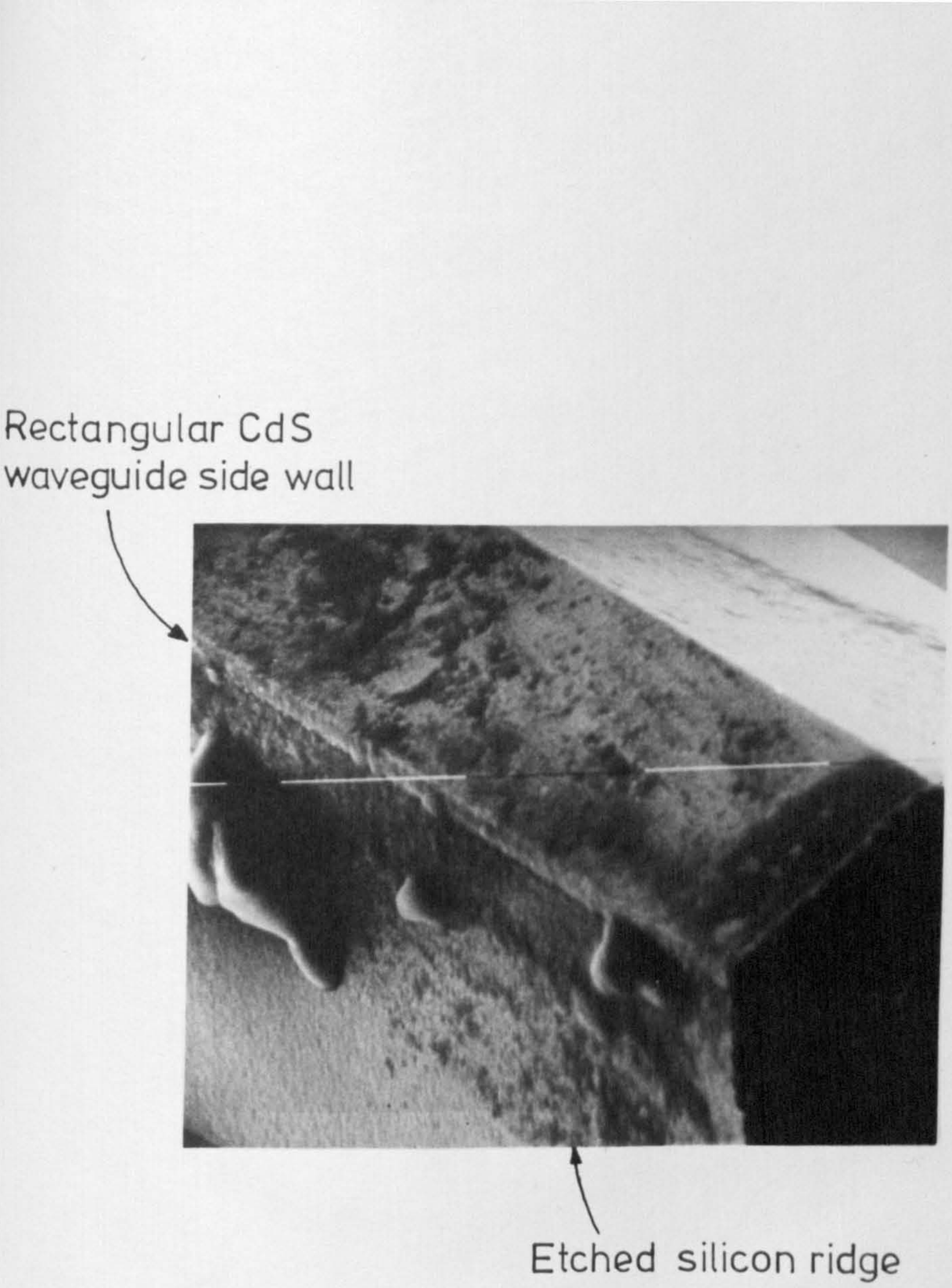

FIGURE 7.12 Scanning electron micrograph of cadmium sulphide on an etched silicon ridge (magnification 2.5K)

Table 7.2 Summary of cadmium sulphide rectangular waveguide losses

Waveguide Fabrication Process	Waveguide dimensions		Minimum loss of lowest order TE mode
	Width (μm)	Thickness (μm)	
Chemical etching	50.0	1.5	> 30 $dBcm^{-1}$
Ion beam etching	50.0	1.5	20-25 $dBcm^{-1}$
Deposition on selectively etched silicon substrates	20.0	2.0	15 $dBcm^{-1}$
Selenium diffusion	5.0	4.0	15 $dBcm^{-1}$

a loss of 15 $dBcm^{-1}$ for waveguide geometry of 20 μm by 1.5 μm thick while the same loss can be achieved in a CdS_xSe_{1-x} waveguide 5 μm wide x 4 μm thick.

For a rectangular waveguide electrooptic phase modulator the confinement offered by the cadmium sulphide waveguide deposited on an etched silicon substrate will produce a low power per unit bandwidth device. The width of the guide will not permit discrete transverse modes to be excited but this is not necessary in the modulator. However, for the optical switch based on an electro-optically switched directional coupler, discussed in chapter 8, single mode operation is essential and the CdS_xSe_{1-x} waveguide represents the better technology. Both fabrication techniques are still based on the vacuum evaporation of polycrystalline cadmium sulphide thin films onto amorphous substrates and thus the possibility of efficient fibre-film coupling discussed in chapter 6 will still apply to the rectangular waveguides.

7.4 EXPERIMENTAL ELECTROOPTIC PHASE MODULATOR BASED ON RECTANGULAR WAVEGUIDES

An electrooptic phase modulator was built to illustrate the feasibility of the low power per unit bandwidth modulator proposed in part II. Since the waveguide-losses of the rectangular waveguides were higher than those for the slab guides of chapter 4 the device length had to be reduced with a concomitant increase in the power per unit bandwidth calculated in chapter 6. The multilayer modulator structure (Fig. 7.13) was based on a 20 μm wide ridge of selectively etched n-type silicon described in section 7.2.4. The silicon slice was used as the lower electrode and the back surface was doped n^+ by a thermal diffusion of phosphorous pentoxide to produce an ohmic contact between the silicon and the aluminium contact electrode. After the diffusion it was essential to remove all traces of the thermally grown phosphorous glass to maintain the cadmium sulphide

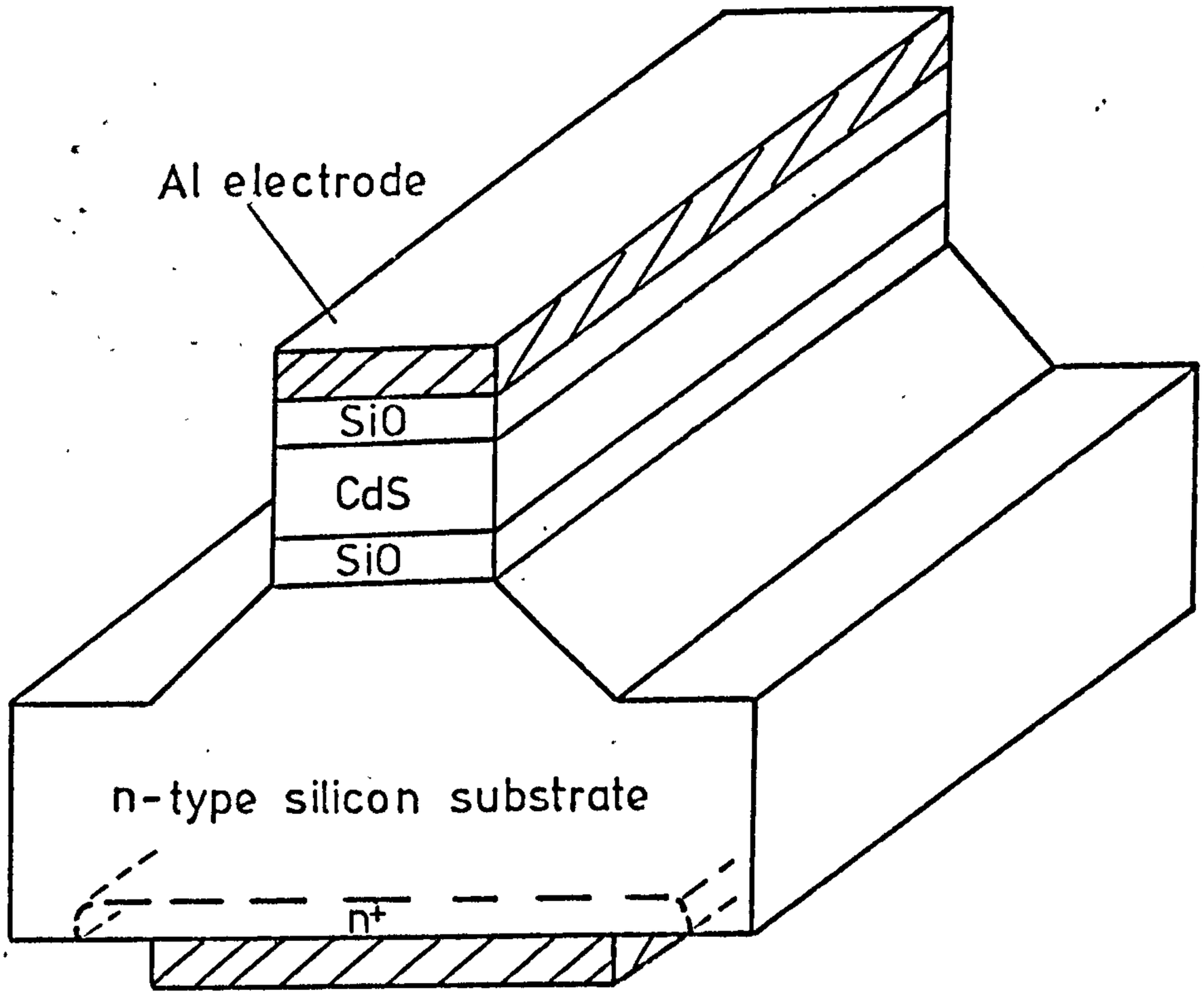

FIGURE 7.13 Schematic diagram of rectangular waveguide modulator

waveguide loss at 15 $dBcm^{-1}$. A 0.6 μm thick buffer layer of silicon monoxide was then evaporated directly onto the etched silicon ridge to eliminate completely any additional waveguide attenuation due to the presence of the silicon substrate. A 2 μm thick cadmium sulphide film was then deposited and the top buffer electrode of silicon monoxide 0.6 μm thick was evaporated through a straight edge mask. It was not possible to define the optimum electrode area of 5x0.02 mm^2 as the 20 μm strip of aluminium would not adhere to the structure. Instead the device was completed by painting a silver electrode 5x2 mm^2 over the silicon ridge.

The phase modulation was detected using the homodyne system described in chapter 6. A combination of two lenses was used to reduce the 1.15 μm beam to a 15 μm diameter spot at the input coupler. The launching efficiency into the lowest order TE mode was 55%. The experimental performance was again in good agreement with the theoretically predicted value. Had an optimised electrode area of 5x0.02 mm^2 been used the power per unit bandwidth would have been 1.45 $mWMHz^{-1}$ for 1 radian phase change with a base bandwidth of 4.7 GHz into a 50Ω load. The drive power figure was, however, higher than the value of 450 $\mu WMHz^{-1}$ predicted in chapter 6. This arises mainly because the basic rectangular waveguide attenuation has limited the interaction length to 5mm and partly because the buffer layer thicknesses had a safety factor included and were not of optimum thickness. The insertion loss of the device was approximately 10 dB.

7.5 DISCUSSION OF RESULTS

An electrooptic modulator using a 20 μm wide rectangular waveguide of polycrystalline cadmium sulphide evaporated onto a selectively etched silicon substrate has been demonstrated. With the present rectangular waveguide fabrication techniques the optical

attenuation precludes the use of narrower waveguides and longer interaction lengths. To define the optimum electrode area of 5x0.02 mm^2 a high conductivity n^+ region should be diffused into the waveguide ridge through the silicon dioxide mask. The width of the top electrode would then be unimportant and with all contacts on the top surface of the silicon wafer a truely planar device technology would result. With the optimum guide and buffer thickness of 1.15 μm and 0.45 μm respectively a minimum power per unit bandwidth of 900 $\mu WMHz^{-1}$ for one radian phase change would result.

Although the evaporation of cadmium sulphide onto etched silicon provides an improved modulator performance the multimode nature of these guides will preclude their incorporation in a directional coupler. However, the single mode nature of the CdS_xSe_{1-x} guides should enable the fabrication of a directional coupler. A theoretical design study of directional couplers and electrooptically controlled switches using directional couplers is detailed in chapter 8.

CHAPTER 8: DESIGN STUDY OF ELECTROOPTICALLY CONTROLLED DIRECTIONAL COUPLER SWITCHES

A device which can switch light from one guide to another separate guide will be an important element of any optical communications system. The directional coupler has been shown[1] to be capable of transferring light from one guide to another by electrooptically controlling the phase of the mode in the coupler. Recently two experimental realisations of this type of switching have been reported[48,49]. However, they suffer the disadvantage of requiring high refractive index single crystal substrates and films, with the associated problem of efficiently coupling the light to and from optical fibres. An electrooptically controlled directional coupler switch based on thin films of cadmium sulphide would overcome this deficiency in an analogous manner to the phase modulator of chapter 6 and hence would be an interesting device.

This chapter considers existing directional coupler theories and points out their limitations. A general expression for the coupling length is derived from an extension of a prism-film coupler theory based on a scatter matrix approach. The tolerances on directional coupler fabrication are discussed in section 8.2 in the context of the two possible mechanisms by which light can be induced to transfer from one guide to another. Specific designs of directional couplers based on cadmium sulphide waveguides are outlined in section 8.3. The results are summarised and discussed in section 8.4 along with a detailed design for the most realistic structure.

8.1 DIRECTIONAL COUPLER THEORY

Extensive theoretical analyses of directional coupling between dielectric waveguides have been published and the results derived from these are briefly summarised in section 8.1.1. In section 8.1.2 a theory for directional couplers is adapted from a scatter matrix

approach to prism-film coupling developed by Dunsmuir et al[107]. The equations derived for a completely general lossless directional coupler are shown to be compatible with the existing theories.

8.1.1 SUMMARY OF PUBLISHED ANALYSES

The directional coupler shown in Fig. 8.1a has two identical waveguides with the modes carrying the optical power in the same direction and is known as a codirectional coupler. Yariv[108] has used coupled mode theory to show that if only guidel is initially excited then the electric field amplitudes of guides 1 and 2 vary as

$$E_1(z) = E_o e^{\frac{i\Delta z}{2}} \left[\cos\left[\tfrac{1}{2}(4\kappa^2+\Delta^2)^{\frac{1}{2}}z\right] - i\,\frac{\Delta}{(4\kappa^2+\Delta^2)^{\frac{1}{2}}} \sin\left[\tfrac{1}{2}(4\kappa^2+\Delta^2)^{\frac{1}{2}}z\right] \right] \tag{8.1}$$

$$E_2(z) = E_o e^{\frac{-i\Delta z}{2}} \frac{2\kappa}{(4\kappa^2+\Delta^2)^{\frac{1}{2}}} \sin\left[\tfrac{1}{2}(4\kappa^2+\Delta^2)^{\frac{1}{2}}z\right] \tag{8.2}$$

where $\Delta = \beta_1 - \beta_2$, β_1 and β_2 are the uncoupled propagation constants of guides 1 and 2 respectively, κ is the overall coupling coefficient and E_o is the initial field amplitude in guide 1. For perfect phase matching between the guides (ie $\Delta=0$) there is complete, periodic power transfer between the two guides with period $L_c = \frac{\pi}{2\kappa}$, the coupling length.

Marcuse[109] has shown that for a non-symmetric coupler structure (Fig. 8.1b) the overall coupling coefficient is given by

$$\kappa = \sqrt{\kappa_1 \kappa_2} \tag{8.3}$$

where κ_1 and κ_2 are the coupling coefficients for the symmetrical couplers of Fig. 8.1c and 8.1d respectively.

The relationship between the waveguide parameters and the coupling coefficient (coupling length) is the most important expression in directional coupler design and several such relationships have been obtained for the symmetric case[110] (Fig. 8.1a). Of these the

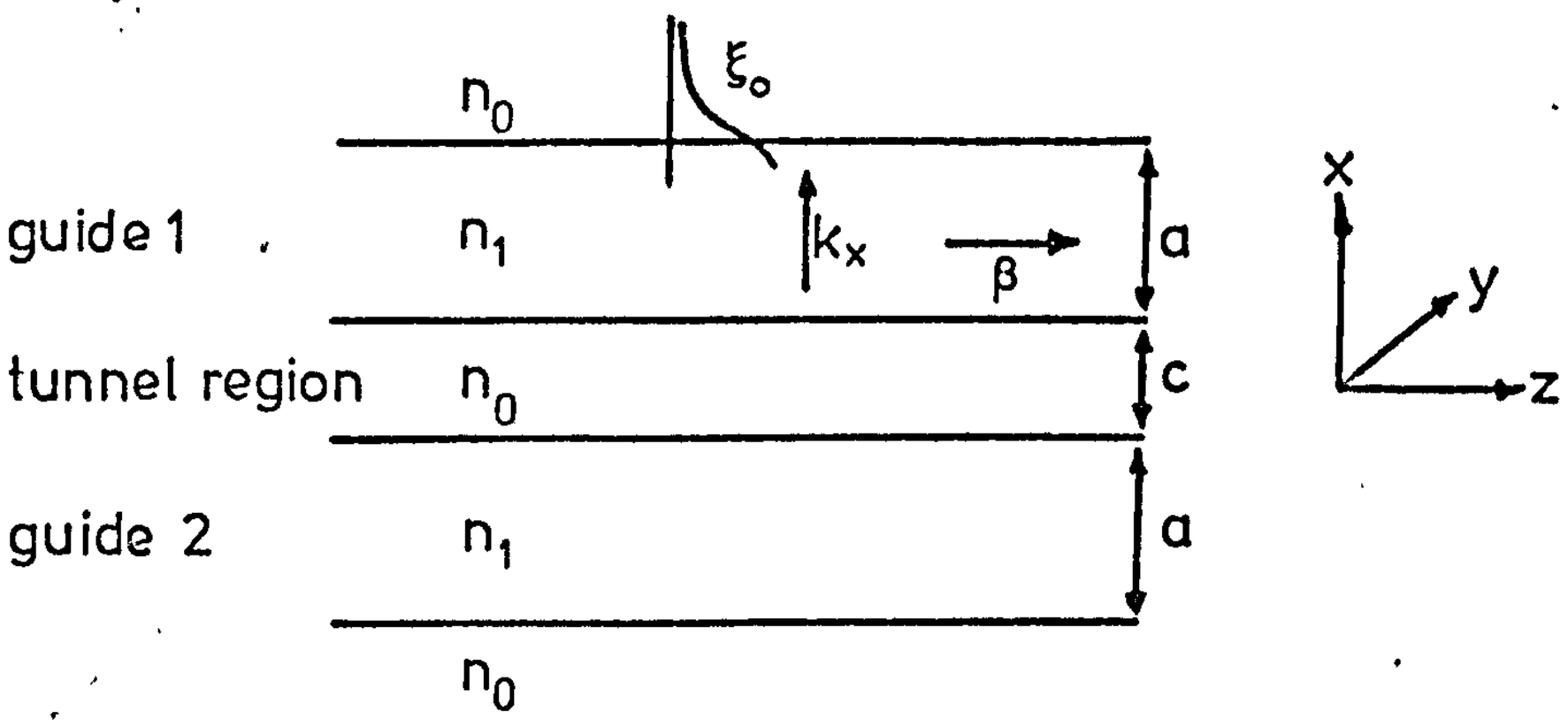

(a) Symmetric case

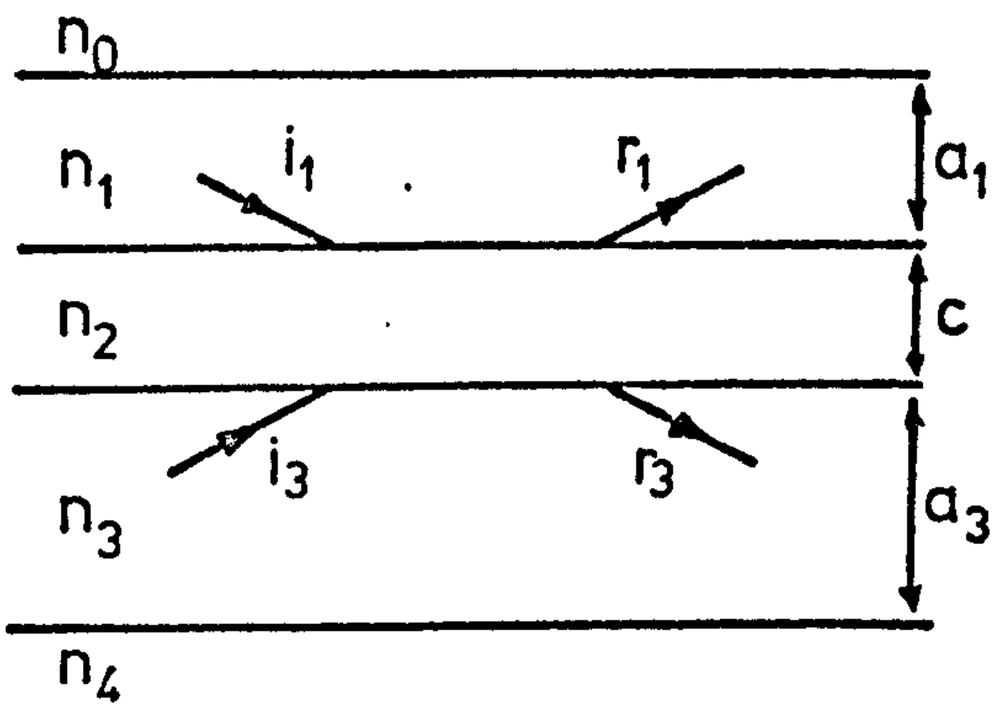

(b) Non-symmetric case

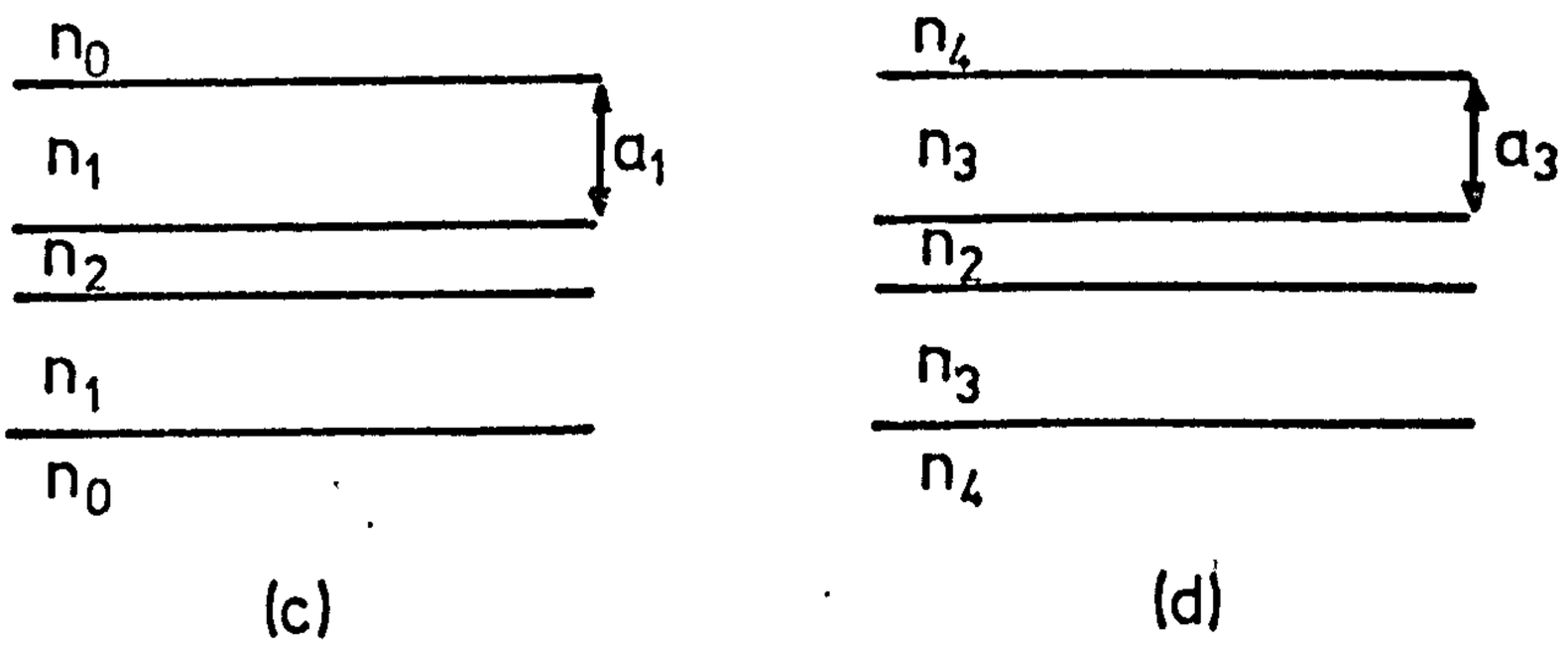

(c) (d)

FIGURE 8.1 Directional coupler schemes

expression obtained by Marcatili[102] (equation (8.4)) is the most commonly used result[48,49].

$$-i\mu = \frac{2\pi}{L_c} = 2\,\frac{k_x^2\,\xi_o \exp(-c/\xi_o)}{\beta\, a\, (1+k_x^2\,\xi_o^2)} \qquad (8.4)$$

where L_c is the coupling length and the rest of the variables are defined in Fig. 8.1a. However, several authors have stated that the effective widths of the waveguides must be considered[111] and other expressions have been derived with a of equation (8.4) replaced by $(a+2\xi_o)$ - the effective guide width. In a coupler the modes are coupled through the penetration of the evanescent fields of one guide into the other. Such fields are therefore large and make a significant change to the values of coupling length calculated from equation (8.4) The expression of Marcatili is only approximate since it has been derived assuming well guided modes.

8.1.2 SCATTERING MATRIX APPROACH

For a complete understanding of directional coupler action the scattering matrix approach was adopted as it could be solved for a completely general (non-symmetric) directional coupler. All the salient equations of section 8.1.1-are readily derived from a unified theory. The basis of this theory is a completely general scattering matrix (equation (8.5)) relating the incident and reflected plane waves at a dielectric boundary (Fig. 8.1b). Dunsmuir et al[107] derived the scattering matrix and then used it to describe the performance of a prism-film coupler but here it is used to provide a theoretical understanding of the lossless, reciprocal directional coupler.

Dunsmuir et al[107] show that

$$\begin{vmatrix} r_1 \\ r_3 \end{vmatrix} = |s| \begin{vmatrix} i_1 \\ i_3 \end{vmatrix} \qquad (8.5)$$

where i_1, i_3, r_1 and r_3 are defined in Fig. 8.1b and $|s|$ is given as

$$|s| = \begin{vmatrix} \dfrac{\exp j2\phi_{12} - u^2 \exp j2\phi_{32}}{1 - u^2 \exp j(2\phi_{12}+2\phi_{32})} & \dfrac{u(1-\exp 4j\phi_{12})^{\frac{1}{2}}(1-\exp j4\phi_{32})^{\frac{1}{2}}}{1 - u^2 \exp j(2\phi_{12}+2\phi_{32})} \\ \dfrac{u(1-\exp j4\phi_{12})^{\frac{1}{2}}(1-\exp j4\phi_{32})^{\frac{1}{2}}}{1 - u^2 \exp j(2\phi_{12}+2\phi_{32})} & \dfrac{\exp j2\phi_{32} - u^2 \exp j2\phi_{12}}{1 - u^2 \exp j(2\phi_{12}+2\phi_{32})} \end{vmatrix} \quad (8.6)$$

where

$$\phi_{12} = \tan^{-1}\left[(\beta/_k^2 - n_2^2)^{\frac{1}{2}} \,/\, (n_1^2 - \beta/_k^2)^{\frac{1}{2}} \right] = \tan^{-1}(k_2/k_1) \quad (8.7)$$

$$\phi_{32} = \tan^{-1}\left[(\beta/_k^2 - n_2^2)^{\frac{1}{2}} \,/\, (n_3^2 - \beta/_k^2)^{\frac{1}{2}} \right] = \tan^{-1}(k_2/k_3) \quad (8.8)$$

for TE waves, and

$$u = \exp(-k_2 c) \quad (8.9)$$

With reference to Fig. 8.1b consider the reflection of a plane wave at the 1-0 and 3-4 dielectric boundaries then

$$i_1 = r_1 \, e^{-j2k_1 a_1 + j2\phi_{10}} \quad (8.10)$$

and

$$i_3 = r_3 \, e^{-j2k_3 a_3 + j2\phi_{34}} \quad (8.11)$$

where ϕ_{10} and ϕ_{34} are defined in a similar manner to ϕ_{12} and ϕ_{32}.

Equations (8.5), (8.10) and (8.11) can then be combined to form equations linking i_1 to i_3 directly.

$$\left\{\left[1-\exp(j2\phi_{12}+j2\phi_{10}-j2a_1k_1)\right]+u^2\exp j(2\phi_{32}-2\phi_{12})\left[\exp(j2\phi_{12}+j2\phi_{10}-j2a_1k_1)\right] - u^2\exp j(2\phi_{12}+2\phi_{32})\right\} i_1 =$$

$$\left\{u(1-\exp j4\phi_{12})^{\frac{1}{2}}(1-\exp j4\phi_{32})^{\frac{1}{2}}\, e^{-j2\phi_{12}} \exp(j2\phi_{12}+j2\phi_{10}-j2k_1a_1)\right\} i_3 \quad (8.12)$$

$$\left\{\left[1-\exp(j2\phi_{32}+j2\phi_{34}-j2a_3k_3)\right]+u^2\exp j(2\phi_{12}-2\phi_{32})\left[\exp(j2\phi_{32}+j2\phi_{34}-j2a_3k_3)\right]\right.$$
$$\left.-u^2\exp j(2\phi_{12}+2\phi_{32})\right\} i_3 =$$
$$\left\{u(1-\exp j4\phi_{12})^{\frac{1}{2}}(1-\exp j4\phi_{32})^{\frac{1}{2}}e^{-j2\phi_{32}}\exp(j2\phi_{32}+j2\phi_{34}-j2k_3a_3)\right\} i_1 \qquad (8.13)$$

Defining

$$P_1 = 1 - \exp(j2\phi_{12}+j2\phi_{10}-j2a_1k_1) \qquad (8.14)$$

and

$$P_3 = 1 - \exp(j2\phi_{32}+j2\phi_{34}-j2a_3k_3) \qquad (8.15)$$

it can be seen that for the two guides in an unperturbed situation

$P_1 = P_3 = 0$ since $(2\phi_{12}+2\phi_{10}-2a_1k_1) = n2\pi$ and $(2\phi_{32}+2\phi_{34}-2a_3k_3) = m2\pi$ (n and m integers) for a mode propagating in the waveguide.

Assuming that the tunnel region 2 is now sufficiently narrow to allow the modes in the two guides to be slightly perturbed by amounts ΔP_1 and ΔP_3 defined as

$$\Delta P_1 = 1 - \exp(j2\phi_{12}+j2\phi_{10}-j2a_1k_1) \qquad (8.16)$$

$$\Delta P_3 = 1 - \exp(j2\phi_{32}+j2\phi_{34}-j2a_3k_3) \qquad (8.17)$$

then equations (8.12) and (8.13) reduce to

$$\left\{\Delta P_1+u^2\exp j(2\phi_{32}-2\phi_{12})-u^2\exp j(2\phi_{12}+2\phi_{32})\right\}i_1=\left\{u(1-e^{j4\phi_{12}})^{\frac{1}{2}}u(1-e^{j4\phi_{32}})^{\frac{1}{2}}e^{-j2\phi_{12}}\right\}i_3 \qquad (8.18)$$

and

$$\left\{\Delta P_3+u^2\exp j(2\phi_{12}-2\phi_{32})-u^2\exp j(2\phi_{12}+2\phi_{32})\right\}i_3=\left\{u(1-e^{j4\phi_{12}})^{\frac{1}{2}}u(1-e^{j4\phi_{32}})^{\frac{1}{2}}e^{-j2\phi_{32}}\right\}i_1 \qquad (8.19)$$

Combining equations (8.18) and (8,19) and neglecting terms of order smaller than u^2 yields

$$\Delta P_1\Delta P_3 = u^2(e^{-j2\phi_{12}}-e^{j2\phi_{12}})(e^{-j2\phi_{32}}-e^{j2\phi_{32}}) \qquad (8.20)$$

Differentiation of equations (8.14) and (8.15) with respect to β yields

$$\Delta P_1 = - j\frac{2\beta(a_1+{}^1/k_o+{}^1/k_2)}{k_1}\,\kappa \qquad (8.21)$$

and

$$\Delta P_3 = - j\frac{2\beta(a_3+{}^1/k_2+{}^1/k_4)}{k_3}\,\kappa \qquad (8.22)$$

where κ is the coupling coefficient. Substituting equations (8.21) and (8.22) in equation (8.20) yields the expression for the overall coupling coefficient as

$$\kappa = \frac{\pm\, 2k_1k_3\exp(-k_2c)}{\beta k_2\sqrt{\left(1+\frac{k_1^2}{k_2^2}\right)\left(1+\frac{k_3^2}{k_2^2}\right)\left(a_1+{}^1/k_o+{}^1/k_2\right)\left(a_3+{}^1/k_4+{}^1/k_2\right)}} \qquad (8.23)$$

For the symmetric case of Fig. 8.1a $a_1 = a_3$, $k_0 = k_2 = k_4$, $k_1 = k_3$ and equation (8.23) reduces to

$$\kappa_1 = \frac{2k_1^2\exp(-k_oc)}{\beta k_o(a_1+{}^2/k_o)\left(1+\frac{k_1^2}{k_o^2}\right)} \qquad (8.24)$$

giving

$$\kappa = \sqrt{\kappa_1\kappa_3} \qquad (8.25)$$

For a non-symmetrical waveguide structure the overall coupling coefficient is the geometric mean of the coupling coefficients for the symmetric cases. Equation (8.24) agrees with Marcatili's equation (8.4) with the important exception that the waveguide width has been replaced by the effective guide width. Equation (8.25) is in agreement with equation (8.3) derived by Marcuse[109] thus substantiating the scatter matrix solution to the directional coupler. Dunsmuir has also shown[112] that the analysis can be extended to derive the fields in each guide and has obtained correlation with equations (8.1) and (8.2) derived by Yariv[108].

Equation (8.1), (8.2) and (8.23) contain all the information needed to design a directional coupler.

8.2 DIRECTIONAL COUPLER TOLERANCE CONSIDERATIONS AND SWITCHING SCHEMES

8.2.1 TOLERANCE CONSIDERATIONS

If a directional coupler is to periodically transfer 100% of the power from one guide to the other then equations (8.1) and (8.2) demand that perfect phase matching occurs between the modes in the two guides (ie $\beta_1 = \beta_2$). The maximum power transferred in the case of a slight mismatch is given by

$$\text{Percentage of driven guide power transferred} = \left[\frac{4\kappa^2}{(4\kappa^2+\Delta^2)}\right] \times 100 \quad (8.26)$$

Figure 8.2 illustrates the effect of mismatch and shows that not only is the maximum power transfer reduced but the coupling length is also shortened. Equation (8.26) indicates that the shorter the coupling length then the larger the phase mismatch that can be tolerated for a given percentage power transfer. The mismatch of the waveguide propagation constants can arise during device fabrication if any of the guide parameters vary only slightly from the calculated values. Tolerances are calculated on the basis of one parameter varying while all the others are fixed at their correct values, with the additional constraintthat the waveguides are uncoupled. Equation (8.26) gives the maximum value of Δ for a specified rejection ratio between the two guides. The phase difference can then be related to the particular refractive index or thickness by differentiation of the appropriate mode equation defining the guide. The tolerance calculated will indicate the maximum transfer of power.

Variation of the width of the tunnelling gap and, in the case of a structure that possesses symmetry about the tunnelling gap, the refractive index of this tunnelling gap will not induce a phase mismatch between the modes. However, the coupling length does depend on these parameters. Tolerances on these parameters are therefore

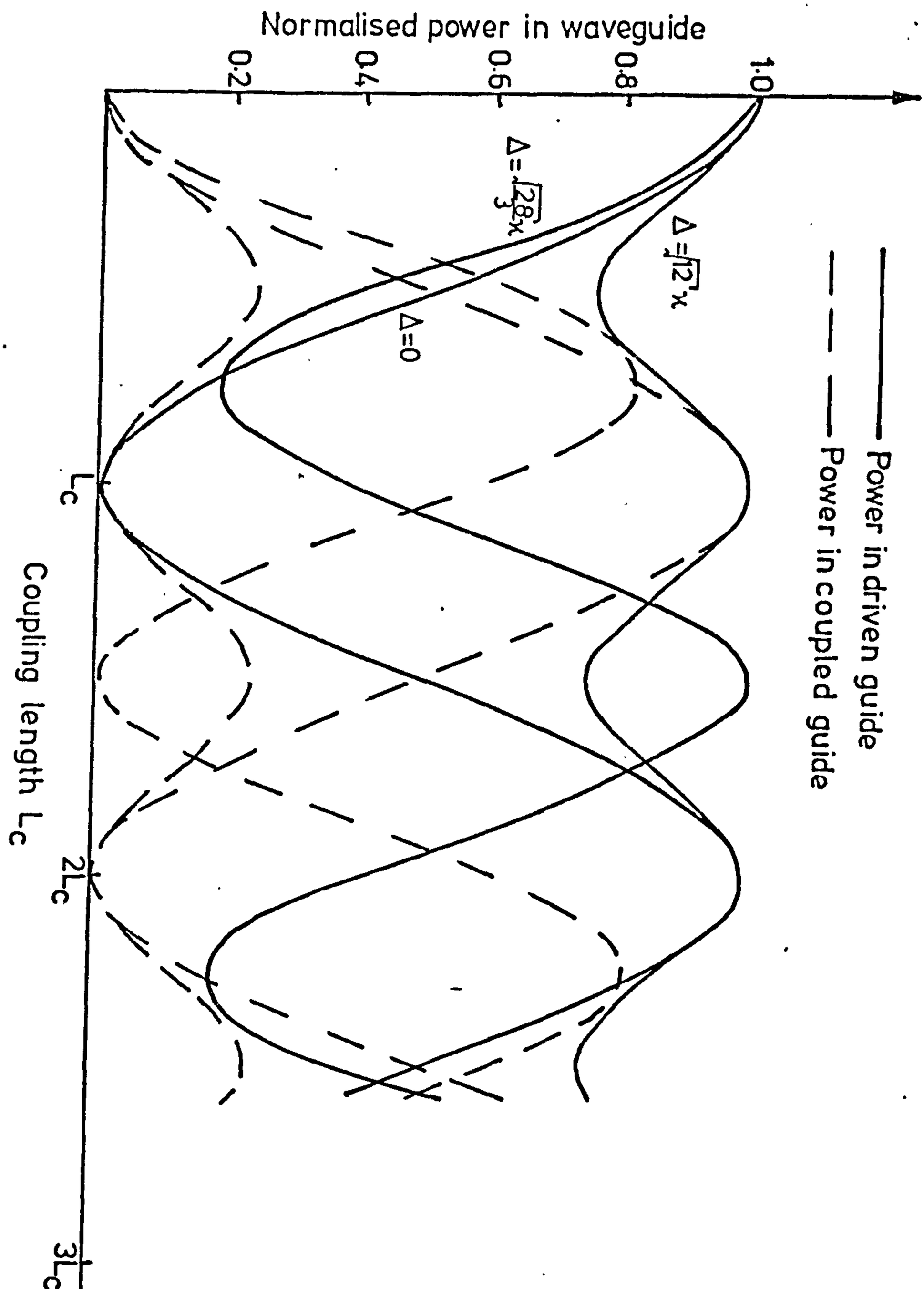

FIGURE 8.2 Waveguide power versus coupling length, illustrating the effect of phase mismatch between the guides

calculated by stipulating that a certain power must be transferred at the point where 100% transfer should have been achieved (100% power transfer will always occur provided perfect phase matching is maintained).

The above methods provide a means of assessing the feasibility of fabricating a directional coupler structure. Clearly those designs which demand a level of accuracy greater than the available technology permits must be rejected.

8.2.2 SWITCHING SCHEMES

The underlying principle of an electrooptically controlled directional coupler switch is the alteration of the passive coupling conditions of the directional coupler, with an odd number of coupling lengths, through the electrooptic effect in one medium and so induce a transfer of the power back to the driven guide. This can be achieved by maintaining the phase match between the two guides and altering the coupling length by inducing a symmetric phase change (Fig. 8.3a) or by inducing an asymmetric phase change thus destroying the phase matching condition (Fig. 8.3b). For each type of switching both a long coupling length and a large number of coupling lengths reduce the voltage required for switching through an increase in the interaction length. However, a finite limit to the device size will exist on account of the length over which the required fabrication tolerances can be maintained. In addition limitations will be imposed by the scattering which occurs on each coupling transition leading to a reduction in the rejection ratio between the two guides. Lower voltages are required for switching when an electrooptic waveguide is used in preference to an eletrooptic material as the tunnelling gap or substrate.

The voltages required for switching are calculated from a knowledge of the structure geometry and the electrooptic equation (5.3)

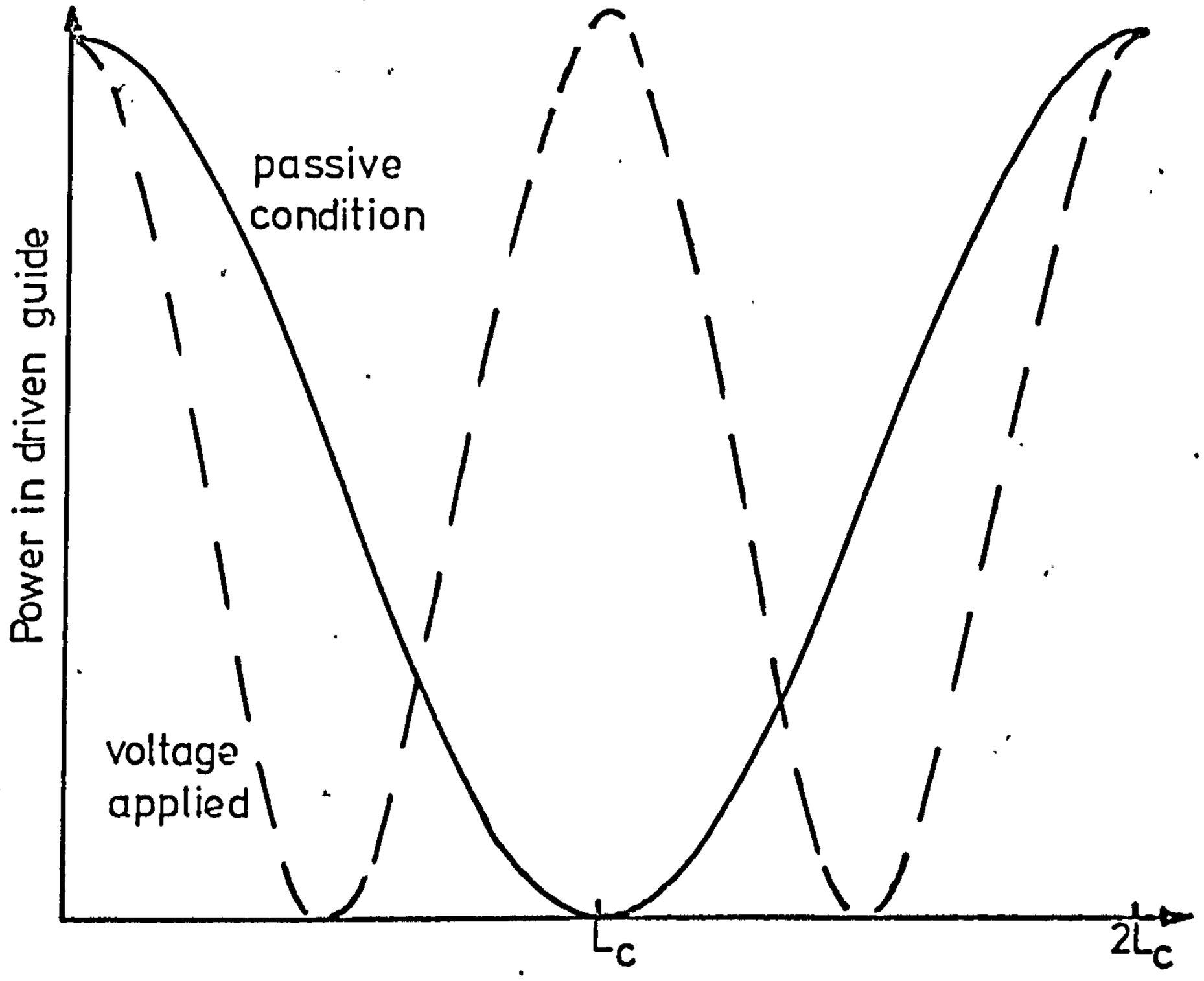

(a) Phase matched

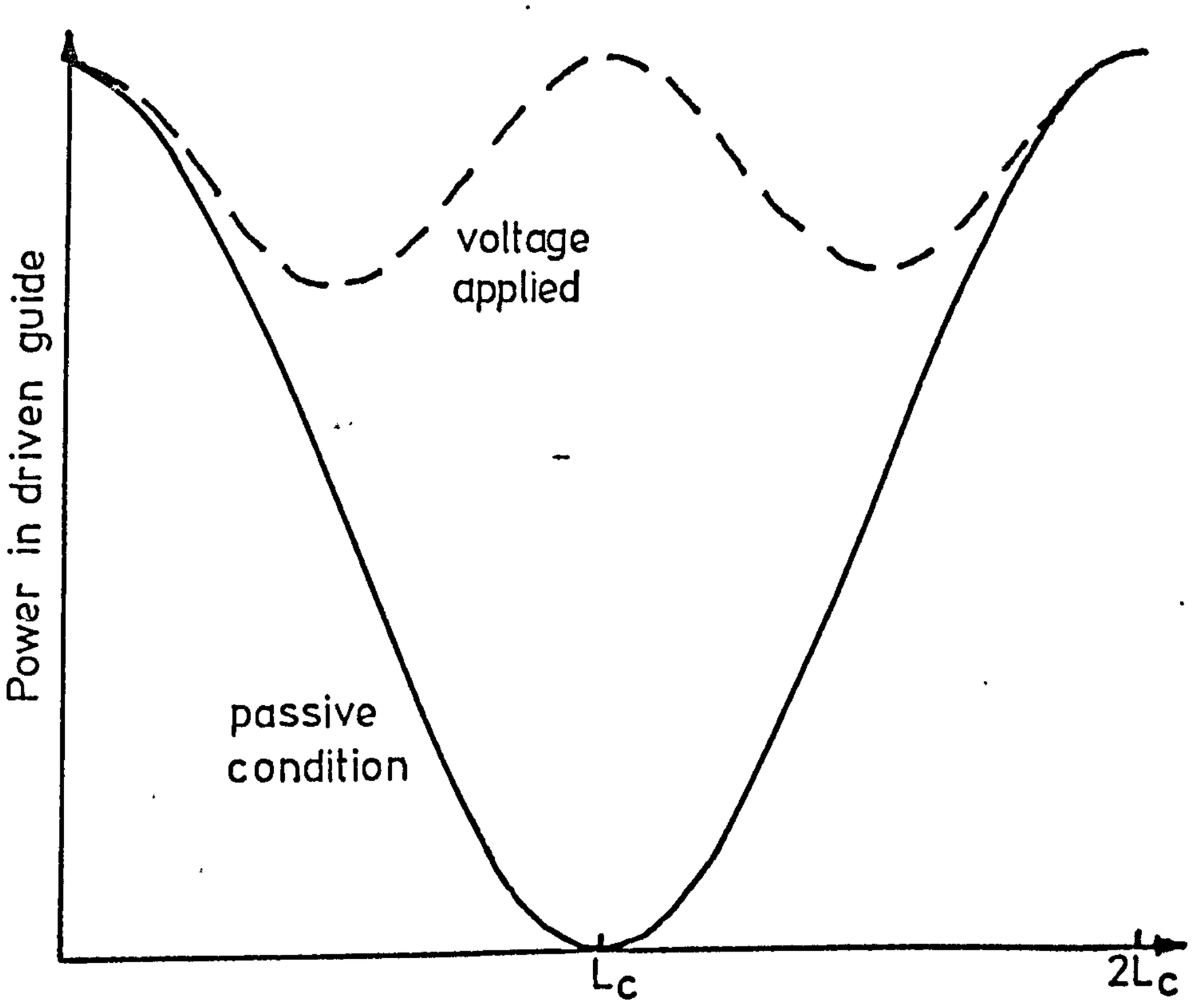

(b) Phase mismatched

FIGURE 8.3 Electrooptic switching schemes

yielding an expression linking applied voltage to induced refractive index change. In the phase mismatched switching the refractive index change is related to the change in phase propagation constant $d\beta$ by differentiation of the relevant mode equation. For a structure which relies on switching by altering the coupling length the refractive index change is related to the coupling coefficient by equation (8.27) which was obtained from differentiation of equation (8.24).

$$d\kappa = \kappa\left[\frac{2k^2n_1}{k_1^2} - \frac{2\beta x}{k_1^2} - \frac{c\beta x}{k_o} - \frac{\beta x}{k_o^2} - \frac{x}{\beta} - \frac{2k^2n_1}{k_o^2(1+(\frac{k_1}{k_o})^2)} + \frac{2\beta x}{k_o^2(1+(\frac{k_1}{k_o})^2)} + \frac{2k_1^2\beta x}{k_o^4(1+(\frac{k_1}{k_o})^2)}\right]dn_1 \qquad (8.27)$$

where $d\beta = xdn_1$ (obtained from differentiation of the appropriate mode equation).

$d\kappa$ and $d\beta$ are defined by the coupler geometry through equations (8.1) and (8.2).

The phase matching of the modes in a directional coupler is very critical for 100% power transfer and thus destroying the phase matched condition between the two coupled guides requires a much lower voltage (smaller refractive index change) than the corresponding coupling length change switching[13]. If opposite polarity voltages can be applied to the two guides the former effect is further enhanced by a factor of two for a given applied voltage. Recently, Kogelnik et al[113] demonstrated that with a split electrode geometry, independent voltage control between the two guides and phase mismatched switching, small fabrication errors could be eliminated by applying a fixed voltage to the structure. A greatly enhanced rejection ratio between the guides results, Kogelnik et al[113] having measured a value of 26 dB.

For the above reasons phase mismatched switching will be

employed whenever the structure geometry permits. The voltages in section 8.3 are calculated on the basis of 100% of the power in the coupler guide being switched back to the driven guide in the same coupler length (device interaction length).

It should be noted that the two criteria, switching voltage and fabrication tolerances, have opposing trends and hence in any switch design a compromise will be necessary.

8.3 ELECTROOPTICALLY CONTROLLED DIRECTIONAL COUPLER SWITCH DESIGNS

The electrooptically controlled directional coupler switch will be a potentially useful device for any optical communications system. Having demonstrated the electrooptic properties of the cadmium sulphide waveguides and the possibility of efficient coupling to and from optical fibres, a similar technology is applicable to directional coupler switches. This section describes the possible directional coupler configurations for both planar and rectangular cadmium sulphide waveguides, and the equations for deriving the tolerance requirements and switching voltages. Numerical results were computed for the various cadmium sulphide structures and the most feasible design is discussed. TE modes in the case of planar guides and E^x modes for rectangular guides will be assumed throughout the subsequent analyses. The guides will be assumed scatter free with no crosstalk occurring by that mechanism. Rejection ratios of 10 dB, 15 dB and 20 dB will be considered although the final rejection ratio required for a workable digital communications system may well need to exceed the most stringent of these values.

8.3.1 THE MULTILAYER PLANAR STACK DESIGN

Three designs for an electrooptically controlled switch using a stacked slab directional coupler are illustrated in Fig. 8.4. Design (a) is based on the silicon monoxide-cadmium sulphide stack

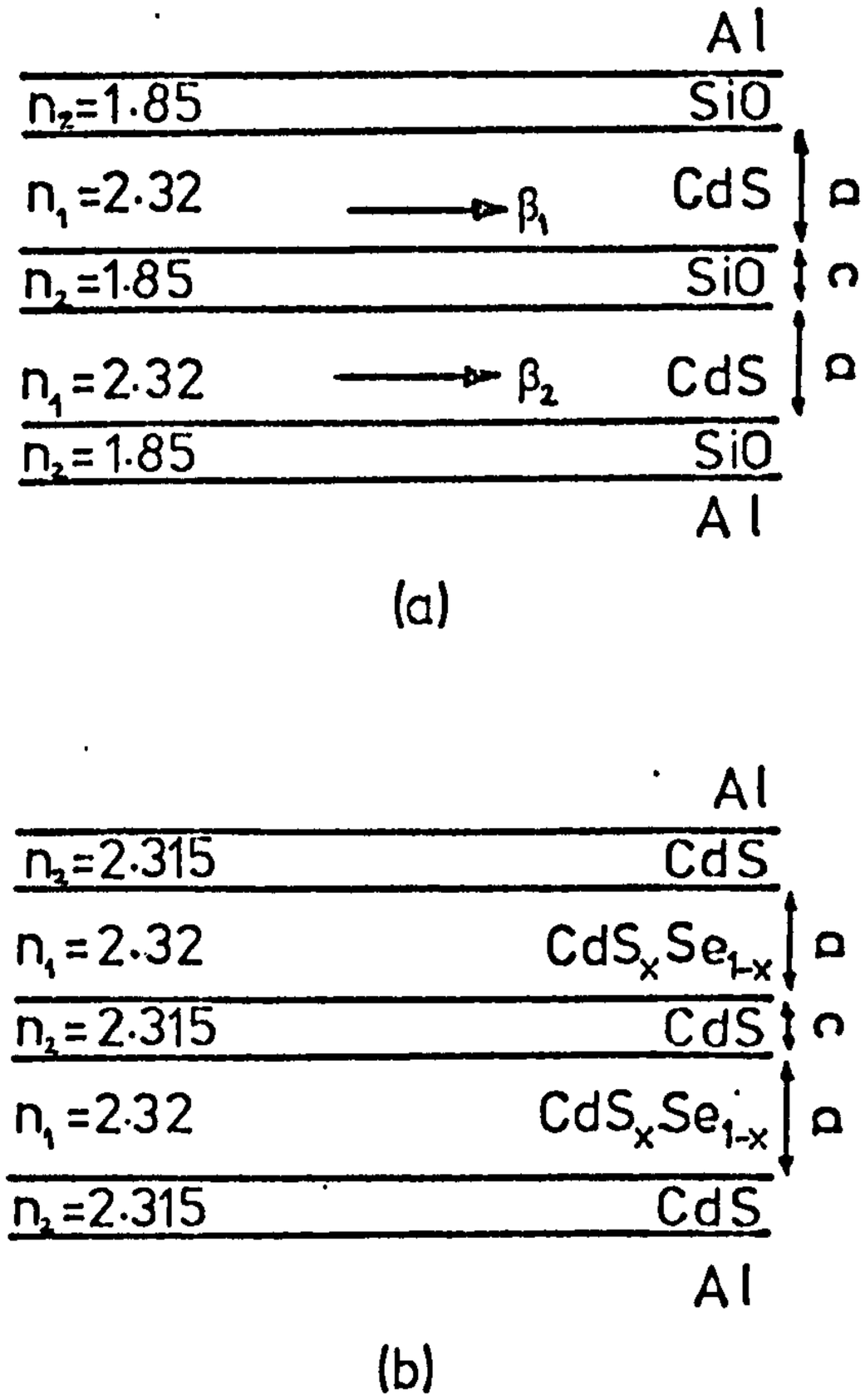

FIGURE 8.4 Directional coupler switch schemes for planar cadmium sulphide waveguides

used for the phase modulator but because the large refractive index difference between the two materials the waveguide tolerances are very exacting. Coupler structure (b) overcomes this tolerance problem by producing a CdS_xSe_{1-x} - cadmium sulphide stack with a smaller refractive index difference. However, a major problem with both designs (a) and (b) is that any applied voltage will induce a symmetric phase change to each guide and switching will thus occur by a change of coupling length with a concomitant increase in the required switching voltage. Design (c) relies on the coupling of two different modes in each waveguide and consequently the applied voltage will induce a phase mismatch between the two guides with a corresponding reduction in switching voltage. The coupling of different modes may have severe practical problems since different propagation losses affect the directional coupling properties of the two guides[114]. In all these designs the fabrication errors that arise will limit the final rejection ratio between the two guides since independent voltage control over each guide cannot be achieved.

The tolerances for the waveguide parameters which induce a phase mismatch between the coupled waveguides were derived from differentiation of the mode equation for planar waveguides (equation (2.8)) and are given in equations(8.28) - (8.30). The tolerance for the waveguide refractive index is calculated from,

$$d\beta = \frac{kn_1}{\beta/k}\left[\frac{ka + \dfrac{2(\beta^2/k - n_2^2)^{\frac{1}{2}}}{(n_1^2 - n_2^2)}}{ka + \dfrac{2}{(\beta^2/k - n_2^2)^{\frac{1}{2}}}}\right] dn_1 \qquad (8.28)$$

for the waveguide thickness, from

$$d\beta = \frac{k(n_1^2-\beta^2/k)}{\beta/k}\left[a + \frac{2}{k(\beta^2/k-n_2^2)^{\frac{1}{2}}}\right]^{-1} da \qquad (8.29)$$

and for the surrounding refractive index, from

$$d\beta = \frac{n_2 k}{\beta/k} \left[\frac{n_1^2 - \beta/k^2}{(\beta/k^2 - n_2^2)^{\frac{1}{2}}(n_1^2 - n_2^2)} \Big/ ka + \frac{2}{(\beta/k^2 - n_2^2)^{\frac{1}{2}}} \right] dn_2 \qquad (8.30)$$

where the variables are defined in Fig. 8.4. The tolerances which induce a phase matched change (and hence a change in coupling length) are derived from differentiation of equation (8.24) and are given in equations (8.31) and (8.32);

$$d\varkappa = - k_o \varkappa dc \qquad (8.31)$$

for the tunnelling gap thickness, and

$$d\varkappa = \varkappa \left[c + 1/k_2 - \frac{1}{ak_2^2 + 2k_2} - \frac{2k_1^2}{(k_2^3 + k_1^2 k_2)} \right] \frac{k^2 n_2}{k_2} \, dn_2 \qquad (8.32)$$

for the tunnelling gap refractive index where the variables are defined in Fig. 8.4. For designs (a) and (b) the tolerance on tunnelling layer refractive index is given by equation (8.32) but for the non-symmetric structure of design (c) the change in tunnelling layer refractive index will induce a phase mismatch and equation (8.30) should be employed. $d\beta$ and $d\varkappa$ are related to the rejection ratio between the guides through equations (8.1) and (8.2).

The switching voltages for designs (a) and (b) were calculated from equation (8.27) while those for the asymmetric design (c) were derived using equation (8.28).

Tables 8.1, 8.2 and 8.3 contain the numerical results for waveguide tolerances and switching voltages for designs (a), (b) and (c) respectively. Each table contains a range of rejection ratios and device interaction lengths. It can be seen that for designs (a) and (b) the switching voltages make the devices impracticable. How-

Coupling Length 1mm

Rejection Ratio Between Guides	Tolerances					Voltage Requirements	
	Guide Thickness	Guide Refractive Index	Surrounding Refractive Index	Tunnelling Gap Refractive Index	Tunnelling Gap Thickness	Length of Coupler .	Voltage Across Guide
10 dB	$1.5\mu m \pm 85A^{o}$	$2.32 \pm 2.2\times10^{-4}$	$1.85 \pm 6.7\times10^{-2}$	$1.85 \pm 9.1\times10^{-2}$	$0.4\mu m \pm 330A^{o}$	1mm	$2.18\times10^{4}v$
15 dB	$1.5\mu m \pm 46A^{o}$	$2.32 \pm 1.2\times10^{-4}$	$1.85 \pm 3.6\times10^{-2}$	$1.85 \pm 5.0\times10^{-2}$	$0.4\mu m \pm 183A^{o}$	5mm	$7.26\times10^{3}v$
20 dB	$1.5\mu m \pm 26A^{o}$	$2.32 \pm 6.6\times10^{-5}$	$1.8 \pm 2\times10^{-2}$	$1.85 \pm 2.84\times10^{-2}$	$0.4\mu m \pm 103A^{o}$	10mm	$4.37\times10^{3}v$

Coupling Length 100μm

10 dB	$1.5\mu m \pm 700A^{o}$	$2.32 \pm 1.7\times10^{-3}$	1.85 ± 0.62	1.85 ± 0.184	$0.12\mu m \pm 330A^{o}$	100μm	$4.4\times10^{4}v$
15 dB	$1.5\mu m \pm 379A^{o}$	$2.32 \pm 9.4\times10^{-4}$	1.85 ± 0.334	1.85 ± 0.1	$0.12\mu m \pm 183A^{o}$	1mm	$8\times10^{3}v$
20 dB	$1.5\mu m \pm 211A^{o}$	$2.32 \pm 5\times10^{-4}$	1.85 ± 0.186	$1.85 \pm 5.7\times10^{-2}$	$0.12\mu m \pm 103A^{o}$	10mm	800v

Table 8.1 Tolerances and Voltage Requirements for Directional Coupler 8.4a.

Coupling Length 1mm

Rejection Ratio Between Guides	Tolerances					Voltage Requirements	
	Guide Thickness	Guide Refractive Index	Surrounding Refractive Index	Tunnelling Gap Refractive Index	Tunnelling Gap Thickness	Length of Coupler	Voltage Across Guide
10 dB	$2.3\mu m \pm 0.206\mu m$	$2.32 \pm 3.0 \times 10^{-4}$	$2.315 \pm 1.2 \times 10^{-3}$	$2.315 \pm 4.9 \times 10^{-4}$	$3.0\mu m \pm 0.37\mu m$	1mm	600v
15 dB	$2.3\mu m \pm 0.112\mu m$	$2.32 \pm 1.6 \times 10^{-4}$	$2.315 \pm 6 \times 10^{-4}$	$2.315 \pm 2.7 \times 10^{-4}$	$3.0\mu m \pm 0.205\mu m$	5mm	210v
20 dB	$2.3\mu m \pm 0.062\mu m$	$2.32 \pm 9.0 \times 10^{-5}$	$2.315 \pm 3.5 \times 10^{-4}$	$2.315 \pm 1.5 \times 10^{-4}$	$3.0\mu m \pm 0.116\mu m$	10mm	109v

Coupling Length 500μm

10 dB	$2.3\mu m \pm 0.37\mu m$	$2.32 \pm 5.0 \times 10^{-4}$	$2.315 \pm 2.1 \times 10^{-3}$	$2.315 \pm 5.7 \times 10^{-4}$	$1.9\mu m \pm 0.37\mu m$	500μm	1.1×10^{3}v
15 dB	$2.3\mu m \pm 0.198\mu m$	$2.32 \pm 2.9 \times 10^{-4}$	$2.315 \pm 1.1 \times 10^{-3}$	$2.315 \pm 3.2 \times 10^{-4}$	$1.9\mu m \pm 0.205\mu m$	5mm	218v
20 dB	$2.3\mu m \pm 0.11\mu m$	$2.32 \pm 1.6 \times 10^{-4}$	$2.315 \pm 6 \times 10^{-4}$	$2.315 \pm 1.8 \times 10^{-4}$	$1.9\mu m \pm 0.116\mu m$	10mm	105v

Table 8.2 Tolerances and Voltage Requirements for Directional Coupler 8.4b.

Coupling Length 1mm Coupling Between TE_0 mode and TE_3 mode

Rejection Ratio Between Guides	Tolerances					Voltage Requirements	
	Guide Thickness	Guide Refractive Index	Surrounding Refractive Index	Tunnelling Gap Refractive Index	Tunnelling Gap Thickness	Length of Coupler	Voltage Across Guide
10 dB	TE_0 0.083μm ± 0.6A° TE_3 1.37μm ± 64 A°	2.32 ± 2.0×10^{-4}	1.85 ± 1.0×10^{-3}	1.85 ± 4.4×10^{-3}	2.1μm ± 796A°	1mm	343v
15 dB	TE_0 0.083μm ± 0.3A° TE_3 1.37μm ± 34A°	2.32 ± 1.1×10^{-4}	1.85 ± 5.4×10^{-4}	1.85 ± 2.4×10^{-3}	2.1μm ± 442A°	3mm	174v
20 dB	TE_0 0.083μm ± 0.2A° TE_3 1.37μm ± 19 A°	2.32 ± 6.0×10^{-5}	1.85 ± 3.0×10^{-4}	1.85 ± 1.3×10^{-3}	2.1μm ± 248A°	9mm	96v

Coupling Length 1mm Coupling Between TE_0 Mode and TE_1 Mode

10 dB	TE_0 0.097μm ± 0.7A° TE_1 0.53μm ± 6.8A°	2.32 ± 2.0×10^{-4}	1.85 ± 1.0×10^{-3}	1.85 ± 5.2×10^{-3}	2.1μm ± 810A°	1mm	243v
15 dB	TE_0 0.097μm ± 0.4A° TE_1 0.53μm ± 3.7A°	2.32 ± 1.1×10^{-4}	1.85 ± 5.4×10^{-4}	1.85 ± 2.8×10^{-3}	2.1μm ± 450A°	3mm	124v
20 dB	TE_0 0.097μm ± 0.2A° TE_1 0.53μm ± 2A°	2.32 ± 6.0×10^{-5}	1.85 ± 3.0×10^{-4}	1.85 ± 1.6×10^{-3}	2.1μm ± 253A°	9mm	68v

Table 8.3 Tolerance and Voltage Requirements for Directional Coupler 8.4c.

ever the waveguide tolerances would allow the fabrication of a passive directional coupler in both these structures. Design (c), although having acceptable switching voltages, would be totally unrealistic owing to the exceptionally small thicknesses required for the TE_o waveguide and the correspondingly stringent tolerance requirements. It is thus unreasonable to produce an optical switch using a stacked planar waveguide technology.

8.3.2 THE RECTANGULAR WAVEGUIDE DESIGN

The rectangular waveguides allow independent voltage control to be applied to each guide and hence the voltage across the structure is reduced, fabrication errors can be reduced and the advantages of asymmetric phase mismatched switching can be used. Two designs based on selenium diffused waveguides in thin films of cadmium sulphide are illustrated in Fig. 8.5. Design (a) is based on a refractive index difference of $5x10^{-3}$ between the cadmium sulphide and the CdS_xSe_{1-x} and design (b) is for a refractive index difference of $2.5x10^{-2}$. The first design is based on the refractive index difference reported in chapter 7 while the latter design represents the best structure assuming the refractive index of the CdS_xSe_{1-x} can be further increased without detriment to the waveguide loss.

The waveguide tolerances for the phase matched changes were derived from equations (8.31) and (8.32) while the phase mismatched tolerances were obtained from differentiation of the closed form approximation of equation (7.1) assuming waveguide symmetry (ie $n_2=n_4$ and $n_3=n_5$). The tolerance for the waveguide width is calculated from;

$$d\beta = \frac{1}{\beta}\left[\frac{(\pi p)^2}{a^3}\left(1+\frac{2n_3^2A_3}{\pi n_1^2 a}\right)^{-2} - \left(\frac{\pi p}{a}\right)^2\left(1+\frac{2n_3^2A_3}{\pi n_1^2 a}\right)^{-3}\left(\frac{2n_3^2A_3}{\pi n_1^2 a^2}\right)\right]da \qquad (8.33)$$

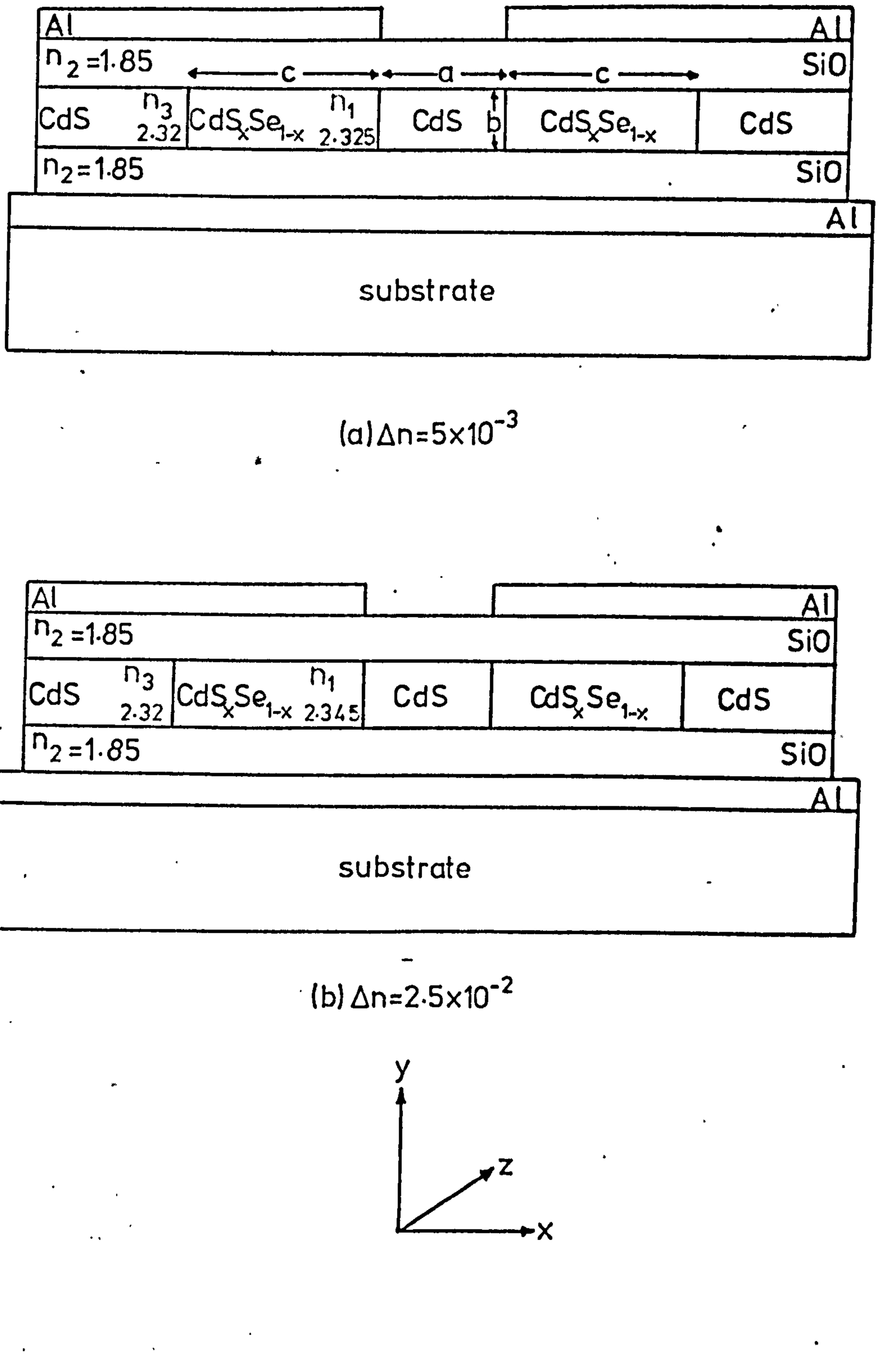

FIGURE 8.5 Directional coupler switch schemes for CdS_xSe_{1-x} diffused rectangular waveguides

for the waveguide thickness, from

$$d\beta = \frac{1}{\beta}\left[\frac{(\pi q)^2}{b^3}\left(1+\frac{2A_2}{\pi b}\right)^{-2} - \left(\frac{\pi q}{b}\right)^2\left(1+\frac{2A_2}{\pi b}\right)^{-3}\left(\frac{2A_2}{\pi b^2}\right)\right] db \qquad (8.34)$$

for the waveguide refractive index, from

$$d\beta = \frac{1}{\beta}\left[\frac{4\pi^2}{\lambda^2} n_1 - \left(\frac{\pi p}{a}\right)^2\left(1+\frac{2n_3^2 A_3}{\pi n_1^2 a}\right)^{-3}\left(\frac{2\pi n_1^3 a A_3\left(\frac{n_3^2}{n_1^2-n_3^2}\right)+4\pi n_1 a n_3^2 A_3}{\pi^2 n_1^4 a^2}\right)\right.$$
$$\left. -\left(\frac{\pi q}{b}\right)\left(1+\frac{2A_2}{\pi b}\right)^{-3}\left(\frac{2A_2\left(\frac{n_1}{n_1^2-n_2^2}\right)}{\pi b}\right)\right] dn_1 \qquad (8.35)$$

for upper and lower surrounding refractive indices, from

$$d\beta = \frac{1}{\beta}\left[\left(\frac{\pi p}{a}\right)^2\left(1+\frac{2n_3^2 A_3}{\pi n_1^2 a}\right)^{-3}\left(\frac{4n_3 A_3+2n_3^2 A_3\left(\frac{n_3}{n_1^2-n_3^2}\right)}{\pi n_1^2 a}\right)\right] dn_3 \qquad (8.36)$$

and for the left and right surrounding refractive indices, from

$$d\beta = \frac{1}{\beta}\left[\left(\frac{\pi q}{b}\right)^2\left(1+\frac{2A_2}{\pi b}\right)^{-3}\left(\frac{2A_2\left(\frac{n_2}{n_1^2-n_2^2}\right)}{\pi b}\right)\right] dn_2 \qquad (8.37)$$

where $A_i = \dfrac{\lambda}{2(n_1^2-n_i^2)^{\frac{1}{2}}}$, p and q are the x and y mode numbers and the other variables are defined in Fig. 8.5.

The switching voltages are calculated using equation (8.35) to relate the applied voltage to the phase change through the induced refractive index change. Opposite polarity voltages are assumed on the two electrodes. The widths of the waveguides have been chosen to produce the desired coupling length while the thickness is selected for maximum phase change to minimise the required switching

voltage. Phase change in a rectangular guide has similar behaviour to the planar waveguide case of Fig. 5.7.

The numerical results for waveguide tolerances and switching voltages are given in Tables 8.4 and 8.5 for the designs (a) and (b) respectively. Because the rectangular waveguides are fabricated simultaneously refractive index tolerances are less significant with the major considerations being the tolerances on the waveguide and tunnelling gap widths. In both designs the tolerances can be met by existing technologies and any small error remaining could be eliminated using the electrode geometry of Kogelnik et al[113]. The switching voltages for design (a) are high due to the large guide thicknesses required for 2-d confinement; therefore a switch of that design would be impracticable. However, design (b) appears feasible both from the point of view of the waveguide tolerances and the switching voltages. Although the structure will withstand the voltage required for switching, 61 volts does not compare favourably with the 6 volts required for the switch fabricated in titanium diffused lithium niobate[48]. This arises because of the large difference between the electrooptic coefficients of cadmium sulphide and lithium niobate[92], ($r_{33}(LiNbO_3) = 30.8 \times 10^{-12} mV^{-1}$ and r_{13} (CdS) = $1.1 \times 10^{-12} mV^{-1}$).

8.3.3 ALTERNATIVE COUPLER DESIGNS

Two further types of waveguide structure, which provide two dimensional confinement of an optical beam, are the rib guide (Fig. 8.6a) and the strip loaded film guide (Fig. 8.6b). They are of interest in the fabrication of a directional coupler due to the large field penetrations which exist beyond the confining medium[115]. Much larger waveguide dimensions are therefore possible for acceptable coupling lengths with a corresponding relaxation in the fabrication tolerances. Little work has been done on such devices and only approximate theories[115] exist to describe the modes in both rib and strip loaded structures.

Coupling Length 1.3mm

Rejection Ratio Between Guides	Tolerances					Voltage Requirements	
	Guide Dimensions	Guide Refractive Index	Surrounding Refractive Index	Tunnelling Gap Refractive Index	Tunnelling Gap Thickness	Length of Coupler	Voltage Across Structure
10 dB	a 5.0μm ± 0.41μm b 4.4μm ± 182A°	2.325 ± 2.81x10^{-4}	1.85 ± 0.34 2.32 ± 1.72x10^{-3}	2.32 ± 1.43x10^{-3}	2.0μm ± 0.57μm	1.3mm	403v
15 dB	a 5.0μm ± 0.22μm b 4.4μm ± 99A°	2.325 ± 1.52x10^{-4}	1.85 ± 0.18 2.32 ± 9.35x10^{-4}	2.32 ± 7.9x10^{-4}	2.0μm ± 0.32μm	3.9mm	205v
20 dB	a 5.0μm ± 0.12μm b 4.4μm ± 55A°	2.325 ± 8.5x10^{-5}	1.85 ± 0.1 2.32 ± 5.2x10^{-4}	2.32 ± 4.5x10^{-4}	2.0μm ± 0.18μm	11.7mm	113v

Coupling Length 760μm

10 dB	a 3.0μm ± 0.28μm b 5.4μm ± 0.32μm	2.325 ± 1.6x10^{-4}	1.85 ± 1.3 2.32 ± 1.15x10^{-3}	2.32 ± 1.26x10^{-2}	2.0μm ± 0.51μm	760μm	977v
15 dB	a 3.0μm ± 0.15μm b 5.4μm ± 0.17μm	2.325 ± 8.67x10^{-5}	1.85 ± 0.71 2.32 ± 6.22x10^{-4}	2.32 ± 7.0x10^{-3}	2.0μm ± 0.28μm	2.28mm	497v
20 dB	a 3.0μm ± 835A° b 5.4μm ± 967A°	2.325 ± 4.81x10^{-5}	1.85 ± 0.4 2.32 ± 3.46x10^{-4}	2.32 ± 3.9x10^{-3}	2.0μm ± 0.16μm	6.84mm	273v

Table 8.4 Tolerances and Voltage Requirements for Directional Coupler 8.5 $\Delta n = 5x10^{-3}$

Coupling Length 1.65mm

Rejection Ratio Between Guides	Tolerances					Voltage Requirements	
	Guide Dimensions	Guide Refractive Index	Surrounding Refractive Index	Tunnelling Gap Refractive Index	Tunnelling Gap Thickness	Length of Coupler	Voltage Across Structure
10 dB	a $5.0\mu m \pm 0.18\mu m$ b $1.6\mu m \pm 52A^{o}$	$2.345 \pm 1.17\times10^{-4}$	1.85 ± 0.023 $2.32 \pm 8.28\times10^{-3}$	$2.32 \pm 3.6\times10^{-3}$	$2.0\mu m \pm 0.31\mu m$	1.65mm	120v
15 dB	a $5.0\mu m \pm 978A^{o}$ b $1.6\mu m \pm 28A^{o}$	$2.345 \pm 6.33\times10^{-5}$	1.85 ± 0.012 $2.32 \pm 4.5\times10^{-3}$	$2.32 \pm 2.0\times10^{-3}$	$2.0\mu m \pm 0.17\mu m$	4.95mm	61v
20 dB	a $5.0\mu m \pm 544A^{o}$ b $1.6\mu m \pm 16A^{o}$	$2.345 \pm 3.52\times10^{-5}$	$1.85 \pm 6.9\times10^{-3}$ $2.32 \pm 2.5\times10^{-3}$	$2.32 \pm 1.1\times10^{-3}$	$2.0\mu m \pm 957A^{o}$	14.85mm	34v

Coupling Length 740μm

10 dB	a $3.0\mu m \pm 0.12\mu m$ b $1.6\mu m \pm 115A^{o}$	$2.345 \pm 2.7\times10^{-4}$	1.85 ± 0.051 $2.32 \pm 5.52\times10^{-3}$	$2.32 \pm 1.7\times10^{-2}$	$2.0\mu m \pm 0.36\mu m$	740μm	327v
15 dB	a $3.0\mu m \pm 652A^{o}$ b $1.6\mu m \pm 63A^{o}$	$2.345 \pm 1.46\times10^{-4}$	1.85 ± 0.028 $2.32 \pm 3.0\times10^{-3}$	$2.32 \pm 9.4\times10^{-3}$	$2.0\mu m \pm 0.2\ \mu m$	2.22mm	167v
20 dB	a $3.0\mu m \pm 362A^{o}$ b $1.6\mu m \pm 35A^{o}$	$2.345 \pm 8.14\times10^{-5}$	1.85 ± 0.015 $2.32 \pm 1.67\times10^{-3}$	$2.32 \pm 5.3\times10^{-3}$	$2.0\mu m \pm 0.11\mu m$	6.66mm	91v

Table 8.5 Tolerances and Voltage Requirements for Directional Coupler 8.5 $\Delta n = 2.5\times10^{-2}$

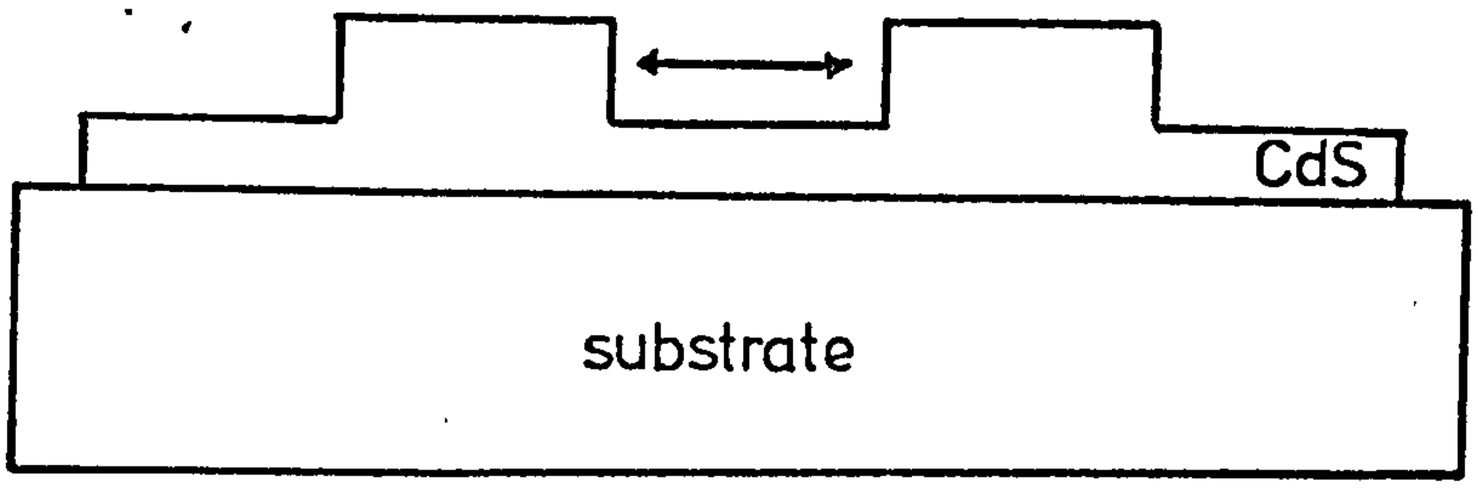

(a)Cadmium sulphide rib waveguides

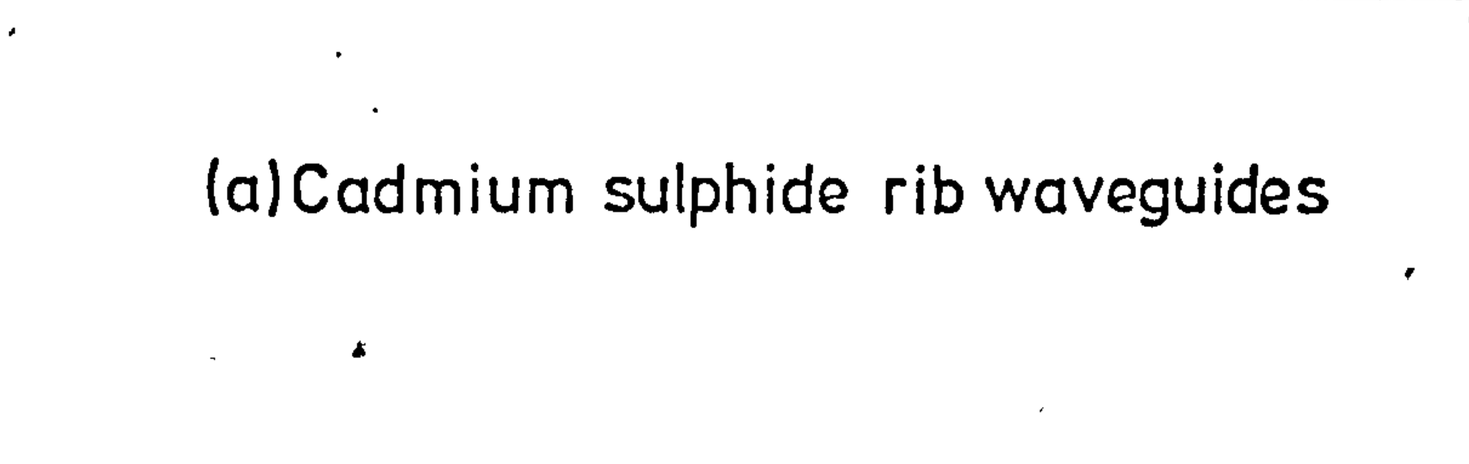

(b) Strip-loaded cadmium sulphide waveguides

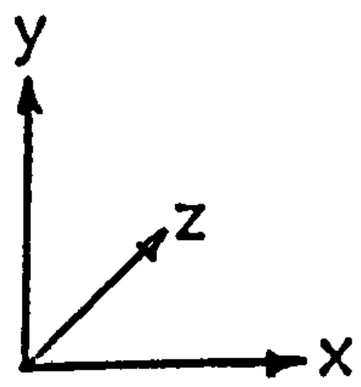

FIGURE 8.6 Further 2-d waveguide structures

The analyses are limited in accuracy near cut-off, the situation prevailing with a directional coupler. These devices, however, are not considered practical in the case of cadmium sulphide as the waveguide thickness would need to be less than 1μm and would consequently result in a large waveguide attenuation.

Another possible directional coupler, shown in Fig. 8.7, was proposed by Auracher et al[116] as a means of producing directional coupling between two uncoupled rectangular waveguides through a third intermediary layer placed over or under the two guides. It was also predicted that although phase matching between the two guides (1) and (2) must be maintained the third guide need not be exactly phase matched to the other two to permit 100% power transfer. Since the top two guides are uncoupled their sizes can be increased (ie mode is further from cut-off) thus relaxing the tolerance requirements and so simplifying device fabrication. This structure could have particular relevance to the case of cadmium sulphide rectangular waveguides where the ultimate waveguide loss could prevent the fabrication of guides with small enough dimensions to couple laterally (cf. cadmium sulphide waveguides grown on etched silicon substrates). Since guides (1) and (2) must be phase matched for 100% power transfer switching of the light would be possible by electrooptically inducing a phase mismatch between these guides. The severe drawback of this structure is that it is multimode and in a practical situation scattering between the modes will exist. A coupler fabricated in 7059-glass and quartz using the three coupled waveguide system of Fig. 8.7 is discussed in Appendix D. It is concluded that multimode waveguides cannot be used for reliable directional coupling.

8.4 DISCUSSION OF RESULTS

The numerical analyses have shown that a directional coupler could be fabricated using either a planar stacked structure or a

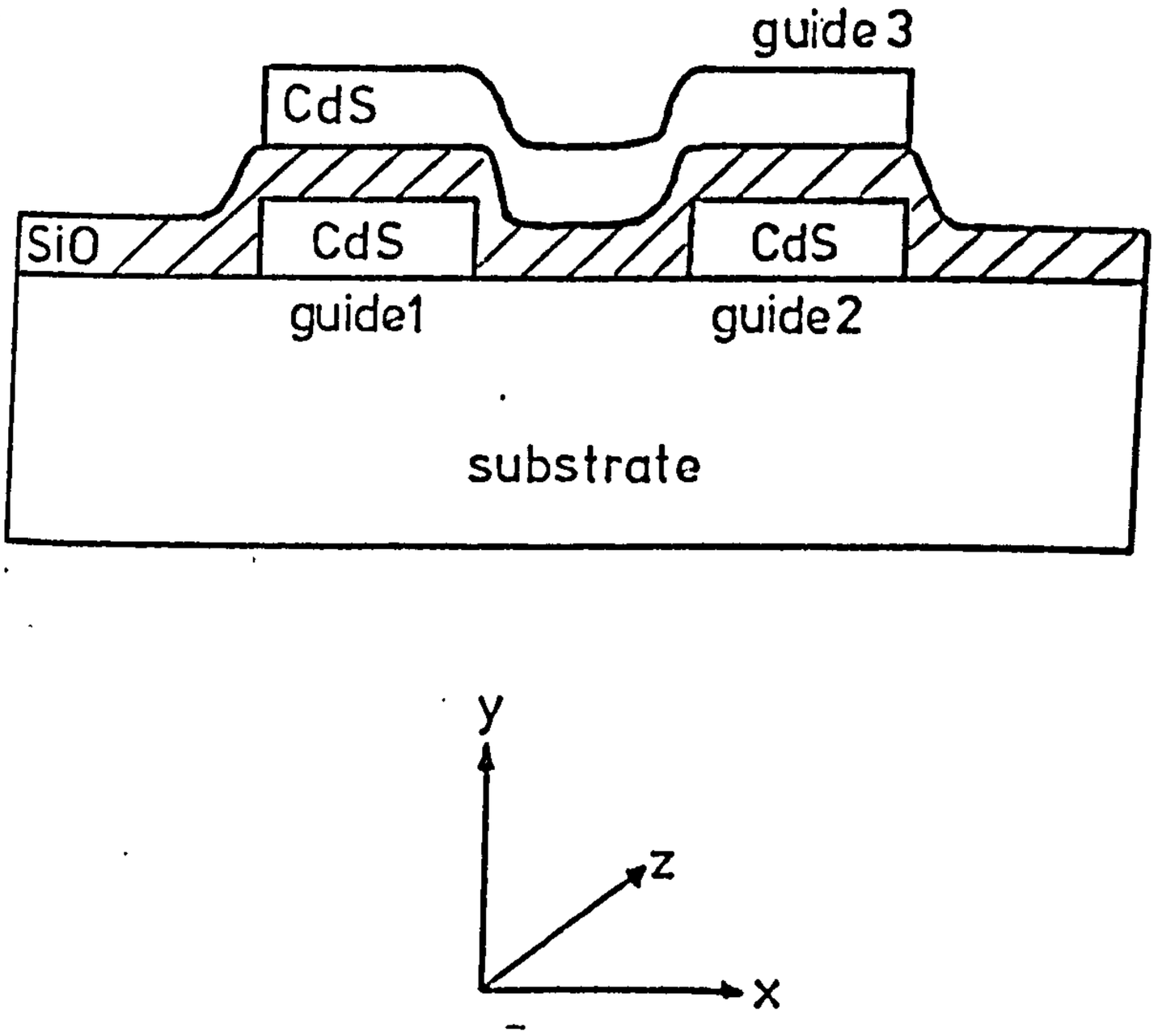

FIGURE 8.7 Three coupled waveguide directional coupler

rectangular waveguide configuration. However, only the rectangular waveguide system provides a means of switching the light between the waveguides. Single mode operation of the guides used for a directional coupler would appear essential and this is another point in favour of the CdS_xSe_{1-x} waveguides. Tolerance requirements for the coplanar structure will also be more readily achieved because the two waveguides are fabricated simultaneously within a very small area. Any remaining fabrication errors can be further alleviated by the electrode scheme of Kogelnik et al[113] whereby separate voltage control can be applied to the two coupled guides. The switching voltage is also reduced since opposite polarity voltages can be applied.

An electrooptic directional coupler switch requiring 61 volts for complete power transfer is possible with selenium diffusion into a thin film of cadmium sulphide ($\Delta n=2.5x10^{-2}$) to produce two CdS_xSe_{1-x} guides 5 μmx1.6 μn, separated by 2 μm with L_c = 1.65 mm. The device interaction length would be 4.95 mm. The voltage for switching is considerably greater than for the titanium diffused lithium niobate structure of Papuchon et al[48] and although efficient fibre-film coupling may be possible to the cadmium sulphide device the voltage would exclude its use in any practical integrated optical circuit. The technology, however, is still of interest and the possibility of a material with a larger electrooptic coefficient being amenable to the same fabrication technique would clearly stimulate further interest in this approach.

PART IV

CONCLUSIONS

CHAPTER 9. CONCLUDING DISCUSSION

9.1 CONCLUSIONS

It has been shown that thin films of cadmium sulphide can be evaporated with good reproducibility by an electron beam gun, from compound cadmium sulphide source materials. The films grown on amorphous substrates have a highly orientated polycrystalline structure with the c-axis perpendicular to the incident vapour stream. Those films grown on single crystal < 111 > spinel substrates are epitaxial films. The use of cadmium sulphide films as optical waveguides was demonstrated for 1.15 μm radiation with a minimum attenuation of 5 $dBcm^{-1}$ for films on amorphous substrates and 2 $dBcm^{-1}$ for those grown on spinel substrates. The minimum in waveguide loss was found to be synonymous with optimum film stoichiometry and structure. In particular a slow growth rate was found to be beneficial in improving the initial highly disordered region of the films grown on amorphous substrates. Once an initial growth layer had been established the evaporation rate was less critical. The rationale for this research, the techniques for evaporating a highly oriented active waveguide on an amorphous substrate, still stands as to date no comparable results have been reported. Most other active waveguides have relied on epitaxial growth and single crystal substrates.

The realisation of low loss rectangular waveguides based on thin polycrystalline films of cadmium sulphide was the most complex aspect of this research and to date has not been completely solved. For a well confined mode the waveguides formed by evaporation onto selectively etched silicon substrates have shown the lowest attenuation, 15 $dBcm^{-1}$ for a 20 μm wide guide formed with a 2 μm thick film. For a 5 μm wide guide formed by diffusion of selenium into polycrystalline cadmium sulphide thin films losses of 15 $dBcm^{-1}$ have also been attained but in this situation the waveguide mode is less tightly confined. The above losses are higher than those quoted for rectangular waveguides formed by ion bombardment and diffusion into other semiconductor

materials[9] but again these all required the use of single crystal substrates. The major problems associated with the formation of the cadmium sulphide waveguides was its chemical reactivity and the side wall roughness which contributed to the large scatter loss. The lower losses in the CdS_xSe_{1-x} diffused guides were due to the amelioration of edge roughness caused by the diffused profile at the side wall boundaries.

A general theory for five lossy waveguiding layers has been developed for use in the calculation of phase change for any multi-layer-type waveguide phase modulator. The results of a specific design study for the case of an Al-SiO-CdS-SiO-Al modulator have been presented and show that, provided waveguide loss is not a significant factor, an optimised structure can have a comparable modulation drive power to the lithium niobate type modulator[10]. Although lithium niobate has a much larger electrooptic coefficient the improved structure efficiency of the parallel plate electrode scheme compensates in the case of cadmium sulphide.

The phase modulation properties of the Al-SiO-CdS-SiO-Al planar modulator structure have been shown to agree with the theoretical predictions implying that the r_{13} electrooptic coefficient of the polycrystalline cadmium sulphide films is close to the value of $1.1 \times 10^{-12} m.V^{-1}$ for bulk single crystals. The optimum figure of merit could not be attained due to the practical limitations of waveguide loss. The minimum realisable power per unit bandwidth was $11.5 mW MHz^{-1}$ for one radian phase change in a diffraction limited structure with electrode area $10 \times 0.5 mm^2$. Tapered film coupling between 7059-glass and cadmium sulphide waveguides with phase modulation in the composite structure was also demonstrated for planar guides. This technology has three advantages; first the bulk of the guiding could be carried out in the low loss glass thus

reducing the device insertion loss, second highly efficient fibre-film coupling can be achieved to 7059-glass waveguides[100] and third it permits the use of a hybrid thin film technology where devices can be built in the best materials and interconnected by means of a low refractive index overlay guide. The final phase modulator reported was one in which lateral confinement of the mode was achieved using a rectangular waveguide. For an electrode area of 5x0.02 mm^2 the modulator will have a power per unit bandwidth of 900 $\mu W MHz^{-1}$ for one radian phase change. The figure is larger than the values reported for lithium niobate[55] because of the large waveguide loss limiting the device length and also the wavelength of operation at 1.15 μm (cf. 0.633 μm for lithium niobate). All these structures were based on vacuum evaporated layers with the active film, a polycrystalline layer, grown on an amorphous substrate and these are the best modulators to be reported using such a technology.

Equations have been derived for calculating the tolerance requirements on a directional coupler to any required rejection ratio between the guides. Several designs for directional coupler with electrooptically controlled switching were investigated. For a selenium diffused cadmium sulphide coplanar rectangular waveguide system a switching voltage of 61 volts would be needed for two 5μm x 1.6μm guides ($\Delta n = 2.5 \times 10^{-2}$) 4.95mm long and 2 μm apart. The switching would occur through an electrooptically induced phase mismatch between the two coupled guides. Recently a number of electro-optically controlled directional coupler switches requiring single crystal substrates have been reported[48,49,113]. The low switching voltages required for these modulators make it unlikely that the selenium diffused cadmium sulphide waveguide switch would be used in preference.

Thin polycrystalline films of cadmium sulphide have been developed from the initial demonstration of optical waveguiding in planar films to the achievement of electrooptic phase modulation in both planar and 2-d multilayered structures. While the cadmium sulphide devices do not possess competitive performances for practical applications the technologies used have been shown to provide a solution to the fibre-film coupling problem. In addition the waveguide and device fabrication techniques would lead to low drive power devices capable of a higher packing density due to the stacked electrode configuration. The fabrication of competitive devices, however, awaits the adaptation of a material, with superior optical properties, amenable to the fabrication techniques described in this thesis.

9.2 FUTURE WORK

The final limiting factor on the cadmium sulphide modulator performance (apart from the relatively small r_{13} electrooptic coefficient which is fixed) has been the minimum attainable waveguide loss. In any further studies on cadmium sulphide the sources of the remaining waveguide attenuation should be investigated by considering the film structure formation and growth kinetics in more detail. To facilitate such a study evaporation by molecular beam epitaxy should be adopted as the impinging rate of the atoms and the film stoichiometry can be more accurately controlled. In particular the elimination of the source of the large photoconductivity at 0.633 μm would permit waveguiding in the visible with a concomitant improvement in the electrooptic effect[63]. Improvements in the planar waveguide loss would help the attenuation in the rectangular waveguides. However, the amelioration of the side wall roughness would have to be studied further. In particular the selenium diffusion technique deserves further study to solve the problems of high waveguide loss for high selenium concentrations and a closer study of the

diffusion mechanisms involved may prove valuable. The guides formed by evaporation onto the selectively etched silicon could also be studied further as the silicon substrate would enable the integration of optics and electronics.

If the above improvements could be made to the basic cadmium sulphide waveguides then the electrooptic modulator performance could be made comparable to the best quoted results[55]. Although tapered film coupling between slab waveguides has been investigated a detailed theoretical and experimental study of this coupling between rectangular waveguides would be a fruitful area of work.

The small electrooptic effect of cadmium sulphide means that an electrooptically controlled directional coupler switch requires a large voltage (cf lithium niobate) and thus some alternative switching schemes, possibly based on the Mach-Zehnder interferometer[50], should be investigated. Fabrication the amplitude modulator illustrated schematically in Fig. 9.1 could be attempted. The device would produce an amplitude modulation of the light in the fibre and would possess rigidity, fibre-fibre coupling and temperature stability, all features required of an integrated optical system[1].

Some theoretical studies on a conductivity modulator based on a cadmium sulphide waveguide are described in Appendix E. The study assumes that the voltage on the gate of a thin film depletion mode insulated gate field effect transistor controls the number of free carriers injected into the cadmium sulphide thus modulating, by absorption, the propagating mode. No previous attempt has been made to induce optical loss modulation by electrical injection of free carriers. However, cadmium sulphide would appear a good choice of material due to the low mobilities and effective masses of its free carriers[117]. The principle advantage of such a device would be for use at longer wavelengths (eg 10.6 μm) where the conductivity modulator becomes more efficient, unlike the electrooptic modulator

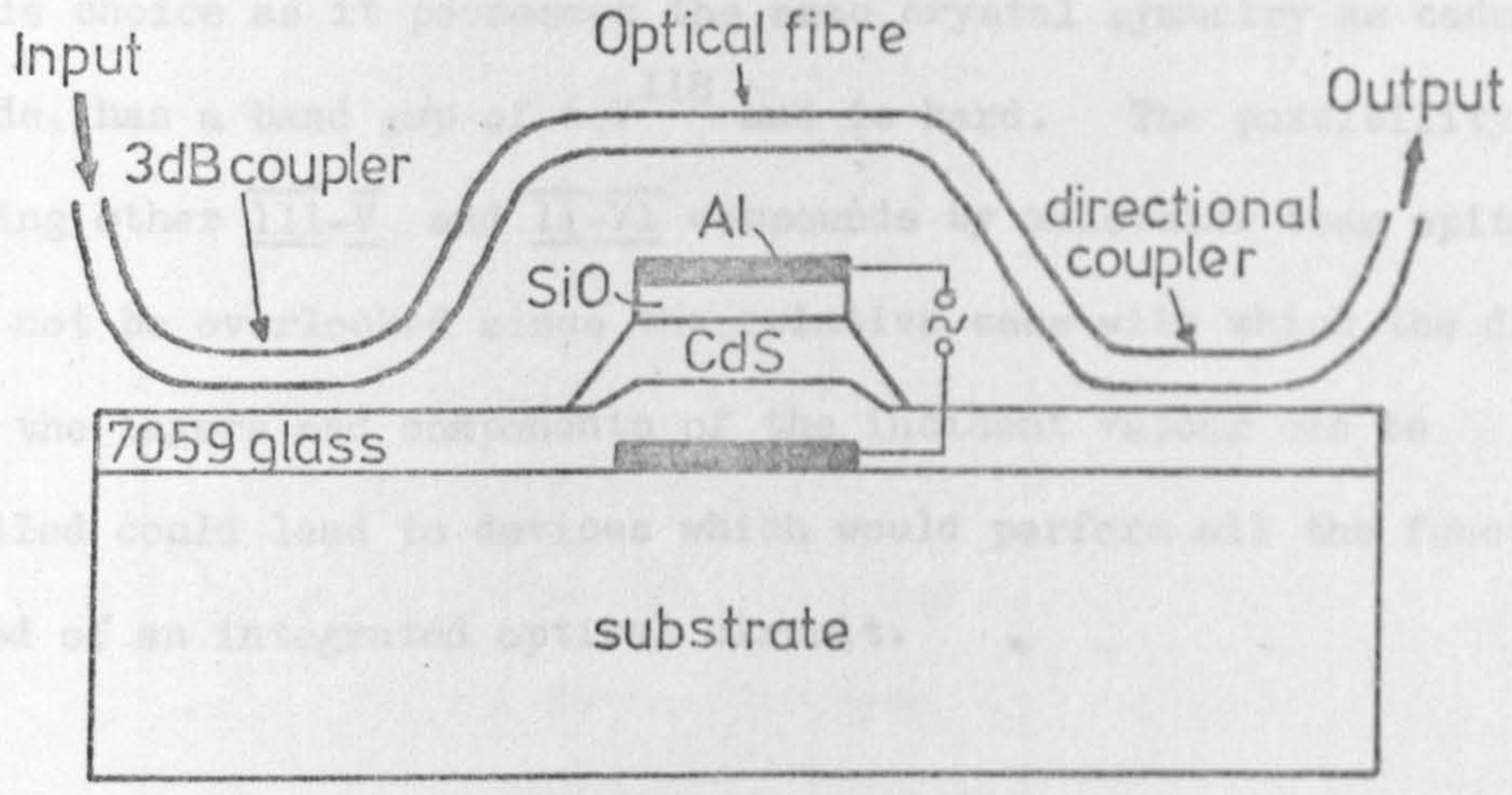

FIGURE 9.1 Schematic diagram of fibre-fibre amplitude modulator based on a cadmium sulphide phase modulator

for which the converse is true.

The limitations of cadmium sulphide are that it is an infrared material, is soft, has a relatively small electrooptic coefficient and does not possess low waveguide attenuation. However, the technologies developed are potentially useful if a more suitable material could be found. Of the III-V semiconductor compounds the nitrides have not been extensively studied. They are wide band gap materials[118] and epitaxial growth of some has been achieved[119]. Aluminium nitride grown by chemical vapour deposition could be a suitable choice as it possesses the same crystal symmetry as cadmium sulphide, has a band gap of 6eV[118] and is hard. The possibility of producing other III-V and II-VI compounds by molecular beam epitaxy should not be overlooked since the relative ease with which the doping of the layers and components of the incident vapour can be controlled could lead to devices which would perform all the functions required of an integrated optical circuit.

APPENDIX A1: COMPUTER FLOW DIAGRAM OF PROGRAM FOR CALCULATING PROPAGATION CONSTANT (β/k) AND GUIDE THICKNESS W

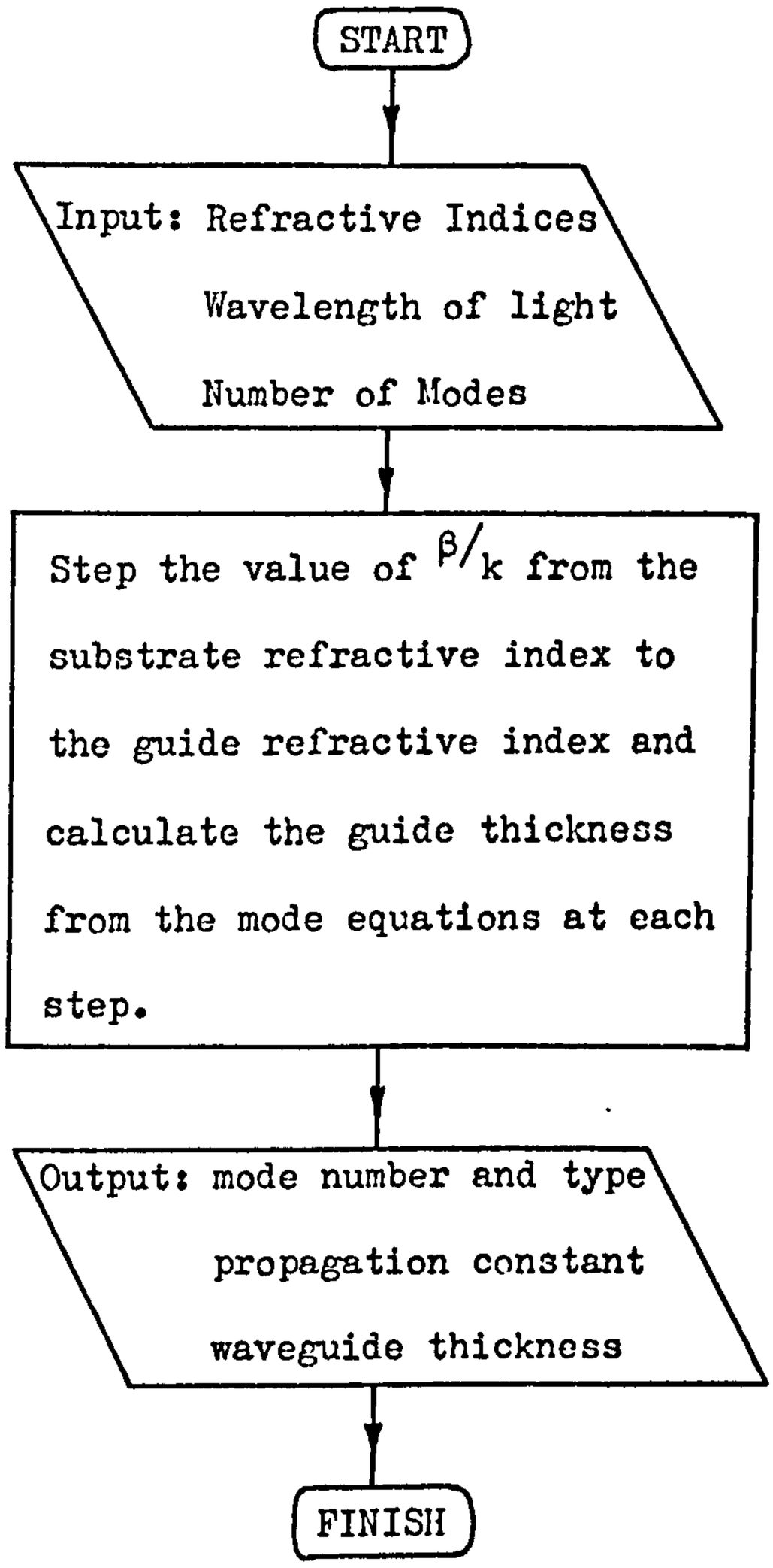

APPENDIX A2: COMPUTER FLOW DIAGRAM OF PROGRAM FOR CALCULATING GUIDE REFRACTIVE INDEX AND THICKNESS FROM THE SYNCHRONOUS COUPLING ANGLES FOR THE MODES

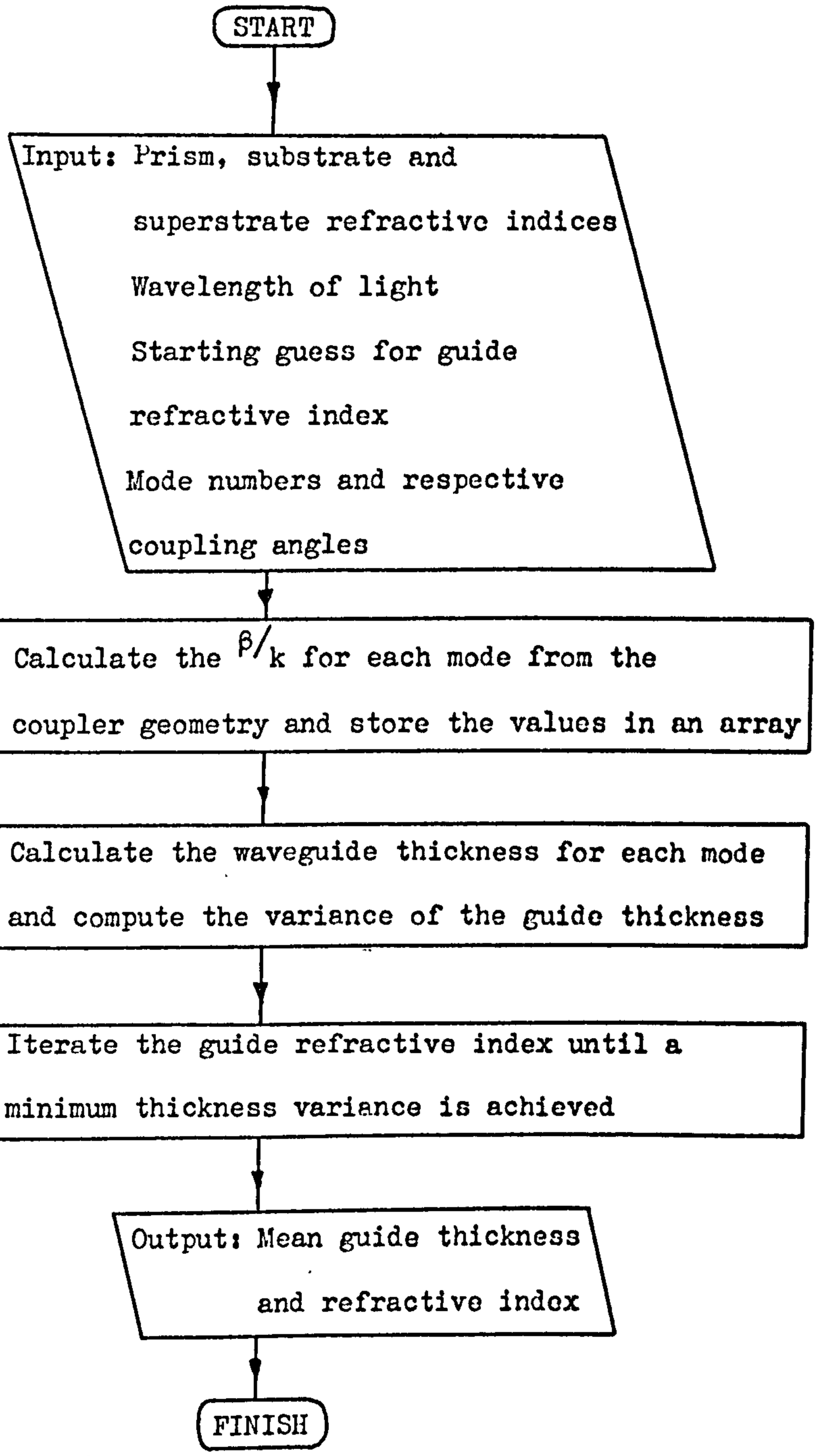

APPENDIX A3: COMPUTER FLOW DIAGRAM OF PROGRAM FOR CALCULATING COMPLEX β AND WAVEGUIDE THICKNESS FOR THE FIVE LAYER LOSSY WAVEGUIDE SYSTEM

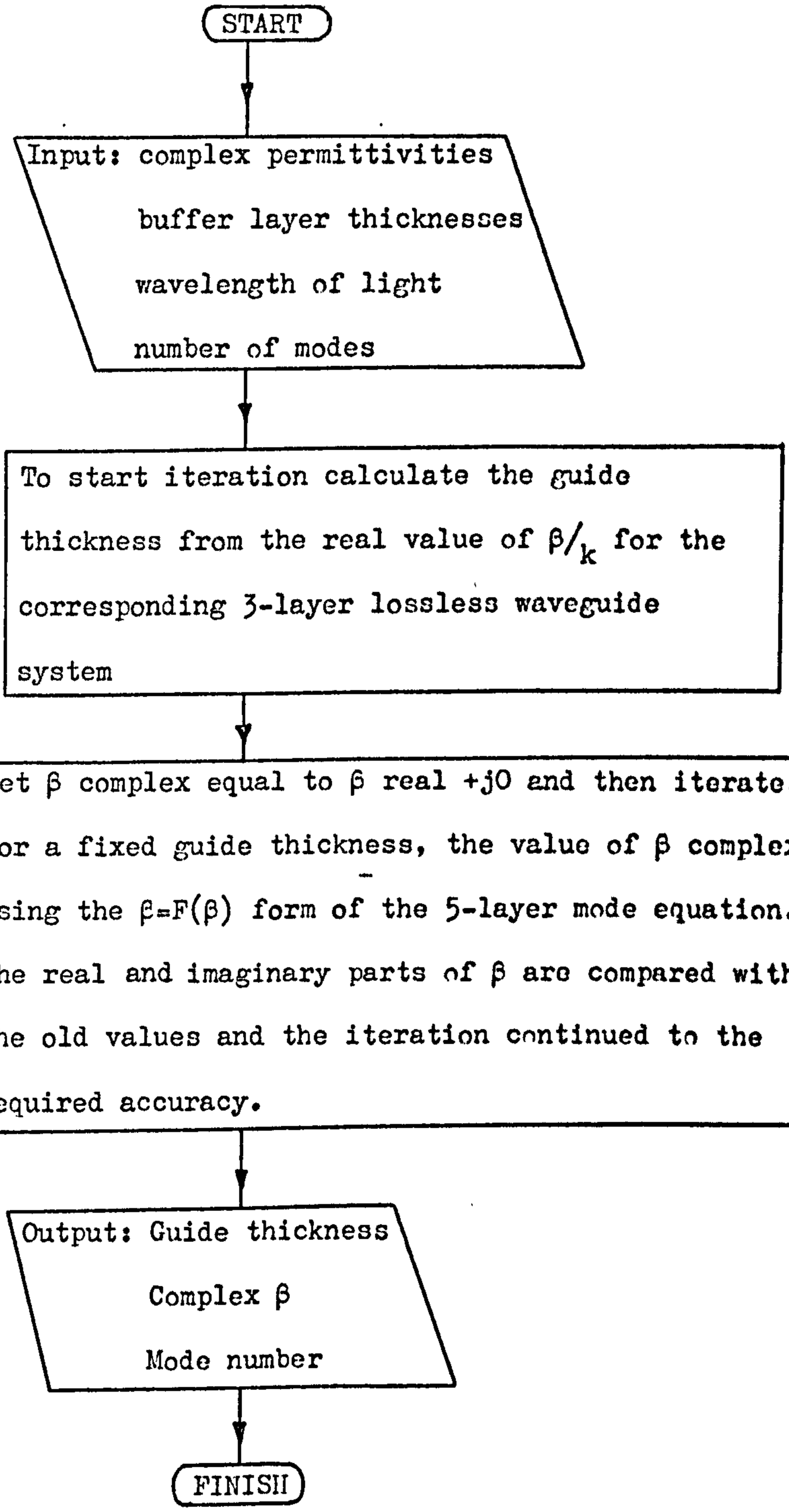

APPENDIX B: THE TE-TM PRISM-FILM COUPLER

The large birefringence of a rutile crystal allows a prism coupler to be cut so that the two refractive indices seen by a TE and a TM mode can compensate for their propagation constant difference and permit equal powers to be launched into the modes at the same synchronous coupling angle. Such a system would be of benefit in converting an electrooptic phase modulator into an amplitude modulator. However, the coupler has the disadvantage that it must be designed for a particular waveguide geometry.

If equal powers of a TE and a TM mode are to be launched at the same synchronous coupling angle then equation (B.1) must hold

$$n_{PTE}\sin\left[\sin^{-1}\left(\frac{\beta_{TE}}{kn_{PTE}}\right) - \alpha\right] = n_{PTM}\sin\left[\sin^{-1}\left(\frac{\beta_{TM}}{kn_{PTM}}\right) - \alpha\right] \qquad (B.1)$$

where n_{PTE} and n_{PTM} are the prism refractive indices for the TE and TM waves respectively, α is the prism angle and air has been assumed to be the medium surrounding the prism. β_{TE} and β_{TM} are obtained from the appropriate mode equation of chapter 2.

The relationship between n_{PTE} and the angle ξ at which the rutile c-axis is cut to the prism base is obtained from Fig. B.1 as

$$\frac{1}{n_{PTE}^2} = \frac{\sin^2\xi}{n_{Po}^2} + \frac{\cos^2\xi}{n_{Pe}^2} \qquad (B.2)$$

where n_{Po} and n_{Pe} are the prism ordinary and extraordinary refractive indices respectively.

The relationship between n_{PTM} and ξ is more complex due to the E-field vector being dependent on the direction of propagation through the prism. From Fig. B.2a the refractive index along y is given by

$$\frac{1}{n_y^2} = \frac{\sin^2\xi}{n_{Pe}^2} + \frac{\cos^2\xi}{n_{Po}^2} \qquad (B.3)$$

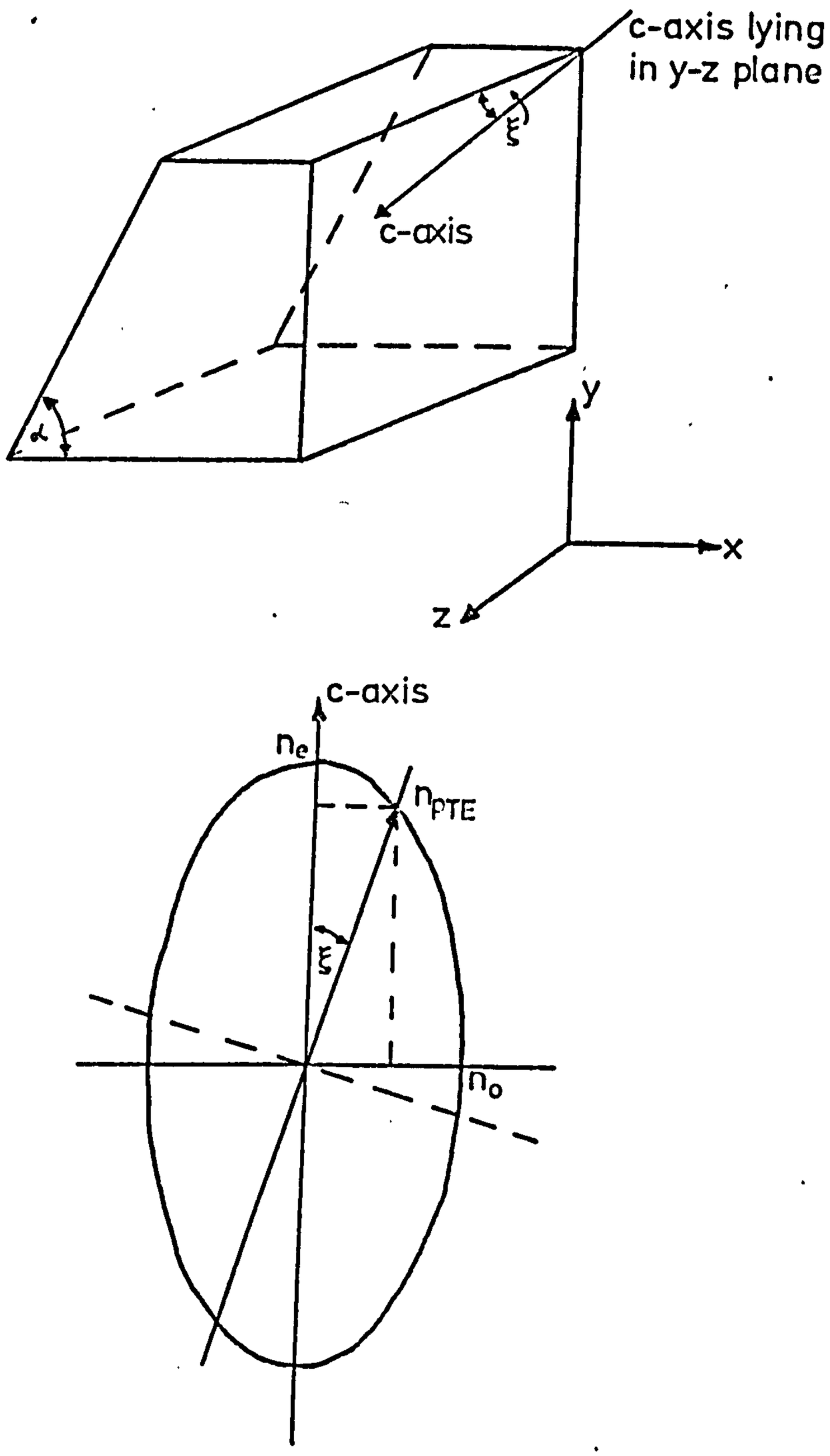

FIGURE B.1 Relationship between n_{PTE} and ξ

for a birefringent prism coupler

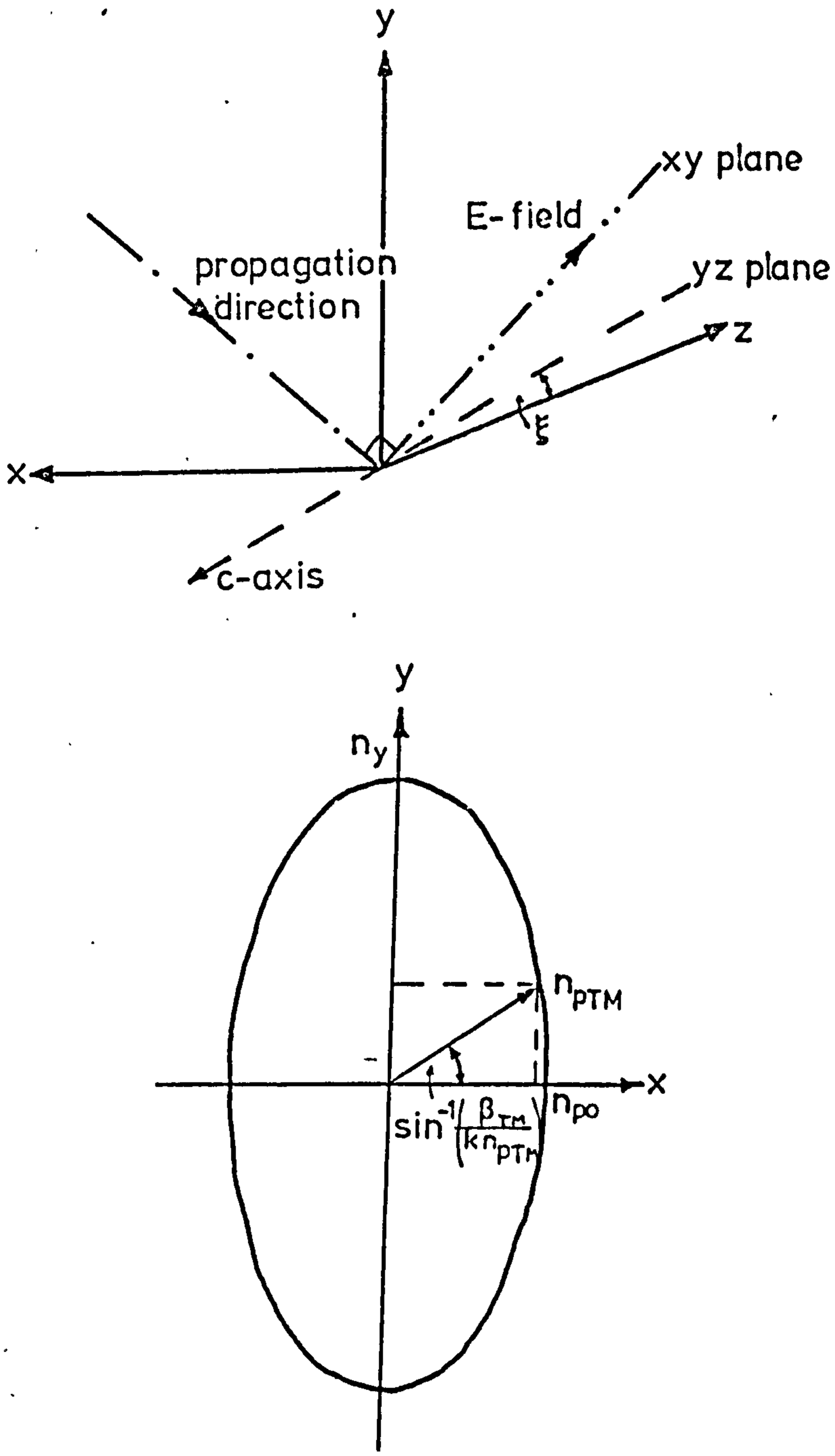

FIGURE B.2 Relationship between n_{pTM} and ξ for a birefringent prism coupler

Fig. B.2b forms an index ellipsoid round n_{Po} and n_y with n_{PTM} being defined by

$$\frac{1}{n_{PTM}^2} = \frac{\sin^2\left[\sin^{-1}\frac{\beta_{TM}}{kn_{PTM}}\right]}{n_y^2} + \frac{\cos^2\left[\sin^{-1}\frac{\beta_{TM}}{kn_{PTM}}\right]}{n_{Po}^2} \qquad (B.4)$$

Substituting for n_{PTE} from equation (B.2) in equation (B.1) yields

$$\frac{n_{Po}\, n_{Pe}}{(\sin^2\xi n_{Pe}^2+\cos^2\xi n_{Po}^2)^{\frac{1}{2}}} \sin\left[\sin^{-1}\left(\frac{\beta_{TE}(\sin^2\xi n_{Pe}^2+\cos^2\xi n_{Po}^2)^{\frac{1}{2}}}{kn_{Po}n_{Pe}}\right)-\alpha\right]$$

$$= n_{PTM}\sin\left[\sin^{-1}\left(\frac{\beta_{TM}}{kn_{PTM}}\right)-\alpha\right] \qquad (B.5)$$

and substituting for n_y^2 from equation (B.3) in equation (B.4) yields

$$n_{TM}^2 = \frac{n_{Po}^4\, n_{Pe}^2}{(n_{Po}^2\sin^2\xi+n_{Pe}^2\cos^2\xi)\left[\frac{\beta_{TM}^2 n_{Po}^2}{k^2 n_{PTM}^2}+\cos^2\left(\sin^{-1}\frac{\beta_{TM}}{kn_{PTM}}\right)\frac{n_{Po}^2\, n_{Pe}^2}{(n_{Po}^2\sin^2\xi+n_{Pe}^2\cos^2\xi)}\right]} \qquad (B.6)$$

Equations (B.5) and (B.6) can be solved numerically for ξ and n_{TM} given the characteristics of the modes that have to be launched at the same synchronous coupling angle.

For a 1 μm thick cadmium sulphide waveguide on a glass substrate the TE_o and TM_o modes will be launched at the same synchronous coupling angle if $\alpha = 60^o$ and $\xi = 47^o$ giving $n_{PTE} = 2.583$ and $n_{PTM} = 2.568$.

APPENDIX C: CALCULATION OF PHASE CHANGE FOR TM MODES IN A BIREFRINGENT FILM

The crystal axes are defined in Fig. C.1 with respect to the waveguide propagation direction. A TM mode thus has a resultant E-field vector which has components affected by both changes in the ordinary and extraordinary refractive indices. These changes were defined in equations (5.3a) and (5.3b) respectively. Although the two refractive indices are very similar the electrooptic coefficients differ by more than a factor of two (r_{13}=1.1x10^{-12}m.V^{-1} and r_{33} = 2.4x10^{-12}m.V^{-1} [92]) and the cadmium sulphide must therefore be considered birefringent when calculating the phase change $\Delta\phi_{TM}$. The phase change for a TM mode is thus given by equation (C.1)

$$\Delta\phi_{TM} = \frac{-\frac{1}{2}\left[\frac{\partial\beta}{\partial n_o} r_{13} n_o^3 + \frac{\partial\beta}{\partial n_e} r_{33} n_e^2\right] V_{TOT} \varepsilon_1'^2}{(2d_1\varepsilon_1'\varepsilon_2' + W\varepsilon_1'^2)} \qquad (C.1)$$

where the variables are defined in equation (5.29) and the partial derivatives $\frac{\partial\beta}{\partial n_o}$ and $\frac{\partial\beta}{\partial n_e}$ are defined in equations (C.2) and (C.3) which are obtained by differentiation of equation (2.22) with the surrounding indices assumed the same (Fig. C.1).

$$\frac{\partial\beta}{\partial n_o} = \frac{\frac{\sin 2\phi\beta^2}{[k^2n_o^2-\beta^2]n_o} + \frac{Wn_e\beta^2}{[k^2n_o^2-\beta^2]^{\frac{1}{2}}n_o^2}}{\frac{\sin 2\phi\beta}{(\beta^2-k^2n_2^2)} + \frac{\sin 2\phi\beta}{(k^2n_o^2-\beta^2)} + \frac{new\beta}{n_o(k^2n_o^2-\beta^2)^{\frac{1}{2}}}} \qquad (C.2)$$

$$\frac{\partial\beta}{\partial n_e} = \frac{\frac{W(k^2n_o^2-\beta^2)^{\frac{1}{2}}}{n_o} - \frac{\sin 2\phi}{n_e}}{\frac{\sin 2\phi\beta}{(\beta^2-k^2n_2^2)} + \frac{\sin 2\phi\beta}{(k^2n_o^2-\beta^2)} + \frac{n_e w\beta}{n_o(k^2n_o^2-\beta^2)^{\frac{1}{2}}}} \qquad (C.2)$$

where

$$\phi = \tan^{-1}\left[\frac{n_e n_o}{n_2^2}\frac{(\beta^2-k^2n_2^2)^{\frac{1}{2}}}{(k^2n_o^2-\beta^2)^{\frac{1}{2}}}\right] \qquad (C.3)$$

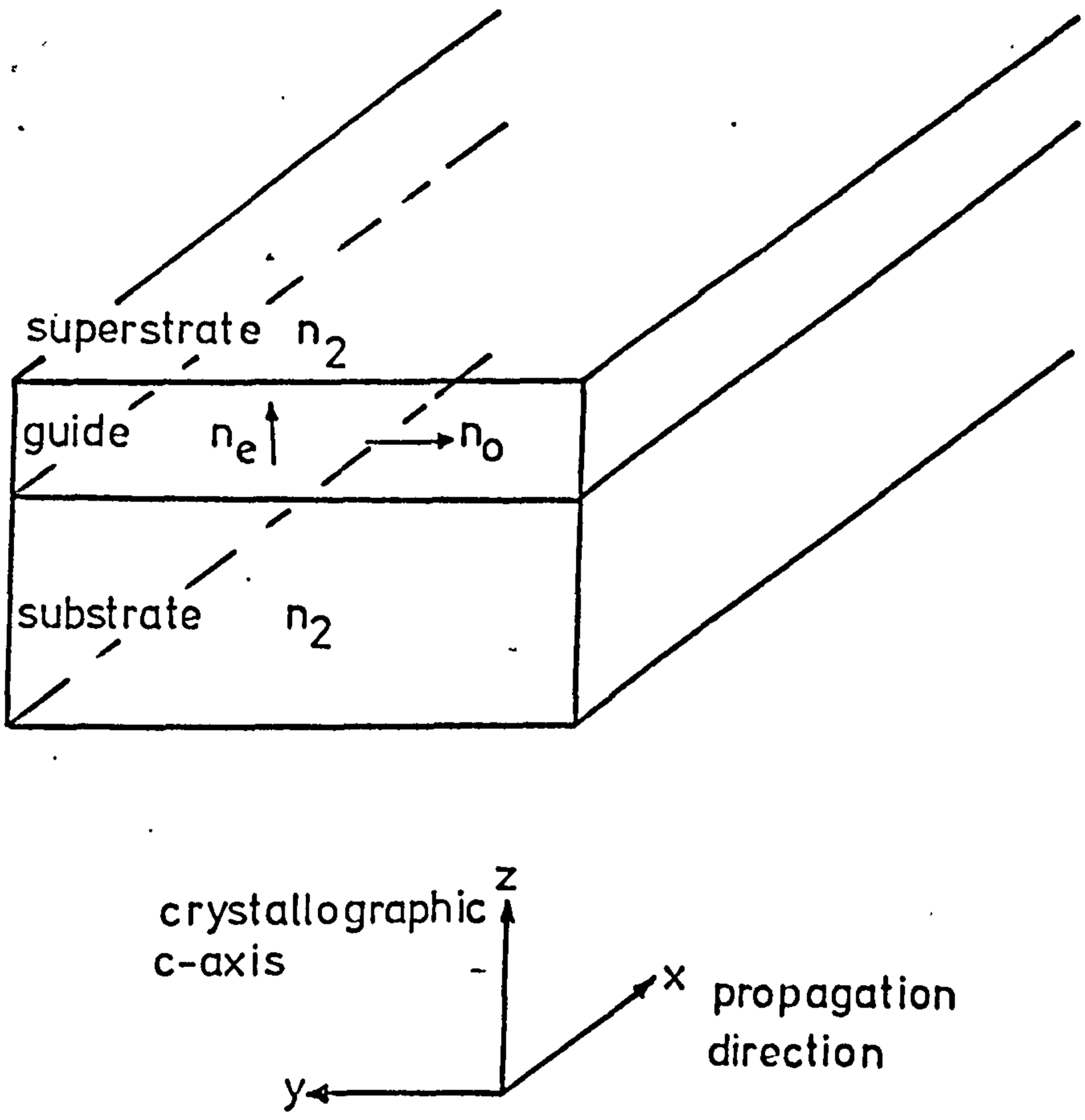

FIGURE C.1 Planar anisotropic waveguide geometry

For a 1 μm thick cadmium sulphide film a phase change of π radians is possible in 10 mm with 8 volts applied across the guide for the TE_0 mode. For the TM_0 mode in the same guide 7.5 volts are required for a π phase change.

APPENDIX D: EXPERIMENTS WITH AN AURACHER DIRECTIONAL COUPLER FABRICATED IN 7059-GLASS AND FUSED SILICA

Auracher et al[116] have proposed the directional coupler structure illustrated in Fig. D.1 but no substantiating experimental work has been reported. This structure might represent a possible directional coupler system for rectangular waveguides formed by cadmium sulphide where the optical attenuation precludes direct coupling of the two coplanar guides. Firstly, however, the coupler structure of Fig. D.1 was built using 7059-glass waveguides and a fused silica tunnelling region to check the validity of the theory. The dimensions of the structures are given in Fig. D.1 and accurate control over the layer thicknesses was achieved using a laser thickness monitor[120]. The rectangular waveguides were defined by ion beam etching through baked photoresist masks.

The waveguides supported two modes in the y-direction and because of the large widths of the guides supported many modes in the transverse x-direction. It thus proved impossible to selectively excite a single mode and even when only two or three modes were launched the light scattered into all the possible modes after only a very short distance due to the waveguide imperfections. The observed result was that after less than one coupling length the light had distributed itself equally between the two guides. This was caused by the coupling of a large number of modes, all with different coupling lengths, tending to distribute the power equally between the two guides. It would thus appear that, experimentally, single mode operation of all three waveguides is necessary. With the third guide larger than the other two it would seem an unlikely condition to be fulfilled.

For the case of rectangular cadmium sulphide waveguides evaporated onto selectively etched silicon substrates this coupler structure would not provide a practical solution as single mode waveguides are not feasible with the present technology.

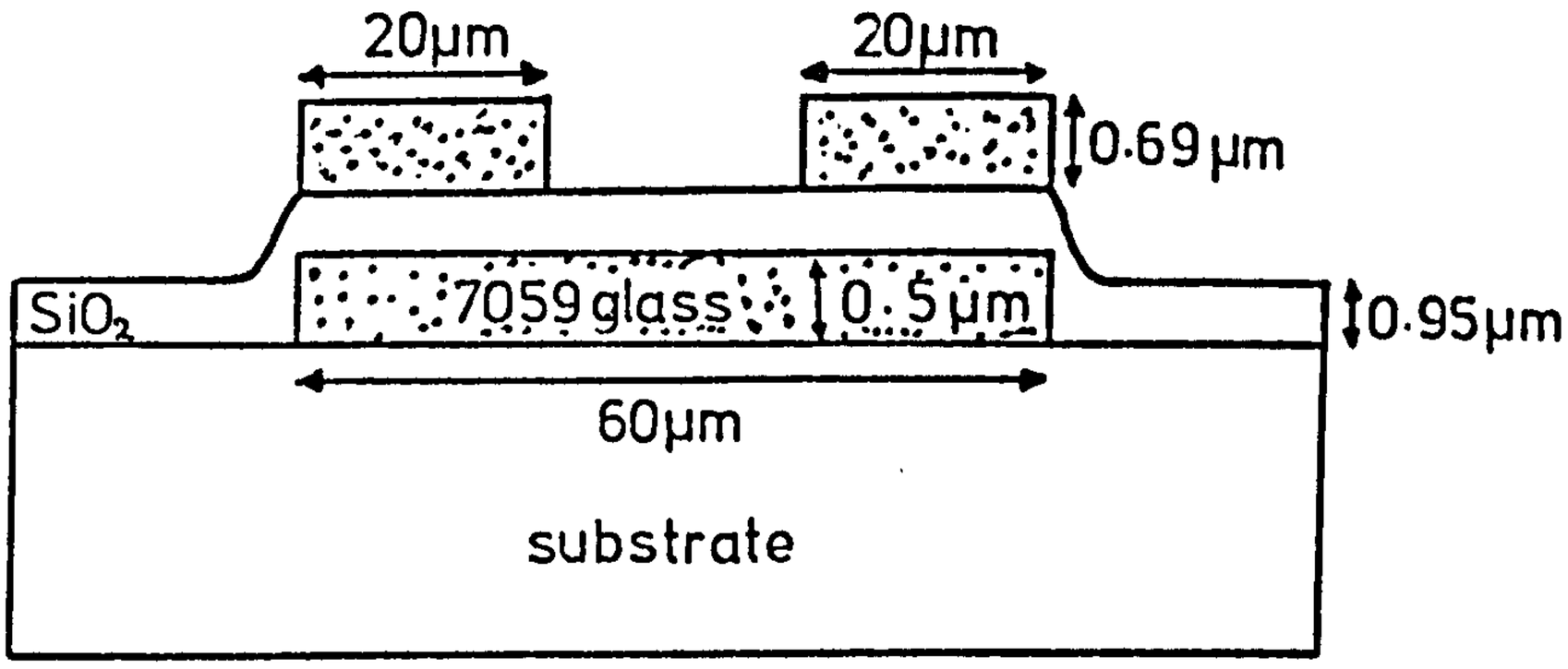

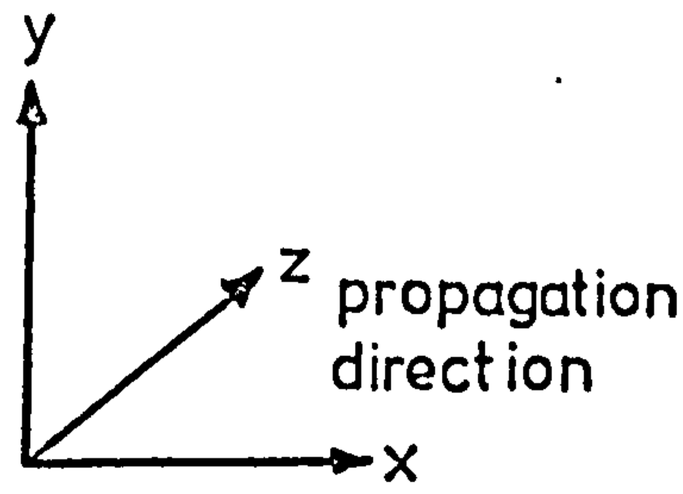

FIGURE D.1 Three coupled 7059glass waveguide directional coupler

APPENDIX E: CONDUCTIVITY MODULATION IN CADMIUM SULPHIDE WAVEGUIDES

An analysis of Weimer[121] for a depletion mode thin film insulated gate field effect transistor (Fig. E.1) derives an expression relating a variation in gate voltage to a change in source-drain current below saturation (equation (E.1)).

$$\frac{\Delta I}{\Delta V_g} = \frac{\mu_d C_g V_D}{L^2} \qquad (E.1)$$

where μ_d is the effective drift mobility, C_g is the capacitance across the insulator and V_D is the source drain voltage. The current density in a semiconductor is related to the number of injected carriers by equation (E.2) which is derived from the equation of charge continuity

$$\Delta J = E\Delta N_n \mu_n e \qquad (E.2)$$

where E is the electric field, ΔN_n the number of injected carriers, μ_n the mobility of electrons and e the charge on an electron.

Combining equations (E.1) and (E.2) relates variations in the gate voltage to the number of injected carriers (equation E.3)

$$\Delta V_g = \frac{\Delta N_n eht}{\varepsilon_o \varepsilon_r} \qquad (E.3)$$

where ε_r is the relative permittivity of the insulator material, t the insulator thickness and h the semiconductor thickness.

Moss[122] derives an expression relating the number of injected carriers to the absorption coefficient α;

$$\alpha = \frac{\lambda^2 e^3}{4\pi^2 c^3 n \varepsilon_o} \left[\frac{\Delta N_n}{m_n^2 \mu_n}\right] \qquad (E.4)$$

where m_n is the effective mass of electrons, c is the speed of light and n the semiconductor refractive index. Combining equations (E.3) and (E.4) yields an equation linking a change in gate voltage to a change in absorption in the semiconductor waveguide.

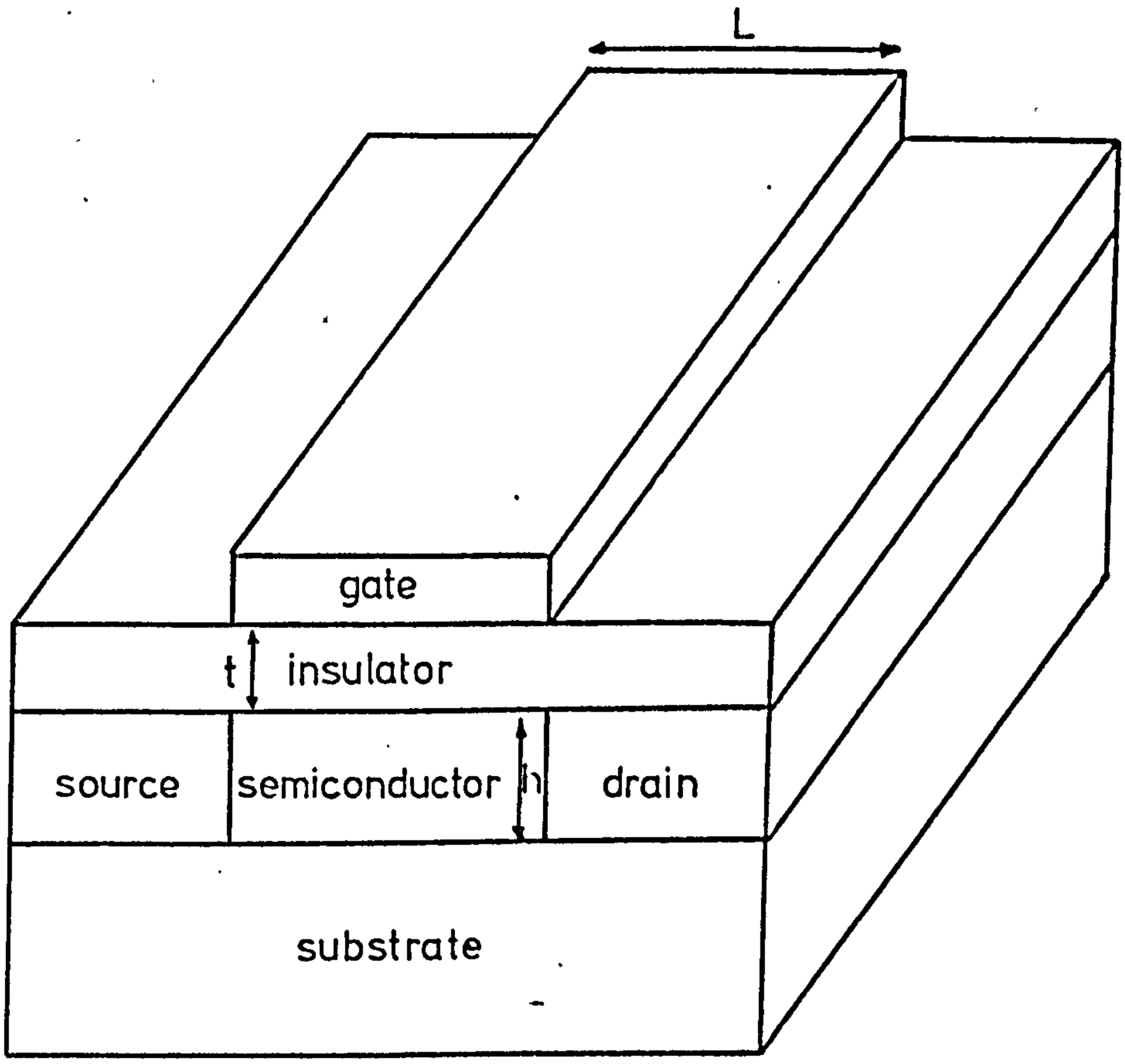

FIGURE E·1 Thin film conductivity modulator

$$\alpha = \frac{\lambda^2 e^2 \varepsilon_r}{4\pi^2 c^3 n m_n^2 \mu_n h t} V_g \qquad \text{(E.5)}$$

Equation (E.5) provides the necessary information to calculate the performance of a conductivity modulator. It can be seen that the smaller the effective mass and mobility of the semiconductor and the larger the wavelength of operation then the more efficient is the conductivity modulation.

For a cadmium sulphide waveguide 2 μm thick, a silicon monoxide insulating layer 0.2 μm thick, W = 10 mm and L = 20 μm then 90% amplitude modulation could be achieved for 20 volts applied to the gate electrode and 10.6 μm as the wavelength of operation.

APPENDIX F: LIST OF PUBLISHED WORK

1. Stanley C.R., Duncan W and McMurray J.A., "Infrared Waveguides in Thin Films of CdS", Applied Physics Letters 24, 8, P380-382 (1974).

2. McMurray J.A. and Stanley C.R., "The Use of Compound Semiconductor Films in Integrated Optics", 8th Thin Films Conference, C.15 (1974).

3. McMurray J.A. and Stanley C.R., "Electrooptic Modulation in CdS Optical Waveguides", 5th European Solid State Device Research Conference, S10-B3-11 (1975).

4. McMurray J.A. and Stanley C.R., "CdS Optical Waveguide Modulators", 2nd National Quantum Electronics Conference, 54 (1975).

5. McMurray J.A. and Stanley C.R., "Taper Coupling between 7059-glass and CdS Films and Phase Modulation in the Composite Waveguide Structure", Applied Physics Letters 28, 3, P126-128 (1976).

6. McMurray J.A. and Stanley C.R., "Assessment of Thin Film Modulator Performance by Homodyne Detection of Optical Phase Change", Journal of Physics E: Scientific Instruments 9, 4, P317-319 (1976).

7. McMurray J.A. and Stanley C.R., "Electrooptic Phase Modulation in CdS Optical Waveguides", IEEE Journal of Quantum Electronics, 12, 5, P307-310 (1976).

8. McMurray J.A. and Stanley C.R., "Electrooptic Modulation and Switching in Optical Waveguides" British Association of Crystal Growers-Colloquium on Crystals for Optical Devices (1976).

REFERENCES

1. Miller S.E., "Integrated Optics - An Introduction", Bell System Technical Journal 48, 7, P2059-2069 (1969).

2. Kaplan R.A., "Optical Waveguide of Macroscopic Dimensions in Single Mode Operation", Proc. IEEE 51, 8, P1144-1145 (1963).

3. Bond W.L. et al, "Observation of the Dielectric-Waveguide Mode of Light Propagation in p-n Junctions" Applied Physics Letters 2, 3, P57-59 (1963).

4. Tien P.K. et al, "Modes of Propagating Light Waves in Thin Deposited Semiconductor Films", Applied Physics Letters, 14, 9, P291-294 (1969).

5. Goell J.E. et al, "Sputtered Glass Waveguide for Integrated Optical Circuits", Bell System Technical Journal 48, 10, P3445-3448 (1969).

6. Ulrich R, "Theory of Prism-Film Coupler by Plane Wave Analysis", Journal of the Optical Society of America, 60, 10, P1337-1350 (1970).

7. Tien P.K. et al, "Theory of Prism-Film Coupler and Thin Film Light Guides" Journal of the Optical Society of America 60, 10, P1325-1337 (1970).

8. Midwinter J.E. et al, "Experimental Studies of Evanescent Wave Coupling into a Thin Film Waveguide", Applied Physics Letters, 16, 5, P198-200 (1970).

9. Martin W.E. et al, "Optical Waveguides by Diffusion in II-VI Compounds", Applied Physics Letters 21, 7, P325-327 (1972).

10. Kaminow I.P. et al, "Thin Film $LiNbO_3$ Electrooptic Light Modulator", Applied Physics Letters 22, 10, P540-542 (1973).

11. Martin W.E., "Waveguide Electrooptic Modulation in II-VI Compounds", Journal of Applied Physics 44, 8, P3703-3707 (1973).

12. d'Auria L. et al, "Composants pour Liaisons par Faisceaux de Fibres Optiques", Revue Technique Thomson C.S.F., 7, 4, P651-675 (1975).

13. Somekh S. et al, "Channel Optical Waveguides and Directional Couplers in GaAs - Imbedded and Ridged", Applied Optics, 13, 2, P327-330 (1974).

14. Harper J. et al, "High Resolution Lens for Optical Waveguides", Topical Meeting on Integrated Optics, WB11, (1974).

15. Tien P.K. et al, "Two-layer Construction of Integrated Optical Circuits and Formation of Thin Film Prisms, Lenses and Reflectors", Applied Physics Letters 24, 11, P547-549 (1974).

16. Parish M.B. "Heterostructure Injection Lasers", IEEE Trans. MTT, 23, 1, P20-30 (1975).

17. Tien P.K. et al, "Optical Second Harmonic Generation in Form of Coherent Cerenkov Radiation from a Thin-Film Waveguide", Applied Physics Letters, 17,10, P447-450 (1970).

18. Schmidt R.V. et al, "Acoustooptic Bragg Deflection in $LiNbO_3$ Ti-diffused Waveguides", IEEE Journal of Quantum Electronics 11, 1, P57-59 (1975).

19. Hall D. et al, "Observation of Propagation Cut-off and its Control in Thin Optical Waveguides" Applied Physics Letters 17, 3, P127-129 (1970).

20. Kaminow I.P., "Optical Waveguide Modulators" IEEE Trans. MTT, 23, 1, P57-70 (1975).

21. de Barros MARP et al, "Nanosecond Baseband Optical Diffraction Modulator" Electronics Letters 23, 10, P267-269 (1971).

22. Hall D. et al, "Optical Guiding and Electrooptic Modulation in GaAs Epitaxial Layers", Optics Communications 1, 9, P403-405 (1970).

23. Blum F.A. et al, "Monolithic GaAs Circuit Elements for Integrated Optics", Toptical Meeting on Integrated Optics, MA4, (1976).

24. Schmidt R.V. et al, "Metal Diffused Optical Waveguides in $LiNbO_3$", Applied Physics Letters, 25, 8, P458-460 (1974).

25. Papuchon M., Private Communication.

26. Maurer R.D., "Glass Fibres for Optical Communication", Proc IEEE 61, 4, P452-462 (1973).

27. Gedeon A., "Spectral Properties of TE_o and TM_o Modes in Dielectric Thin Film Waveguides Excited with a Prism Light Coupler", Optica Acta 19, 9, P765-779 (1972).

28. Pitt C.W. et al, "R.F. Sputtered Thin Films for Integrated Optical Components", Thin Solid Films 26, 1, P25-51 (1975).

29. Valette S. et al, "Optical Wavcguides in Ion Implanted ZnTe", Journal of Applied Physics 46, 6, P2731-2732 (1975).

30. Taylor, H.F. et al, "Fabrication of Single Crystal Semiconductor Optical Waveguides by Solid State Diffusion", Applied Physics Letters, 21, 3, P95-98 (1972).

31. Kaminow I.P. et al, "Optical Waveguiding Layers in $LiNbO_3$ and $LiTaO_3$" Applied Physics Letters 22, 7, P326-328 (1973).

32. Giallorenzi T.G. et al, "Optical Waveguides Formed by Thermal Migration of Ions in Glass" Applied Optics, 12, 6, P1240-1245 (1973).

33. Hutchins R.H., Private Communication.

34. Chang M.S. et al, "GaAs Optical Waveguide Structures at 10.6 μm Wavelength", Applied Optics 14, 7, P1572-1578 (1975).

35. Hammer J.M. et al, "Low loss Epitaxial ZnO Optical Waveguides", Applied Physics Letters, 21, 8, P358-360 (1972).

36. Westwood W.D. et al, "Sputtered ZnO Optical Waveguides", Wave Electronics 1, 2, P139-151 (1975).

37. Hammer J. M. et al, "Low loss Single Mode Optical Waveguides and Efficient High Speed Modulators of $LiNb_xTa_{1-x}O_3$ on $LiTaO_3$", Applied Physics Letters 24,11, P545-547 (1974).

38. Kleinknecht H.P. et al, "(GaAl)P Optical Waveguide Modulators Fabricated by Liquid Phase Epitaxy" Journal of Applied Physics 45, 8, P3453-3459 (1974).

39. Chen F.S. et al, "A Lithium Niobate Light Modulator for Integrated Optics", Proc. IEEE, 62, 1, P133-134 (1974).

40. Martin W.E., "A New Waveguide Switch/Modulator for Integrated Optics" Applied Physics Letters 26, 10, P562-564 (1975).

41. Takada S. et al, "Optical Waveguides of Single Crystal $LiNbO_3$ Film Deposited by RF Sputtering " Applied Physcis Letters, 24, 10, P490-492 (1974).

42. Reinhart F.K. et al, "Electroabsorption in $Al_yCa_{1-y}AsAl_xCa_{1-x}As$ Double Heterostructures" Applied Physics Letters 22, 8, P372-374 (1973).

43. Tien P.K. et al, "Switching and Modulation of Light in Magnetooptic Waveguides of Garnet Films" Applied Physics Letters, 21, 8, P394-396 (1972).

44. Chang W.S.C., "Acoustooptic Deflections in Thin Films", IEEE Journal of Quantum Electronics, 7, 4, P167-170 (1971).

45. Kerr J., "A New Relation between Electricity and Light: Dielectrified Media Birefringent" Philosophical Magazine 50, 4, P337-348 and P446-458 (1875).

46. Pockels F, "Lehrbuch der Kristalloptik", Bibliotheca Mathematica Teubneriana Series, Teuhner Leipzig (1906).

47. Hammer J.M. "Digital Electrooptic Grating Deflector and Modulator" Applied Physics Letters 18, 4, P147-149 (1971).

48. Papuchon M. et al, "Electrically Switched Optical Directional Coupler: COBRA" Applied Physics Letters 27, 5, P289-291 (1975).

49. Campbell J.C. et al, "GaAs Electrooptic Directional Coupler Switch" Applied Physics Letters 27, 4, P202-205 (1975).

50. Zernike F., "Integrated Optics Switch", Topical Meeting on Integrated Optics, WA5 (1974).

51. Webster J.C. et al, "Push-pull Thin Film Optical Modulator" Applied Physics Letters 26, 8, P465-467 (1975).

52. Campbell J.C. et al, "GaAs Electrooptic Channel Waveguide Modulator" Applied Physics Letters 26, 11, P640-642 (1975).

53. Papuchon M. et al, "Electrooptic Modulation in a Multimode Exodiffused Waveguide" Optics Communications 13, 4, P418-421 (1975).

54. Wright S., PhD Thesis, University of London (1976).

55. Kaminow I.P. et al, "Efficient Strip Waveguide Modulator", Applied Physics Letters 27, 10, P555-557 (1975).

56. Foster N.F. "Structure of CdS Evaporated Films in Relation to their Use as Ultrasonic Transducers", Journal of Applied Physics 38, 1, P149-159 (1976).

57. Tien P.K. "Light Waves in Thin Films and Integrated Optics", Applied Optics 10, 11, P2395-2413 (1971).

58. Andrews R.A., "Optical Waveguides and Integrated Optics Technology", Naval Research Report 7291, Washington D.C. USA (1971).

59. Marcuse D., "Mode Conversion Caused by Surface Imperfections of a Dielectric Slab Waveguide", Bell System Technical Journal 48, 9, P3187-3215 (1969).

60. Born M. et al, "Principles of Optics" 4th Edition, Pergamon Press, London (1970).

61. Lotsch H.K.V., "Reflection and Refraction of a Beam of Light at a Plane Interface", Journal of the Optical Society of America 58, 4, P551-561 (1968).

62. Gia Russo D.P. et al, "Wave Propagation in Anisotropic Thin Film Optical Waveguides", Journal of the Optical Society of America 63, 2, P138-145 (1973).

63. Yariv A., "Quantum Electronics", Wilcy, New York (1967)

64. Yamamoto S. et al, "Normal Mode Analysis of Anisotropic and Gyrotropic Thin Film Waveguides for Integrated Optics", Journal of Applied Physics 43, 12, P5090-5097 (1972).

65. Cryzak S. J. et al, "Refractive Indices of Single Synthetic ZnS and CdS Crystals", Journal of the Optical Society of America 47, 3, P240-243 (1957).

66. Shubert R. et al, "Optical Surface Waves on Thin Films and their Application to Integrated Data Processors" IEEE Trans. MTT, 16, 12, P1048-1054 (1968).

67. Tien P.K. et al, "Experiments on Light Waves in a Thin Tapered Film and a New Light Wave Coupler" Applied Physics Letters 18, 9, P398-401 (1971).

68. Kogelnik H. et al, "Holographic Thin Film Coupler", Bell System Technical Journal 49, 7, P1602-1608 (1970).

69. Dakss M.L. et al, "Grating Coupler for Efficient Excitation of Optical Guided Waves in Thin Films" Applied Physics Letters 16, 12, P523-525 (1970).

70. Dalgoutte D.G. "A High Efficiency Thin Grating Coupler for Integrated Optics", Optics Communications 8, 2, P124-127 (1973).

71. de Vore J.R., "Refractive Indices of Rutile and Sphalerite", Journal of the Optical Society of America 41, 6, P416-419 (1951).

72. Fraser D.B. et al, "Sputter Deposited CdS Films with High Photoconductivity Through Film Thickness", Journal of Applied Physics, 43, 7, P3120-3127 (1972).

73. Wilson J.I.B. et al, "The Electrical Properties of Evaporated Films of Cadmium Sulphide" Journal of Physics and Chemistry of Solids 34, 2, P171-181 (1973).

74. Berkowitz J. et al, "Equilibrium Concentration of Sulphur Vapour" Journal of Chemical Physics 39, 2, P275-283 (1963)

75. Somarjai G.A. et al, "Evaporation Mechanism of CdS Single Crystals" Journal of Chemical Physics 41, 5, P1389-1399 (1964).

76. Somarjai G.A. et al, "Compound Change of Binary Compounds Under Conditions of Equilibrium and Vacuum Vaporization", Journal of Chemical Physics 42, 12, P4140-4144 (1965).

77. Chopra K.L. "Thin Film Phenomena", McGraw-Hill, New York (1969).

78. Gunther K.G. "Interfacial and Condensation Processes Occurring with Multicomponent Vapours", "The Use of Thin Films in Physical Investigations", P213-231, New York (1966).

79. Campbell D.S., "Film Formation and Structural Problems", Journal of Vacuum Science and Technology 6, 4, P442-448 (1969).

80. Honjo G. et al, "Studies of Epitaxial Growth of Metal and Nonmetallic Films by Means of High Resolution Cine and Still Electron Microscopy" Journal of Vacuum Science and Technology 6, 4, P576-582 (1969).

81. Matthews J.W., "Evaporated Single Crystal Films", Physics of Thin Films, IV, P137-190 Academic Press, New York (1967).

82. Van der Drift A., "Evolutionary Selection, A Principle Governing Growth Orientation in Vapour Deposited Layers" Philips Research Reports 22, 2, P267-288 (1967).

83. Shimaoka G., "Structure and Epitaxy of Evaporated Cadmium Sulphide Films", Thin Solid Films 7, 3, P405-414 (1971).

84. Simov S., "Cubic Forms in the Surface Morphology of CdS Evaporated Films" Thin Solid Films 15,1, P79-86 (1973).

85. Francis A.B. et al, "Cadmium Sulphide Infrared Optical Material", Journal of the Optical Society of America 50, 2, P118-121 (1960).

86. Valdes L.B., "Resistivity Measurements on Germanium for Transistors", Proc IRE 42, 2, P420-427 (1954).

87. Look D.C., "High Temperature Annealing in Electron-Irradiated CdS", Journal of Applied Physics 45, 1, P492-493 (1974).

88. Wilcox D.M. et al, "Epitaxial Growth of CdS on Ionic Substrates", Journal of Material Science, 4, 7, P672-680 (1969).

89. Dalgoutte D.G., PhD Thesis, Glasgow University (1973).

90. Abeles F., "La Determination de L'indice et de L'epaisseur des Couches Minces Transparentes", Le Journal de Physique et Le Radium 11, 7, P310-314 (1950).

91. Yariv A., "An Introduction to Optical Electronics", Holt, Reinhart and Wiston Inc., New York (1971).

92. Kaminow I.P. et al, "Electrooptic Light Modulators", Applied Optics, 5, 10, P1612-1628 (1966).

93. Nye J.F., "Physical Properties of Crystals", Oxford Press, Oxford, (1957).

94. Lotspeich J.F., "Modulation Sensitivity Enhancement in Electrooptic Slab Waveguides" Journal of the Optical Society of America 65, 7, P797-803 (1975).

95. Chang W.S.C. et al, "Theoretical Design of Guided Wave Structure for Electrooptical Modulation at 10.6 μm", IEEE Journal of Quantum Electronics 8, 6, P463-470 (1972).

96. Pratt W.K., "Laser Communication Systems", Wiley, New York (1969).

97. Ross M. "Laser Receivers", Wiley, New York (1966).

98. De la Rue R.M., PhD Thesis, University of London (1972).

99. Tien P.K. et al, "Formation of Light Guiding Interconnections in an Integrated Optical Circuit by Composite Tapered Film Coupling", Applied Optics 12, 8, P1909-1916 (1973).

100. Millar C.A., PhD Thesis, Glasgow University (1976).

101. Goell J.E., "A Circular-Harmonic Computer Analysis of Rectangular Dielectric Waveguides", Bell System Technical Journal 48, 7, P2133-2160 (1969).

102. Marcatili E.A.J., "Dielectric Rectangular Waveguide and Directional Coupler for Integrated Optics" Bell System Technical Journal 48, 7, P2071-2102 (1969).

103. Spencer E.G. et al, "Ion Beam Techniques for Device Fabrication" Journal of Vacuum Science and Technology, 8, 5, PS52-S70 (1972).

104. Brillson L.J. et al, "Optical Guided Waves in CdS_xSe_{1-x} Diffused Layers" Journal of Applied Physics 45. 12, P5289-5293 (1974).

105. Finne R.M. et al, "A Water-Amine-Complexing Agent System for Etching Silicon" Journal of the Electrochemical Society 114, 9, P965-970 (1967).

106. Tsang W.T. et al, "Optical Waveguides Fabricated by Preferential Etching" Applied Optics 14,5, P1200-1206 (1975).

107. Dunsmuir R. et al, "Thin Film Dielectric Waveguides and Prism-Film Couplers" submitted to Proc IEE for publication.

108. Yariv A. "Coupled Mode Theory for Guided Wave Optics" IEEE Journal of Quantum Electronics 9, 9, P919-933 (1973).

109. Marcuse D., "The Coupling of Degenerate Modes in Two Parallel Dielectric Waveguides" Bell System Technical Journal 50, 6, P1791-1816 (1971).

110. Gedeon A., "Effective Thickness of Optical Waveguides in Tunable Directional Couplers" Journal of the Optical Society of America 64, 5, P615-618 (1974).

111. Kapany N.S., "Fibre Optics", Academic Press, New York (1967).

112. Dunsmuir R., Private Communication.

113. Kogelnik H. et al, "Switched Directional Coupler with Stepped Δβ-Reversal", Topical Meeting on Integrated Optics, MD5 (1976).

114. Miller S.E., "Coupled Wave Theory and Waveguide Applications", Bell System Technical Journal, 33, 3, P661-719 (1954).

115. Marcatili E.A.J., "Slab-Coupled Waveguides", Bell System Technical Journal 53, 4, P645-674 (1974).

116. Auracher F. et al, "New Directional Coupler for Integrated Optics" Journal of Applied Physics 45, 11, P4997-4999 (1974).

117. Milnes A.G. et al, "Heterojunctions and Metal Semiconductor Junctions", Academic Press, New York (1972).

118. Jones D. et al, "The Electronic Band Structures of the Wide Band Gap Semiconductors GaN and AlN", Solid State Communications 11, 5, P701-705 (1972).

119. Yim W.M. et al, "Epitaxially Grown AlN and its Optical Band Gap", Journal of Applied Physics 44, 1, P292-296 (1973).

120. Hutchins R.H. et al, Internal Report, Glasgow University (1973).

121. Weimer P.K. "The Insulated-Gate Thin Film Transistor", Physics of Thin Films, 2, P147-192, Academic Press, New York (1964).

122. Moss T.S. "Optical Properties of Semiconductors", Butterworths, London (1959).